CENTRO INTERNACIONAL DE ESTUDOS
DE DOUTORAMENTO E AVANZADOS
DA USC (CIEDUS)

TESIS DE DOCTORADO

DEVELOPMENT OF LUMINESCENT TECHNIQUES FOR THE ENHANCED DETECTION OF IMMUNOSUPPRESSANTS

Francesca Salis

ESCUELA DE DOCTORADO INTERNACIONAL

PROGRAMA DE DOCTORADO EN CIENCIA Y TECNOLOGÍA QUÍMICA

SANTIAGO DE COMPOSTELA / LUGO

AÑO 2018

USC
UNIVERSIDADE
DE SANTIAGO
DE COMPOSTELA

DECLARACIÓN DEL AUTOR DE LA TESIS

DEVELOPMENT OF LUMINESCENT TECHNIQUES FOR THE ENHANCED DETECTION OF IMMUNOSUPPRESSANTS

D./Dña. FRANCESCA SALIS

Presento mi tesis, siguiendo el procedimiento adecuado al Reglamento, y declaro que:

1) *La tesis abarca los resultados de la elaboración de mi trabajo.*
2) *En su caso, en la tesis se hace referencia a las colaboraciones que tuvo este trabajo.*
3) *La tesis es la versión definitiva presentada para su defensa y coincide con la versión enviada en formato electrónico.*
4) *Confirmo que la tesis no incurre en ningún tipo de plagio de otros autores ni de trabajos presentados por mí para la obtención de otros títulos.*

En Leganés, a 27 de Julio de 2018

Fdo.: Francesca Salis

USC
UNIVERSIDADE
DE SANTIAGO
DE COMPOSTELA

AUTORIZACIÓN DEL DIRECTOR DE LA TESIS

DEVELOPMENT OF LUMINESCENT TECHNIQUES FOR THE ENHANCED DETECTION OF IMMUNOSUPPRESSANTS

D. .....GUILLERMO ORELLANA MORALEDA.....
Dña. .....ANA BELÉN DESCALZO LÓPEZ.....

INFORMAN:

Que la presente tesis, corresponde con el trabajo realizado por D/Dña. ***FRANCESCA SALIS****, bajo nuestra dirección, y autorizamos su presentación, considerando que reúne los requisitos exigidos en el Reglamento de Estudios de Doctorado de la USC y que, como directores de ésta, no incurre en las causas de abstención establecidas en Ley 40/2015.*

En Madrid, a 27 de Julio de 2018

Fdo.: Guillermo Orellana

Fdo.: Ana Belén Descalzo

USC
UNIVERSIDADE
DE SANTIAGO
DE COMPOSTELA

A mio padre

USC
UNIVERSIDADE
DE SANTIAGO
DE COMPOSTELA

Acknowledgments

Este trabajo fue financiado por la Unión Europea a través del Proyecto FP7-ICT "NANODEM" (NANOphotonic DEvice for Multiple therapeutic drug monitoring) bajo contrato no. 318372.

Quiero agradecer a todas las personas que en estos años han contribuido a llevar a cabo esta tesis.

En primer lugar, a mis directores de tesis el Prof. Guillermo Orellana Moraleda y la Prof. Ana Belén Descalzo López que han creído en mí eligiéndome para trabajar en el grupo, me han enseñado continuamente, tratando de trasmitirme su pasión por el trabajo que hacen. Gracias por vuestros consejos y vuestro seguimiento en mi trabajo, por vuestro trato siempre amable y por vuestra disponibilidad. Gracias porque me habéis hecho crecer personalmente y profesionalmente.

Quiero agradecer el Prof. Ramón José Estévez Cabanas por haberme aceptado en el Programa de Doctorado en Ciencia y Tecnología Química y de esta manera, facilitarme todos los trámites burocráticos y hacer que esta tesis se pudiera leer cuanto antes.

Quiero agradecer todos los miembros del grupo GSOLFA, sobre todo a las Prof. Mª Cruz Moreno Bondi por sus constructivas reuniones y la Prof. Elena Benito Peña por su ayuda y colaboración en estas tesis y en el proyecto Nanodem.

En estos años he tenido muchísima surte de tener unos compañer@s majisim@s. Desde el principio me habéis aceptado como parte de la familia, me habéis ayudado siempre, animado y apoyado. Espero haber aprendido algo de cada un@s de vosotr@s. En particular, tengo que dar mil gracias al Prof. Javier Lucas Urraca Ruiz, que tiene buena parte del merito que el GSOLFA sea un grupo dentro y fuera del laboratorio, el Dr. Maximino Bedoya Gutiérrez siempre amable y disponible, la Dra. Irene Núñez González mi ángel de la guarda, una ayuda imprescindible los primeros años, la Dr. Mª Nieves Fresno López y Dr. Pramiti Hui por sus consejos y experiencias, José Ángel de la Torre González y Idoia Urriza Arsuaga por vuestra infinita alegría que dió al laboratorio una nueva luz, he trabajado muy a gusto con vosotros. También quería agradecer a Dr. David Haigh Flórez, Keurison Figueredo Magalhaes, Guido Ielasi per le nostre chiaccherate sempre produttive, Silvia Vaghini per la tua tenecia e forza, Cristina de la Hera Hernanz por tu positividad, Alexandre Vieira Silva, Raquel Chamorro Mendiluce, Clara Somoza Colino, Rahma A. Gebril Abou-Hany por su astucia, Lidia N. Gómez Arribas, Alberto Rico Yuste, Riikka Peltomaa, Dr. Francisco Amaro Torres, Prof. Fernando Navarro Villoslada, Dr. Sergio Carrasco Garrido Prof. Mª Concepción Pérez Conde, Ana Bettina Glahn Martinez, Beatriz Bedoya Gutiérrez, Dra. Mª Victoria González de Vallejo por su simpatía, Dr. Tomás C. Engel, Aleksandra Chechelska, Dr. André Eduardo Pereira Guedes Ribeiro dos Santos, y a Nuria Martín el grupo sin ti ya no será lo mismo.

I would like to thank all the members of the NANODEM project for the fruitful collaboration, constructive confrontation and to share the same desire in achieving the final goal of the project.

Tengo que agradecer a todo el grupo de química medica de la Prof. Mª Luz López Rodríguez del departamento de química orgánica de la UCM por la amable concesión del reactor de microondas sin el cual un parte importante de la tesis no hubiera visto la luz.

Un ringraziamento speciale ai miei genitori che mi hanno sempre spronato nello studio, nel fare nuove esperienze, mio padre oggi sarebbe orgogliosissimo. Grazie a mio padre che mi ha dato una motivazione per andare avanti, mi manchi. Grazie a mia mamma per essere un esempio nell'affrontare e superare le difficoltà. Grazie per avermi lasciato libera di fare le mie scelte e per esserci sempre.

Grazie a mia figlia, Vera che ha dovuto sorbirsi la fase di correzioni della tesi e che mi ha dato tanta gioia e voglia di continuare. Questa tesi e questo sforzo sono stati fatti anche per te, spero che servano a farci stare bene e meglio.

Gracias a mi amor, Víctor que me ha salvado la vida, que me ha dado fuerza, apoyado y aguantado en estos años.

Grazie a mia nonna Vicenzina che se fosse nata sessant'anni dopo avrebbe ottenuto il dottorato più in fretta di me.

Grazie a tutta la mia famiglia e amici di famiglia, perché mi volete bene, anche se siamo lontani, vi sento sempre vicino. A mia Zia Nicoletta, Anna Giulia, Massimo e M. Teresa, Padrino, Lucy, Fabrizio e Giorgio, Teresa, Antonello, Valentina e Speranza, Efisio, Gianni, Antonellino, Francesco, grazie anche a tutti gli altri zie e zie e cugini.

Grazie anche alle amiche di mia madre soprattutto Maura, Luciana e Graziella, mi avete sempre dato buoni consigli.

Gracias a toda mi familia española, sobre todo a mis suegros Lourdes y Manolo por haber cuidado de Vera cuando tenía que trabajar en las correcciones, sois una referencia para todos. Gracias a mis cuñados Rocío y Javi y mi sobrino Adrián por haber estado conmigo siempre. Gracias a todos y todas los demás tíos, tías y primas que siempre se han interesado por mi y que me han animado siempre.

Gracias también a mis compañer@s de piso y mis amig@s.

Index

INTRODUCTION

INTRODUCTION **2**

1. THE IMPORTANCE OF ORGAN TRANSPLANTATIONS **2**

1.1. Spain as world leader in organ transplantation 4

2. IMMUNOSUPPRESSANT THERAPY **5**

2.1. History 5

2.2. Complication of immunosuppressive medication 5

2.3. Therapeutic drug monitoring 7

3. IMMUNOSUPPRESSIVE DRUGS **9**

3.1. Cyclosporine A (CyA) 10

3.1.1. Mechanism of action of cyclosporine A 11

3.1.2. Chemical reactivity 12

3.2. Tacrolimus (FK506) 13

3.2.1. Mechanism of action of tacrolimus 14

3.2.2. Chemical reactivity 15

3.3. Mycophenolic acid (MPA) 16

3.3.1. Mechanism of action 17

3.4. Chemical reactivity 17

4. THE NANODEM PROJECT **18**

4.1. NANODEM limits of detection and strategies to enhance the analytical signal 20

4.2. Homogeneous assay 21

4.3. Heterogeneous assay 22

5. METHODS OF ANALYSIS OF IMMUNOSUPPRESSANTS **23**

5.1. Chromatographic methods 24

5.2. Immunoassays 24

5.2.1. Fluorescence immunoassays (FIAs) 25

5.2.2. Fluorescence polarization immunoassay (FPIA) 25

5.2.3. Basic principles of fluorescence polarization-based methods 27

5.2.4. Binding assay based on detection of chemiluminescence initiated by $^1O_2$ photoproduction. 28

5.2.5. Photochemical production of singlet oxygen 31

6. NEAR-INFRARED FLUORESCENT LABELS 34
6.1. Cyanine dyes 35
6.2. BODIPY dyes 37
6.3. Benzophenoxazines 40
7. FLUORESCENT MAGNETIC NANOPARTICLES AS LABELS FOR FIAS 42
7.1. Methods for preparing dye-doped nanoparticles (DDNPs) 45
OBJECTIVES 47
GENERAL OBJECTIVES OF THE THESIS WORK 48
RESULTS AND DISCUSSION
DERIVATIZATION OF IMMUNOSUPPRESSIVE DRUGS FOR FLUORESCENT LABELING AND IMMOBILIZATION ONTO SURFACES
1. INTRODUCTION 53
2. MODIFICATION OF THE IMMUNOSUPPRESSANTS WITH A CARBOXYLIC ACID GROUP 54
2.1. Synthesis of cyclosporine A derivatives 55
2.1.1. Routes 1 and 2. Previous protection of the hydroxy group of CyA 56
2.1.2. Route 1, synthesis of CyA-S-COOH 59
2.1.3. Route 2, synthesis of CyA-N-COOH 61
2.1.4. Route 3, synthesis of CyA-O-COOH 64
2.2. Synthesis of a carboxylic derivative of tacrolimus 65
3. LABELING OF IMMUNOSUPPRESSANTS WITH A NIR FLUORESCENT LABEL 67
3.1. Reaction mechanism of amide bond formation mediated by carbodiimides 67
3.1. Synthesis of FK506-DIC 68
3.2. Labeling of FK506-COOH with Dy636-NH_2 69
3.3. Labeling of immunosuppressants with Amino Nile Blue 71
3.3.1. Synthesis of an alternative NIR label: Amino Nile Blue (ANB) 72
3.3.2. Spectroscopic characterization of Amino Nile Blue (ANB) 73
3.3.3. Coupling of CyA-COOH with Amino Nile Blue 76
3.3.4. Coupling of FK506-COOH with Amino Nile Blue 79
3.3.5. Coupling of MPA to Amino Nile Blue 80
3.3.6. Comparison of the spectroscopy data of the different immunosuppressants labeled with ANB 81
4. BINDING ANALYSIS OF IS-ANB LABELS WITH HUMAN SERUM ALBUMIN WITH FLUORESCENCE POLARIZATION 84

4.1. Free fraction of ISs 84
4.2. Fluorescence polarization technique 85
4.3. How to obtain the free fraction α from the dissociation constant K_D 86
4.4. Optimization of the condition for the FP binding assay 88
4.4.1. Fluorescent emission of IS-ANB in the presence of HSA 88
4.4.2. Concentration of the labeled immunosuppressant 89
4.4.3. Preliminary FP binding assay with BSA 90
4.5. Biding assay for CyA-S-ANB, FK506-ANB and MPA-ANB 91
5. APPLICATIONS OF THE SYNTHETIZED IMMUNOSUPPRESSANT DERIVATIVES 96
5.1. Fluorescence polarization immunoassay (FPIA) 96
5.2. Collaborations with the NANODEM EU Project Partners 97
FLUORESCENT NANOPARTICLES AS MARKERS FOR SENSITIVE IMMUNOASSAYS
1. INTRODUCTION 98
2. COBALT CORE MAGNETIC NPs 102
2.1. Co@SiO_2 MNPs 102
2.1.1. Co@PSt MNPs 102
2.2. Co@SiO_2@PSt magnetic NPs 103
2.2.1. Fluorescent doping of Co@SiO_2 NPs 104
3. FERRITE-DECORATED POLYSTYRENE NPs 107
3.1. Synthesis and characterization of BODIPY dyes 108
3.2. Synthesis of PFB-515 and PFB-641 BODIPY dyes 109
3.3. Spectroscopic characterization of PFB-515 and PFB-641 110
3.4. Protocol for doping polystyrene Estapor® NPs with BODIPY dyes 116
3.5. Spectroscopic characterization of NPs doped with BODIPY dyes (FMNPs) 116
3.6. Intra-particle Förster resonance energy transfer 120
3.7. Magnetic characterization of the fluoromagnetic nanoparticles (INESC-MS) 122
4. APPLICATION OF THE FRET NPs: HETEROGENEOUS IMMUNOASSAY FOR TACROLIMUS 122
4.1. Coupling of capture antibodies to the fluoromagnetic nanoparticles 122
4.2. FMNPs-based competitive immunoassay for Tacrolimus 124
4.3. Stability of the FMNPs in the presence of surfactant 127
PHOTOSENSITIZING NANOPARTICLES FOR SINGLET OXYGEN PRODUCTION 129
1. OBJECTIVE 129
2. RUTHENIUM COMPLEXES AS PHOTOSENSITIZER DYES 130

3. BODIPY DYES AS PHOTOSENSITIZER 132
3.1. Electrophilic substitution reactions: halogenation 132
4. DOPING OF NPs WITH THE BODIPY PHOTOSENSITIZING DYES 135
5. DOPING OF POLYSTYRENE NPs WITH THE RUTHENIUM PHOTOSENSITIZING DYES 139
5.1. Polystyrene carboxylated nanoparticle (PSt-COOH NPs) doped with RD3 139
5.1.1. Nanoparticles swelling with different solvents 140
5.1.2. Study of the swelling with different methanol-THF mixture 141
5.1.3. Study of the dye leaching 143
5.1.4. Optimum loading of the RD3 photosensitizer in 390 nm PSt-COOH NPs 144
5.1.5. Preparation of 200 nm PSt-COOH NPs 145
5.1.6. Preparation of doped RD3 26 nm PSt-COOH NPs 146
6. MAGNETIC NANOPARTICLES (MNPs-COOH) DOPED WITH RD3 148
7. PHOSPHORESCENCE KINETICS OF 390 NM PST-COOH NPs DOPED WITH RD3 149
8. QUANTUM YIELD OF SINGLET OXYGEN PRODUCTION OF THE RD3-DOPED NPs 153

EXPERIMENTAL PART

1. MATERIALS AND INSTRUMENTATIONS 167
2. SYNTHESIS OF CYCLOSPORINE A DERIVATIVES 170
2.1. Synthesis of Cyclosporine A acetate (CyA-Ac) for the synthesis of CyA-S-COOH and CyA-N-COOH 171
2.2. Synthesis of CyA-S-COOH 172
2.2.1. Synthesis of Cyclosporine A 6-bromo-2-methylhex-4-en-1-yl acetate (CyA-Br) 172
2.2.2. Synthesis of Cyclosporine-6-acetoxy-thiopropanoate 173
2.2.3. Synthesis of Cyclosporine A thiopropanoic acid (CyA-S-COOH) 173
2.3. Synthesis of CyA-N-COOH 174
2.3.1. Synthesis of Epoxy Cyclosporine A (CyA-EPO) 174
2.3.2. Synthesis of Cyclosporine A ((2-yl)amino)hexanoic acid (CyA-N-COOH) 175
2.4. Synthesis of Cyclosporine A (2-oxoethoxy) acetic acid (CyA-O-COOH) 177
3. SYNTHESIS OF TACROLIMUS DERIVATIVES 178
3.1. Synthesis of carboxylated tacrolimus (FK506-COOH) 178
3.2. Synthesis of Diisopropylcarbodiimide Tacrolimus (FK506-DIC) 179
4. SYNTHESIS OF FLUORESCENT CONJUGATE OF IMMUNOSUPPRESSIVE DRUGS 179
4.1. Labeling of tacrolimus with Dy636-NH_2 (FK506-DY-636) 180
4.2. Synthesis of Amino Nile Blue (ANB) 180

4.2.1. Synthesis of 5-ethylamino-4-mathyl-2-nitrosophenol. 181
4.2.2. Synthesis of N^1-1-naphthalenyl-1,3-propanediamine 181
4.2.3. Synthesis propylamino Nile Blue (ANB) 182
4.3. Synthesis of Cyclosporne A-(oxoethoxy)(acetamido)(propylamino)-NileBlue (CyA-O-ANB) 182
4.4. Synthesis of Cyclosporine A(thio)(propanamido)(propylamino)-Nile Blue (CyA-S-ANB) 184
4.5. Synthesis of Tacrolimus-propylamino Nile Blue (FK506-ANB) 185
4.6. Synthesis of Mycophenolic propylamino Nile Blue (MPA-ANB) 186
5. BINDING ASSAY WITH IMMUNOSUPPRESSANT USING FLUORESCENCE POLARIZATION 187
5.1. Preparation of stock solutions 187
5.2. Filling of a 96 wells microplate for the FP binding assay 187
6. COBALT CORE MAGNETIC NANOPARTICLES 190
6.1. Synthesis of Co@SiO_2 MNPs 190
6.2. Fluorescent doping of Co@SiO_2 NPs 190
6.2.1. Synthesis of Dy630-TES 190
6.2.2. Doping of Co@SiO_2 NPs with Dy630-TES 191
7. SYNTHESIS OF FLUORESCENT BODIPY DYES 192
7.1. Synthesis of PFB-515 192
7.2. Synthesis of PFB-641 193
8. FLUORESCENT DOPING OF MNPs-COOH WITH BODIPY DYES 194
8.1. General protocol 194
8.2. Preparation of FRET fluorescent magnetic nanoparticle (FMNPs-ET) 195
9. FOSTER RESONANCE ENERGY TRANSFER (FRET) ASSAY 195
9.1. Coupling of the fluoromagnetic nanoparticles to capture antibodies 195
9.2. Functionalization of the microwell plates bottom with tacrolimus 196
9.3. Immunoassay protocol 196
10. SYNTHESIS OF BODIPY PHOTOSENSITIZING DYES FOR PRODUCTION OF $^1O_2$ 197
10.1. Synthesis of 5,5-difluoro-1,3,7,9-tetramethyl-10-phenyl-5H-dipyrrolo[1,2-c:2',1'-f][1,3,2]diazaborinin-4-ium-5-uide (B1) 197
10.2. Synthesis of 5,5-difluoro-2,8-diiodo-1,3,7,9-tetramethyl-10-phenyl-5H-dipyrrolo[1,2-c:2',1'-f][1,3,2]diazaborinin-4-ium-5-uide (BI2-5) 198
10.3. Synthesis of 5,5-difluoro-2,8-diiodo-1,9-dimethyl-10-phenyl-3,7-di((E)-styryl)-5H-dipyrrolo[1,2-c:2',1'-f][1,3,2]diazaborinin-4-ium-5-uide (BI2-6) 198

11. DOPING OF NPs WITH THE BODIPY PHOTOSENSITIZING DYES 199

12. DOPING OF POLYSTYRENE NPs WITH RUTHENIUM PHOTOSENSITIZING DYES 199

12.1. Nanoparticles swelling with different solvent (390 nm PSt-COOH NPs) 199

12.2. Swelling with different MeOH-THF proportion (390 nm PSt-COOH NPs) 200

12.3. Study of RD3 dye loading (390 nm PSt-COOH NPs) 201

12.4. Preparation of PSt-COOH NPs of 200 nm 202

12.5. Preparation of PSt-COOH NPs of 26 nm 203

12.6. Magnetic nanoparticles doped with RD3 204

13. DETERMINATION OF THE FINAL CONCENTRATION OF PST-COOH NP_S AQ. SUSPENSIONS 204

14. SINGLET OXYGEN PRODUCTION QUANTUM YIELD 206

CONCLUSIONS

1. DERIVATIZATION OF IMMUNOSUPPRESSIVE DRUGS FOR FLUORESCENT LABELING AND COVALENT IMMOBILIZATION ONTO SURFACES. 210

2. FLUORESCENT NANOPARTICLES AS MARKERS FOR SENSITIVE IMMUNOASSAYS 212

3. PHOTOSENSITIZING NANOPARTICLES FOR SINGLET OXYGEN PRODUCTION 213

ANNEX PART

1. NMR AND MASS SPECTRA OF THE SYNTHETIZED COMPOUNDS 216

1.1. Cyclosporine A acetate (CyA-Ac) 216

1.2. CyA-Br 218

1.3. CyA-S-COOH 220

1.4. CyA-EPO 223

1.5. CyA-N-COOH 225

1.6. CyA-O-COOH 227

1.7. FK506-COOH 229

1.8. FK506-DIC 231

1.9. FK506-DY636 232

1.10. 5-ethylamino-4-methyl-2-nitrosophenol 233

1.11. *N*-(naphtalen-1-yl)propane-1,3-diamine 234

1.12. Propylamino Nile Blue (ANB) 236

1.13. CyA-S-ANB 238

1.14. CyA-O-ANB 240

1.15. FK506-ANB 242

1.16. MPA-ANB 244

1.17. Dy630-TES 245
1.18. PFB-515 245
1.19. PFB-641 247
1.20. B1 248
1.21. BI2-5 249
1.22. BI2-6 250
2. FTIR SPECTRA 251
2.1. $Co@SiO_2$ NPs 251
3. TEM IMAGES 251
3.1. $Co\text{-}NH_2$ magnetic nanoparticles 251
3.2. $Co@SiO_2$ magnetic nanoparticles 252
3.3. TurboBeads® with vinyl groups 253
3.4. NPs provided by Bangs Laboratories® 253
3.5. Magnetic NPs provided by Estapor®, Merck Millipore 254
RESUMEN I
1. INTRODUCCIÓN II
2. DERIVATIZACIÓN DE FÁRMACOS INMUNOSUPRESORES PARA EL ETIQUETADO FLUORESCENTE Y LA INMOVILIZACIÓN EN SUPERFICIES. IV
2.1. Inmunosupresores carboxilados (ISs-COOH). IV
2.2. Etiquetado de inmunosupresores con sonda fluorescente NIR. V
3. NANOPARTÍCULAS FLUORESCENTES COMO MARCADORES PARA INMUNOENSAYOS SENSIBLES. VI
3.1. Nanopartículas dopadas con sistemas de transferencia de energía resonante Förster (FRET) intraparticula. VI
3.2. Inmunoensayo competitivo basado en FMNP para tacrolimus. VII
4. NANOPARTÍCULAS FOTOSENSIBILIZADORAS PARA LA PRODUCCIÓN DE OXÍGENO SINGLETE VIII
5. CONCLUSIONES. IX

USC
UNIVERSIDADE
DE SANTIAGO
DE COMPOSTELA

Introduction

Introduction

1. The importance of organ transplantations

Transplantation is the transfer of human cells, tissues or organs from a donor to an ill patient with the aim of reestablishing function in his/her body.[1] During the last 50 years, transplantation has become a worldwide successful practice and remains the only successful treatment for persons with end-stage failure of solid organs such as liver, heart, lung and pancreas. Additionally, it has been demonstrated that transplantation considerably increases the duration and quality of life of transplanted patients.[2] For example, although end-stage renal disease patients can be treated through other renal therapies, kidney transplantation, the most commonly globally realized transplantation, is the best and most cost-effective treatment. According to WHO (World Health Organization), kidney transplants are carried out in 91 countries.[3]

Kidney donations together with (part of) liver are the only organ donations that can be done from well selected living donors. Nevertheless donations from deceased persons should be developed to their maximum therapeutic potential avoiding, whenever possible, the inherent risks to live donors.[4]

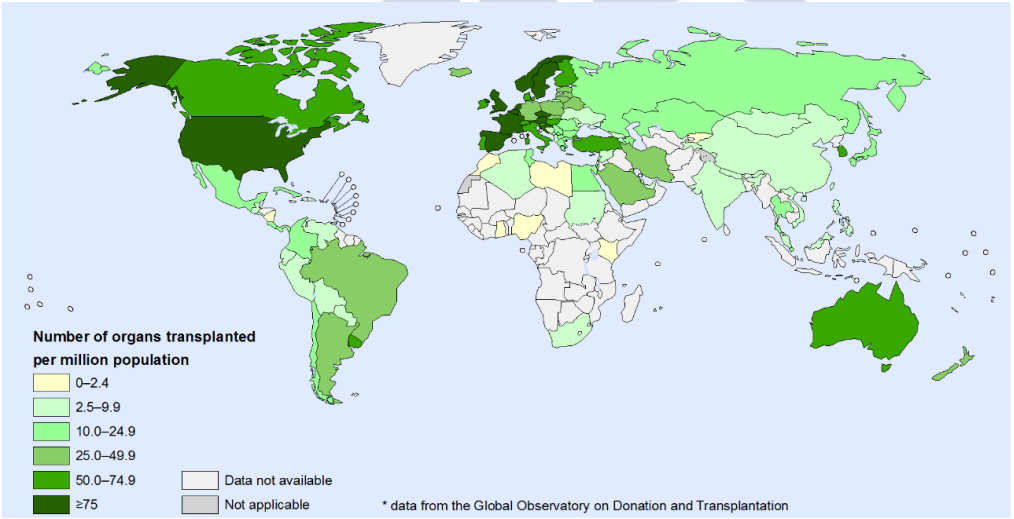


Figure 1. Global transplantation activity of solid organ. Data from: Global Observatory of Donation and Transplantation GODT 2016.

[1] Health topic, transplantation, World Health Organization. http://www.who.int/topics/transplantation/en/. **09/01/2017**

[2] Report of the Madrid Consultation, *Transplantation*, **2011**, *91*, S36–S66

[3] Y. Shimazono, Bulletin of the World Health Organization, **2007**, 85, 955–962.

[4] Global Observatory of Donation and Transplantation GODT, Orgnizacion Nacional de transpante ONT and World Health Organization WHO, *Organ Donation and Transplantation Activities* **2014**.

As it is shown in Figure 1, there are large differences between countries in accessing to suitable transplantation which mainly take place in the more economically developed ones. More than 25% of the transplants worldwide took place in the European Union in 2012.

In the decade between 2004 and 2013 the total number of organs transplanted in the European Union (Figure 2) has boosted a 33% (18% for the deceased donations and a 86% for living donations). In 2014 almost 200.000 solid organ transplantations were done in the word, with an increase of 1.8% with respect to the previous year. Table 1 reports the data of transplantation done in 2014.[5] It is reasonable to think that this trend will continue in the future. In fact, despite this considerable growth in organ donation from deceased or living persons, the availability of organs (and tissues) for transplantation is still insufficient to satisfy the demand, and 4.100 patients died in the course of 2013 while officially placed on waiting lists.

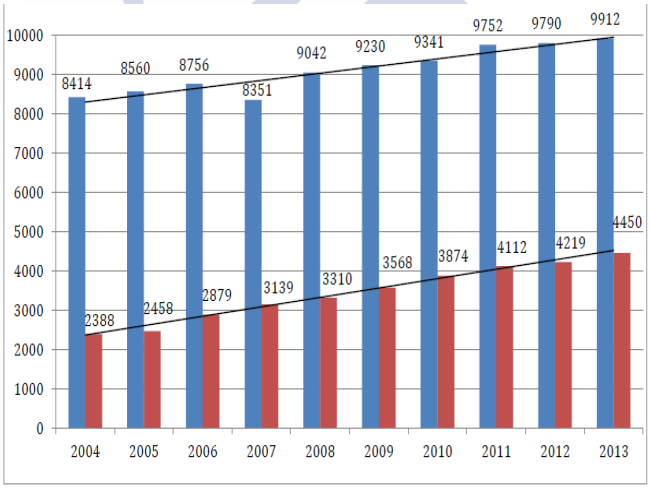


Figure 2. Organ transplanted in the European Union from 2004 to 2013. In pale blue, deceased donations and in red, living donations. All the 28 EU Member States in 2014 are included for all the years considered.[5]

Table 1. Global activity in organ transplantation in 2014 estimates. [4]

Kidney	Liver	Heart	Lung	Pancreas	Small bowel
79948	26151	6542	4689	2328	215

[5] European Commission, *Journalist Workshop on Organ donation and transplantation Recent Facts & Figures*, 26 November **2014** – Brussels.

From the medical and technological point of view, it is obvious that transplantations protocols must be optimized in order to minimize loses of precious donated organs. Nowadays, one of the critical points for a successful organ transplant normally relies in avoiding tissue or organ rejection after the operation. This implies that methods of immunosuppressant administration have to be optimized. A way of improving patient immunosuppressant dosage –and with this, diminishing the risk of organ rejection–, is having dedicated analytical methods allowing for a closer, continuous or semi-continuous monitoring of the immunosuppressant levels in blood.

1.1. Spain as world leader in organ transplantation

The Spanish model of organ donation is recognized worldwide. In fact during the last 25 years Spain achieves a continuous increase of organ donations.[6] This is due to the combination of an efficient system for organ donor identification, detection and procurement. In particular the success is due to the presence of a key professional: "transplant donor coordinators" whose main responsibility is to develop a proactive donor detection program. The ONT (*Organización Nacional de Trasplantes, National Organization for Transplants*) states that the improved results come from the better coordination with physicians working in accidents and emergencies to identify possible donors.[7]

Donation rates increased in Spain from 14 donors pmp (per million people) in 1989 to 43.4 donors pmp in 2016 (Scheme 1), with a total of 2018 donors and 4818 transplants.[8] Consequently, Spain has the shortest waiting time (3 month for heart and 18 for kidney transplant) worldwide.[9]

Table 2. Spain activity in organ transplantation in 2016. Source: *Organización Nacional de Trasplantes*.

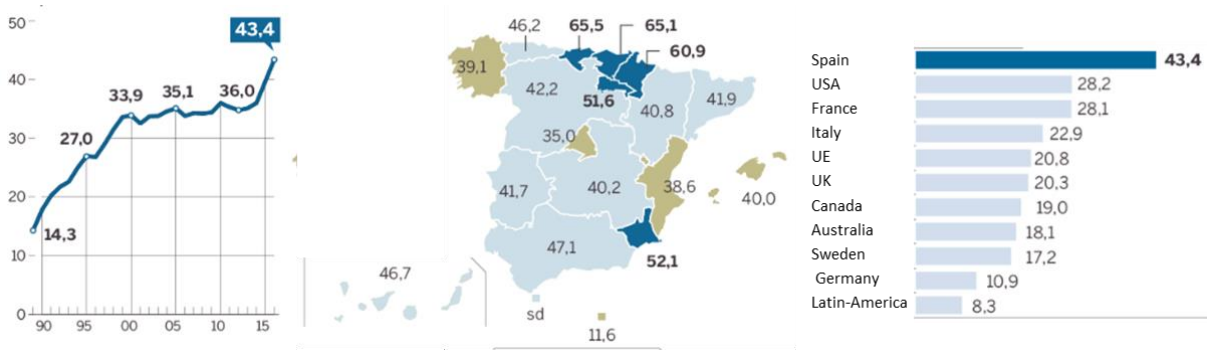
Kidney	Liver	Heart	Lung	Pancreas	Small bowel
2994	1159	281	307	73	4

[6] Ministerio de Sanidad, Servicios Sociales e Igualdad, *NOTA DE PRENSA*, **24/02/2016**.

[7] Redacción BBC Mundo, *BBC*, 3 lecciones de España, el país líder mundial en donación de órganos, **16/01/2017**. http://www.bbc.com/mundo/noticias–38638038.

[8] A. Laborde, *El País*, España vuelve a ser líder de trasplantes y logra reducir las listas de espera, **11/01/2017**.

[9] R. R. García-Abadillo, *El Mundo*, España pulveriza su propio récord en donación y trasplantes, **11/01/2017**.



Scheme 1. *Left*: graphic of donation evolution from 1990 to 2015 in Spain. *Center*: Donation of per million habitants in Spain: in dark blue the five regions with more donations, in pale blue, regions with an average number of donations and, in beige, the five regions with lower donation rates. *Right*: rates of donors per million habitants in 2016 (world-wide).[8]

2. Immunosuppressant therapy

2.1. History

Transplantation has been practiced since ancient times but the birth of clinical organ transplantation, as we currently know, can be ascribed to the second half of last century.[10] The first successful transplant, a kidney transplantation in 1954, came about by avoiding an immune response altogether, which Joseph Murray's team achieved by performing a kidney transplant between identical twins.[11]

Peter Brian Medawar in 1960 shared a Nobel Prize for his work on acquired immunologic tolerance. He was the first to identify organ rejection and to argue that immunosuppressive drugs (ISs) could be used to increase the survival of the recipients.[12,13] Cortisone and azathioprine were the first immunosuppressive drugs identified, but transplant surgery underwent a dramatic improvement just when the more potent immunosuppressive drug cyclosporine was discovered in 1970.

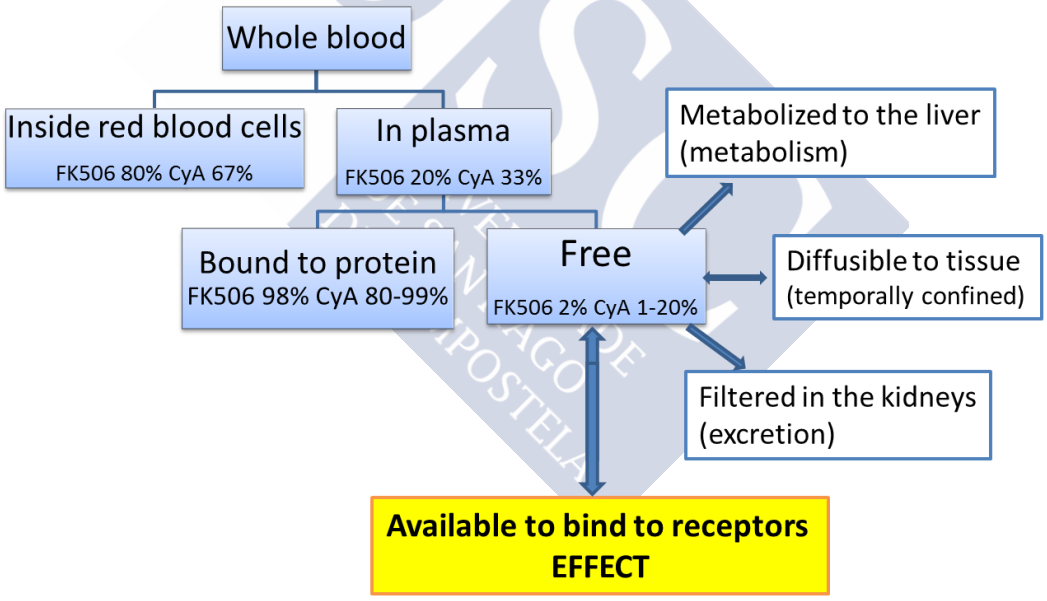
2.2. Complication of immunosuppressive medication

The first human heart transplant was made in 1967 by Dr. Christiaan Barnard. The recipient of the first heart transplantation was Louis Washkansky who lived only 18

[10] T. E. Starzl, *J. Am. Coll. Surg.*, **2001**, *192*, 431–446.
[11] J.P. Merrill, J.E. Murray , J.H. Harrison, W.R. Guild, *J. Am. Med. Assoc.*, **1956**; *160*, 277–282.
[12] P. B. Medawar, *J. Am. Coll. Surg.*, 1995, 180, 332–336.
[13] P. B. Medawar, *Nobel Lecture*, **12/ 1960**.
https://www.nobelprize.org/nobel_prizes/medicine/laureates/1960/medawar–lecture.html

days after the operation. He died not because its new heart failed but due to a severe infection as a consequence of the immunosuppressive drug therapy he received to avoid organ rejection.

Until now transplantation and post-transplant care are some of the most challenging and complex areas of modern medicine. Patients must be treated with antirejection medications and these drugs compromise seriously the immune system increasing the risk of life-threatening infections. One of the major complications that the doctors have to face with immunosuppressive medications is their narrow therapeutic window. Immunosuppressive drugs can easily be underdosed (with possible transplanted organ rejection) or overdosed (resulting in dangerous side effects). Moreover, the high inter- and intra-patient variability in the pharmacokinetic parameters due to polymorphic metabolism suggests that a continuous and personalized therapy is required, making more challenging the drug administration, especially in the early post-transplant settings.[14] It has been demonstrated that there is a clear relationship between drug concentration and side effects: a wrongly calculated dose could cause severe side effects.



Scheme 2. Distribution of immunosuppressive drugs in the body. Tacrolimus (FK506) and cyclosporine A (CyA) are used in the scheme as representative examples.[15]

[14] N.A. Stienstra, M.A. Sikma, A. van Dapperen, D.W. de Lange, E.M. van Maarseveen, *Ther. Drug Monit.*, **2016**, *8*, 722–727.

[15] A) K. Nagase, K. Iwasaki, K. Nozaki, K. Noda, *J. Pharm. Pharmacol.*, **1994**, *46*, 113–117; B) H. Bittersohl, B. Schniedewind, U. Christians, P. B. Luppa, *J. Chromatogr. A*, **2018**, *1547*, 45–52; C) H. Bittersohl, J. Herbinger, M. Wen, L. Renders, W. Steimer, P. B. Luppa, *Ther. Drug Monit.*, **2017**, *3*, 211–219.

Some of the side effects that immunosuppressive drugs may have are neuro- and nephrotoxicity, decreasing the possibility of survival of transplanted patients.[16,17] Recent studies suggest that side effects can be predicted by analyzing the free (i.e. unbound) immunosuppressants concentration. The free fraction can provide better information than the overall immunosuppressive drug concentration in whole blood.[18,19] In fact, it was observed that there are higher levels of unbound drug fraction in patients undergoing severe side effects.[20,21] This can be related to the fact that just the free fraction is the pharmacologically active form because it is the only one which can reach the receptor or tissue compartments (Scheme 2).[22] As shown on Scheme 2, the free immunosuppressant concentration in the case of cyclosporine A or tacrolimus is very low (sometimes reaching only the 1% of the whole-blood concentration).[23] Therefore monitoring the unbound fraction is very challenging because extremely low limits of detection are required (Table 3).

Table 3. Therapeutic ranges of the most common immunosuppressive drugs in whole blood and the required detection limits for therapeutic drug monitoring using free fraction (table adapted from K. Freudenberger et al.[25]).

Immunosuppressant	***Therapeutic range in whole blood [ng/mL]***	***Free drug fraction [%]***	***Limit of detection (LOD) [ng/mL]***
Cyclosporine A (CyA)	150-350	1-3	1
Tacrolimus (FK506)	5-20	1	0.05
Mycophenolic Acid (MPA)	1000-3500	1-3	10

2.3. Therapeutic drug monitoring

Therapeutic drug monitoring (TDM) consists in the measurement of medication concentration in the blood to ensure that drug levels remain within the desired range. There are two main ways in which the drug levels are measured: the so called "*trough level*" and the area under the drug concentration vs. time curve (AUC).

[16] M.F. Hebert, S. Zheng, K. Hays K, *Transplantation*, **2013**, *95*, 908–915.
[17] E.M. Yoshida, P.J. Marotta, P.D. Greig, *Liver Transpl*., **2005**, *11*, 1064–1072.
[18] A. Dasgupta, In *Personalized Immunosuppression in Transplantation: Role of Biomarker Monitoring and Therapeutic Drug Monitoring*, Oellerich, M.; Dasgupta, A. (Eds.), Elsevier, **2015**; pp. 83-108.
[19] I. Nowak, L.M. Shaw, *Clin. Chem.* **1995**, *41*, 1011-1017.
[20] H. Zahir, G. McCaughan, M. Gleeson, *Ther. Drug Monit*., **2004**, *26*, 506–515.
[21] T. Bohnert, L.S. Gan, *J. Pharm. Sci.,* **2013**, *102*, 2953–2994.
[22] M. Musteata , *Ther. Drug Monit*., Newer Drugs Biomarkers, first edit., **2012**, 468.
[23] K. Iwasaki , Y. Miyazaki, Y. Teramura, *Res Commun. Mol. Pathol. Pharmacol.*, **1994**, *94*, 251–257.

The so called "trough level" is the concentration of medication in blood immediately before the next dose. In post transplanted patients TDM is regularly performed with a blood sample taken immediately before each immunosuppressant dose. Measurements are normally performed by liquid chromatographic methods coupled to mass spectrometry detection, and provide information on the total (free and bound to proteins) IS levels with an appropriate sample preparation.

The area under the drug concentration vs. time curve (AUC)[24] reflects the body exposure to drug after administration of a dose. The AUC is inversely proportional to the elimination of the drug from the body. In the absence of continuous sensing, it can be estimated by measuring the drug concentration in plasma at several time points in a semi-continuous manner. This method gives precious information on the pharmacokinetic behavior of a drug.

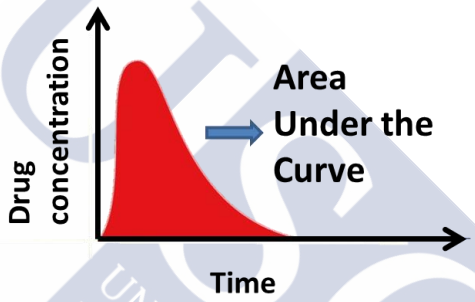


Figure 3. The area under the drug concentration vs time curve (AUC) as indication of better dosing strategies.

Therefore, the area under the drug concentration vs. time curve (AUC) (Figure 3) is a better indicator than the "trough level". In fact there is a general agreement that improved patient outcomes derive from pharmacokinetic dosing strategies based on multiple blood sample collection. This makes it possible to adjust the dosage in the next drug administration. Moreover, it should be feasible to measure the patient's individual pharmacokinetic and to calculate rates of absorption, distribution and elimination, helping to provide an optimal personalized immunosuppressant drug therapy.

However, obtaining accurate information from the AUC implies regular and frequent monitoring of the immunosuppressant concentration in the blood over a period of time. Consequently the increased number of samples required, has made AUC monitoring so far impractical for routine clinical use.

[24] J.R. Turner, *Area Under the Curve (AUC)*. In: Gellman M.D., Turner J.R. (eds) *Encyclopedia of Behavioral Medicine. Springer*, New York, NY, **2013.**

Recent studies show that further substantial progress can be expected from continuous measurement rather than estimation of the AUC. Moreover, continuous monitoring of protein unbound (free) immunosuppressive drugs would be a significant step forward in TDM. Free drug fractions might better reflect toxic or insufficient drug levels and, in consequence, better predict the clinical outcome compared to conventional drug monitoring based on infrequent sampling and time- and resource-consuming analyses.

3. Immunosuppressive drugs

Immunosuppressive drugs (ISs) are medications that inhibit and reduce the strength of the immune system. Therefore they are used to treat diseases of autoimmune origin such as psoriasis, arthritis, Crohn's disease, lupus or multiple sclerosis. However the ISs are mostly employed after organ and tissue transplantations (heart, liver, kidney, bone marrow, etc.) to prevent organ rejection.

Immunosuppressive drugs can be classified according to their mechanism of action. Among the ISs there are corticosteroids, monoclonal antibodies. The most applied immunosuppressive drugs are calcineurin inhibitors such as cyclosporine A (CyA) and tacrolimus (FK506); serine/threonine kinase inhibitors, such as sirolimus (SIR), and everolimus (EvE); and inosine monophosphate dehydrogenase inhibitors, with mycophenolic acid (MPA) as a representative example.[25]

To avoid or reduce their side effects, ISs are usually given as combination of at least two drugs of different type: for instance, a calcineurin inhibitor together with an inosine monophosphate dehydrogenase inhibitor. This practice is today widely used and drugs interactions have been extensively documented.[26] Usually tacrolimus and cyclosporine are never administered together. The most common regimes are a combination of CyA and MPA or FK506 and MPA. [27]

In this thesis the attention will be focused in some of the most relevant ISs used nowadays for clinical pourposes: cyclosporine A (CyA), tacrolimus (FK506) and mycophenolic acid (MPA) (Figure 4). The main aim will be to introduce chemical modifications in these molecules, that would allow either their fluorescent labeling or their immobilization onto different surfaces. It is very important to know how the immunosuppressants are being recognized by their corresponding cell receptors. Cyclosporine A and tacrolimus are two macromolecular cyclic polypeptides with a rather complex structure, therefore, their chemical modification is not a straightforward task, and the examples describing chemical modification of these macromolecules is very scarce in the literature. Their transformation usually requires multi-step reactions,

[25] K. Freudenberger, U. Hilbig, G. Gauglitz, *Trac-Trends Anal. Chem.*, **2015**, *79*, 257–268.

[26] R. A. Wolfe, E. C. Roys, R. M. Merion, *Am. J. Transpl.*, **2010**, *10*, 961–972.

[27] C. C. Almeida, M. R. Silveira, V. E. de Araújo, L. L. P. de Lemos, J. de Oliveira Costa, C. A. L. Reis, *Pharmaceuticals*, **2013**, *6*, 1170–1194.

and the use of protecting groups. MPA on the other hand is a smaller molecule with a –COOH group present on its structure that can be profited for further chemical derivatization. In the next parts 3.1 to 3.3, biological recognition sites, mechanism of action, and chemical reactivity of the three ISs will be described.[28]

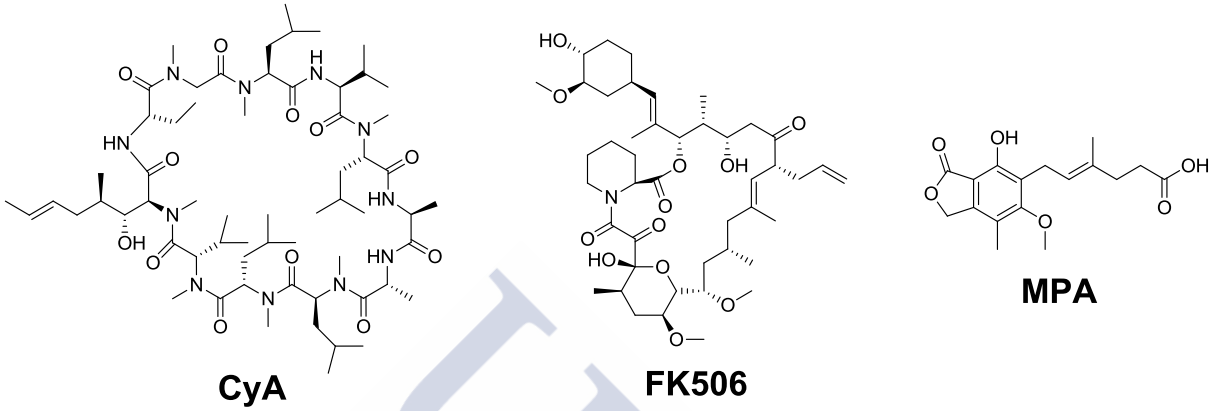


Figure 4. Chemical structures of the selected immunosuppressants: cyclosporine A (CyA), tacrolimus (FK506) and mycophenolic acid (MPA).

3.1. Cyclosporine A (CyA)

Cyclosporine A is a cyclic undecapeptide that was isolated from the fungus *Tolypocladium inflatum* in 1970. Its chemical structure was clarified six years later. It was the first immunosuppressant discovered of the polypeptide type.[29] The structure of CyA is usually drawn as shown in Figure 5. The amino acid at position 1, Bmt, or (4*R*)-4-[(*E*)-2-butenyl]-4-methyl-L-threonine, was previously unknown. Cyclosporine can adopt different conformations depending on the polarity of its surrounding.[30] In non-polar solvents or in crystalline form, intramolecular hydrogen bonds are formed between the hydrogen atoms of the four N-H amide groups and the oxygen atoms of the closed subsequent amide bonds. Due to its hydrophobic nature, cyclosporine is scarcely water soluble.

[28] M. Malachowska–Ugarte, G. Cholewinski, K. Dzierzbicka, P. Trzonkowski, *Eur. J. Med. Chem.*, **2012**, *54*, 197–201.

[29] A. Ruegger, M. Kuhn, H. Lichti, H.–R. Loosli, R. Huguenin, C. Quiquerez, A. von Wartburg, *Helv. Chim. Acta*, **1976**, *59*, 1075–1092.

[30] N. El Tayar, A. E. Mark, P. Vallat, R. M. Brunne, B. Testa, W. F. van Gunsteren, *J. Med. Chem.*, **1993**, *36*, 3757–3764.

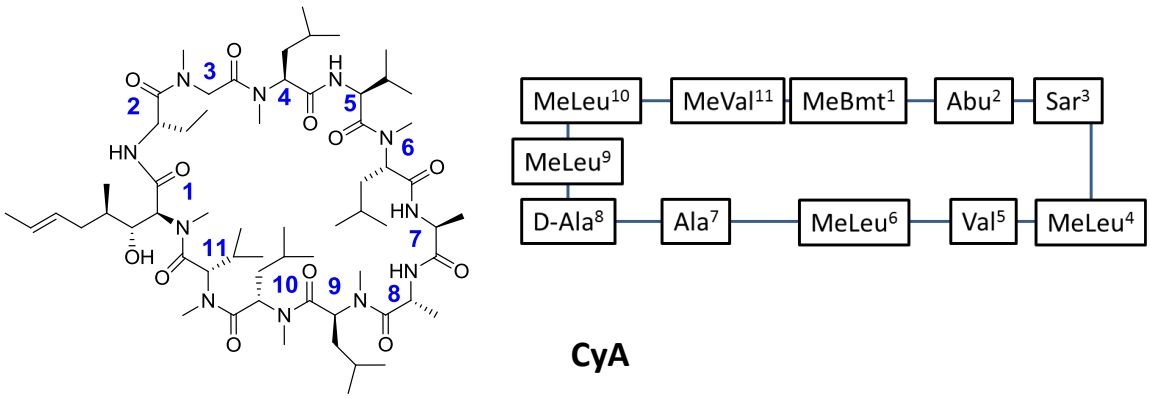
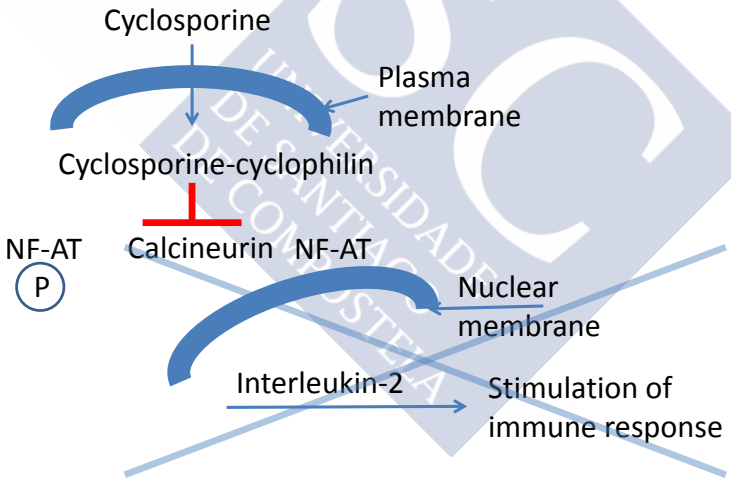


Figure 5. Left: Chemical structure of CyA. Left: the amino acids are numbered clockwise according to Peel and Scribner.[31] Right: aminoacid sequence of CyA after Lawen.[32] Bmt is (4*R*)-4-[(*E*)-2-butenyl]-4-methyl-l-threonine [=(2S, 3R, 4R, 6E)-2-amino-3-hydroxy-4-methyl-6-octenoic acid; Abu: L-2-aminobutyric acid; Sar: sarcosine; Lue: leucine; Val: valine; Ala: alanine.

3.1.1. Mechanism of action of cyclosporine A



Scheme 3. Cyclosporine A binds to the cyclophilin protein forming a complex able to inhibit the calcineurin enzyme, reducing in this way the immune response (from G. J. Nabel.[33])

The mechanism of action of CyA relies on the disruption of the function of the enzyme calcineurin; for this reason, it is clasified as a "calcineurin inhibitor (CI)". Calcineurin is in charge of dephosphorylation of specific transcription factors, proteins that command the rate of transcription of genetic information, the NFATc (Nuclear Factor of Activated

[31] M. Peel, A. Scribner, *Biochim. Biophys. Acta*, **2015**, *1850*, 2121–2144.
[32] A. Lawen, *Biochim. Biophys. Acta*, **2015**, *1850*, 2111–2120.

T-Cells). NFATc are essential for the immune response because they promote the synthesis of cytokines (small proteins important in cell signaling), including IL2, the protein that regulates the work of leukocytes. When CyA is bound to the cyclophilin protein, the complex CyA-cyclophilin is able to inhibit the enzyme. This inhibition causes a decrease on the number of T-lymphocytes and, consequently, an inhibition of the immune response.[33]

Amino acids 1, 2, 9, 10 and 11 of CyA belong to the cyclophilin binding domain, whereas amino acids 4 to 7 belong to the domain of the calcineurin binding site (Figure 6). [31]

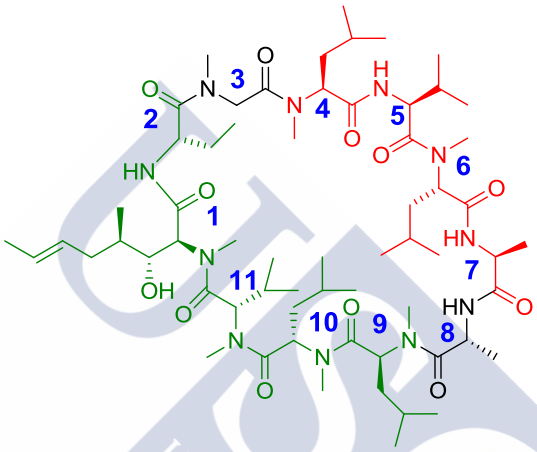


Figure 6. Binding domain of cyclosporine A: in green the cyclophilin binding domain and in red the calcinerium binding domain as described by Peel and Scribner.[31]

3.1.2. Chemical reactivity

In cyclosporine A there are eight reactive sites: each of the four N-H amide groups can be alkylated, and [Sar]^3 (Figure 5) can also undergo chemical reactions. However these synthetic routes (see yellow sites in Figure 7) demand harsh reaction conditions and their products are obtained with low yield. Alternative chemical modifications can be performed through the MeBmt subunit. The CyA crystal structure shows that this unit sticks out of the binding pocket and it is solvent accessible.[34] Moreover, it is the only amino acid of cyclosporine A that has a double bond and a heteroatom in its side-chain. Reactions of MeBmt can be performed either on the 3′-OH, on the C6′-C7′ double bond, or on the terminal carbon C8′ positions (see Figure 7 for atom numbering).[31] The 3'-OH group can be used for oxidation, acylation or alkylation reactions yielding, in the latter case, the corresponding ether derivative. The double bond in the C6'-C7'position is more reactive and may undergo oxidation providing the corresponding aldehyde or epoxide.

[33] G. J. Nabel, *Nature*, **1999**, *397*, 471–472.

[34] S. Gaali, C. Kozany, B. Hoogeland, M. Klein, F. Hausch, *ACS Med. Chem. Lett.*, **2010**, *1*, 536–539.

It can also be used for olefin cross-metathesis, or alternatively, it can be reduced to the corresponding alkane. The terminal carbon C8′ can be modified with allylic bromination.[31]

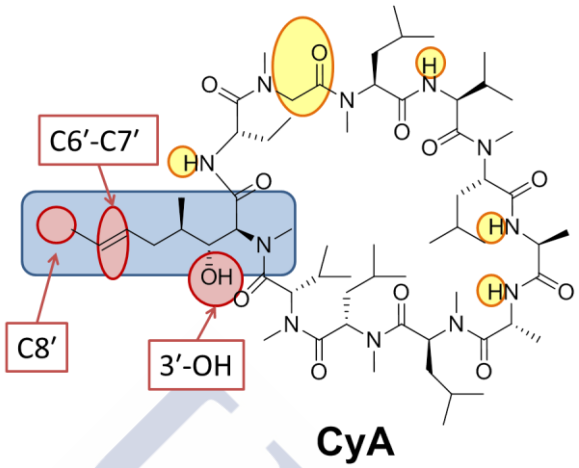


Figure 7. Cyclosporine A reactive sites. In yellow the sites which need harsh conditions to react, in red the sites in the MeBmt which will be exploited in this thesis for the CyA modifications.

There are very few examples in the literature describing **fluorescent conjugates** of immunosuppressive drugs. Regarding CyA labelling, just two recent examples were described by Grote *et al.*[35] and by Gaali *et al.*[36] Grote et al. synthetized a cyclosporine-*fluorescein* conjugate via derivatization through the –OH group of the MeBmt chain. This method requires very harsh conditions (chloroformylation with phosgene in toluene) with the need of using specific laboratory material to avoid the corrosive effects of phosgene. Attempts to substitute phosgene with safer analogues led to unsatisfactory results, with very long reaction times (one week). Furthermore, HPLC purification was necessary and very low reactions yields were obtained.[35] A more convenient method was developed by Gaali et al. by attaching an amine functionality to the C6′-C7′ double bond of CyA through a cross-metathesis reaction. The amino-modified CyA was then attached to the 5/6-carboxyfluorescein *N*-hydroxysuccinimide fluorophore with good reaction yield. The potential disadvantages of this procedure are the need of using a catalyst and HPLC for the purification.[36]

3.2. Tacrolimus (FK506)

Tacrolimus, also known as FK506 by the original manufacturer (Fujisawa, Japan), (Figure 4) was first discovered in 1987 by T. Kino *et al.* while searching for cyclosporine

[35] J. Grote, J. Fishpaugh, S. Rege, *Org. Process Res. Dev.*, **2005**, *9*, 822–824
[36] S. Gaali, C. Kozany, B. Hoogeland, M. Klein, F. Hausch, *ACS Med. Chem. Lett.*, **2010**, *1*, 536–539.

derivatives.[37] Tacrolimus is a hydrophobic 23-membered macrolide lactone produced by *Streptomyces tsukubaensis*, and its name is an acronym derived from "**t**sukuba m**acroli**de im**mu**no**s**uppressant". It is a highly functionalized molecule with 14 stereocenters, three free hydroxyl groups, three double bonds, and several carbonyl groups. Despite the presence of three hydroxyl groups, tacrolimus is very hydrophobic. The amide bond in the pipecolic acid moiety (see orange highlighted site in Figure 8) causes a restriction in the rotation resulting in equilibrium between *cis*- and *trans*-rotamers in solution.[38,39]

3.2.1. Mechanism of action of tacrolimus

Tacrolimus, like CyA, is a calcineurin inhibitor and exerts its immunosuppressive effects in the same manner as cyclosporine. The only difference is that FK506 binds to the immunophilin FKBPs (FK506-binding proteins), while CyA binds to the immunophilin cyclophilin. Both inhibit the calcium-dependent protein phosphatase activity of calcineurin-calmodulin complex, reducing the production of T lymphocytes and IL-2 which are fundamental for an effective immune response.[40] Although their immunosuppressive mechanism is now well understood, the way how these ISs cause side effects is not completely clear yet. Some side effects of tacrolimus and cyclosporine A are vasoconstriction in the kidney and overexpression of transforming growth factors, which can provoke lung disease such as interstitial fibrosis.[41] Other side effects are chronic nephrotoxicity or cell apoptosis.[42] Figure 8 shows how tacrolimus interacts with the amino acids of one of its target FKBP proteins.[43]

[37] H. Tanaka, A. Kuroda, H. Marusawa, H. Hatanaka, T. Kino, T. Goto, M. Hashimoto*, J. Am. Chem.,* **1987***, 109,* 5031–5033.

[38] P. Karuso, H. Kessler, D. F. Mierke, *J. Am. Chem. Soc*., **1990**, *112*, 9434–9436.

[39] D. M. Skytte, J. W. Jaroszewski, K. T. Johansen, S. Honoré Hansen, L. Hansen, P. G. Nielsen, K. Frydenvang, *Eur. J. Pharm. Sci.*, **2013**, *48*, 514–522.

[40] W. M. Flanagan, B. Corthesy, R. J. Bram, G. R. Crabtree, *Nature*, **1991**, *352*, 803–807.

[41] E. A. Burdmann, T. F. Andoh, L. Yu, W.M. Bennett, *Semin. Nephrol*., **2003**, *23*, 465–476.

[42] X. Zhang, *J. Chromatogr. A*, **2014**, *1359*, 84–90.

[43] A. Prakash, S. Rajan, H. Sup Yoon, *Protein Sci.*, **2016,** *25*,905–910.

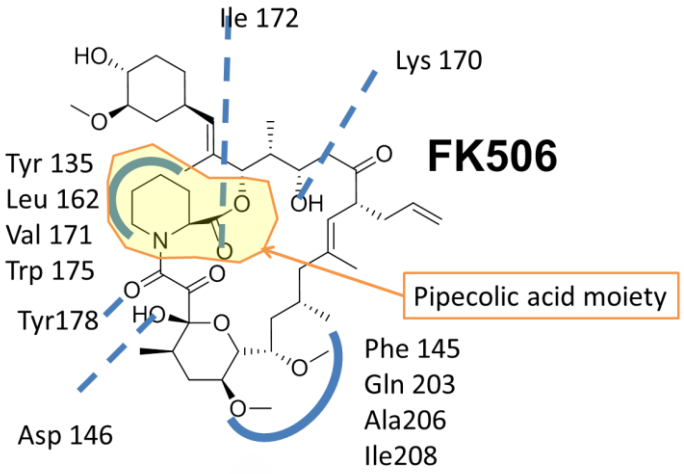


Figure 8. Crystal structure of the hFKBD25–FK506 complex. Two-dimensional representation of the interactions made by hFKBD25 with their corresponding inhibitors FK506 as describe by Prakash et all.[43] In orange, the pipecolic acid moiety.

3.2.2. Chemical reactivity

Tacrolimus contains two reactive hydroxyl groups, one at the O-C(24) and the other at the O-C(32) (see Figure 9 for atom numbering). The O-C(24) is less reactive because it is sterically hindered; consequently, selective reactions can be performed on O-C(32) without protecting the O-C(24).[44] The terminal olefin (C39-C40) of FK506 protrudes out, making this an attractive moiety for derivatization by olefin metathesis.[45,46] Thiol–ene click (TEC) reaction has been employed to generate FK506 derivatives through its unique exocyclic alkene group with excellent yield (over 95%).[47] The FK506 derivatization has also been made in high yield through the C22 carbonyl group to obtain a FK506-carboxymethoxyloxime,[48] which has then been used to synthetize a fluorescent *dansyl* derivative of tacrolimus following a straightforward method (Cañadas *et al.*[49]). To the best of our knowledge, this is the only example in the literature reporting fluorescent labelling of tacrolimus.

[44] R. Hersperger, K.–H. Buchheit, S. Cammisuli, A. Enz, O. Lohse, M. Ponelle, W. Schuler, A. Schweitzer, C. Walker, H. Zehender, G. Zenke, A. G. Zimmerlin, M. Zollinger, L. Mazzoni, J. R. Fozard, *J. Med. Chem.*, **2004**, *47*, 4950-4957.

[45] P. A. Clemons, B. G. Gladstone, A. Seth, E. D. Chao, M. A. Foley, S. L. Schreiber, *Chem. Biol*, **2002**, *9*, 49–61.

[46] P. S. Marinec, C. G. Evans, G. S. Gibbons, M. A. Tarnowski, D. L. Overbeek, J. E. Gestwicki, *Bioorg. Med. Chem.*, **2009**, *17*, 5763–5768.

[47] Z.–F. Guo, R. Zhang, F.–S. Liang, *RSC Adv.*, **2014**, *4*, 11400–11403.

[48] O. Cañadas, A. Sacénz, G. Orellana, C. Casals, *Anal. Biochem.*, **2005**, *340*, 57–65.

[49] O. Cañadas, R. Guerrero, R. García–Cañero, G. Orellana, M. Menéndez, C. Casals, *Biochemistry,* **2004**, *43*, 9926–9938.

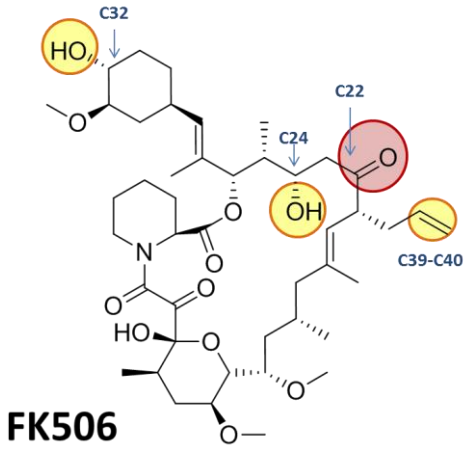


Figure 9. Tacrolimus reactive sites. In red, the C22 used to obtain a FK506-carboxymethoxyloxime; in yellow, the C32 with hydroxyl group and the terminal olefin (C39-C40).

3.3. Mycophenolic acid (MPA)

Mycophenolic acid (MPA in Figure 4), (4*E*)-6-(4-hydroxy-6-methoxy-7-methyl-3-oxo-5-phthalanyl)-4-methyl-4-hexenoic acid, is a natural product isolated from *Pennicillium stoloniferum* in 1896 by Gosio, and used as antibiotic.[50] Its use as immunosuppressant was first described in 1991,[51] and it was approved for its use in transplantation in 1995. Nowadays, it is the second most widely immunosuppressant prescribed.[52] MPA has the simplest chemical structure of the three ISs studied in this Thesis, and the main functional group in its native form is its carboxylic acid. MPA can also be prepared as its sodium salt or in the form of mycophenolate mofetil (MMF) ester (Figure 10).

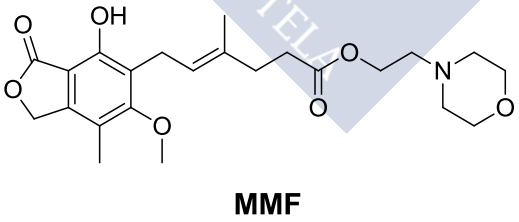


Figure 10. Chemical structure of mycophenolate mofetil (MMF).

[50] B. Gosio, *Rivista d'Igiene e Sanità pubblica*, **1896**, 7, 825–868.

[51] A. C. Allison, S. J. Almquist, C. D. Muller, E. M. Eugui, *Transplant. Proc.*, **1991**, *23*, 10–14.

[52] D. B. Kaufmann, R. Shapiro, M. R. Lucey, W. S. Cherikh, R. T. Bustami, D. B. Dyke, *Am. J. Transplant.*, **2004**, *4* , 38–53.

3.3.1. Mechanism of action

The target of the MPA immunosuppressant is the inosine monophosphate dehydrogenase (IMPDH) enzyme which is involved in the synthesis of the guanine nucleobase. The production of B and T lymphocytes depends essentially on this biochemical pathway; therefore, MPA inhibits their proliferation. MPA has also potential anti-cancer activity.[53] Typical adverse effects of long-term treatment with MMF include diarrhea, leukopenia, sepsis, vomiting, and a higher incidence of certain infections.[54] Figure 11 displays the biorecognition site of mycophenolic acid.[55,56]

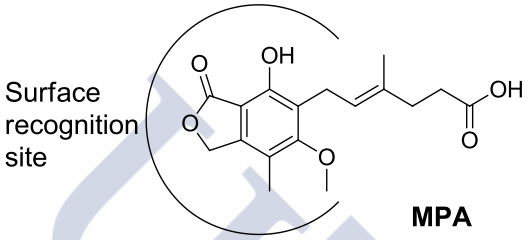


Figure 11. Recognition site of MPA as described by Batovska *et al.*[55] and Malachowska-Ugarte.[56]

3.4. Chemical reactivity

Chemical derivatization of MPA is relatively straightforward thanks to the presence of the carboxylic function –COOH, which is not involved in the binding to the recognition antibodies for immunoassays (Figure 11). Coupling reactions can be carried out through the –COOH group without the need of protecting the phenol group.[57]

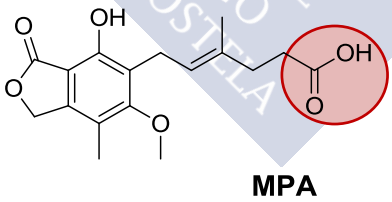


Figure 12. The reactive moiety of MPA used for derivatization.

[53] A. C. Allison, E. M. Eugui, I*mmunopharmacology*, **2000**, *47*, 85–118.

[54] E. Usleber, M. Dade, E. Schneider, R. Dietrich, J. Bauer, E. Martlbauer, *J. Agric. Food Chem.*, **2008**, *16*, 6857–6862.

[55] D. I. Batovska, D. H. Kim; S. Mitsuhashi, Y. S. Cho, H. J. Kwon, M. Ubukata, *Biosci., Biotechnol., Biochem.* **2008**, *72*, 2623–2631.

[56] M. Malachowska–Ugarte, G. Cholewinski, K. Dzierzbicka, P. Trzonkowski, *Eur. J. Med. Chem.*, **2012**, *54*, 197–201.

[57] D. Iwaszkiewicz–Grzes, G. Cholewinski, A. Kot–Wasik, P. Trzonkowski, K. Dzierzbicka., *Eur. J. Med. Chem.*, **2013**, *69*, 863–871.

In the case of fluorescently-labeled MPA, only one example was found in the literature, which unfortunately did not provide many synthetic details. In the work reported by Baiga *et al.* MPA is conjugated to a derivate of *apigenin*, a yellow fluorophore, after activation of the carboxylic group of MPA with HATU (*o*-(7-azabenzotriazol-1-yl)-*N,N,N',N'*-tetramethyluronium hexafluorophosphate).[58]

4. The NANODEM Project

Immunosuppressive drugs are ideal for therapeutic drug monitoring due to their beneficial effects but they have a very narrow therapeutic window (Section 2.2), with considerable problems in initial and ongoing dosing. In this context, the FP7 ICT Program-funded European project "NANODEM" (**NANO**photonic **DE**vice for **M**ultiple therapeutic drug monitoring)[59] was conceived with the aim of developing an **optical biosensor** able to fulfill the strict *requirements* of high sensitivity for achieving the very low limit of detection needed to determine *in situ* (i.e. in the point-of-care or the patient "bedside"), the concentration of selected free immunosuppressive drugs (CyA, FK506 and MPA), and the possibility of performing a continuous or at least, semi-continuous rapid monitoring of the free ISs levels in the blood of the transplanted patient over the following 2 to 7 days. The aim was to develop a miniaturized POCT (point-of-care testing) device based on laser-induced fluorescence detection methods (for the highest sensitivity) to carry out the simultaneous (semi)continuous monitoring of the ISs free fraction levels in the blood. To achieve the low LODs required, fluorescent magnetic nanobeads, endowed with the corresponding antibodies to the different IS drugs, where designed to be used as the recognition elements.

The NANODEM consortium has been a collaboration between partners of different EU countries that includes academic institutions, research centers, and private companies: Consiglio Nazionale delle Ricerche (IFAC and IREA Institutes of CNR, Florence and Naples, Italy); Klinikum rechts der Isar der Technischen Universität München (TUM, Munich, Germany); Probe Scientific Ltd. (PROBE, Coventry, United Kingdom); Datamed S.r.L. (DM, Rodano, Milan, Italy); Microfluidic ChipShop GmbH (MFCS, Jena, Germany); Universidad Complutense de Madrid (UCM, Madrid, Spain); University of Tübingen (EKUT, Tübingen, Germany); University of Stuttgart (USTUTT, Stuttgart, Germany), and INESC Microsystems and Nanotechnologies Institut (INESC-MN, Lisbon, Portugal).

The working principle of the NANODEM POCT device is summarized in Figure 13 and Figure 14. The biological sample is automatically withdrawn from the patient's blood by

[58] T. J. Baiga, H. Guo, Y. Xing, G. A. O'Doherty, A. Dillin, M. B. Austin, J. P. Noel, J. J. La Clair, *ACS Chem. Biol.*, **2008**, *3*, 294–304.

[59] https://cordis.europa.eu/project/rcn/104915_en.html; http://nanodem.ifac.cnr.it/ (accessed 15/05/2018)

means of *microdialysis* through a microfluidic circuit necessary to pump the perfusate solution to the microdialysis catheter (PROBE). Here, the dialysate is mixed with the reagents required to unattendedly perform the bioassay. The proposed approach of combining microdialysis with an extracorporeal sensor has the advantages of analyzing the physiological fluids outside the body, providing less invasive protocols. The need of mixing the dialysate with the chemical reagents and incubation for the bioassay implementation, implies that a continuous measurement of such analytes is not feasible. However, the miniaturization down to micro scale will lead to very short reaction time intervals, ideally on the order of a few minutes. Analytes and reagents will successively be pumped through a nanostructured chip (MFCS), where the determination of the different analytes will take place. The chip must have two important characteristics: the ability to perform multianalyte assays and the inclusion of magnetic traps for efficiently capturing the fluorescent magnetic nanolabels.

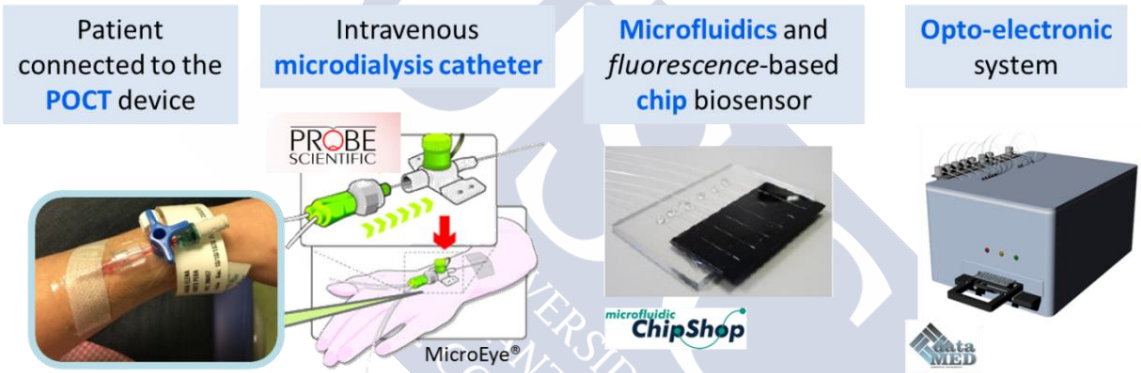


Figure 13. Scheme of the NANODEM POCT device underlining the companies contribution.

The heart of the monitoring system is a compact optoelectronic system (DATAMED) which has been developed for the control, acquisition and processing of the fluorescent signals. A user interface, optimized for the end-user needs, allows an easy instrument handling with respect to instrument operation, data storage, display of results and device calibration. The different parts will be integrated in a stand-alone device to be used at the patient bedside (typically, ICU rooms or boxes). The data can be used to calculate the individual pharmacokinetics of the drug of interest by applying the AUC concept (Figure 3). The resulting clinical benefit will be an optimized and personalized dosage of the respective therapeutic drugs.

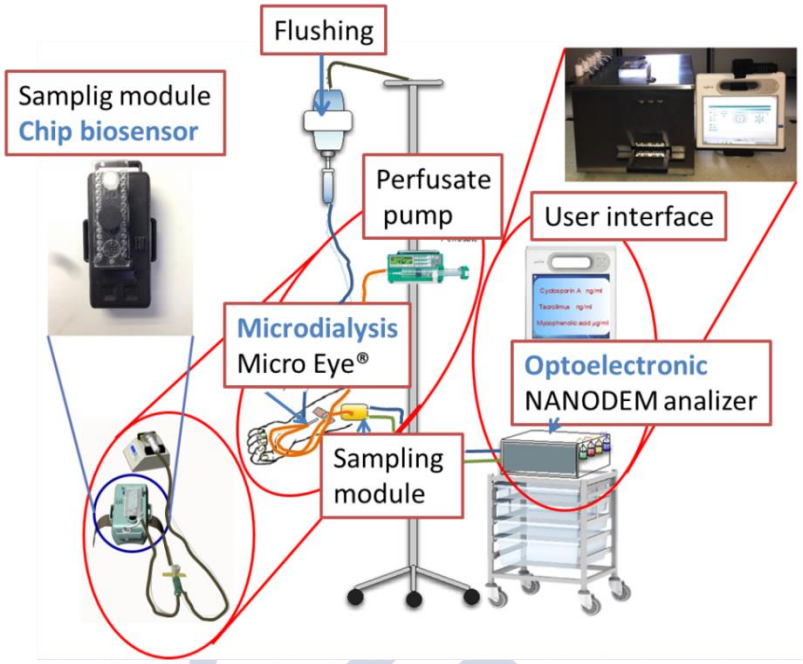


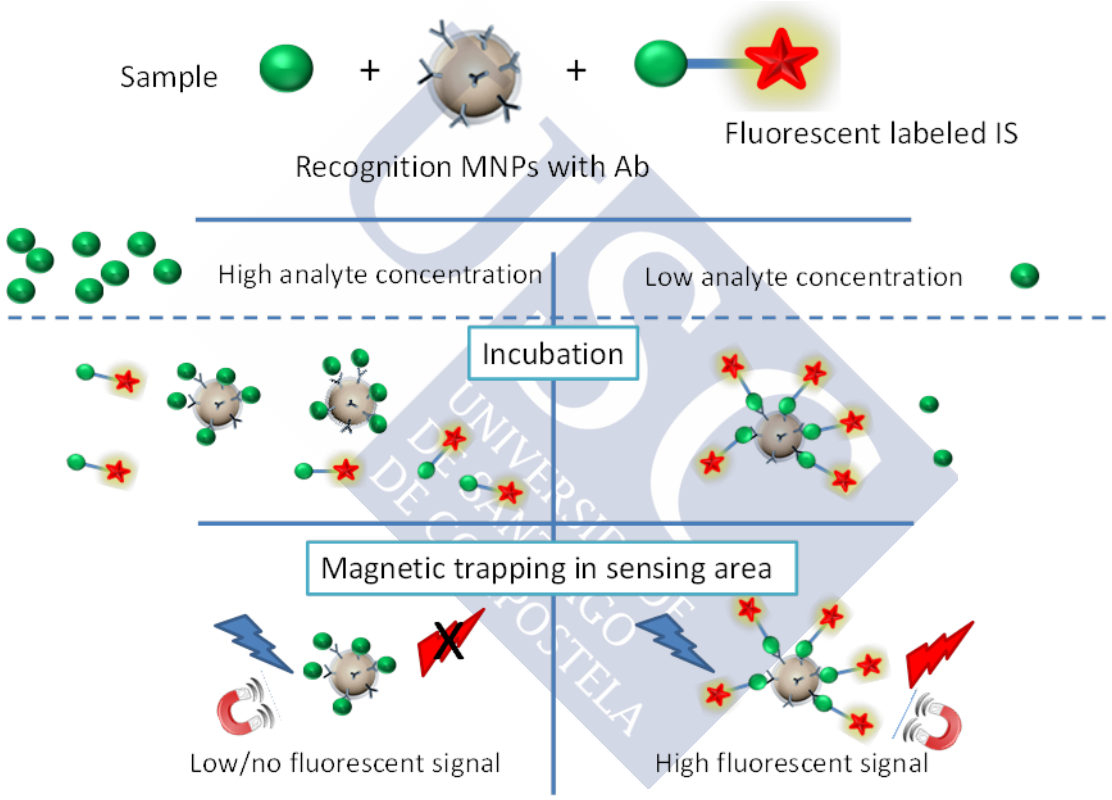
Figure 14. Schematic view of the final POCT device (courtesy of Datamed Ltd.).

4.1. NANODEM limits of detection and strategies to enhance the analytical signal

As stated above, the aim of the NANODEM POCT device is the measurement of plasma concentrations of the free fraction of selected immunosuppressants. Since unspecific binding of ISs drugs to blood proteins such as human serum albumin and immunoglobulins is very important (>90%), the free drug concentration will be very low. In the case of the NANODEM Project, the target limits of detection are even lower because of the limited efficiency of the microdialysis extraction process. Expected recoveries from the blood free fraction are on the order of 25% for FK506 and CyA and 50% for MPA. Taking into account the LOD reported in Table 3 the actual target NANODEM LODs are 0.250 ng/mL for CyA, 0.038 ng/mL for FK506, and 5.000 ng/mL for MPA. Consequently, the use of strategies to enhance the fluorescence signal is essential to reach the level of sensitivity required. In this context, **Nanotechnology** plays an important role. One of the aims of the Project is exploring *signal amplification* strategies (chemical and photochemical) for improving the biosensor performance. The Project relies on the development of optical biosensors using magnetic nanobeads for allowing sample pre-concentration and location on the detecting area, together with fluorescent labelling. It is well known that fluorescence-based detection methods are among the most sensitive ones. Sensitivity in fluorescence detection can be additionally boosted by using very brilliant labels emitting in the background fluorescence-free near-infrared region of the spectrum.

Two different formats of competitive immunoassays were considered: i) an *homogeneous* assay format (Scheme 4), and ii) an *heterogeneous* assay type (Scheme 5). In both cases, the assay is based on the competition between the analyte (the selected IS), and a *modified analyte*, either derivatized with a fluorescent label (homogeneous assay, Scheme 4), or attached onto the microchip surface for binding the recognition antibody (heterogeneous assay, Scheme 5). In any case, the higher the analyte concentration in the sample, the lower the fluorescent signal will be. Therefore, the intensity of the analytical signal is inversely proportional to the amount of IS.

4.2. Homogeneous assay

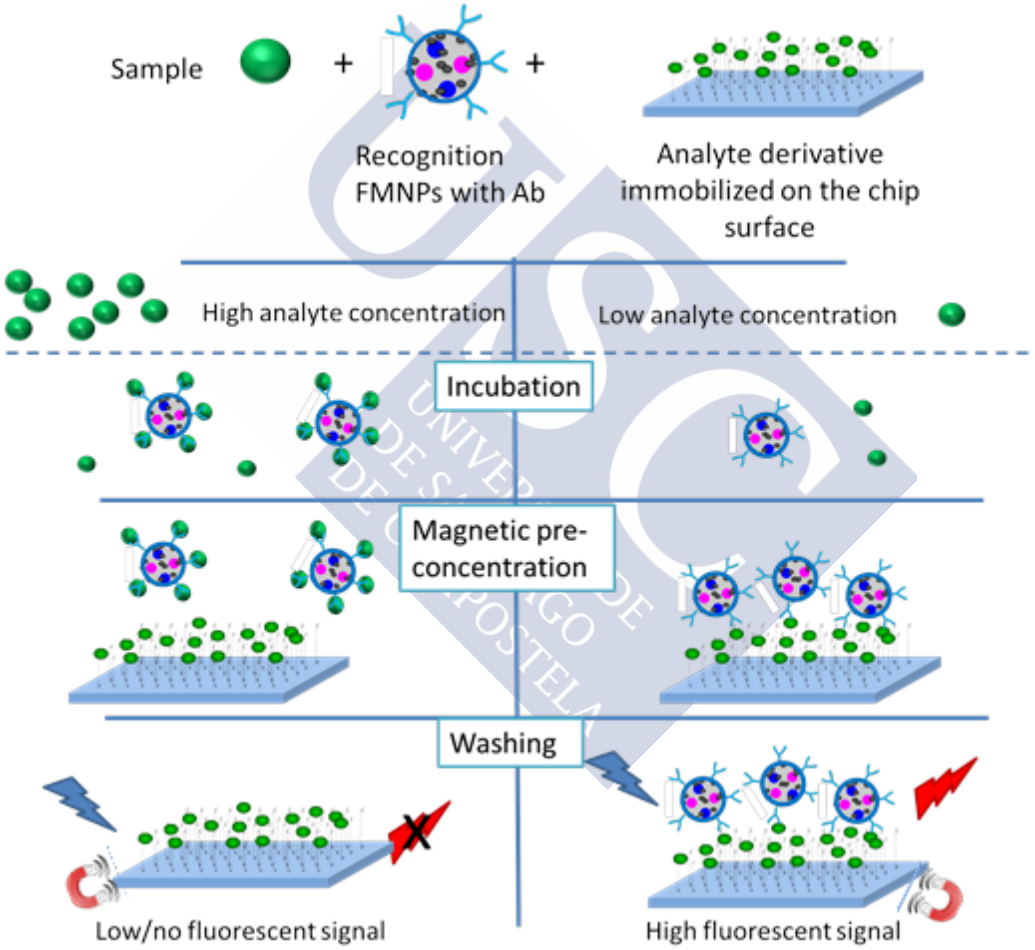


Scheme 4. Homogeneous fluorescent immunoassay format designed for the NANODEM analyzer.

In the case of the homogeneous assay, none of the reagents is immobilized onto a solid support, and everything is mixed in an aqueous phase. Magnetic nanoparticles (MNPs) are functionalized with the antibody in charge of selective IS recognition and binding in addition to an immunosuppressant fluorescent derivative employed as the tracer. If the sample contains the specific IS, a competition is established between the free IS and the fluorescently labelled IS for binding to the specific antibody. In the absence of drug, the labelled IS remains attached to the MNPs, while if the sample IS concentration increases,

less fluorescent labels remain attached to the MNPs surface because the free IS is occupying the antibodies binding sites. After a period of incubation, MNPs are trapped at the bottom of a microfluidic chip with a magnet, while a washing solution is circulated through the microfluidic setup. The labelled IS molecules that are not specifically bound to the MNPs will be washed out; therefore, the fluorescence signal will decrease as the concentration of IS in the sample increases (Scheme 4). Once the measurement is finished, the magnet is removed and the microfluidic chip can be regenerated by proper washing.

4.3. Heterogeneous assay



Scheme 5 Heterogeneous fluorescent immunoassay format designed for the NANODEM analyzer.

In the case of the heterogeneous assay, a derivative of the analyte is immobilized on the surface of the microfluidic chip, where (laser) excitation and detection of the fluorescence (see below) will take place. Magnetic nanoparticles are also functionalized with the recognition antibody. The difference with the previous assay format is that, in

this case, the recognition MNPs act also as the fluorescent label (they are doped with fluorophores). In the absence of analyte, the fluorescent magnetic nanoparticles (FMNPs) remain attached onto the chip surface because the antibody binds the chip surface-immobilized IS. If the sample contains IS, it will compete with the IS attached to chip for binding to the FMNPs, in a way that, the higher the concentration of the free IS, the fewer FMNPs will remain bound to the chip surface after washing, so that the weaker the fluorescent signal will be. The magnetic properties of the FMNPs facilitate the interaction with the sensing chip surface if a magnetic field is applied in the proper position. When the magnet is removed, the FMNPs which are not specifically bound to the chip surface can be readily washed out. The drawback of this assay format is the difficulties for regenerating the sensing surface because FMNPs which remain specifically bound will not be so easy to remove.

5. Methods of analysis of immunosuppressants

Standard practice today for routine TDM of ISs in central laboratories is the measurement of the drug plasma levels before administering the next dose (the "trough" concentration) using liquid chromatographic techniques such as, HPLC with MS or MS/MS detection. The limitation of these methods is that they normally determine the IS total fraction (free + protein bound), which may sometimes be misleading, and limits the possibility of studying individual pharmacokinetics and thus the optimal application of personalized medicine as discussed above.

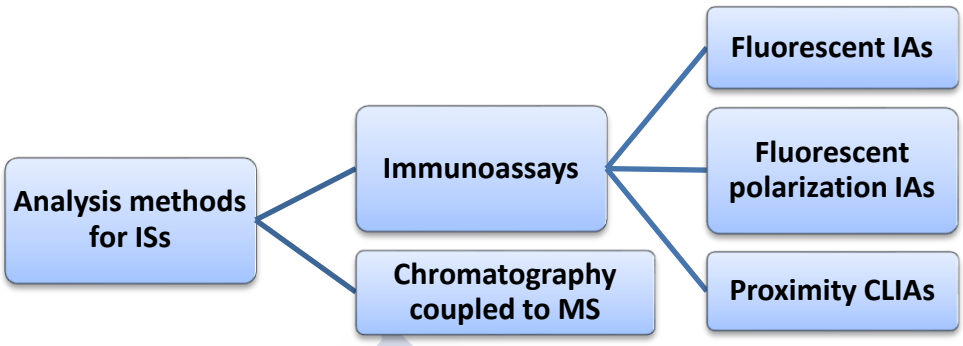
Nowadays there are techniques to separate the free fraction from venous blood such as ultrafiltration, equilibrium dialysis, ultracentrifugation or erytrocyte partitioning. Sometimes, oral fluid concentration in saliva can be associated with the free drug fraction, avoiding sample pretreatments.[60] Despite the free fraction is more scientifically relevant, in the clinical practice it is normally not determined because the process to measure it is time consuming and expensive, and because routine methods of analysis in the hospital laboratories generally do not possess sufficient sensitivity to reach the required limits of detection. Therefore, there is an urgent need for improving bioanalytical methods to quantify the ISs free fraction in order to investigate and monitoring the relationship between unbound ISs fraction and clinical outcomes in early post-transplanted patients. The low drug concentration levels of the free fraction require ambitious analytical methods and specific devices with high sensitivity.

In addition to the standard chromatographic methods, alternative analytical strategies are arising, and in fact, some of the novel methods are already implemented in clinical laboratories and have become commercially available.[61,25] In this respect, **immunoanalytical methods** play a significant role (Scheme 6). In this work, three

[60] M. Ghareeb, F. Akhlaghi, *J. Chromatogr. B*, **2016**, *1038*, 136–141.

[61] D. G. Wild (Ed.), *The Immunoassay Handbook. 3rd edn*. North Holland: Elsevier B V; **2006**.

different kinds of *immunoassays* (IAs) will be described: 1) fluorescence immunoassays (FIAs); 2) fluorescence polarization immunoassays (FPIAs), and 3) proximity chemiluminescence immunoassays (CLIAs).



Scheme 6. Classification of analytical methods employed for ISs detection.

5.1. Chromatographic methods

Liquid chromatography combined with mass spectrometry detection (LC-MS or LC-MS/MS) are routinely used by central clinical laboratories to bolster organ transplantation practices.[62,63] There are plenty of validated protocols to measure immunosuppressive drugs using LC-MS/MS methods, which are then employed as standard reference methods to validate new immunoassays. The advantages of LC-MS/MS techniques are excellent specificity, versatility, lack of interference from other metabolites and feasibility of simultaneous measurements of more than one IS, decreasing the analysis time and volume of the sample required and, consequently, amortizing the high cost of the technique.[64] A disadvantage however is the duration of runtime per sample because it is usually long.[65] The initial significant cost of the equipment is also a major obstacle. Another important drawback is the difficulty to recruit technicians with high experience in LC-MS/MS, and usually an expensive training of the personnel is required.

5.2. Immunoassays

There is a continuous demand for fast and simple analytical methods; in this respect immunoassays (IAs) provide a useful mean of analysis. IAs can be divided into homogeneous or heterogeneous, competitive or non-competitive, and can be classified

[62] D. A. Whitman, V. Abbott, K. Fregien, L. D. Bowers, *Ther. Drug. Monit.*, **1993**; *15*, 552–556.
[63] L. Zhou, D. Tan, J. Theng, *J. Chromatogr. B Biomed. Sci. Appl.*, **2001**, *754*, 201–207.
[64] P. J. Taylor, *The. Drug Monit.*, **2004**, *26*, 215–219.
[65] P. Salm, P.J. Taylor, S.V. Lynch, *Clin. Biochem.*, **2005**, *38*, 667–673.

according to the type of signal transduction.[66] The advantages of IAs are manifold: simplicity, short analysis times, low start-up costs and the hospitals personnel does not require specialized training because the instruments are easy to operate. All these advantages overshadow the extremely sensitivity of LC-MS/MS techniques and many experts argue that LC-MS/MS analysis may be progressively replaced by IAs as a routine technique.[67] The drawback of IAs for ISs analysis is that they may suffer from significant metabolite cross-reactivity (i.e. lack of the required specificity).

5.2.1. Fluorescence immunoassays (FIAs)

Fluorescence immunoassays are receiving an increasing interest in the field of clinical immunology, not only as a safer alternative to radioimmunoassays, but also because fluorescence measurements offer high sensitivity and are very easy and rapid to perform. FIAs are nowadays one of the most employed methodologies applied to optical biosensors in many research fields, especially in drug monitoring and biomarkers.[61,68]

Most FIA methods are based on the use of well-known organic fluorescent probes or fluorescent nanoparticles, which have opened new possibilities towards more sensitive immunoassays.[69] An optimal fluorescent probe should exhibit high fluorescent quantum yield, good photostability, large Stoke shifts and its conjugation to antigens should not affect the properties of the latter.

Some of the problems that FIAs face are the light scattering (i.e. in solutions containing high concentrations of proteins) and the fluorescence background produced by intrinsically fluorescent compounds in the sample (i.e. serum). These drawbacks can be overcome by the use of near infrared (NIR) fluorescent labels, as it will be described in Section 6 (Near-infrared fluorescent labels).

5.2.2. Fluorescence polarization immunoassay (FPIA)

Fluorescence polarization (FP) was applied in Biochemistry for the first time in the 50s after G. Weber studies.[70] However, since the 80s, fluorescence polarization had not been paid much attention by the scientific community due to the lack of affordable commercial instrumentation equipped with polarizers or the lack of appropriate commercial fluorescent probes. Since the 80s, due to the development of new commercial devices and innovative fluorophores, the number of studies in fluorescence polarization rose significantly. FP can be used advantageously to study the interaction

[66] M. Hasanzadeh, N. Shadjou, *Microchim. Acta*, **2017**, *184*, 389–414.

[67] K. A. Kelly, A.W. Butch, *Immunosuppressive drug monitoring: limitations of immunoassays and the application of liquid chromatography mass spectrometry*, Chapter 15, in: A. Dasgupta (Editor), *Therapeutic Drug Monitoring*, Academic Press, Boston, **2012**, 323–348.

[68] J. Zhang, S. Wang, K. Liu, Y. Wei, X. Wang, Y. Duan, *Anal. Chem*., **2015**, *87*, 2959–2965.

[69] X. Pei, B. Zhang, J. Tang, B. Liu, W. Lai, D. Tang, *Anal. Chim. Acta*, **2013**, *758*, 1–18.

[70] G. Weber, *Biochem. J.*, **1952**, *51*, 145–155.

between antigen and antibody and it has become popular mainly in Clinical Chemistry for its application in high-throughput studies.[71]

As discussed in Section 2.2 (Complication of immunosuppressive medication), measurement of the free ISs concentration in plasma, serum or whole blood, rather than the total amount, provides a better correlation with the clinical efficacy of the drug. The challenge of quantifying the free ISs in blood for semi-continuous monitoring with point-of-care-testing devices can be overcome with FPIA. Indeed FPIA is a type of the homogeneous fluorescence-based immunoassay in which no washing is required to eliminate the fluorescent-labeled analyte that is not bound to the protein. Therefore advantages of anisotropy-based fluoroimmunoassays include the feasibility of measuring the bound/free ratio without the need of previous separation of the free fraction from the bound ligand, and their capability for automation, as demonstrated by the incorporation of the FPIA technology in some commercial analyzers.[72]

Khoschsorur has compared FPIAs with HPLC methods for the determination of everolimus in 52 just transplanted patients. He concluded that the results obtained with FPIAs can be correlated with those of HPLC opening a promising path for FPIAs.[73] The great advantage of these immunoassays is that there is no need of separate the free fraction,[72,77] reducing in this way the time of analysis. In fact, FPIA are so simple to perform that the rate-determining step is usually the pipetting of reagents. A typical FPIA can be summarized as follows: a fluorescent analogue of the ligand (i.e. a labelled analyte) is added to the cuvette and FP is measured. Then, the sample (the corresponding biological fluid) is also added and a decrease of FP is observed due to the displacement of the fluorescent analogue of the ligand from the target molecule.[74] When the labelled analyte is no longer bound to the corresponding protein, it can freely rotate in the solution, and the degree of fluorescence polarization decreases. The synthesis of a fluorescent analogue of the target molecule may represent the most challenging step for the design of a FPIA (see Chapter 1 of "Results and discussion"). The disadvantages of FPIA are the same of every FIA: interferences due to light scattering and fluorescent background. The last one can be overcome by utilizing brilliant labels absorbing and emitting in the NIR, such as the Nile Blue dye,[75] or by using dyes with long emission decay times (i.e. luminescent ruthenium complexes,[76]) that allow introduction of a time gate between the pulse of excitation and the detection of emission.

[71] J. C. Owicki, *J. Bimolecular Screening*, **2000**, *5*, 297–306.

[72] D. M. Jameson, W. H. Sawyer, *Methods Enzymol*., **1995**, *246*, 283–300.

[73] G. A. Khoschsorur, F. Fruehwirth, S. Zelzer, M. Stettin M. G. Halwachs Baumann, *Clin. Chim. Acta*, **2007**, *380*, 217–221.

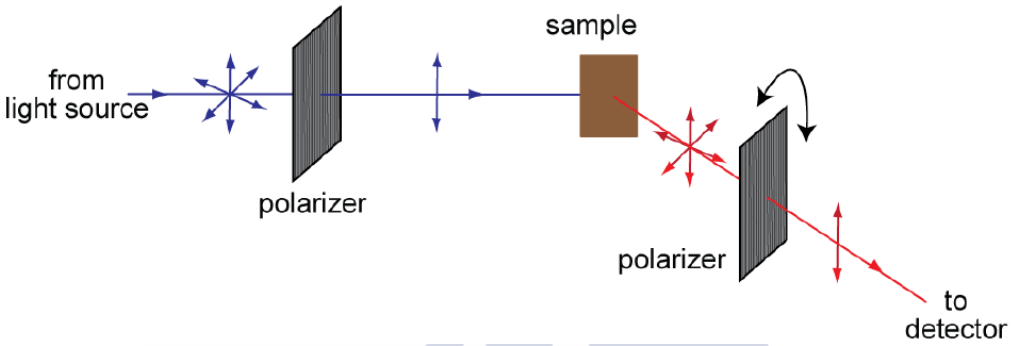
[74] D. S. Smith, S. A. Eremin, *Anal. Bioanal. Chem*., **2008**, *391*, 1499–1507.

[75] M. L. Sanchez–Martınez, M.P. Aguilar–Caballos, S.A. Eremin, A.Gomez–Hens, *Talanta*, **2007**, *72*, 243–248.

[76] M. L. Sanchez–Martınez, M.P. Aguilar–Caballos, A. Gomez–Hens, *Anal. Chem*. **2007**, *79*, 7424–7430.

5.2.3. Basic principles of fluorescence polarization-based methods

In a FP experiment, the sample is excited with only one direction of the electronic vector of the light, which is isolated by passing the light from the source through a polarizer (Scheme 7). When the light reaches the sample, only fluorophores with a certain orientation of their transition moments will absorb the light. This is known as a *photoselection* process: if a fluorophore is excited with polarized light, only the population of those fluorophores which have their transition moments lined up with the plane-polarized light are excited. This selective excitation results in (partially) polarized fluorescence emission.



Scheme 7. Representation of a conventional fluorescence polarization experiment.

Then, the direction of the emitted light is determined by a second polarizer, which can be oriented orthogonally or in parallel to the electric field of excitation (the *reference* plane). *Polarization* is then defined as a function of the observed parallel ($I_{//}$) and perpendicular ($I_{\perp}$) fluorescence intensities:

$$P = \frac{I_{\parallel} - I_{\perp}}{I_{\parallel} + I_{\perp}} \qquad (1)$$

This concept can be also expressed as *anisotropy*, as introduced by Jablonski (Eq. 2.):

$$r = \frac{I_{\parallel} - I_{\perp}}{I_{\parallel} + 2I_{\perp}} \qquad (2)$$

From Eq.1 and Eq.2 it can be concluded that when the emission is totally polarized in the parallel direction, polarization P equals 1. However, if the emitted light is completely polarized in the perpendicular direction then P equals -1. However, these P limiting values of +1 and -1 can be only reached in a crystal because it is a completely oriented system. In solution it is impossible to observe these values because of the photoselection process mentioned above and the tumbling of the molecules. The Perrin equation (Eq. 3)

describes this intrinsic limitation; for explicit derivation, the reader should consult the work of Jameson.[72,77] The treatment here will not enter into all the rigorous details.

The limiting or intrinsic polarization, denoted as P_0, are the polarization values in the absence of rotation.

$$\frac{1}{P_0} - \frac{1}{3} = \frac{1}{5}\left(\frac{2}{3\cos^2\varphi - 1}\right) \quad (3)$$

Moreover, the fluorescence polarization depends on the fluorescence lifetime (Eq. 4). The Perrin equation can be expressed (in terms of anisotropy) in this alternative way:

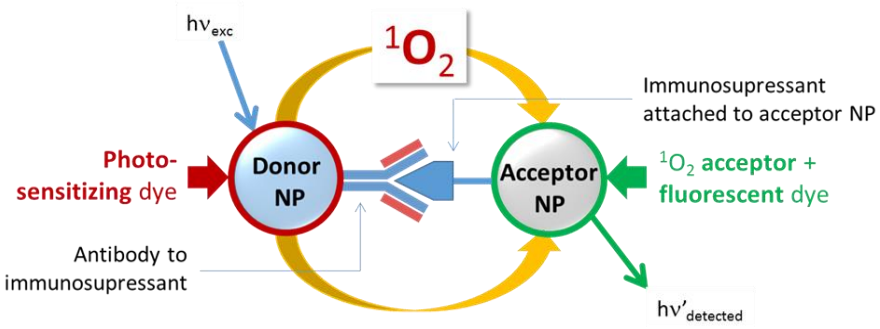
$$\frac{r}{r_0} = \left(1 + \frac{\tau}{\tau_c}\right) \quad (4)$$

where τ_c is the rotational relaxation time, a parameter describing the time-dependence of the tumbling of a molecular entity in a medium of viscosity η as originally defined by Debye. The shorter the lifetime, the higher the anisotropy (or polarization) will be. Furthermore, since FP depends on how fast the fluorophore molecules can rotate before they emit a photon, the molecular mass of the fluorophore and the solvent viscosity will also have an effect on the fluorescence polarization.

5.2.4. Binding assay based on detection of chemiluminescence initiated by $^1O_2$ photoproduction.

Alternatively to FPIAs, the so called *proximity chemiluminescence immunoassay (CLIA*) can also be used for monitoring a binding process in homogeneous phase. In this assay, one type of nanoparticles are encoded with a photosensitizer that produces large concentrations of singlet molecular oxygen (abbreviated $^1O_2$) upon irradiation with visible light (typically, red). These *donor* (D) nanoparticles (Scheme 8) are functionalized with the required recognition antibody. Additionally, a second set of NPs are derivatized with the corresponding hapten (the analyte; in our case, the IS drug) and doped with a singlet oxygen scavenger that provides the energy for the chemoluminescent reaction, and with a fluorescent dye. These are the *acceptor* NPs (A, Scheme 8).

[77] D. M. Jameson, J. A. Ross, *Chem. Rev.*, **2010**, *110*, 2685–2708.



Scheme 8. Working principle of the proximity chemiluminescence immunoassay CLIA.

When the suspension is irradiated with the appropriate light, the photosensitizer (PS) embedded in the D particles generates $^1O_2$ that can diffuse to the acceptor NPs provided that they are close enough (otherwise, $^1O_2$ deactivates to $^3O_2$ within 3–4 μs in aqueous solution). The photosensitizer is a dye molecule that undergoes an efficient intersystem crossing so that it can very rapidly (in the ns range) decay from the lowest-lying singlet excited state to its triplet state PS(T_1). This spin configuration matches that of the molecular oxygen in its ground state (O_2 has two unpaired electrons in degenerated orbitals), and energy transfer from the excited PS(T_1) to $^3O_2$ is possible via a Dexter-type mechanism (Figure 15).[78,79] This energy transfer promotes $^3O_2$ to its excited state, generating $^1O_2$, a very reactive species. Taking into account the $^1O_2$ lifetime in water (τ = 3–4 μs) and its diffusion coefficient D the maximum distance d ($\sqrt{2\tau D}$) that the active oxygen molecule can cover before decaying is approximately 125 nm in water at ambient temperature.[80] In the absence of the analyte, both types of NPs remain bound by the Ab-Ag interaction, and $^1O_2$ diffusion to the acceptor NPs is feasible. The arrival of $^1O_2$ at the A NPs activates a chemiluminescent reaction because the $^1O_2$ scavenger, –normally a dioxene–, can be oxidized by singlet oxygen generating a dioxane endoperoxide.[81] The opening of this endoperoxide generates an electronically excited diester (Figure 16). This excess of energy can be transferred to the fluorophore F, because both molecules are close enough due to their co-encapsulation into de NPs. The electronically excited fluorophore decays then quickly to its ground state by the emission of a photon, which is used for the detection in the assay.[82] At low analyte concentrations, the chemiluminescence signal is strong because the D-A NPs remain

[78] C. Schweitzer, R. Schmidt, *Chem. Rev.*, **2003**, *103,* 1685–1757.
[79] N. Turro, V. Ramamurthy, J. C. Scaiano, *Principles of Molecular Photochemistry: An introduction*, **2009** University Science Book.
[80] M. Klaper, W. Fudickar, T. Linker, *J. Am. Chem. Soc.*, **2016**, *138*, 7024–7029.
[81] S. Singh, E. F. Ullman, *Chem. Commun.*, **2003**, *14*, 1756–1757.
[82] O. Jilani, T. M. Donahue, M. O. Mitchell, *J. Chem. Educ.*, **2011**, *88*, 786–787.

bound. If the analyte concentration in the sample increases, it will disrupt the D-A NPs interaction, decreasing the chemiluminescence signal.

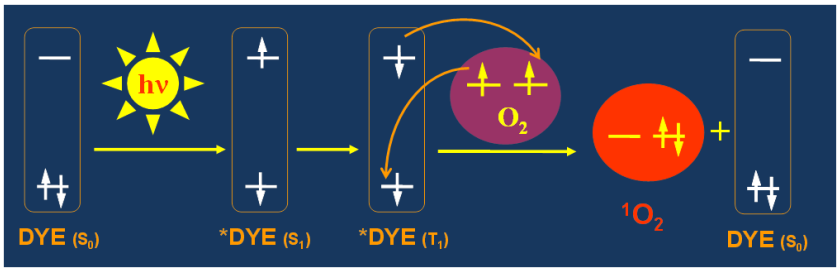


Figure 15. Mechanism of singlet oxygen production in the donor NPs via a photosensitization process.

This proximity CLIA is commercialized by PerkinElmer with the name AlphaScreen™. The acronym ALPHA stands for *Amplified Luminescent Proximity Homogeneous Assay* but it was originally named LOCI® (*Luminescent Oxygen Channeling Immunoassay*) by Ullman.[83] In the AlphaScreen™ assay the NPs are made of latex and have a diameter of approximately 250 nm. They are functionalized on the surface with reactive aldehyde groups needed for conjugation of biomolecules. As photosensitizer, the AlphaScreen™ uses a phthalocyanine which is excited at 680 nm. The acceptor NPs are doped with a thioxene derivative as $^1O_2$ acceptor, and rubrene is used as the fluorophore. The energy transferred from the singlet oxygen finally yields light at 520–620 nm.

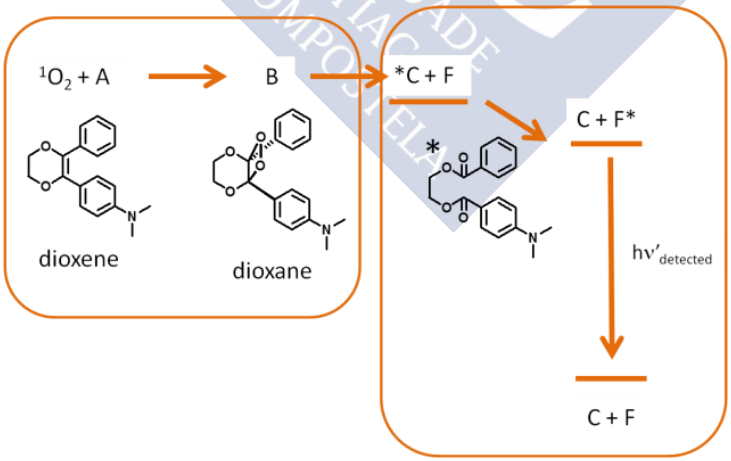


Figure 16. Mechanism of light production in the acceptor nanoparticles, in the presence of $^1O_2$. A dioxene ***A*** is oxidized with $^1O_2$ yielding a dioxane endoperoxide ***B*** which, upon ring opening, liberates the diester ***C*** with an excess of energy that is transferred to a fluorophore molecule (***F***). The emission of a photon is then observed after electronic relaxation of the excited ***F***.

[83] E. F. Ullman, H. Kirakossian, S. Singh, Z. P. Wu, B. R. Irvin, J. S. Pease, A. C. Switchenko, J. D. Irvine, A. Dafforn, C. N. Skold, D. B. Wagner. *Proc. Natl. Acad. Sci. USA,* **1994**, *91*, 5426–5430.

The advantage of this type of proximity assay is its very high sensitivity due to the almost negligible background signal during the measurements because: 1) it is based on the detection of chemiluminescence: after the pulse of light needed for $^1O_2$ generation, the light source can be switched off for a few microseconds (time needed for $^1O_2$ diffusion to the A-NPs) and then the emission of the photon can be detected against a "dark background"; 2) additionally, the detection wavelength is lower than the excitation wavelength and are well separated. In consequence, the signal-to-noise ratio is very high. Moreover, the AlphaScreen assay has an extreme versatility for different analytes.[84]

The effective production of singlet oxygen is a key issue in this assay. The next section is providing a more detailed description about the basic photochemical processes involved in its generation.

5.2.5. Photochemical production of singlet oxygen

Singlet oxygen is a high energy form of molecular oxygen. It was discovered in 1924 but it became the focus of research studies in 1963 after Khan and Kasha interpretation of the chemiluminescence produced by the hypochlorite-peroxide reaction.[85]

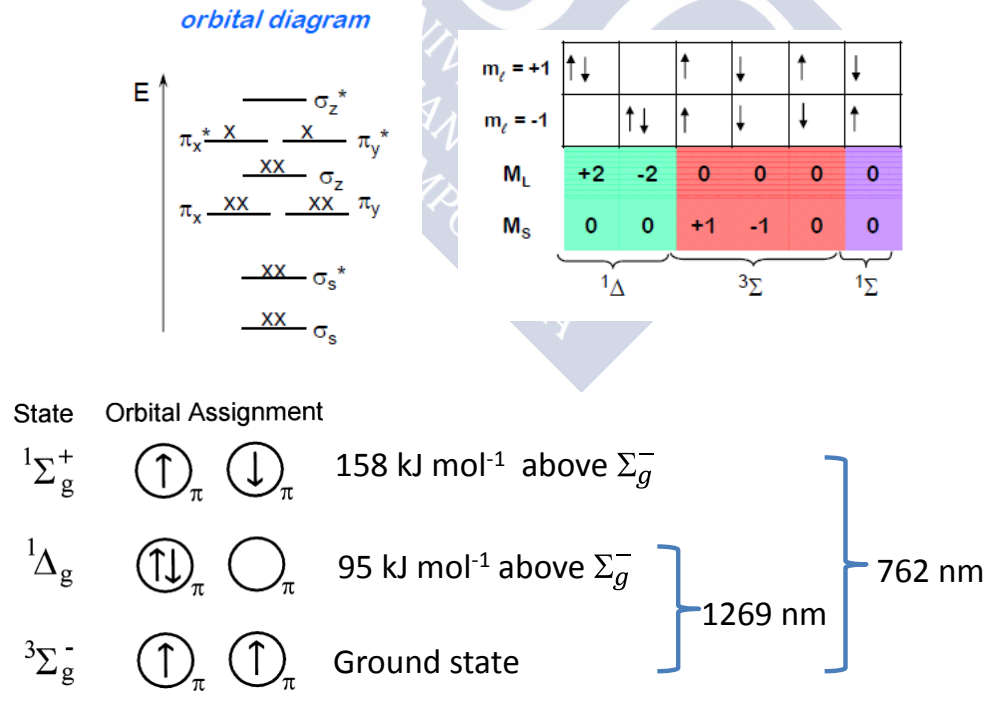


Figure 17. Representation of the molecular orbitals and configuration of states of dioxygen (O_2).

[84] C. Hou, L. Zhao, F. Geng, D. Wang, L.H. Gu, *Anal. Bioanal. Chem.*, **2016**, *408*, 8795–8804.
[85] A. U. Khan, M. Kasha, *J. Chem. Phys.*, **1963**, *39*, 2105.

Molecular oxygen is a triplet in its ground state because, as shown in Figure 17 for the $^3\Sigma$ state (in pink), there are three possibilities in which the two unpaired electrons of the π-antibonding orbitals can be oriented. The first excited state of molecular oxygen ($^1\Delta_g$) is a long-lived singlet in which the two electrons are paired in one of the π-antibonding orbitals. The second excited state ($^1\Sigma_g^+$) has the same configuration than that of the ground state ($^3\Sigma$) except for the last two electrons which have antiparallel spins.

$^1\Delta_g$ O_2 is a relatively long-lived species because the transition from the $^1\Delta_g$ state to the $^3\Sigma_g^-$ state is spin-forbidden ($\tau_r = 10^{-6} – 10^{-3}$ s in solution). The transition from $^1\Sigma_g^+$ to $^3\Sigma_g^-$ is a spin-allowed transition, thus $^1\Sigma_g^+$ is a short-lived species ($\tau_r = 10^{-11} – 10^{-9}$ s in solution).[86] Despite being spin- and symmetry-forbidden, the transition from the $^1\Delta_g$ state to the $^3\Sigma_g^-$ is observed at 1268.7 nm in the absorption and emission spectra due to the metastability of the $^1\Delta_g$ state.[87]

A straightforward method for generating $^1O_2$ from $^3O_2$ is by using light and dyes called *photosensitizers* (PSs). A photosensitizer is a dye molecule that can absorb radiation in the UV-Vis region and rapidly decay to the triplet state by an effective intersystem crossing process yielding PS(T_1) (Figure 18). The PS(T_1) can transfer its excess of energy to the ground state oxygen by collision, promoting it to the singlet excited state ($^1\Delta_g$ or $^1\Sigma_g^+$) The conditions that a dye molecule must meet for being a good photosensitizer are: 1) posses a high absorption coefficient at the wavelength of excitation; 2) the energy of its triplet state must be ≥ 95 kJ mol^{-1} in order to be able to transfer the energy to the $^3O_2$; 3) display a high quantum yield of triplet state formation Φ_T, 4) exhibit a long triplet state lifetime and, 5) show a good photostability.

[86] P. B. Merkel, D. R. Kearns, *J. Am. Chem. Soc.*, **1972**, *94*, 1029.

[87] M. C. De Rosa, R. J. Crutchley, *Coord. Chem. Rev.*, **2002**, *233–234*, 351–371

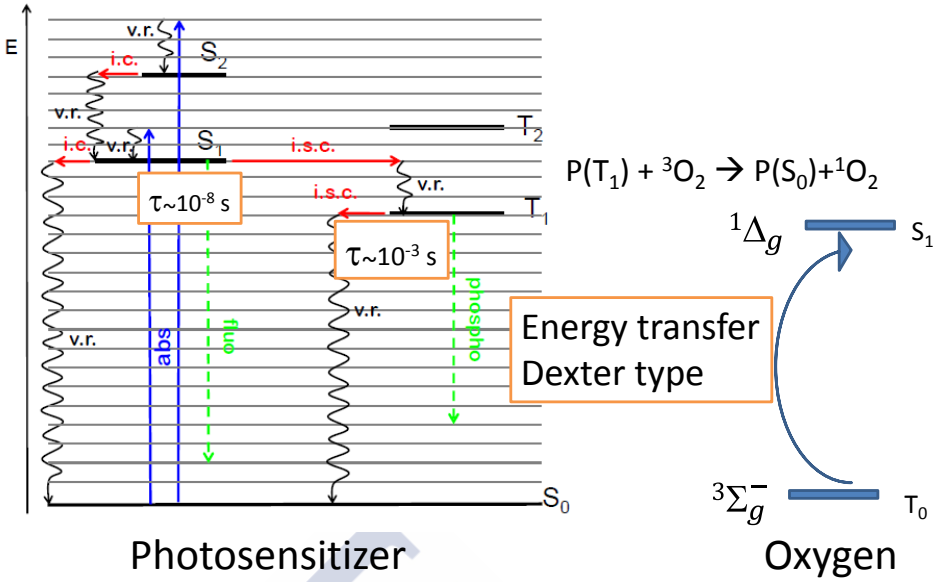


Figure 18. Jablonski diagram with the different processes that may occur after photoexcitation of a chromophore, and singlet oxygen generation via energy transfer. The photosensitizer is excited upon a one-photon transition (hν) to a S_n state. After a rapid internal conversion + vibrational relaxation to the lowest singlet excited state S_1 (Kasha's rule), the triplet state T_1 can be populated by a fast intersystem crossing (ISC) process. The generated PS (T_1) species, is then able to induce the formation of singlet oxygen via an energy transfer process by collision with the ground state oxygen $^3\Sigma_g^-$.

The ability of a photosensitizer to generate $^1O_2$ can be measured by its *quantum yield of singlet oxygen production* (Φ_Δ).[88] Once the triplet state of the PS is formed, there are several radiative (phosphorescence) and non-radiative (vibration and relaxation motions) deactivation pathways that compete with the generation of $^1O_2$. Also there is a competition with bimolecular reactions or electron transfer to oxygen with the production of other reactive oxygen species different to $^1O_2$, such as the superoxide radical anion:

$$PS(T_1) \rightarrow PS(S_0) + h\nu \quad (5)$$

$$PS(T_1) \rightarrow PS(S_0) + \Delta \quad (6)$$

$$PS(T_1) + {}^3O_2 \rightarrow PS(S_0) + {}^1O_2 \quad (7)$$

$$PS(T_1) + \rightarrow PS^+ + {}^3O_2^{\bullet -} \quad (8)$$

The quantum yield of $^1O_2$ production (Φ_Δ) is defined as:

[88] D. E. Wetzler, D. Garcıa-Fresnadillo G. Orellana, *Phys. Chem. Chem. Phys.*, **2006**, *8*, 2249–2256.

$$\Phi_{\Delta} = \Phi_T \varphi_{en} = \Phi_T \left(\frac{k_{en}[O_2]}{k_r + k_{nr} + k_q[O_2]} \right) \quad (9)$$

Where Φ_T is the quantum yield of triplet formation; φ_{en}, is the efficiency of energy transfer; k_r is the radiative deactivation constant; k_{nr} is the sum of all the non-radiative unimolecular deactivation constants and k_q is the sum of all the bimolecular quenching rate constants.

The quantum yield of singlet oxygen generation Φ_{Δ} can be measured by direct methods such as the detection of the luminescence emitted by $^1O_2$ at 1270 nm (by time-resolved or steady-state infrared luminescence, see Chapter 3 of "Results and discussion"), or indirect methods such as photooxidation reactions (loss of absorbance or fluorescence of a scavenger molecule when reacting with $^1O_2$).

There are different types of efficient PSs: organic dyes such as methylene blue, rose Bengal, or different porphyrins and phthalocyanines to mention a few of the most popular; or transition metal complexes. In Chapter 3 of "Results and discussion" section, two different types of photosensitizers will be studied: polypyridyl ruthenium complexes[89] and halogenated BODIPYs.[90]

6. Near-infrared fluorescent labels

Near-infrared (NIR) fluorescent labels absorb and emit light in the near-infrared region of the spectrum. The advantage of these dyes is that they allow to perform measurements in the so called "biological window", a wavelength range covering the 650 – 900 nm interval. This range is considered to be a window "free" of optical interferences in biological samples because biomolecules such as hemoglobin, certain aminoacids such as phenylalanine, tyrosine and triptophan, or cofactors such as FAD or NADH that absorb or emit light in the UV-Vis region, are optically silent in that interval.[91] Also the intensity of scattered light is lower in the red-NIR than in the UV-Vis due to its inverse dependence with the 4th power of the wavelength used for excitation. Especially interesting is the use of NIR dyes for applications that require light that can penetrate into physiological tissues, such as in photodynamic therapy for treatment of certain skin diseases or tumors. In the case of NIR dyes, and due to the above mentioned reasons, the light is able to be transmitted for longer distances than when using UV-Vis radiation. Additionally, NIR light produces less damage to biological samples.[92]

[89] F. Manjón, L. Villén, D. García-Fresnadillo, G. Orellana, *Environ. Sci. Technol.* **2008,** *42,* 301–307.
[90] L. Huang, W. Yang, J. Zhao, *J. Org. Chem.* **2014**, *79*, 10240−10255.
[91] L. Yuan, W Lin, K. Zheng, L. He, W. Huang, *Chem. Soc. Rev.*, **2013**, *42*, 622–661.
[92] J. Xie, C. Li, Y. Li, J. Fei, F. Xu, J. Ou–Yang, J. Liu, *Anal. Chem.*, **2016**, *88*, 9746–9752.

Some of the most popular families of NIR dyes include cyanine dyes, boron-dipyrromethene (BODIPY) dyes, oxazines, squaraines and rhodamine analogues.

6.1. Cyanine dyes

Cyanine dyes were firstly synthesized by Williams in 1856.[93] The classical cyanines are organic dyes, the main structure of which consists of two nitrogen atoms connected through a conjugated polymethine chain with an odd number of carbons and a positive charge delocalized along the whole structure (Figure 19). Generally, the dyes have an all-trans configuration in their most stable form. They are usually named as "Cy" followed by a figure that indicates the number of bridge carbon atoms, as shown for example for the popular pentamethine Cy5 dye in Figure 19.



Figure 19. a) Mesomeric forms of a cyanine chromophore and, b) example of the pentamethine cyanine Cy5 fluorophore ($\lambda_{abs}/\lambda_{em}$ = 647/665 nm).

Cyanine dyes have been applied in different fields, including photography,[94] industrial applications, or to construct photochemical reaction systems such as artificial light harvesting systems,[95] fluorescent probes for labelling biological systems,[96] or as fluorescent indicators for monitoring the presence of metal ions, anions, protons, or reactive oxygen species.[97]

Cyanine dyes can be classified according to their structure. The most common ones are streptocyanines, hemicyanines and closed chain cyanines (Figure 20). In the case of hemicyanines and closed chain cyanines, one or the two nitrogen atoms, respectively, are included in a heteroaromatic ring such as pyrrole, imidazole, pyridine, indole or thiazole.

[93] C. H. G. Williams, *Trans. R. Soc. Edinburg*, **1856**, *21*, 377.
[94] X. Tang, F. Gan, *Proc. SPIE–Int. Soc. Opt. Eng.* **1997**, *3136*, 210.
[95] N. Sato , T. Fujimura, T. Shimada, T. Tani, S. Takag, *Tetrahedron Lett.*, **2015**, *56*, 2902–2905.
[96] M. Z. Hossain, L. A. Ernst, J. Nagy, *Neurosci. Lett.* **1996**,*184*, 183.
[97] A. Mishra, R. K. Behera, P. K. Behera, B. K. Mishra, G. B. Behera, *Chem. Rev.*, **2000**, *100*, 1973–2011.

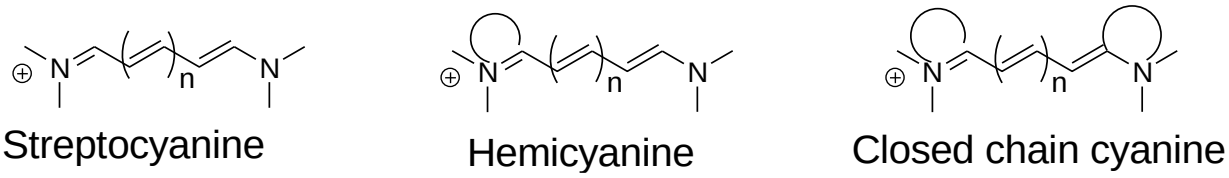


Figure 20. Different types of cyanine dyes classified according to their basic structure.

The principal characteristic of cyanine dyes is the ease to undergo a bathochromic shift by adding vinylene moieties to the chromophore backbone (approximately 100 nm for each vinylene moiety added). For example, while pentamethine cyanines such as Cy5 absorb at ca. 650 nm, the heptamethine dyes, Cy7, have an absorption maximum around 750 nm. Other typical positive features of these type of chromophores are their narrow absorption and emission bands and their high absorption coefficients. Their disadvantages include a moderate-to-low fluorescence quantum yield (Φ_f < 0.25)[98] and their poor photostability. Additionally, they might display undesired aggregation problems in aqueous solution, that gets worse when increasing the length of the polymethine chain. Another drawback of the cyanine dyes is that they are prepared with multistep synthesis, and they are normally obtained with low reaction yields. Moreover, further chemical modification of the dyes is complicated.[99]

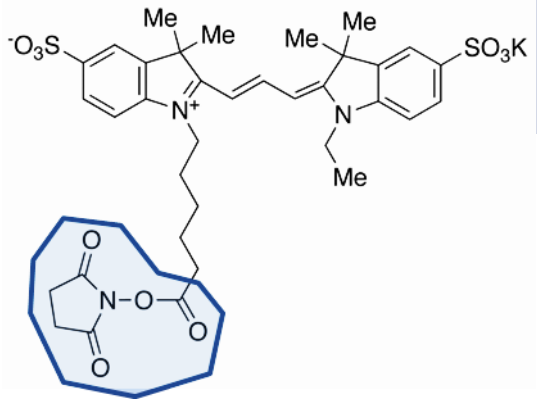


Figure 21. Example of a water soluble sulfoindocyanine; the succinimidyl ester group for labeling is highlighted in blue .

Among the different cyanine dyes, the derivatized sulfoindocyanines (Figure 21) are particularly interesting when they contain a succinimidyl ester group that can be used

[98] K. Rurack, M. Spieles, *Anal. Chem.*, **2011**, *83*, 1232–1242.
[99] Y. Lin, R. Weissleder, C. Tung, *Bioconjugate Chem.* **2002,** *13,* 605–610.

for further (bio)conjugation. Additionally, the negatively charged sulfonate group on the aromatic nucleus of the indocyanine improves its water solubility, minimizing aggregation issues.[100]

6.2. BODIPY dyes

The 4,4-difluoro-4-bora-3a,4a-diaza-*s*-indacene (Figure 23), abbreviated as BODIPY, was firstly described by Treibs and Kreuzer in 1968.[101,102] BODIPY is usually described as a boradiaza-*s*-indacene by analogy with the all-carbon tricyclic *s*-indacene, and the substituents are numbered following the rules set for *s*-indacene (Figure 22). The IUPAC numbering system for BODIPY dyes is not the same to that used for dipyrromethenes and this can lead to confusion. However, the terms "α, β, and *meso*- position" are used in the same way for both systems. BODIPYs are considered as a "rigidified" cyanine by some authors. This rigidization is a consequence of the complexation of the dipyrromethene moiety with a boron difluoride bridge.[103]

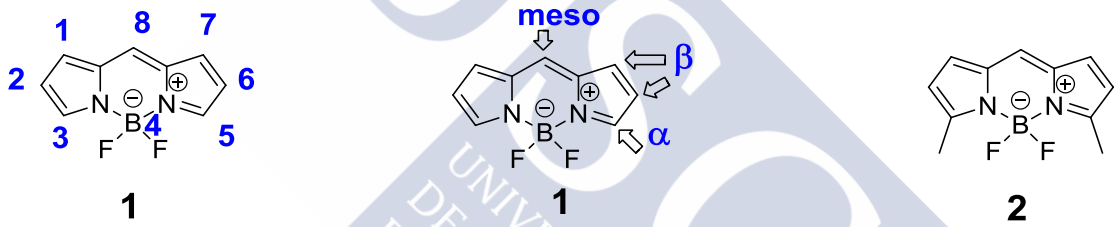


Figure 22. Core structure of a BODIPY dye (**1**) with the atom numbering and the α, β and *meso*-positions indicated, and chemical structure of the simplest BODIPY employed for comparing alkylated BODIPY dyes **2**.

BODIPY 1 (Figure 22), which has no substituents in the core, has never been obtained from the dipyrromethene precursor because none of the pyrrole carbons are blocked from electrophilic attack on the consequence it is very unstable and decomposes even at -40 °C.[104] However BODIPY **1** has been obtained from a BODIPY with a thiomethyl group in the *meso* position through the Fukuyama reaction in which the thioalkyl group serves as a proton surrogate in the aldehyde synthesis.[105] Although BODIPY **2** is not the simplest BODIPY that has been described, it can be considered as a reference compound

[100] L. A. Ernst, R. K. Gupta, R. B. Mujumdar, A. S. Waggonelr, *Cytometry*, **1989**, *10*, 3–10.

[101] N.–H. Ho, R. Weissleder, C.–H. Tung, *Bioorg. Med.Chem. Lett*., **2006**, *16*, 2599–2602.

[102] A. Treibs, F-H. Kreuzer, *Liebigs Ann. Chem*, **1968**; *718*, 208–223.

[103] Y. Nia, J.Wu, *Org. Biomol. Chem*., **2014**, *12*, 3774–3791.

[104] A. Loudet, K. Burgess, *Chem. Rev.* **2007**, *107*, 4891–4932.

[105] I. J. Arroyo, R. Hu, G. Merino, B. Z Tang, E. Peña-Cabrera, *J. Org. Chem*., **2009**, *74*, 5719–5722.

for comparison with other simple alkylated BODIPY dyes. This simple BODIPY absorbs light and fluoresces at *ca.* 500 and 510 nm, respectively, with fluorescence quantum yield approaching unit, and log ε close to 5.[106]

BODIPY dyes are suitable for designing extremely bright probes showing both a high fluorescence quantum yield (Φ_f) as a consequence of their rigid structure, and a high molar absorption coefficient (ε). Moreover, these dyes are largely insensitive to the solvent polarity and to the pH of the solution. They have fluorescence lifetimes in the nanosecond range, have sharp excitation and emission bands contributing to increase their brightness, exhibit good photochemical stability, and display good solubility in many organic solvents.[107] The hydrophobic nature of BODIPY dyes allows their encapsulation into polystyrene beads by simple swelling in an organic solvent.[108] A limitation of BODIPY dyes is that, usually, they display very small Stokes shifts, complicating the proper separation of the fluorescence emitted by the probe from the excitation "leakage" (particularly when particulated fluorescent materials are used, due to the strong scattering). This limitation is aggravated by their narrow absorption and emission bands.

One of the major advantages in using BODIPYs is their easy tunability and versatility. There are plenty of possibilities to obtain a modified BODIPY with the required characteristics. Here the vast chemistry of BODIPY dyes will be not described, but some of the common chemical modifications are listed (Scheme 9).

a) *Modifications to meso-aromatic substituents on the BODIPY core*: a variety of aromatic groups can be introduced at the *meso*-position to achieve appropriately functionalized BODIPY dyes;

b) *Palladium-mediated C-H reactions functionalization*,: this route provides a direct way to extend the conjugation of the BODIPY core without a halogenated or metallated intermediate;[109]

c) *BODIPYs with heteroatom substituents* from electrophilic substitution reactions at 2- and 6-positions of the BODIPY core which bear the least positive charge (i.e. halogenation, sufonation);

d) *Condensation reactions* of the 3,5-dimethyl derivatives with benzaldehyde derivatives to yield alkenyl systems. It has been shown that 3- and 5-methyl BODIPY-substituents are acidic enough to participate in Knoevenagel reactions. Thus, styryl-BODIPY derivatives can be obtained by condensation of 3,5-dimethyl-BODIPYs with aromatic

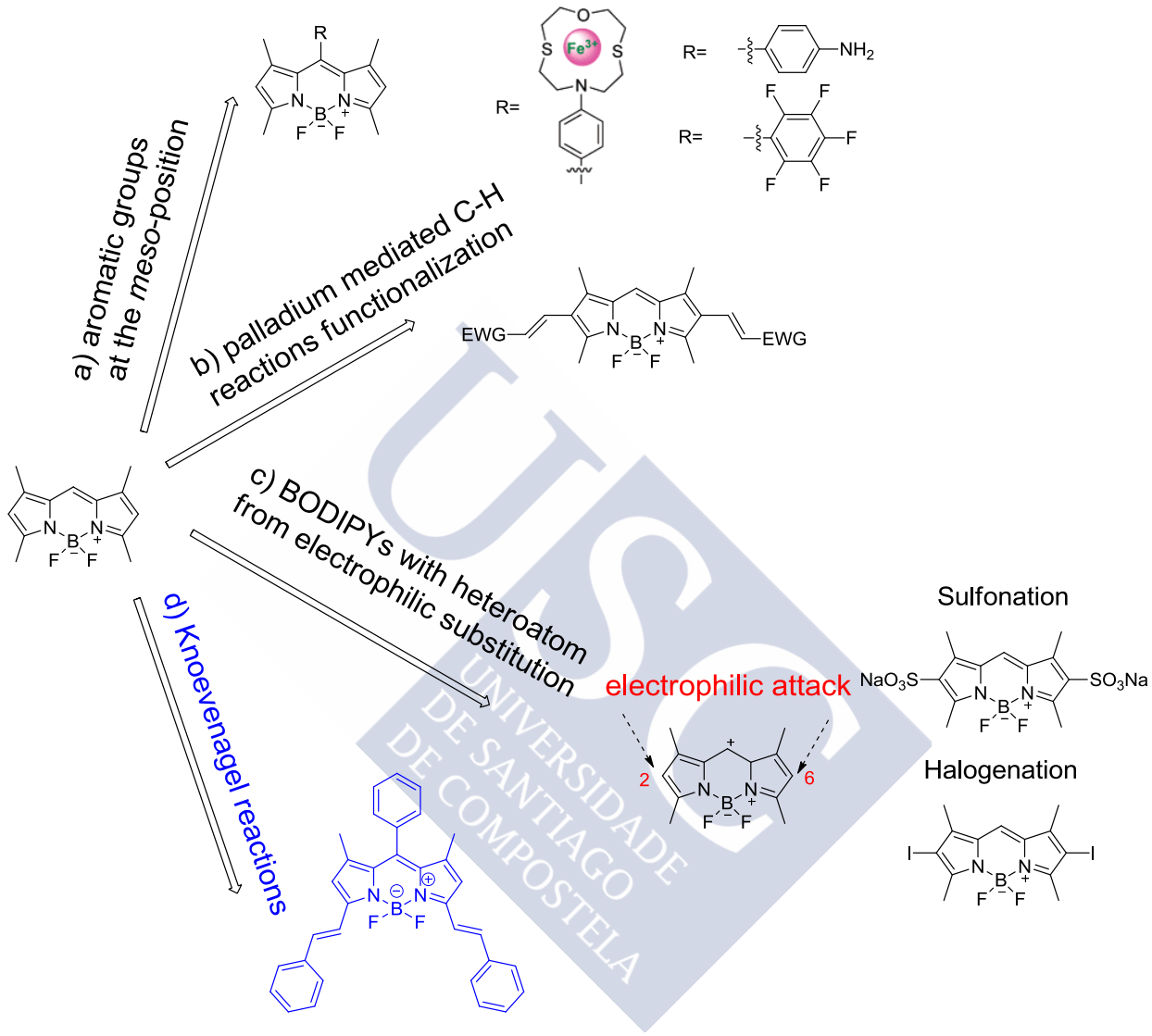
[106] G. Ulrich, R. Ziessel, A. Harriman, *Angew. Chem. Int. Ed.*, **2008**, *47*, 1184–1201

[107] A. B. Descalzo, H.–J. Xu, Z. Shen, K. Rurack, *Ann. N.Y. Acad. Sci.*, **2008**, *1130*, 164–171.

[108] A. B. Descalzo, H.–J. Xu, Z.–L Xue, K. Hoffmann, Z. Shen, M. G. Weller, X.–Z. You, K. Rurack, *Org. Lett.*, **2008**, *10*, 1581–1584.

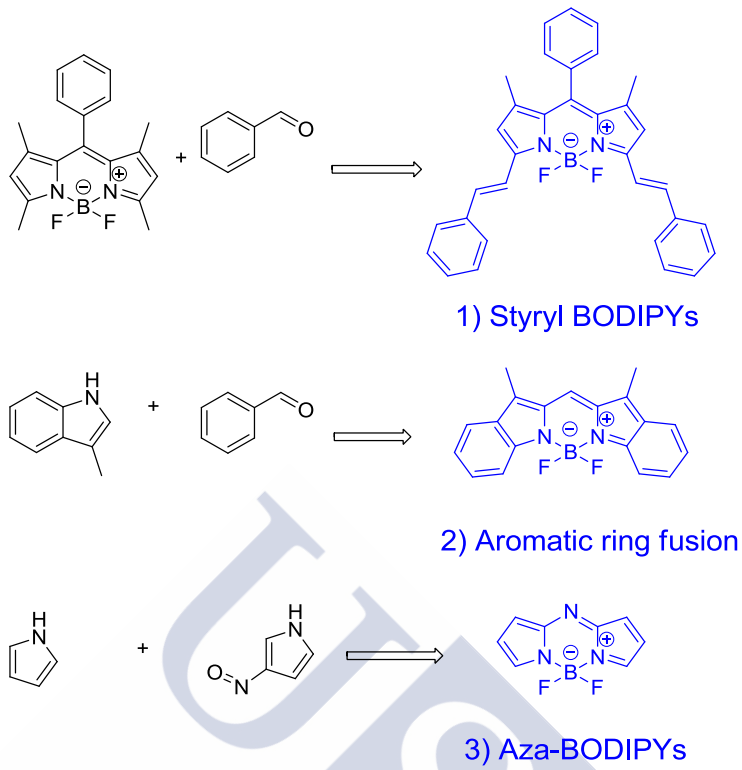
[109] C. Thivierge, R. Bandichhor, K. Burgess, *Org. Lett.*, **2007**, *9*, 2135–2138.

aldehydes. This is the most straightforward method for extending the electron delocalization of BODIPY core and obtain NIR-absorbing BODIPYs.



Scheme 9. Some common modification on the BODIPY core. a) Modifications to *meso*-aromatic substituents on the BODIPY core with some examples. b) BODIPY dye with electron withdrawing groups from palladium-mediated reactions. c) Electrophilic addition to yield BODIPYs with heteroatoms, with two examples. d) π-extended BODIPY dye for absorption in the NIR region of the spectrum by Knoevenagel reactions.

Two other ways to obtain NIR BODIPY dyes are: 1) the use of substituted indole fragments instead of pyrrole in the synthesis of the core BODIPY and 2) the replacement of the meso-carbon by an imine-type nitrogen atom (Scheme 10).



Scheme 10. Additional possible chemical derivatizations for obtaining NIR-absorbing BODIPYs from the simplest BODIPY core.

6.3. Benzophenoxazines

Benzophenoxazines consist of a phenoxazine moiety which has an additional benzene ring (Figure 23). They are positively charged fluorophores with two N atoms connected through a conjugated π–system. Their rigid structure provides high photostability and significant Φ_f at wavelengths above 650 nm. Mendola's blue (MDB, Figure 25) was one of the first fluorescent oxazine dyes discovered, but nowadays Nile Red (NR) and Nile Blue (NB) (Figure 25) are more commonly employed. The phenoxazine skeleton can be extended by adding fused benzene rings. Depending on the orientation of the ring fusion, benzophenoxazines can be 'angular' or 'linear' as illustrated in Figure 24. Figure **23.** Different types of phenoxazine dyes.

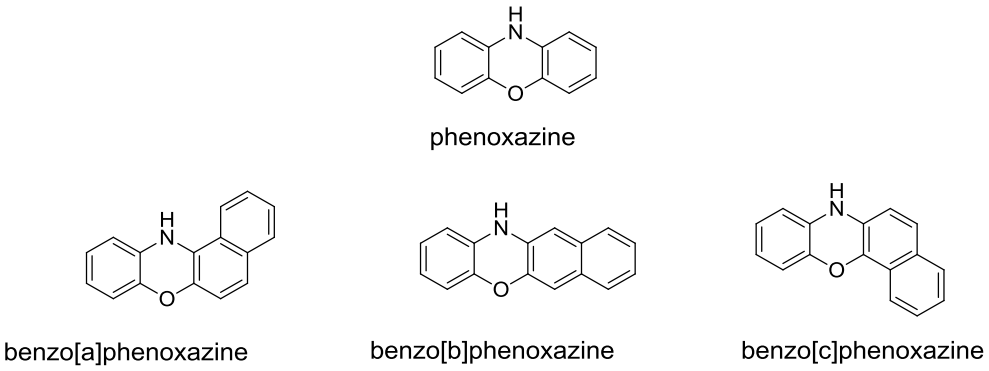


Figure 23. Different types of phenoxazine dyes.

Benzo[*a*]phenoxazines and benzo[*c*]phenoxazines are "angular", while benzo[*b*]phenoxazines display a linear structure. MDB, NR and NB belong to the angular benzo[*a*]phenoxazines. NR is a *push-pull* system with a strong electron donor group in position 9 (a 9-diethylamino substituent) and an electron acceptor (a carbonyl group) conjugated through the π-electron system, in a way that, after light excitation, an intramolecular charge transfer (ICT) process takes place from the donor to the acceptor. In the case of NB, there it is not a neat *push-pull* system, and the positive charge of the iminium substituent is strongly delocalized along the whole π-system. An additional difference between NB and NR is that Nile Red is a rather hydrophobic molecule, while the positive charge of Nile Blue facilitates its solubilization in polar solvents. Actually, it can be said that NB is one of the best water-soluble alternatives to BODIPY dyes.

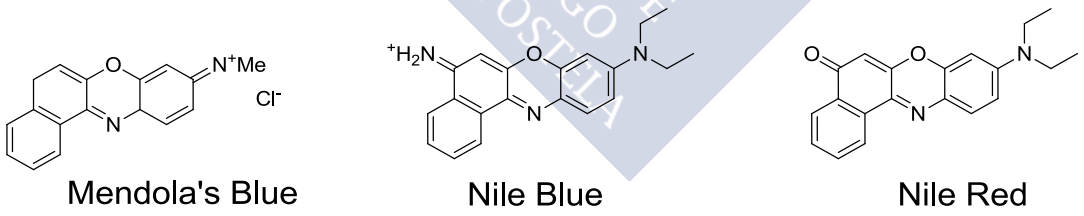


Figure 24. Chemical structure of Mendola's blue, Nile Blue and Nile Red.

Nile Blue is a long wavelength emissive dye with strong fluorescence in aprotic media, but low fluorescent quantum yield in water (about 0.01)[110]. Still this emission is significant in comparison with Nile Red or other NIR fluorescent dyes in water. Its fluorescence lifetime is short (in ethanol for example, 1.42 ns),[110] and it can vary in concentrated solution ($c > 10^{-3}$ M), presumably due to aggregation problems.

[110] J. Jose, K. Burgess, *Tetrahedron*, **2006**, 62, 11021–11037.

Another interesting characteristic of NB is the pH dependence of its optical properties. Under basic conditions the iminium group is deprotonated, whereas under strongly acidic conditions one of the amino groups might even be protonated, resulting in a hypsochromic shift. NB shows a progressive bathochromic shift in absorption and emission maxima as the solvent polarity increases: λ_{em} is 546 nm in hexane, 668 nm in MeOH, and 674 nm in H_2O. This unique property renders these compounds extensively used in scientific applications as fluorescent polarity probes.[111]

Good solubility is an important feature for performing reproducible bioassays in aqueous media, since NIR dyes are normally large, planar, hydrophobic molecules prone to aggregation in water.[112] But this is not the case for NB which in water at micromolar concentrations is perfectly soluble. Burgess and coworkers have reported the synthesis of water-soluble NB derivatives (at a 4 μM concentration level) bearing water-solubilizing substituents in their structure.[113] In spite of the related Nile Blue (NB) dye being a strongly emissive in organic media (Φ_f = 0.27 in ethanol), its fluorescence quantum yield in aqueous solution drops to only 0.01. This quenching of fluorescence is not associated to the aggregation but it is due to due to efficient proton transfer from the solvent.[114]

From this Section, we can conclude that BODIPY dyes and phenoxazine derivatives can be considered excellent fluorophores for the red-NIR spectral region. Both families of dyes are characterized by their strong brightness and their good photostability (at least, in comparison to cyanine dyes). Additionally, the versatile chemistry of BODIPY dyes allows easily tuning their spectroscopic and chemical properties and, despite they have a poor solubility in water, they are very appropriate for straightforward doping of hydrophobic materials such as polystyrene beads. On the other hand, positively charged phenoxazine dyes are a good alternative to BODIPYs when aiming to work with the molecular probes directly in aqueous solution.

7. Fluorescent magnetic nanoparticles as labels for FIAs

A nanomaterial is defined as a solid material characterized by at least one dimension in the nanometer range which has innovative properties and functionalities thanks to their nanometer size.[115] Remarkable properties are for example, their large surface area and the possibility of synthetizing them with different chemical composition or architectures. Nanotechnology is an interesting research field continuously expanding in

[111] S. Naik, C. M. A. Alves, P. J. G. Coutinho, M. S. T. Goncalves, *Eur. J. Org. Chem*., **2011**, *13*, 2491–2497.
[112] D. Hazafy , M.–V. Salvia, A. Mills, M. G. Hutchings ,M. P. Evstigneev, J. A. Parkinson, *Dyes Pigment.*, **2011**, 88, 315–325.
[113] J. Jose; Y. Ueno; K. Burgess, *Chem. Eur. J.* **2009**, *15*, 418–423.
[114] A. Grofcsik, M. Kubinyi, W. J. Jones, *J. Mol. Struct.*, **1995**, *348*, 197–200.
[115] A. D. McNaught , A. Wilkinson, *IUPAC. Compendium of Chemical Terminology, 2nd ed. (the "Gold Book")*, **2006**.

which *nanoparticles* (NPs), which are normally synthesized following a bottom-up approach,[116] are some of the most relevant structures.

NPs are very interesting platforms for the development of sensing systems. Their high surface-to-volume ratio allows immobilization of a high number of target molecules or receptors, and offers rapid assay kinetics. Depending on their functionalization, they can display catalytic activity, magnetic properties, emission of fluorescence, or electrochemical activity.[117] Additionally, their nanometric size plays a crucial role in device miniaturization for the design of compact and portable devices.[118,119]

Fluorescent NPs are able to increase the analytical signal and consequently the signal to noise ratio with respect to the response provided by *conventional* molecular probes. These characteristics satisfy the demand of numerous analytical applications of vast economic and social impact such as medicine diagnostics, imaging techniques, food analysis and environmental monitoring.[120,121] Fluorescent NPs can be classified in two main categories: i) NPs with *intrinsic luminescence* such as semiconductor crystals (also called quantum dots, QDs)[122], upconverting NPs,[123] or NPs made of conjugated polymers;[124] and ii) *dye-doped NPs* (DDNPs), made of optically silent materials such as silica or polystyrene, which are doped with organic dyes that provide them the luminescent properties, as described in the next Section.

Fluorescently-doped *magnetic* nanoparticles, or FMNPs, is a type of nanomaterial that is lately receiving much attention in the field of fluorescence-based immunoassay, because, on the one hand, *fluorescent* (or more generally, luminescent) doping confers the NPs optical properties that allow monitoring the Ab-Ag recognition process with good sensitivity. On the other hand, the *magnetic* properties of the NPs facilitates handling of the labels: no centrifugation is needed for washing, and NPs can be collected in a particular location while, in the case of non-magnetic separation techniques used in microfluidics, a complex geometry is required instead.[125,126]

Magnetic NPs respond to an external magnetic field produced by an electromagnet or permanent magnet and they can be moved to a desired location through magnetic field

[116] K. E. Sapsford, W. R. Algar, L. Berti, K. Boeneman Gemmill, B. J. Casey, E. Oh, M. H. Stewart, I. L. Medintz, *Chem. Rev.* **2013**, *113*, 1904–2074.
[117] Y. K. Lee, R. Smith, R. Kopelman, *Annu. Rev. Anal. Chem.*, **2009,** *2*, 57–76.
[118] T. Chiu, C. Huang, *Sensors*, **2009**, *9*, 10356–10388.
[119] G. Mistlberger, K. Koren, E. Scheucher, D.Aigner, S. M. Borisov, A. Zankel, P. Pölt, I. Klimant, *Adv. Funct. Mater.*, **2010**, *20*, 1842–1851.
[120] K. Hoffmann, T. Behnke, D. Drescher, J. Kneipp, U. Resch–Genger, *ACS Nano*, **2013**, *7*, 6674–6684.
[121] V. K. Sreenivasan, A. Zvyagin, E. M. Goldy, *J. Phys. Condens. Matter,* **2013**, *25*, 194101.
[122] J Gao, H. Gu, B. Xu, *Acc. Chem. Res.*, **2009**, *42*, 1097–1107.
[123] M. Wang, C. Mi, Y. Zhang, J. Liu, F.Li, C. Mao, S. Xu, *J. Phys. Chem. C*, **2009**, *113*, 19021–19027.
[124] J. Pecher, S. Mecking, *Chem. Rev.*, **2010**, *110*, 6260–6279.
[125] Y. Wang, X. Peng, J. Shi, X. Tang, J. Jiang, W. Liu, *Nanoscale Res. Lett.*, **2012**, *7*, 86.
[126] G. Mistlberger, P. Chojnacki, I. Klimant, *J. Phys. D: Appl. Phys.*, **2008**, *41*, 085003.

control. The nanometric size confers these materials different properties with respect to the bulk material, such as a higher coercivity[127] and superparamagnetism, a similar phenomenon to paramagnetism in which magnetization can randomly flip direction under the influence of temperature. Magnetic NPs can be made of magnetite (Fe_3O_4), maghemite (γ-Fe_2O_3), cobalt, nickel, neodymium-iron-boron or FePt alloy[128] and may be synthesized following different procedures, such as: by mechanical attritioning, physical vapor deposition or colloidal chemical approaches.[129,130] Some drawbacks are that the magnetic core can be quite unstable, since it may be oxidized by the air or solvents, and it may undergo pyrolysis. Additionally, only magnetite and maghemite are accepted nontoxic magnetic materials for medical applications. However, these problems can be minimized if the magnetic cores are protected by a suitable shell. This shell can be inorganic silica[131,132] or an organic polymer.[133,134] Alternatively the magnetic core can be directly coated with a semiconducting shell. Besides sensing technologies, magnetic NPs can be applied to a wide range of disciplines including magnetic fluids, biological separation, drug delivery, bacteria detection, protein purification, catalysis, magnetic resonance imaging, biotechnology/biomedicine, data storage, and environmental remediation. [135,136,137]

To summarize, FMNPs are versatile bifunctional nanocomposite materials in which fluorescent and magnetic properties are combined into one object.[138,139] Most of these NPs have a core-shell structure. Due to their bimodal character, FMNPs can be employed in a very wide range of attractive applications such: bioseparation, bioanalysis and medical diagnosis, *in vitro* and *in vivo* bioimaging, biological labeling or in hyperthermia techniques; FMNPs can act also as biocompatible contrast agents in magnetic resonance imaging (MRI) or can be applied in energy storage/conversion and to the development of new nanoscale and photonic devices.

[127] A. Lu, E. L. Salabas, F. Schüth, *Angew. Chem. Int. Ed.* **2007**, *46*, 1222–1244.
[128] L. H. Reddy, J. L. Arias, J. Nicolas, P. Couvreur, *Chem. Rev.*, **2012**, *112*, 5818–5878.
[129] L. L. Vatta, R. D. Sanderson, K. R. Koch, *IUPAC, Pure Appl. Chem.*, **2006**, *78*, 1793–1801.
[130] T. Hyeon, *Chem. Commun*., **2003**, *8*, 927–934.
[131] C. Borgohain, K. K. Senapati, D. Mishra, K. Ch. Sarmac, P. Phukan, *Nanoscale*, **2010**, *2*, 2250–2256.
[132] G. Liu, H. Wu, H. Zheng, L. Tang, H. Hu, H. Yang, S. Yang, *J. Mater. Sci.*, **2011**, *46*, 5959–5968.
[133] S. Xu, W. Ma, L. You, J. Li, J. Guo, J. J. Hu, C. Wang, *Langmuir*, **2012**, *28*, 3271–3278.
[134] J. Ge, Y. Hu, T. Zhang, Y. Yin, *J. Am. Chem. Soc.*, **2007**, *129*, 8974–8975.
[135] G. Wang , X. Su, *Analyst*, **2011**, *136*, 1783–1798.
[136] S. Shylesh, V. Schünemann, W. R. Thiel, *Chem. Eur. J*., **2010**, *16*, 8950–8967.
[137] S. Laurent, D. Forge, M. Port, A. Roch, C. Robic, L. V. Elst, R. N. Muller, *Chem. Rev.* **2008**, *108,* 2064–2110.
[138] S. A. Corr, Y. P. Rakovich, Y. K. Gun'ko, *Nanoscale Res. Lett.*, **2008**, *3*, 87–104.
[139] S. K. Yen, D. Jänczewski, J. L. Lakshmi, S. B. Dolmanan, S. Tripathy,V. H. B. Ho, V. Vijayaragavan, A. Hariharan, P. Padmanabhan, K.K. Bhakoo, T. Sudhaharan, S. Ahmed, Y. Zhang, S. T. Selvan, *ACS Nano*, **2013**, *7*, 6796–6805.

7.1. Methods for preparing dye-doped nanoparticles (DDNPs)

The main methods for NP doping can be divided in i) *covalent* attachment of chromophores or, ii) *physical* adsorption of dopants. For covalent attachment, the corresponding dye must possess suitable functional groups for coupling to the NPs (i.e. alcoxysilane groups for condensation with silica or vinyl/acrylic groups for binding to polymeric materials). Covalent attachment of dyes can also be performed if the NPs surface has been previously derivatized with functional groups such as amino, thiol or glycidoxi groups.[140] On the other hand, physical adsorption relies normally on strong electrostatic interactions (i.e. positively charged dyes remain attached to the negatively charged surface of silica NPs), or hydrophobic interactions in aqueous solution (i.e. lipophilic dyes can be easily encapsulated in hydrophobic polymers such as polystyrene.

Fluorophores that can be used for doping are numerous and many are commercially available. This fact increases the versatility of luminescent DDNPs. Other possibility is to synthesize home-made dyes for fine-tuning of the spectral properties and chemical functions present in the molecule.

One of the features defining the quality of DDNPs is their brightness. Brightness is defined as the product $\varepsilon x \Phi_f$, where ε is the molar absorption coefficient and Φ_f is the fluorescence quantum yield of the dye. Each NP can incorporate a large number of dye molecules. For this reason, the apparent molar absorption coefficient can easily reach a value of 10^6 L $mol^{-1}cm^{-1}$, contributing to increase the overall NP brightness.

Inorganic silica NPs and organic polystyrene NPs are some of the most extensively studied DDNP.[141] Both types satisfy most criteria for their application in biomedical analysis: i) low toxicity, ii) uniform size and transparency to visible light (despite larger NPs have the drawback of producing a strong light scattering), iii) facile synthesis and functionalization with different surface groups that can be chosen for minimizing aggregation of the NPs.

Silica NPs. *Silica* is convenient for many reasons. Its synthesis is well known and can be performed under mild conditions. Silica can be easily functionalized, enabling chemical binding of various fluorescent and biological species (covalent attachment of dyes or biomolecules can be performed via amino- or glycidoxi-silanization procedures, for example).[142] Alternatively, positively charged dyes and biomolecules can be adsorbed onto the negatively charged silica matrix by electrostatic interactions. Moreover, the silica itself is biocompatible, inert and optically transparent. Additionally, silica provides a barrier for protecting luminophores from quenching by external agents such as atmospheric oxygen, solvent molecules or other ions present in solution. All these

[140] S. Bonacchi, D. Genovese, R. Juris, M. Montalti, L. Prodi, E. Rampazzo, N. Zaccheroni, *Angew. Chem. Int. Ed.* **2011**, *50*, 4056–4066.

[141] S. W. Bae, W.Tan, J. Hong, *Chem. Commun.*, **2012**, *48*, 2270–2282.

[142] L. Wang, W. Zhao, W. Tan, *Nano Res.*, **2008**, *1*, 99–115.

effects, together with certain rigidity that silica confers to the luminescent molecules, can enhance of the emission quantum yield of the encapsulated probes.[143]

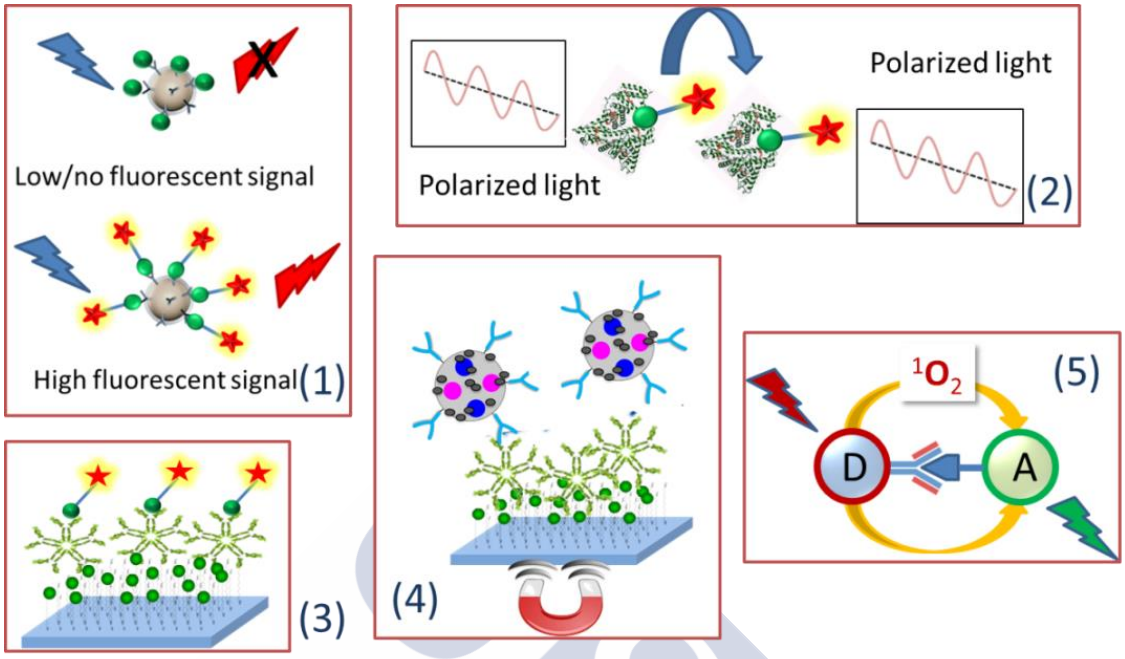
Polystyrene NPs. In the case of *polystyrene* beads, physical adsorption of (hydrophobic) dyes, proteins, or antibodies is possible. Moreover, they are commercially available with surface functional groups that can also be used for further (bio)-conjugation. Due to its hydrophobic character, polystyrene tends to aggregate in aqueous media and its density leads to difficulties in separation from solution after the labeling processes. However, polystyrene NPs satisfy several criteria for being used in biomedical applications: they are non-toxic, do not sediment, have uniform size and uniform size distribution and, normally, no dye leaking is observed in aqueous solution. In the same way as silica, polystyrene is optically inert and it has no influence in the spectroscopic properties of the encapsulated dyes.

USC UNIVERSIDADE DE SANTIAGO DE COMPOSTELA

[143] S. Bonacchi, D. Genovese, R. Juris, M. Montalti, L. Prodi, E.Rampazzo, M. Sgarzi, N. Zaccheroni, *Top Curr. Chem.*, **2011**, *300*, 93–138.

Objectives

General objectives of the Thesis work



Scheme 11. Different microfluidic compatible formats proposed in this Thesis for the sensitive determination of the free IS drug concentration (IS = FK506, CyA or MPA) to be implemented in a final POCT device, developed within the framework of the EU Project NANODEM. (1) Homogeneous analysis with a NIR-fluorescent labeled IS and MNPs. (2) Fluorescent polarization immunoassay with a NIR-fluorescent labeled IS. (3) Heterogeneous format analysis that requires previous immobilization of the target IS onto a chip surface and a fluorescent labeled IS. (4) Heterogeneous format employing FMNPs doped with a couple of BODIPY dyes for recording a FRET that improves the S/N ratio of the analysis. (5) Proximity chemiluminescence immunoassay (CLIA) mediated by singlet oxygen produced by photosensitizer in "donor" NPs.

The main focus of this Thesis work will be the development of innovative analytical strategies for measuring the free fraction of the immunosuppressive drugs FK506, CyA and MPA within the framework of the EU Project NANODEM (**Figure 25.** Chemical structures of the selected immunosuppressants: cyclosporine A (CyA), tacrolimus (FK506) and mycophenolic acid (MPA).Figure 25).

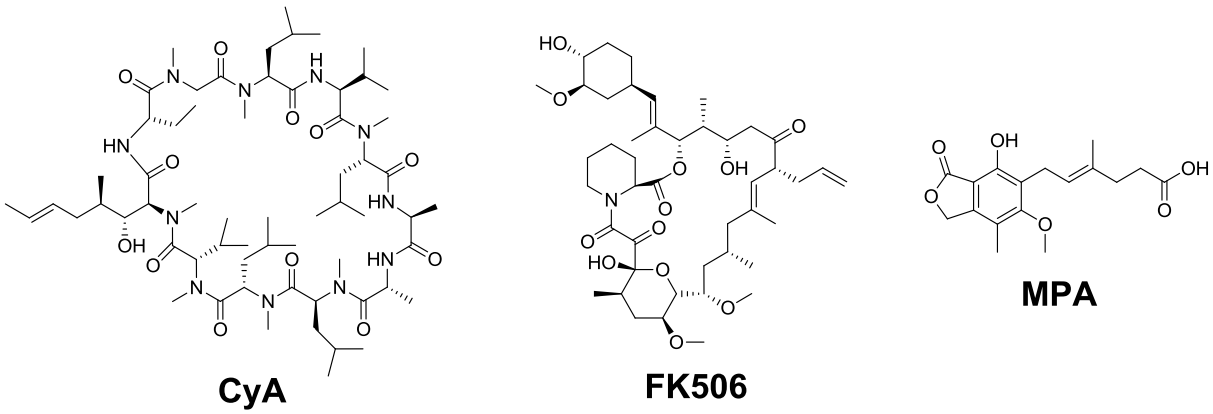


Figure 25. Chemical structures of the selected immunosuppressants: cyclosporine A (CyA), tacrolimus (FK506) and mycophenolic acid (MPA).

The different (photo)chemical strategies explored for the development of novel, sensitive, selective microfluidic-compatible methods of analysis are displayed in Scheme 11. The main tasks will be

i) an adequate chemical derivatization of the IS drugs for further conjugation either to solid surfaces, to fluorescent labels or to NPs;

ii) synthesis of brilliant molecular probes emitting in the near-infrared (NIR) spectral range for highly sensitive detection, and their spectroscopic characterization;

iii) synthesis and characterization of photosensitizers for $^1O_2$ production;

iv) synthesis and doping of polymeric (magnetic) nanoparticles with fluorescent probes for improving analytical performance of the labels;.

v) synthesis and doping of polymeric (magnetic) nanoparticles with photosensitizers for increasing the singlet oxygen production.

The novel fluorescent dye-labeled drugs, functionalized drugs and encoded MNPs will be forwarded to the NANODEM project partner in Italy, Germany and Portugal to manufacture the designed microfluidic device for their implementation into the final POCT NANODEM biosensing system aimed to in situ (bedsite) analysis of the immunosuppressive drugs in the blood of just transplanted patients.

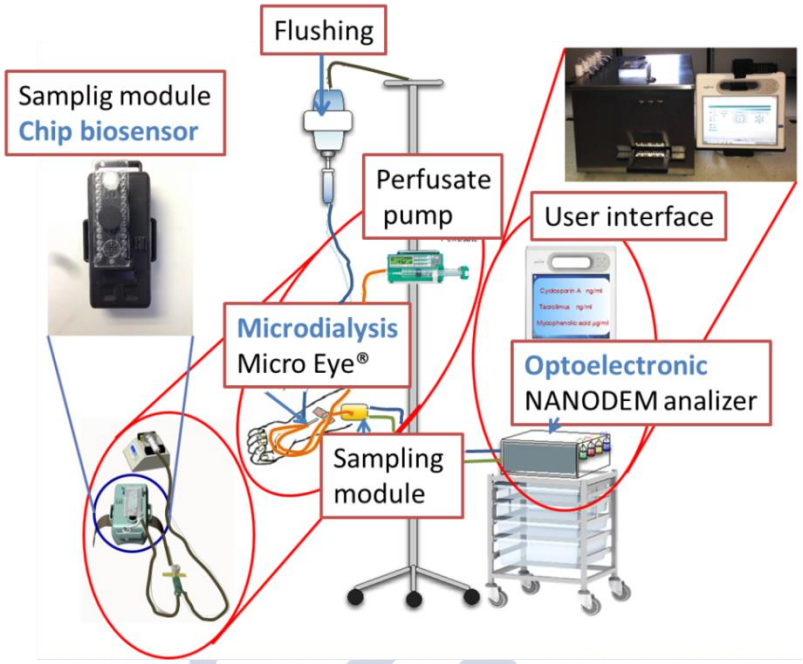


Figure 26. Schematic view of the final POCT device (courtesy of Datamed Ltd.).

Tereofre, the Thesis is divided in three main chapters as follows:

- Chapter 1 describes the chemical derivatization of the three ISs of interest: cyclosporine A (CyA), tacrolimus (FK506) and mycophenolic acid (MPA), with suitable groups (i.e. –COOH groups) suitable for immobilization onto aminated surfaces, or for NIR-fluorescent tags. Good fluorophore candidates are oxazine derivatives (see section 6.3).The latter should have an appropriated group to react with the –COOH function of the IS-COOH molecules, providing the corresponding fluorescent conjugate. The NIR dye labelled ISs are then spectroscopically characterized and applied as fluorescent probes for FPIAs (Scheme 11 (1), (2), (3)). .

- Chapter 2 describes the synthesis of strongly fluorescent BODIPY dyes and their spectroscopic characterization. The lipophilic dyes, or combinations of two of them, are encapsulated into polystyrene NPs by a straightforward swelling method in tetrahydrofuran-water mixtures to yield very brilliant NPs. If two of the BODIPY dyes are co-encapsulated in the same NP, it is possible to observe an intraparticle FRET process that allows increasing the Stokes shift and with that, improving the S/N ratio in a fluorescent immunoassays for tacrolimus detection. Different NPs (silica or polystyrene, with magnetite or cobalt magnetic cores) will be also employed, and diverse strategies (covalent attachment or physical entrapment) for NPs doping will be tested (Scheme 11 (4)).

- Chapter 3. The last chapter describes the development of photoactive beads. Two main aspects will be covered: i) optimization of the doping procedures of polystyrene NPs with suitable molecular photosensitizer; and ii) photophysical characterization of the prepared NPs followed by the development of a method to evaluate the singlet oxygen production quantum yield ($\Phi\Delta$) in NPs. The NPs with the most efficient production of singlet oxygen will be proposed as "$^1O_2$ donor" beads for developing a novel chemiluminescence proximity immunoassays (Scheme 1 (5)).

Finally, the Experimental Part provides a detailed description of the synthesis of FK506, CyA and MPA derivatives, their fluorescent derivatization, and the synthesis of NIR-fluorescent labels, as well as the procedures followed for NPs synthesis and their fluorescent doping. The employed chemicals, solvents and instruments are provided. The characterization data (^1H, ^{13}C and ^{19}F NMR spectra, MS spectrometry results, and electron microscopy images) are also provided at the end of the Thesis as an Annex.

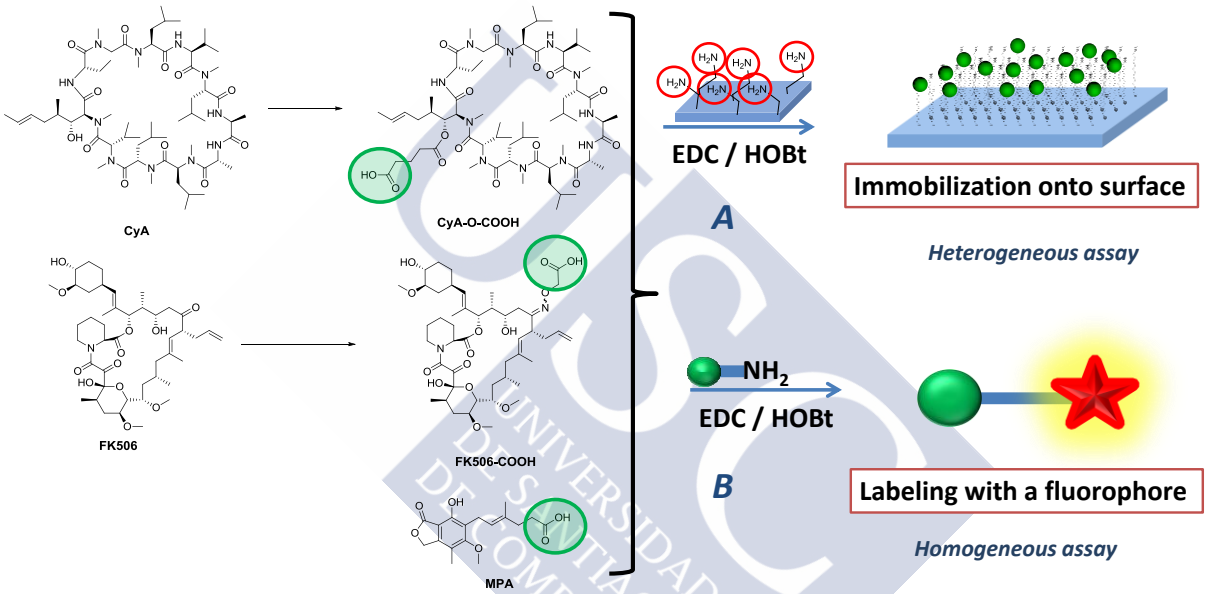
USC UNIVERSIDADE DE SANTIAGO DE COMPOSTELA

Results and discussion

Derivatization of immunosuppressive drugs for fluorescent labeling and immobilization onto surfaces

1. Introduction

The aim of this chapter is the derivatization of IS drugs and its characterization. The immunosuppressants selected are cyclosporine A (CyA), tacrolimus (FK506) and mycophenolic acid (MPA). A new chemical function will be introduced in their structure for allowing either, fluorescent labelling or their immobilization onto aminated surfaces (Scheme 12).



Scheme 12. Left: structures of the immunosuppressants selected CyA and FK506, and MPA and the carboxylic derivatives of CyA and FK506 (in green the carboxylic group). Right: (A) Protocol for IS´s immobilization onto a surface; (B) IS´s labeling with a fluorophore (red star). Both protocols A and B require previous activation of the IS's –COOH function via carbodiimide chemistry.

The chosen chemical function for ISs derivatization is a carboxylic group. In the case of MPA such chemical derivatization is not necessary, since the drug itself is a carboxylic acid. The carboxy derivatives of immunosuppressants (IS-COOHs) can be immobilized in aminated surfaces or they can be tagged with amino fluorescent labels after -COOH activation using carbodiimide chemistry. The second point, fluorescent labeling of the carboxylated immunosuppressants, is also an important aim of this Thesis. It is sought that the selected fluorescent label emits in the red region of the visible spectra in order to minimize the interference from biological samples and scattering. The tag has to contain an amino group for the coupling with the ISs providing a stable amide bond. For

this purpose oxazine derivatives, such as the popular Nile Blue, are well suited.[144] These dyes have an intense red fluorescence and are water soluble, also an important aspect to be taken into account for biological applications. A modified structure of the standard Nile Blue will be synthesized with view to obtain a primary sterically accessible amine (Figure 27) for coupling with the IS-COOHs.

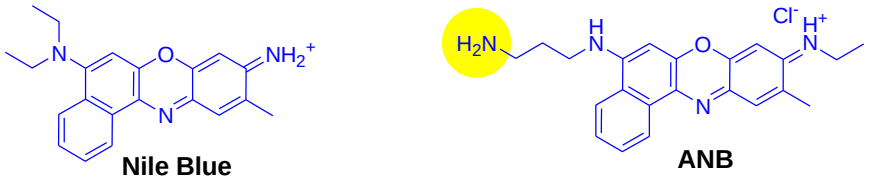


Figure 27. Chemical structure of Nile Blue (left) and of the analogue called Amino Nile Blue (right).

The suitability of the ANB-labeled immunosuppressants for their use in fluorescent immunoassays (FIA or FPIA) (section 5.2.1 in the Introduction) will be evaluated. Also, the fluorescent labels will be applied for fluorescent polarization binding analysis (see section 4 of this Chapter) to determine the free fraction (α) of the immunosuppressants and the association constant K_A to blood proteins.

In the following sections the synthesis, characterization and applications, of carboxylated immunosuppressants and their fluorescent derivatives will be described.

2. Modification of the immunosuppressants with a carboxylic acid group

The immunosuppressants tacrolimus and cyclosporine A were chemically modified with carboxylic group to permit further (bio)conjugation. The –COOH group reacts with an amino group through the activation with carbodimides to form a strong amide bond. Chemical modification of the immunosuppressants should not affect the binding with the recognition antibodies that will be employed afterwards in the FIAs or FPIAs.[145,146]

The synthesis of these immunosuppressant derivatives was a demanding task: the literature found describing ISs derivatization was very scarce; there are few positions in the molecules for chemical modification; and, the large molecular size of CyA and FK506 complicated the analytical characterization of the obtained products by NMR. Only MS could be used as confirmative technique –despite the difficulties, sometimes, for finding the proper conditions for sample ionization–. In addition, monitoring of the reaction by

[144] J. Jose, K. Burgess, *Tetrahedron*, **2006**, *62*, 11021–11037.
[145] K. Sunohara, S. Mitsuhashi, K. Shigetomi, M. Ubukata, *Bioorg. Med. Chem. Lett.*, **2013**, *23*, 5140–5144.
[146] D. Iwaszkiewicz-Grzes, G. Cholewinski, A. Kot-Wasik, P. Trzonkowski, K. Dzierzbicka, *Eur. J. Med. Chem.*, **2013**, *69*, 863–871.

thin layer chromatography (TLC) requires the use of very polar mixtures of eluents such as CH_2Cl_2:EtOAc:MeOH:HOAc, 30:70:11:0.6 *v/v*.[147] Despite in this Thesis it was found that the eluent mixture CH_2Cl_2:MeOH (8:2 *v/v*) was also suitable, still the methanol content was too high to be used for a silica column chromatography. Fortunately, it was observed that liquid-liquid extraction was sufficient for isolation of the pure products.

2.1. Synthesis of cyclosporine A derivatives

Cyclosporine A is a cyclic undecapeptide. Among the eleven amino acids, there is just one that can be used to carry out further modifications of the molecule. This amino acid is the Bmt, or (4*R*)-4-[(*E*)-2-butenyl]-4-methyl-L-threonine, which was previously unknown before cyclosporine A was discovered. The three-dimensional chemical structure of CyA reveals a steric hindrance that makes the Bmt chain less accessible to the corresponding reagents and, consequently, makes more difficult its chemical modification (Figure 28).

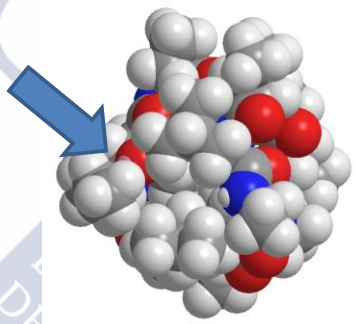


Figure 28. 3-D model of CyA after energy minimization (MM2 method).[148] The arrow points at the Bmt subunit.

There are two functional groups in the Bmt chain that can be used for chemical modification of the immunosuppressant: a carbon–carbon double bond and a hydroxy group.[149]

Still, the most demanding task is not finding a synthetic route for CyA derivatization, but to find a procedure for purification of the reaction products. One of the most common ways to separate a carboxylic acid is by using a significant acidic medium for protonation of the –COOH group. This provokes precipitation of the neutral molecule in aqueous media and, consequently, it could be isolated by filtration. However, we noticed that the original chemical structure of CyA was irreversibly altered under strong acidic

[147] O. Cañadas, Al. Sáenz, G. Orellana, C. Casals, *Anal. Biochem.*, **2005**, *340*, 57–65.
[148] N. L. Allinger, *J. Am. Chem. Soc.*, **1977**, *99*, 8127–8134.
[149] M. Peel, A. Scribner, *Biochim. Biophys. Acta*, **2015**, *1850*, 2121–2144.

conditions. The same observation has been reported by other researchers,[149] who have attributed it to a non-reversible intramolecular acyl transfer within the Bmt amino acid of CyA (Figure 29). Alternative CyA separation methods must be then considered.

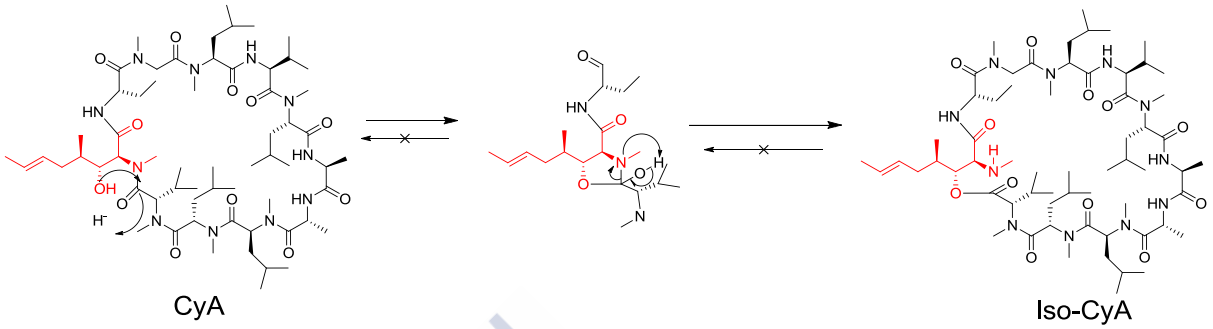


Figure 29. Intramolecular acyl transfer from the 2-nitrogen to the 3- oxygen in the Bmt amino acid (in red) of CyA induced by a strong acid as reported by M. Peel and A. Scribner.[149]

Three different synthetic routes were followed for derivatization of CyA:

(i) The first synthetic path (route 1) involves bromination of the terminal carbon in the Bmt chain following a similar method to that published by M. Schumann;[150] (ii) The second synthetic path (route 2) involves a 4 steps reaction in which the C-C double bond was the starting point with an epoxide as intermediate product;[151] the third route implies direct modification of the secondary hydroxy group of CyA.

2.1.1. Routes 1 and 2. Previous protection of the hydroxy group of CyA

The first step for both synthetic routes 1 and 2 for obtaining CyA-S-COOH and CyA-N-COOH, respectively is the acylation of the hydroxyl group of CyA in order to avoid the deleterious intramolecular formation of cyclic sub-products similar to those depicted in Figure 30.[151]

[150] M. Schumann, G. Jahreis, V. Kahlert, C. Lücke, G. Fischer, *Eur. J. Med. Chem.*, **2011**, *46*, 5556–5561.
[151] Z. Lu, S. Gao, P. Kopeckova, J. Kopecek, *Bioconjugate Chem.*, **2001**, *12*, 129–133.

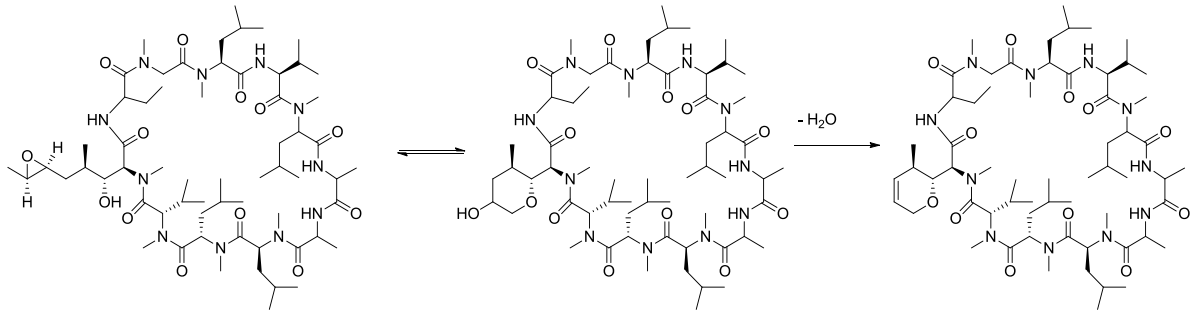
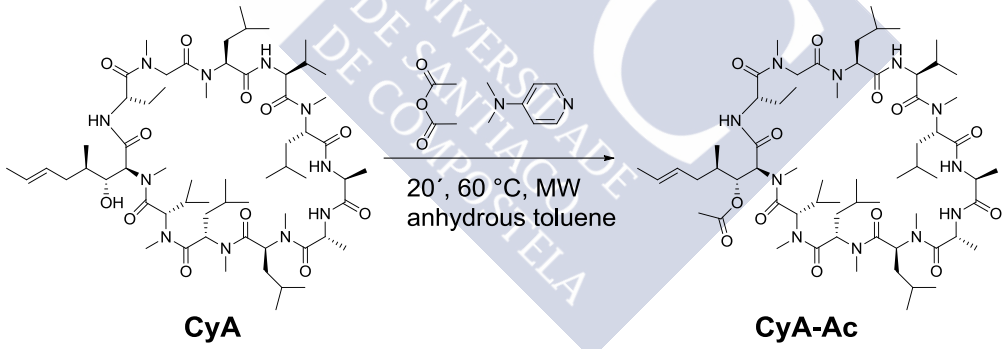


Figure 30. Cyclic form of CyA observed after epoxydation of the double bound without previous protection of the hydroxyl group.

The acylation of cyclosporine A with either acetic or (4-bromophenoxy)-acetic anhydride or chloroacetic anhydride in the presence of pyridine is a well know reaction since the '80s.[152,153] Here we propose the same reaction but using instead acetic anhydride as reagent and a microwaves reactor. The last helped to improve the reaction yield, save time and facilitate the purification (Scheme 13). 4-dimethylamino-pyridine (DMAP) was used as base for increasing the nucleophilic character of the –OH group. The reaction releases acetic acid as subproduct which is eliminated by reduced pressure.



Scheme 13. Reaction of CyA with acetic anhydride in the presence of DMAP for acetylation of the –OH group.

[152] R. Traber, H.-R. Loosli, H. Hofmann, M. Kuhn A. Wartburg, *Helv. Chim. Acta,***1982**, 65, 1655–1677.
[153] A. S. Park, G. P. Meier, *Tetrahedron Lett.*, **1989**, *32*, 4215–4218.

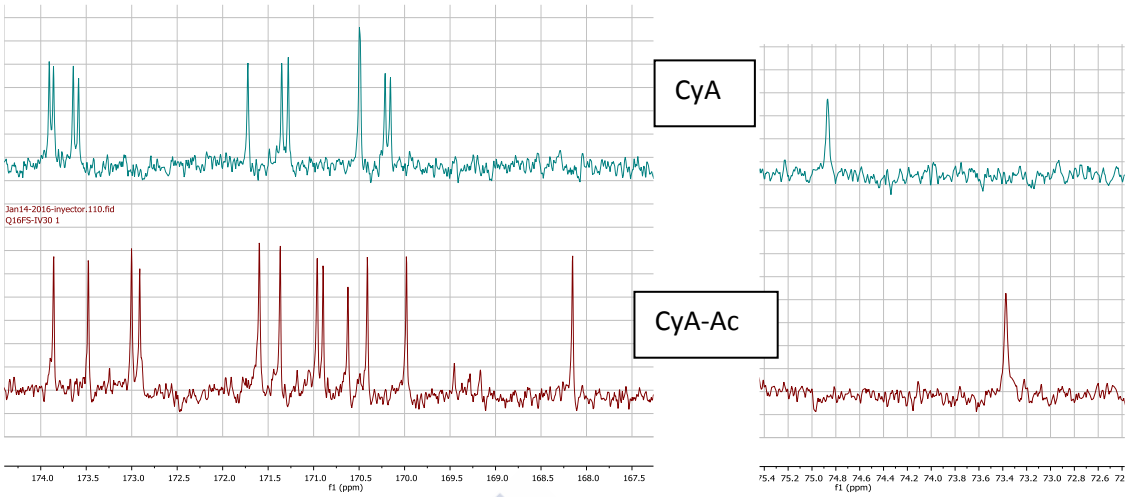
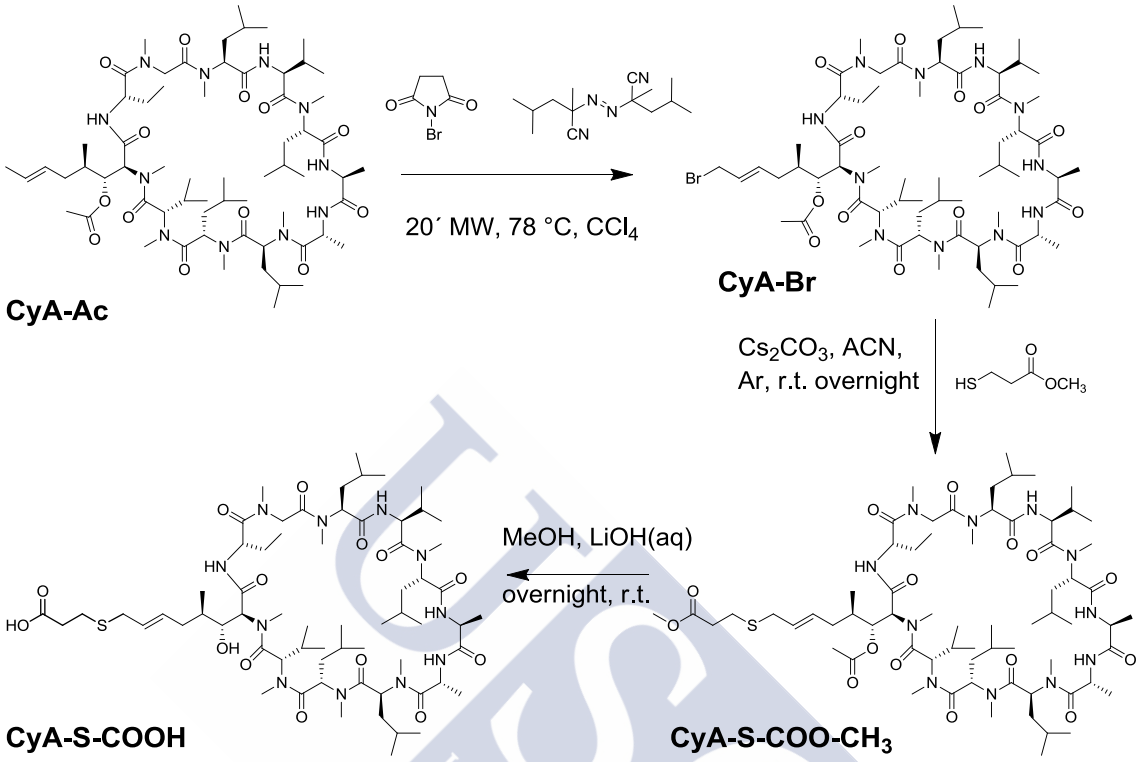


Figure 31. Amplification of the ^{13}C-NMR spectra obtained for CyA (green) and CyA-Ac (brown) in $CDCl_3$. Left (175-167 ppm range): the new –C=O ester group of CyA-Ac can be appreciated at 168.15 ppm; Right (75.5-72.0 ppm range): acylation of the CyA –OH group is confirmed.

The confirmation of the good outcome of the reaction was made by ^{13}C-NMR. Indeed, as a consequence of acylation of the hydroxyl group (i) the signal of the C–OH carbon atom at 75.07 ppm shifted to 73.37 ppm (Figure 31, right), and, (ii) the signal of the new C=O ester bond appeared at 168.15 ppm (Figure 31, left). Mass spectrometry also confirmed the molecular weight of the compound (m/z calculated for $[M+H]^+$ $C_{64}H_{114}N_{11}O_{13}^+$ 1244.8, found 1245.2). CyA-Ac was obtained as pale yellow solid in 97% yield.

2.1.2. Route 1, synthesis of CyA-S-COOH



Scheme 14. Synthesis of CyA-S-COOH in three steps starting from the acylated CyA-Ac derivative.

Starting from the acylated CyA-Ac product, the preparation of this first CyA carboxy-derivative capitalizes on the terminal carbon in the Bmt aminoacid and is performed in three reaction steps (Scheme 14). The first step is the Wohl-Ziegler reaction, an allylic bromination of the cyclosporine using N-bromosuccinimide (NBS) and a radical initiator to yield the reactive halogen derivative CyA-Br. The allylic position is favored for hydrogen abstraction, because the corresponding intermediate radicals are better stabilized, still, a mixture of brominated products can be obtained (Figure 32). The Wohl-Ziegler reaction was performed in a microwave reactor instead of a classical thermal reaction in order to accelerate reaction rate, since we observed that cyclosporine A is quite inert. This reaction resulted difficult to control and a variety of conditions were tested. Different parameters including time, temperature and NBS equivalents were varied in order to try to minimize the formation of the di-bromated CyA-Ac. Unfortunately, splitting of the NMR signals seemed to indicate the formation of several of the brominated product shown on Figure 32.

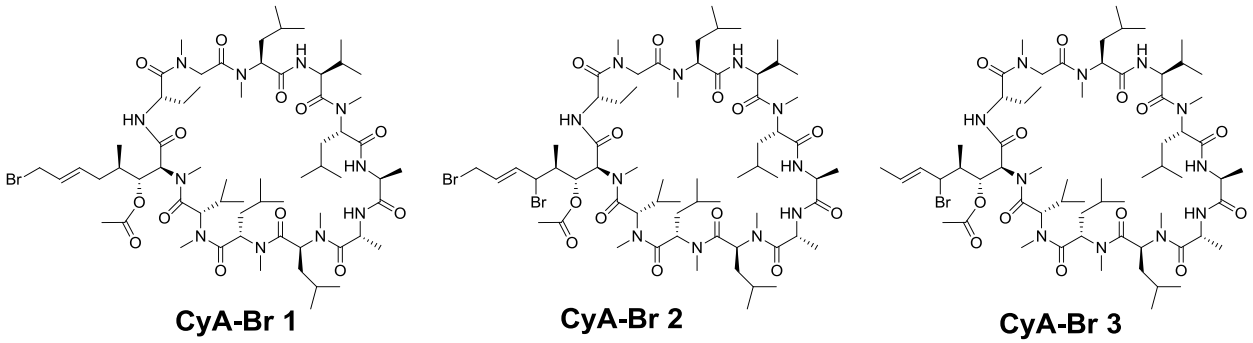


Figure 32. Possible bromination products of CyA-Ac.

The compromise between the complete consumption of the reagents and the less amount of CyA-Br 2 formed was found using 20 minutes of microwaves at 78 °C and 6 equivalents of NBS. The amount of the di-bromide compound was qualitatively estimated measuring the intensity of some ^{1}H-NMR tween signals. The presence of the di-bromide compound was also confirmed by mass spectrometry. An additional confirmation that the reaction worked properly was found by MS with the typical Br isotopic distribution. CyA-Br was obtained as light brown-orange solid in 70% yield.

The latter CyA-Br mixture reacted by a S_N2 reaction with methyl 3-mercaptopropanoate. The alkyl chain between the thiol group and the ester group has been chosen of an appropriate length, neither too large, to avoid a folding into CyA hydrophobic pocket, nor too short to make the carboxylic acid accessible. The reaction works with mild conditions in the presence of cesium carbonate as base. The crude product was used for the next reaction step.

The final step involved an alkaline hydrolysis of the protective ester into the desired carboxylic acid using LiOH with good yield. In this reaction conditions the hydroxylic group was also deprotected. Fortunately the subproducts of all the steps could be eliminated by liquid-liquid extraction. The purified final product was characterized by mass spectrometry and NMR (see Experimental and Annex parts). A broad signal was observed at 3.84 ppm in the ^{1}H-NMR spectrum, indicating that the –OH group was also released (see Annex part), confirming the success of the reaction. CyA-S-COOH was obtained as a light brown solid in 71% yield (47% yield considering the whole process).

The mass of the product was confirmed by MS (with MALDI TOF, ESI and FAB see Experimental and Annex parts). The expected mass for [M] was 1305.8, and the molecular ion was observed for $[M-H]^-$ at m/z 1304.7 by ESI-. The fragment marked in blue in Figure 33 was also detected (m/z = 1198.8), a fragmentation of the C-S bond, a position likely to undergo fragmentation due to the presence of the sulfur heteroatom.

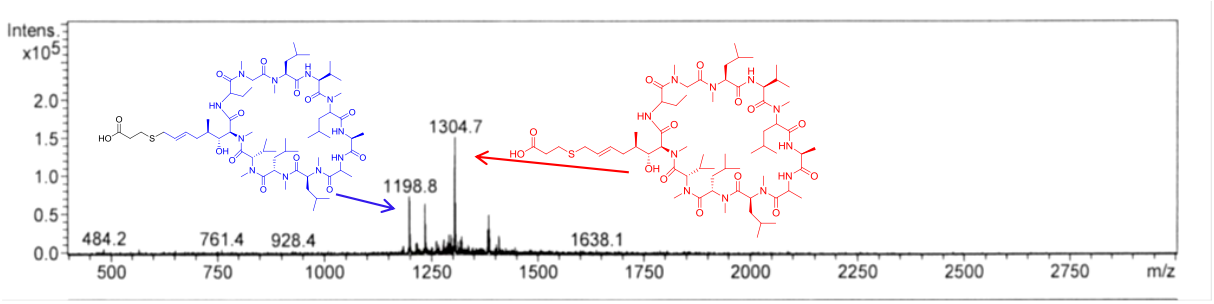
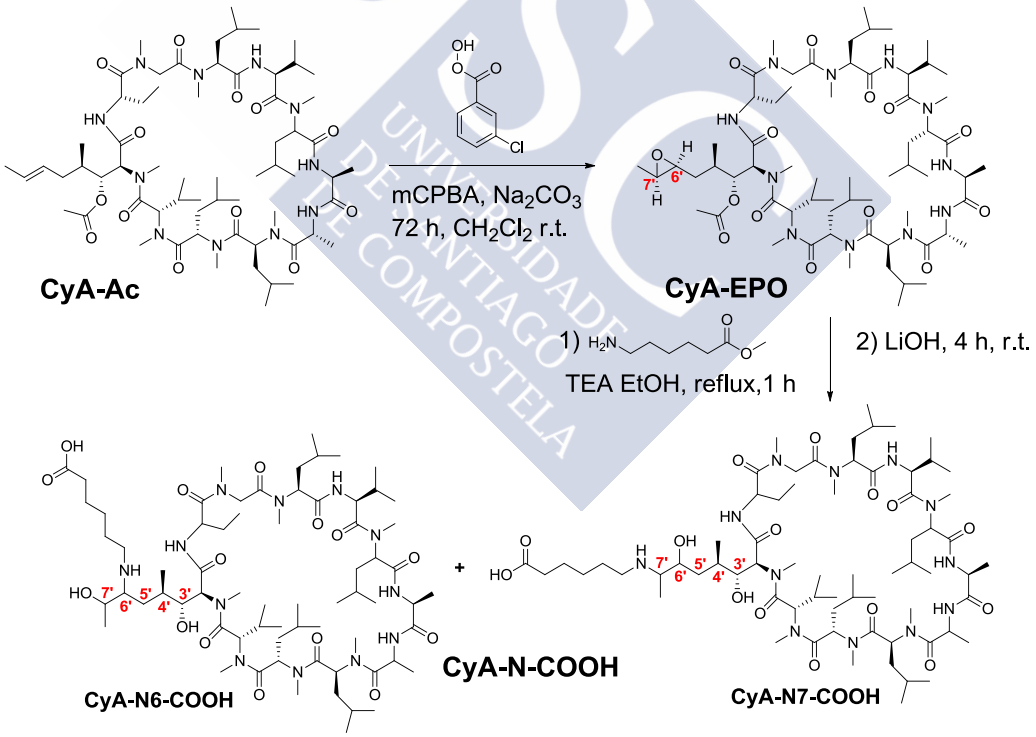


Figure 33. Mass spectrum of CyA-S-COOH recorded in MeOH by electrospray ionization in negative detection mode; m/z: $[M-H]^-$ calculated for $C_{65}H_{114}N_{11}O_{14}S^-$, 1304.8, found 1304.7 (red structure); the fragmentation with a m/z of 1198.8 was also detected (marked in blue).

2.1.3. Route 2, synthesis of CyA-N-COOH



Scheme 15. Synthesis of CyA-N-COOH in two steps starting from CyA-Ac.

The second proposed synthetic route for the preparation of the sought carboxy-cyclosporine A involves oxidation of the C=C bond to yield a reactive epoxide following

similar procedure published by Lu et al. (Scheme 15).[151] The reaction was performed in mild conditions using 3-chloroperoxibenzoic acid (mCPBA) as oxidant agent with Na_2CO_3 in DCM at room temperature. The structure and purity of the product was confirmed by mass spectrometry and NMR. In ^{13}C-NMR the disappearance of the characteristic signals of the double bound at 137.3 and 132.2 ppm (Figure 34, left) and the appearance of the signals at 55.69 and 57.62 ppm (Figure 34, right) of the two C6' and C7' carbons of the epoxide (Scheme 15) confirm the formation of CyA-EPO, that was obtained as a white solid in 78% yield.

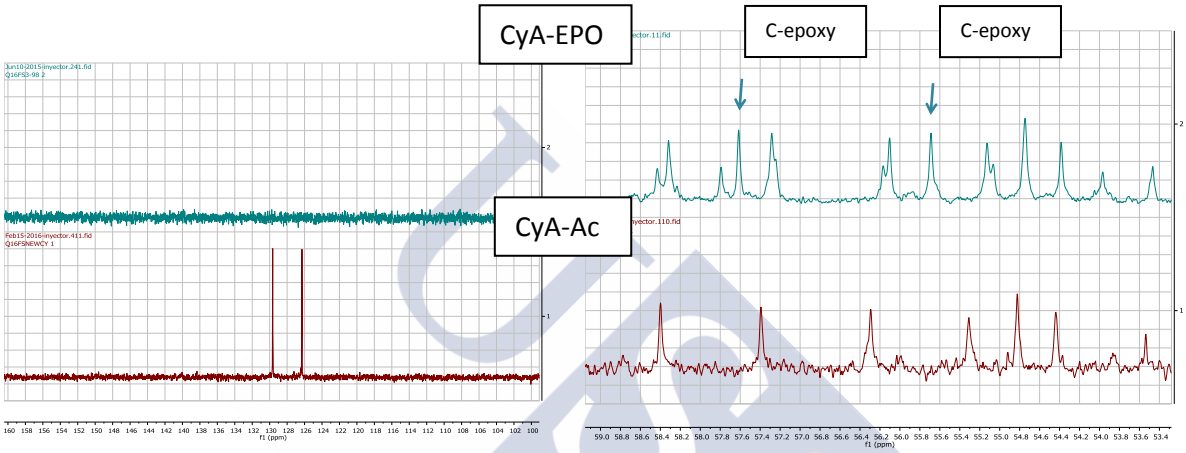


Figure 34. Comparison of the ^{13}C-NMR spectra in $CDCl_3$ of CyA-Ac (brown) and CyA-EPO (green). Left: in the double bond region between 100 and 160 ppm; right between 53 and 60 ppm.

The following step was a S_N2 reaction with an ω-aminoester to open the epoxide. Since the epoxide is similarly substituted, the nucleophilic attack by the amine group may occur on both carbons. The mixture of isomers was isolated by liquid- liquid extraction. CyA-N-ester was obtained as a white solid in 77% yield.

The final step required the alkaline hydrolysis of the ester with LiOH into the desired carboxylic acid. Again, this allowed the simultaneous deprotection of the acylated –OH group. CyA-N-COOH was obtained as a mixture of two regioisomers as shown in Scheme 15, and most of the NMR signals were duplicated.

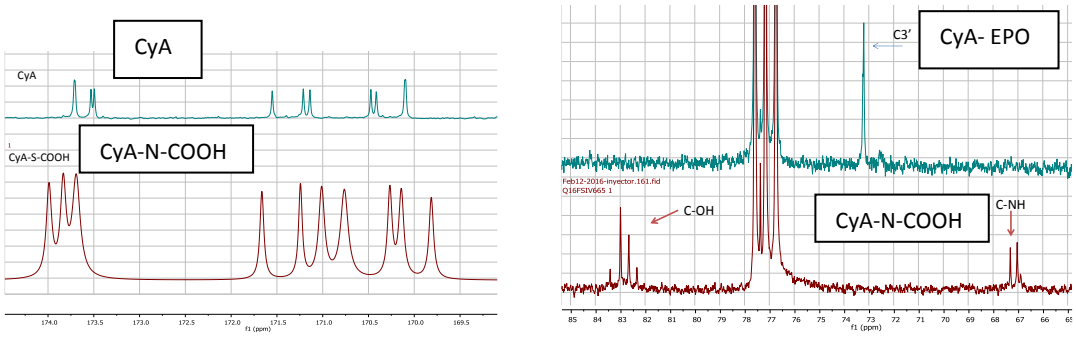


Figure 35. Comparison of ^{13}C-NMR spectra (in $CDCl_3$) for several CyA derivatives. Left: between CyA (green) and CyA-N-COOH (brown) in the 175-169 ppm region. Right: between CyA-EPO (green) and CyA-N-COOH (brown) in the 62-85 ppm range, where the C3' signal of the acylated –OH group of CyA-EPO, and the signal of C-OH and C-NH of CyA-N-COOH can be appreciated.

Due to the presence of the two CyA-N-COOH isomers, assignment of the NMR signals in this case was more complicated. It was not possible to define which of the two isomers of CyA-N-COOH is prevailing. In ^{13}C-NMR some new signals can be assigned as follows: (i) 82.99 and 82.65 ppm to the C–OH group generated upon opening of the epoxide; (ii) 67.31 and 67.03 ppm to the tertiary carbon bound to the C6' nitrogen of CyA-N6-COOH and C7' of CyA-N7-COOH (Scheme 15). The last, toghether with the disappearance of the C-epoxide signals at 55.7 and 57.6 ppm of CyA-EPO, confirm the successful formation of CyA-N-COOH.

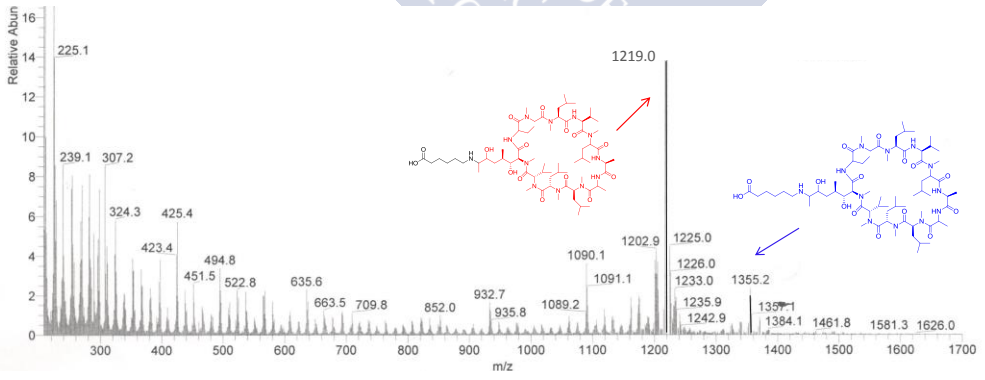


Figure 36. Mass spectrum of CyA-N-COOH by fast atom bombardment ionization in positive mode; m/z $[M + Li]^+$ calculated for $[C_{68}H_{124}LiN_{12}O_{15}]^+$ 1355.9, found 1355.2 (blue structure); the fragment with mass of 1219.0 was also found (red structure).

The main peak observed in mass spectrometry corresponds to the fragment of the red structure in Figure 36: rupture of the C-N bond of the ω-aminoester. The expected

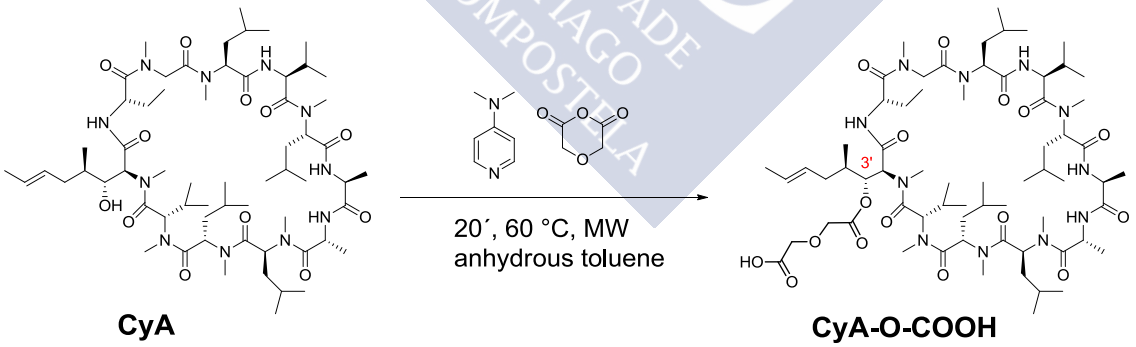
molecular ion at m/z 1355.9 $[C_{68}H_{124}N_{12}O_{15} + Li]^+$ was also observed at 1355.2 (FAB +) (Figure 36).

CyA-N-COOH was obtained as white solid in 81% yield (33% total yield).

2.1.4. Route 3, synthesis of CyA-O-COOH

In this case, taking into account the possibility of acylation of the –OH group of CyA, such as in the case of CyA-Ac (section 2.1.1) we decided to use a cyclic anhydride that, upon reaction with the –OH nucleophile, will yield ring opening and a free carboxylic acid function linked to a spacer (see Scheme 5). The first attempts of acylation with glutaric anhydride using different reaction conditions (i.e. pyridine or toluene as solvent, changing the equivalents of glutaric anhydride, using MW or conventional thermal reaction) did not yield the sought product or only in very few amounts. The low yield of the reaction was probably due to the steric hindrance around the secondary alcohol group.

The reaction was repeated after substituting glutaric anhydride by the more reactive diglycolic anhydride (Scheme 16). A six ring anhyride was selected to obtain a longer spacer and make the –COOH more available for bioconjugation. The reaction follows a typical nucleophilic addition to a carbonyl group which provokes the opening of the ring. In this way, the sought chemical derivatization of CyA with a carboxylic acid group was successfully achieved with very good yield (84%) in only one reaction step.



Scheme 16. Synthesis of CyA-O-COOH using CyA and diglycolic anhydride in the presence of DMAP.

The signal of C3' was found at 71.18 ppm in ^{13}C-NMR in analogy with CyA-Ac. The main peak observed in the mass spectra corresponds to the fragment of the red structure in Figure 37: rupture of the C-O bond. The expected molecular ion at m/z 1318.85 (for

$C_{66}H_{116}N_{11}O_{16}^{+}$, $[M+H]^{+}$) was also found at 1319.28 (FAB +), together with the ion of doubled charge at 663.44 (blue structure in Figure 37).

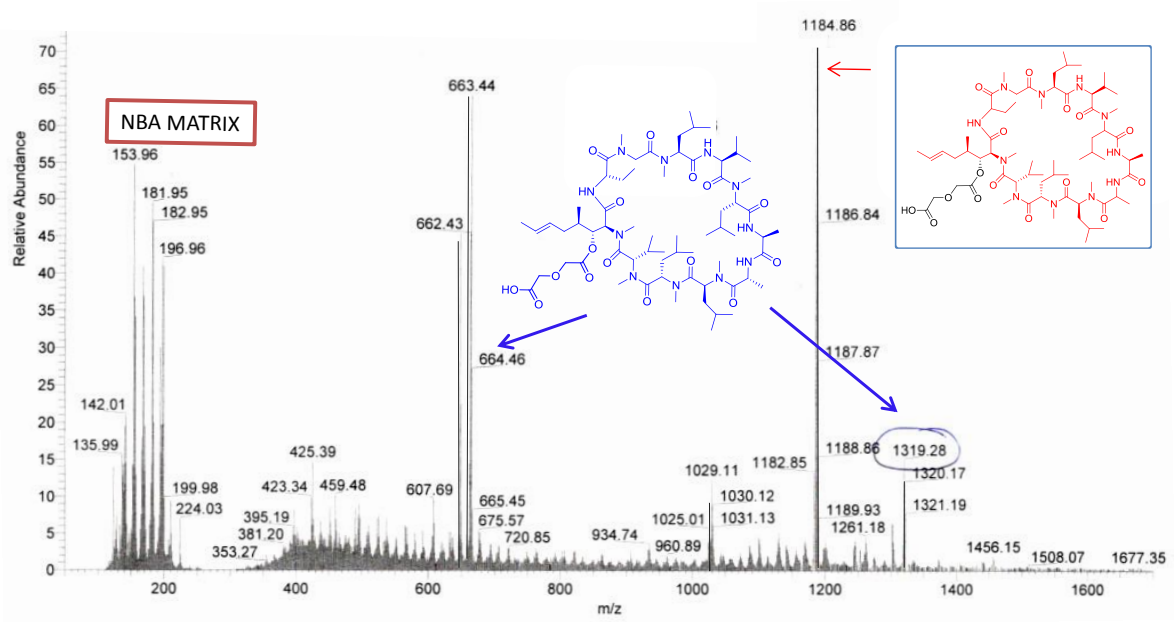
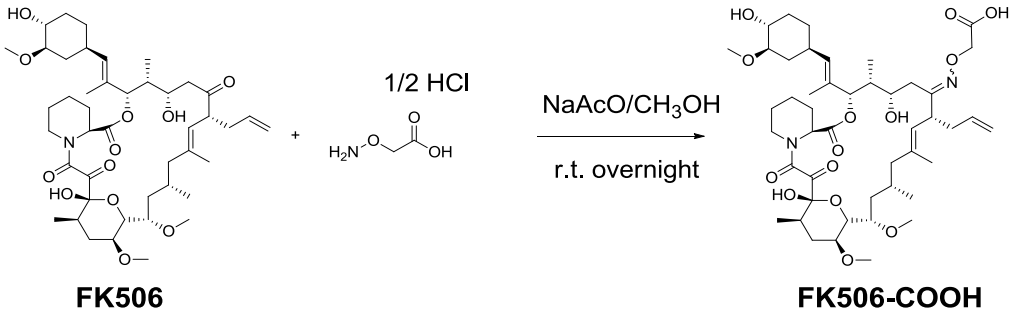


Figure 37. Mass spectrum of CyA-O-COOH by fast atom bombardment ionization in positive mode; m/z $[M+H]^{+}$ calculated for $C_{66}H_{116}N_{11}O_{16}^{+}$ 1318.85, found 1319.28 (blue structure); a fragmentation with a mass of 1184.86 was also observed (red structure).

2.2. Synthesis of a carboxylic derivative of tacrolimus

Tacrolimus (FK506) is a hydrophobic macrolide lactone; it has two positions that can be used for derivatization: the vinyl–$CH=CH_2$ and the carbonyl –C=O groups. The reactions through the vinyl group were discarded because generally they need the presence of a catalyst.[154] The reactivity of the carbonyl group was chosen to prepare the carboxymethoxyloxime derivative of the immunosuppressant, FK506-COOH, following a protocol previously described by O. Cañadas et al. (Scheme 17).[147]

[154] B. M. Dunyak, R. L. Nakamura, A. D. Frankel, J. E. Gestwicki, *ACS Chem. Biol.*, **2015**, *10*, 2441–2447.



Scheme 17. Synthesis of FK506-COOH.

Briefly, FK506 reacts with carboxymethoxylamine hemichlorhydrate in in anhydrous methanol, in the presence of sodium acetate via an addition-elimination reaction to yield the Z/E oxime product. Thus the reaction was performed in mild conditions (room temperature), the purification was rather straightforward (simply by liquid-liquid extraction in mixture water-chloroform) not so laborious and just extraction were needed. Finally the pure product was obtained with a very good yield (> 80%). The compound was confirmed by MS and characterized by NMR.

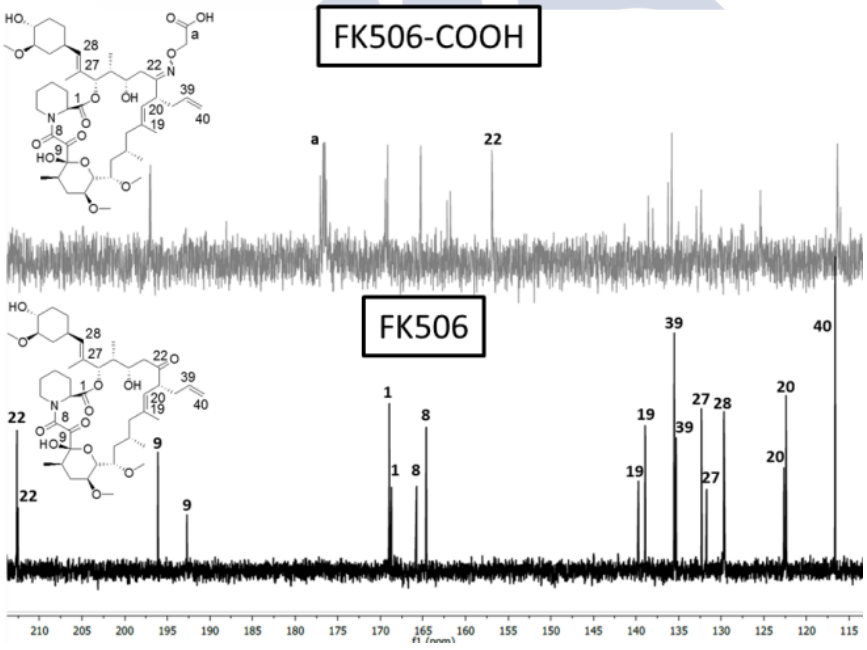


Figure 38. ^{13}C-NMR spectra of FK506-COOH and the starting (commercial) FK506 (75 MHz, in $CDCl_3$). The atom numbering and ^{13}C-NMR assignment for FK506 was from S. Chamni et al.[155]

[155] S. Chamni, Q.-L. He, Y. Dang, S. Bhat, J. O. Liu, D. Romo, *ACS Chem. Biol.* **2011**, *6*, 117–1181.

After FK506 derivatization, the characteristic C=O signals at 212.7 and 212.6 ppm disappear, indicating that functionalization occurs through the carbonyl group at C22. At the same time, a new signal appears in FK506-COOH at 156.9 ppm, typical of an oxime C=N bond. Moreover, the new signal at 177 ppm indicates the presence of the –COOH function (carbon "a", Figure 38). Most signals are multiple because FK506 itself exists as an equilibrium mixture of two isomers in solution.[156]

3. Labeling of immunosuppressants with a NIR fluorescent label

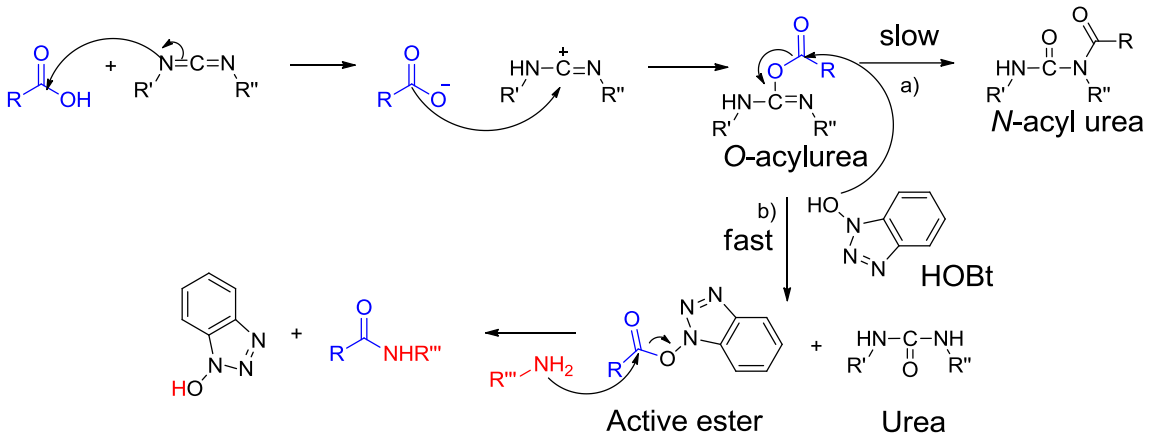
In order to choose an appropriate fluorescent marker for IS labelling we have considered molecules presenting a strong emission in the biological window i.e. 650 to 900 nm, because this spectral region is free from optical interferences as compared to the UV-vis interval. The conjugation of a label to the molecule of interest, in this case, the immunosuppressive drug, is often performed by amide coupling. The amide is a robust functional group which is stable to hydrolysis in a wide pH range.[157]

3.1. Reaction mechanism of amide bond formation mediated by carbodiimides

Since the ISs are carboxylated, the selected fluorescent label has to contain amine functionality for the formation of the amide bond. The carboxylic acid can be activated with carbodiimides. The carbodiimide reacts with the carboxylic acid, to form an *O*-acylurea. This intermediate can then directly react with the amine to yield the desired amide and a urea by-product. However, isolation of the symmetric carboxylic anhydride from the reaction mixture, racemization and acetyl transfer forming the unreactive *N*-acylurea are often observed (Route a, Scheme 18).[158] Alternatively, the coupling agents can be used in the presence of hydroxybenzotriazole (HOBt) and a base like triethylamine (TEA) or 4-dimethylaminopyridine (DMAP) to improve the efficiency of the reaction and avoid the formation of side products. Scheme 18 shows how, in the presence of HOBt, the route b is faster than the undesired competing acyl transfer, yielding the sought activated ester that can then react with the amine and form the corresponding amide bond.

In this Thesis the best results were obtained using 1-ethyl-3-(3-dimethylaminopropyl)carbodiimide (EDC). Additionally, the resulting urea, dimethylaminopropyl-3-ethylurea, is extremely water soluble and can be eliminated by aqueous workup, whereas dicyclohexyl urea, the subproduct formed when using an alternative carbodiimide, DCC (N,N'-dicyclohexylcarbodiimide), must be eliminated by filtration.

[156] H. Tanaka, A. Kuroda, H. Marusawa, H. Hatanaka, T. Kino, T. Goto, M. Hashimoto*, J. Am. Chem. Soc.,* **1987**, *109*, 5031–5033.
[157] K. Prasad, K. Bharathi, B. Haseena–Banu, *Indian J. Pharm. Sci.*, **2011**, *1*, 108–119.
[158] C. A. G. N. Montalbetti, V. Falque, *Tetrahedron*, **2005**, *61*, 10827–10852.



Scheme 18. Mechanism of amide bond formation between a carboxylic acid and primary amine via carbodiimide activation in the presence of HOBt which minimizes the formation of unreactive *N*-acylurea as reported by C. A. G. N. Montalbetti et al.[158]

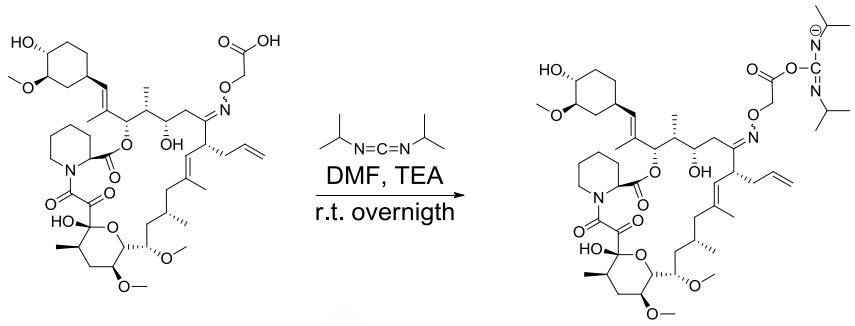
The coupling reaction between the corresponding ISs and the amino fluorescent labels – a commercial dye, Dyomics Dy636-NH_2, and a Nile Blue analogue that was synthesized in our laboratory– was carried out with different coupling agents: DCC/NHS, EDC/HOBt, DCC/HOBt, and PyBOP/HOBt where NHS stands for N-hydroxysuccinimide and PyBOP for (benzotriazol-1-yloxy)tripyrrolidinophosphonium hexafluorophosphate. Fluorescent ISs were obtained with good yield when the Nile Blue analogue (ANB) was used. On the contrary, very low reaction yields were obtained when the commercial label Dy636 was used instead.

As previously mentioned, the method that was finally chosen for the coupling with the ANB was the activation of the IS-COOHs with EDC/HOBt. Conjugation with ANB was then performed with an excess of the dye in DMF or DCM. The crude product was isolated by extraction, using slightly acidic water (pH *ca*. 5) and dichloromethane. For the reaction, DCM is a more convenient solvent because it can be readily eliminated by rotary evaporation. In order to be able to dissolve the cationic dye ANB in DCM, its deprotonation with an excess of a base such as triethylamine (TEA) is required. The protonated form is then regenerated in the acidic conditions used for the extraction.

3.1. Synthesis of FK506-DIC

In order to have a derivative that could be readily immobilized onto an aminated surface or linked to an aminated fluorescent label, an N,N'-diisopropylcarbodiimide derivative of FK506-COOH was prepared and isolated: FK506-DIC . The reaction is a proton exchange between the carboxylic acid and the diisopropylcarbodiimide in DMF with trimethylamine as base at room temperature under argon atmosphere and overnight

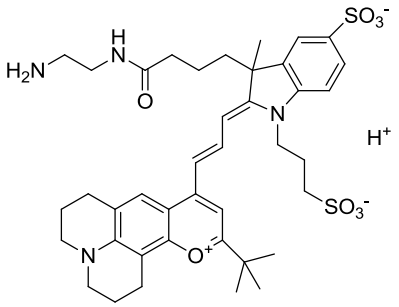
(Scheme 19). The compound was characterized by mass spectrometry (calculated for $[C_{53}H_{85}N_4O_{14}]^-$ 1001.61, found 1001.61 m/z) and stored in the freezer.



Scheme 19. Synthesis of FK506-DIC.

3.2. Labeling of FK506-COOH with Dy636-NH_2

The commercial label, amino-substituted Dy636-NH_2 (Figure 39) was initially proposed as fluorescent tag because of its compatibility with the widespread He-Ne red laser (λ_{em} = 633 nm). The dye displays an absorption maximum at 636 nm and emission at 667 nm in phosphate buffer at pH 7.4, and in ethanol λ_{abs} / λ_{em} values are 637 / 642 nm, meaning that it has a larger Stokes shift in aqueous buffer than in the organic solvent. The normalized absorption and emission spectra for Dy636-NH_2 are shown in Figure 40.



Solvent	λ_{abs} [nm]	λ_{em} [nm]
Ethanol	637	642
PBS 100 mM (pH=7.4)	636	667

Figure 39. Chemical structure of the Dy636-NH_2 dye and its spectroscopic properties (absorption and emission maxima) in EtOH and aq. PBS.

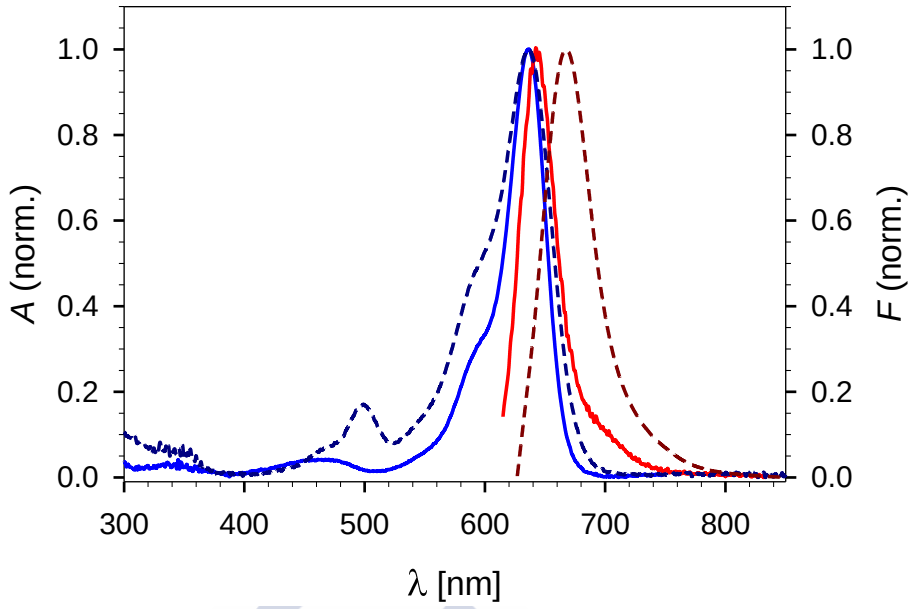
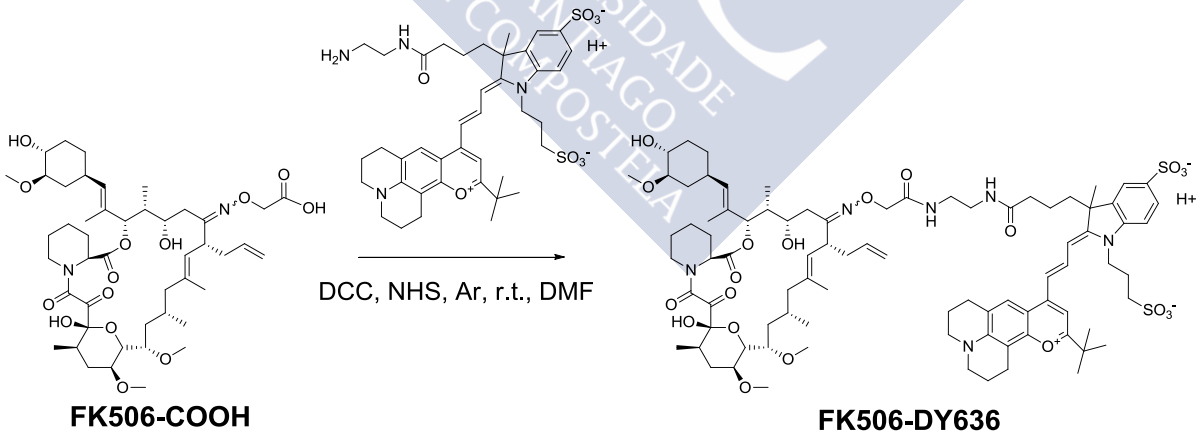


Figure 40. Normalized absorption (blue) and emission (red) spectra of Dy636-NH_2 in ethanol (solid line, λ_{ex} = 610 nm, slits 2-2 nm) and in PBS 100 mM pH 7.4 (dashed line, λ_{ex} = 624 nm, slits 2-2 nm).

The Dy636-NH_2 label was reacted with FK506-COOH following the procedure described in Scheme 20.



Scheme 20. Synthesis of FK506-DY636.

The addition of an excess of the amino reagent is usually essential to displace the chemical equilibrium in a coupling reaction between a carboxylic acid and an amine. In this case, however, this was not feasible due to the high cost of the commercial reactive

dye Dy636-NH_2. Moreover, the purification of the product FK506-Dy636 was very challenging due to the high polarity of the dye. The extraction method was discarded because we could not find a solvents mixture suitable for transferring the product to the organic phase. Recrystallization was not possible with the little amount of FK506-Dy636 available. HPLC was successful but it was a very time and solvent consuming method. Finally reverse phase chromatography using Sephadex® LH20 resin was selected as purification method. The FK506-Dy636 conjugate could only be obtained with a very low reaction yield (<10%). The purified product was characterized by mass spectrometry. The absorption and emission spectra are shown in Figure 41.

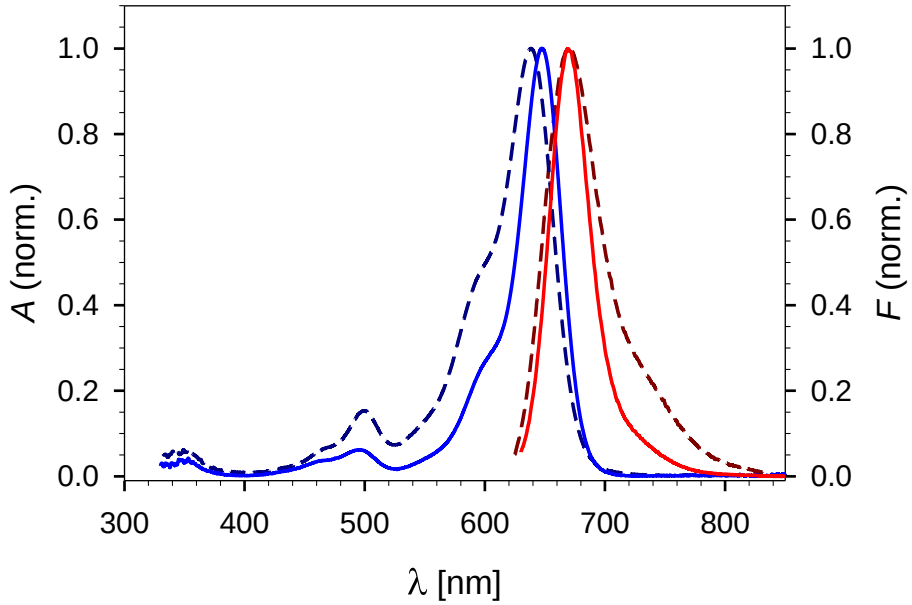


Figure 41. Normalized absorption (blue) and emission (red) spectra of FK506-Dy636 in ethanol (solid lines); and in PBS pH 7.4, 100 mM (dashed lines). λ_{ex} = 624 nm, slits 2-2 nm.

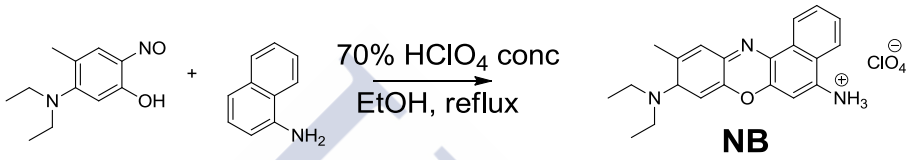
The spectroscopic characteristics of the labeled tacrolimus are very similar to those of the free label. The fluorescence quantum yield of Dy636-NH_2 in ethanol is 0.075 and drops almost to 50% in PBS buffer (Φ_f = 0.039). The weak emission of the dye in aqueous media together with its rather prohibitive price and the low reaction yield for obtaining FK506-Dy636 lead us to discard Dy636-NH_2 as a suitable fluorescent marker for our purposes.

3.3. Labeling of immunosuppressants with Amino Nile Blue

As alternative to Dy636-NH_2, an analogue of the well know dye Nile Blue (NB) (5-amino-9-(diethylamino)-benzo[*a*]phenoxazin-7-ium chloride) was chosen. NB is a positively-

charged phenoxazine system, whit a similar spectral profile (λ_{abs} =630 nm and λ_{em} = 660nm) to that of the Dy636-NH_2 dye, with a fluorescent quantum yield of 27% in ethanol[159] and good water solubility.

The synthesis of benzo[*a*]phenoxazines such as Nile Blue involves the acid-catalyzed condensation of a nitroso compound (5-amino-2-nitrosophenol for NB) and a naphthalene derivative (1-aminonaphthalene for NB) in ethanol with reflux (Scheme 21).[160,161] The majority of the experimental methods reported are straighforward, and considerably good reaction yield can be obtained.



Scheme 21. Synthesis of Nile Blue.

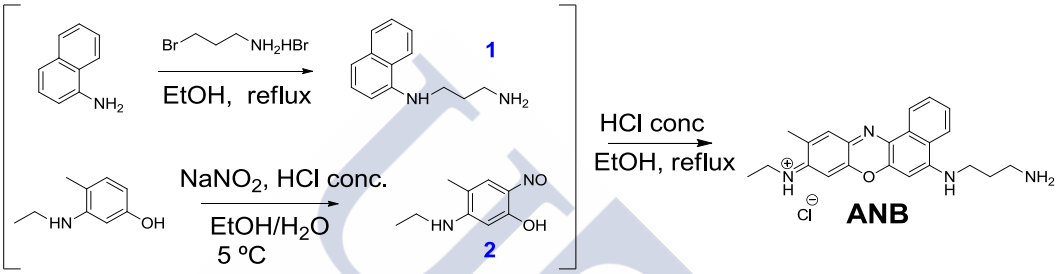
Nile Blue analogues with enhanced water-solubility and/or groups for bioconjugation can be prepared starting from a naphthalene with appropriate N-substituents.[162] A few works have reported the modification of the benzophenoxazine core,[163,164] most of them with the aim of shifting the absorption and emission wavelength to the NIR spectral range.

3.3.1. Synthesis of an alternative NIR label: Amino Nile Blue (ANB)

The chemical structure of Nile Blue itself is not suitable for the conjugation with the carboxylated immunosuppressants because its –NH_2 group is sterically hindered and additionally it is a very poor nucleophile due to its aromatic character and the partial positive charge. Therefore, for introducing a proper –NH_2 substituent in the NB structure, it was necessary to synthetize a sterically accessible primary amino analogue of NB, named Amino Nile Blue (ANB). A similar procedure described by V. H. J. Frade et

[159] H. J. van Staveren, O.C. Speelman, M. J. Witjes, L. Cincotta, W.M. Star, *Photochem. Photobiol.*, **2001**, *73*, 32–38.
[160] M. S. J. Briggs, I. Bruce, J. N. Miller, C. J. Moody, A.C. Simmonds, E. Swann, *J. Chem. Soc.,* **1997**, *7*, 1051–1058.
[161] A. Kanitz, H. Hartmann, *Eur. J. Org. Chem.*, **1999**, 13, 923–930.
[162] V. H. J. Frade, M. Sameiro, T. Gonçalves, J. C. V. P. Moura., *Tetrahedron Lett.*, **2006**, *47*, 8567–8570.
[163] J. Madsen, I. Canton, N. J. Warren, E. Themistou, A. Blanazs, B. Ustbas, X. Tian, R. Pearson, G. Battaglia, A. L. Lewis, Steven P. Armes, *J. Am. Chem. Soc.*, **2013**, *135*, 14863–14870.
[164] B. Wang, J. Fan, X. Wang, H. Zhu, J. Wang, H. Mu, X. Peng, *Chem. Commun.*, **2015**, *5*1, 792–795.

al. was followed.[162] Aminoalkylation of the naphthylamine were carried out in the first place with 3-bromopropylamine. The new added aliphatic $-NH_2$ group is separated from the phenoxazine nucleous by 3 atoms. Since the immunosuppressants are quite bulky, the more sterically available propylamino group in the ANB facilitates the coupling. After nitration of commercially available 3-(ethylamino)-*p*-cresol, the condensation of the two resulting products 1 (N1-(naphthalen-1-yl)propane-1,3-diamine) and 2 (5-(ethylamino)-4-methyl-2-nitrosophenol) of Scheme 22 was carried out in refluxing acidic ethanol yielding a pure ANB in > 60% yield. The NMR results were in agreement with those previously reported.[162]



Scheme 22. Synthesis of propylamino Nile Blue, ANB.

3.3.2. Spectroscopic characterization of Amino Nile Blue (ANB)

Table 4 summarizes the spectroscopic data for the ANB in ethanol, and aqueous buffers such as PBS and HEPES. Absorption and emission spectra are shown in Figure 42. The absorption maxima are centered at 630 nm (ethanol) and 624 nm (aqueous buffers) and the fluorescence bands are centered at 642 nm in ethanol, 650 nm in HEPES and 677 nm in PBS. A bathochromic shift in the emission is observed as the polarity of the solvent increases. ANB has a high molar absorption coefficient, 20282 $cm^{-1}M^{-1}$ in ethanol (as published by Freda et al.) and ca. five-fold larger fluorescent quantum yield in water (Φ_f = 0.18) than Dy636-NH_2. The latter is an important observation, since in spite of the related Nile Blue (NB) dye being a strongly emissive in organic media (Φ_f = 0.27 in ethanol), its fluorescence quantum yield in aqueous solution drops to only 0.01, due to efficient proton transfer from the solvent.[165]

[165]A. Grofcsik, M. Kubinyi, W. J. Jones, *J. Mol. Struct.* **1995**, *348*, 197–200.

Table 4. Spectroscopic characteristic of ANB in ethanol and buffers.

Solvent	λ_{abs} [nm]	λ_{em} [nm]	Φ_f[a]
Ethanol	630	642	0.55
PBS 100 mM (pH =7.4)	624	677	0.18
HEPES 100 mM (pH = 7.0)	624	650	n.d.[b]

[a]Oxazine 170 was used as reference for the determination of the fluorescence quantum yield; [b]Not determined.

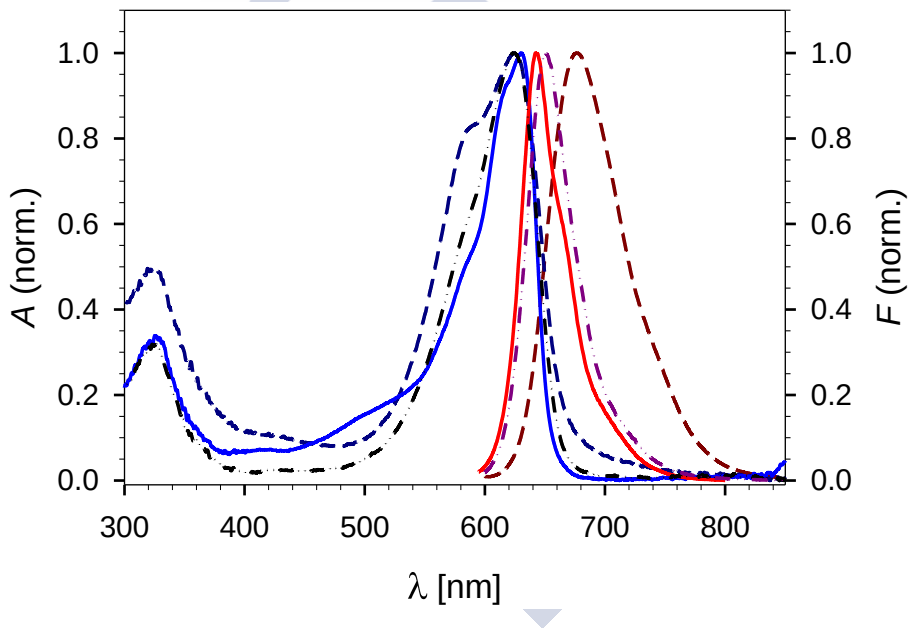


Figure 42. Normalized absorption (blue) and emission (red) of ANB in different solvents (λ_{ex} = 561 nm, slits 5-5 nm): in PBS 100 mM pH 7.4 (dashed line), in ethanol (solid line) and in HEPES 100 mM pH 7.0 (dash-dot line).

Photostability studies with ANB. The photostability of ANB was evaluated using the cyanine 7 dye (Cy7) for comparison because it shows a similar spectral profile (λ_{abs} = 650 nm in EtOH) to that of ANB (λ_{abs} = 630 nm in EtOH). The absorption at of the dyes at the excitation wavelength (635 nm) was adjusted to the same value (0.12, Figure 43, left) in order to have the same optical density.

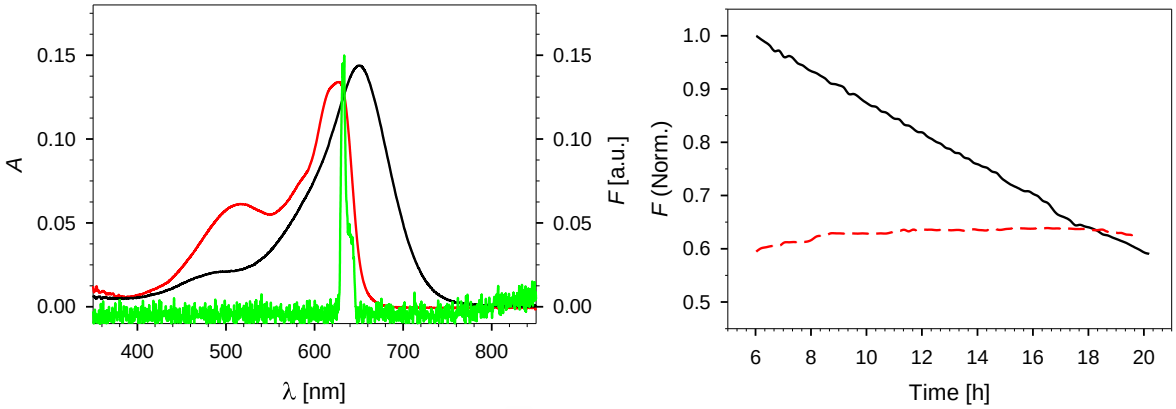


Figure 43. Left: absorption spectra of ANB (red) and Cy7 (black) in ethanol. In green the normalized emission spectrum of the red laser diode (λ_{em} =635 nm, 5mW, Picotronic) used for irradiation. Right: Changes in the emission intensity of ANB (red) and Cy7 (black) in function of irradiation time.

Monitoring was performed with a fiber-optic Maya® Pro Spectrometer (Ocean Optics). Maya® is able to calculate the area under the emission curve, as a function of the illumination time. A 5-mW 635-nm red laser diode from Picotronic was used as excitation source. The laser was connected to the cuvette holder with a homemade piece built with a Velleman 3D printer. The emitted light from the sample is collected at 90° with a fiber optic that is connected to the Maya® detector (Figure 44). The dyes were irradiated for 20 h. The emission intensity was recorded every 10 min during the experiment (Figure 43, right). Emission spectra before and after the irradiation were also collected (Figure 45).

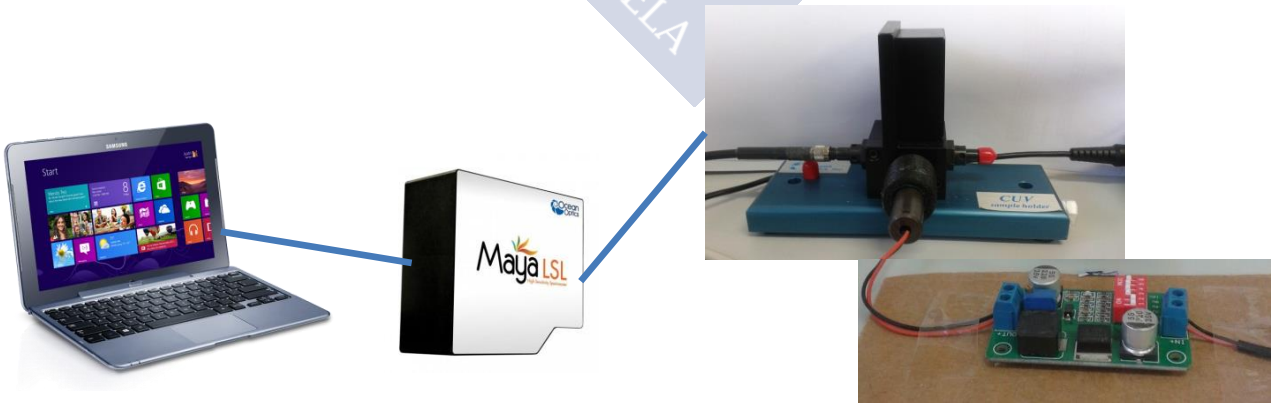


Figure 44. Picture of the setup for the photostability test. From right to left: DC/DC power supply of the laser diode; the laser is attached to the cuvette holder; an optical fiber connects the sample cell and the Maya® detector. The detector is powered from the USB port of a laptop computer running the Ocean Optics Spectrasuite® for the instrument control and data collection.

As it is shown in Figure 45 and Figure 43, Cy7 undergoes quick photodegradation under irradiation: there is a significant decrease of the emission intensity and also a slight modification in the band shape after a few hours. Afetr the 20 h of illumination, the emission intensity of Cy7 had decreased 44% while that of ANB decreased only 0.03% of the initial emission. Amino Nile Blue shows outstanding photostability, and it could be used repeatedly as fluorescent label without losing its sensitivity.

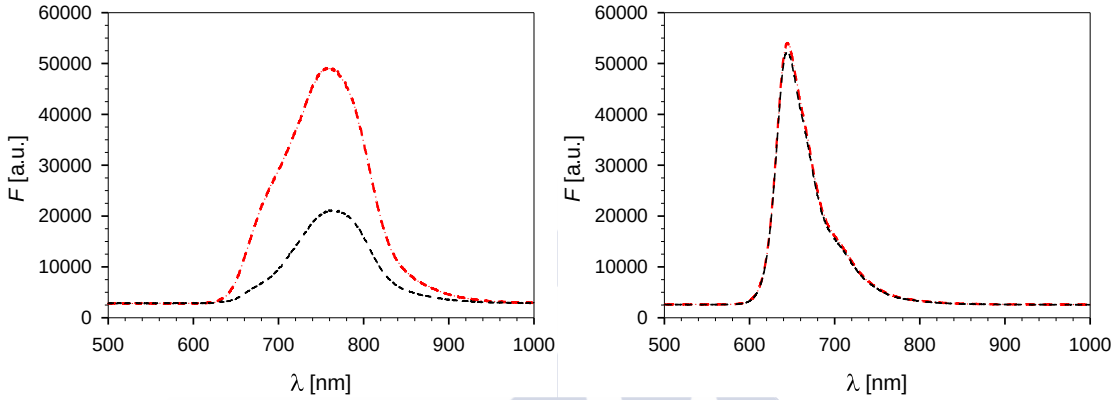
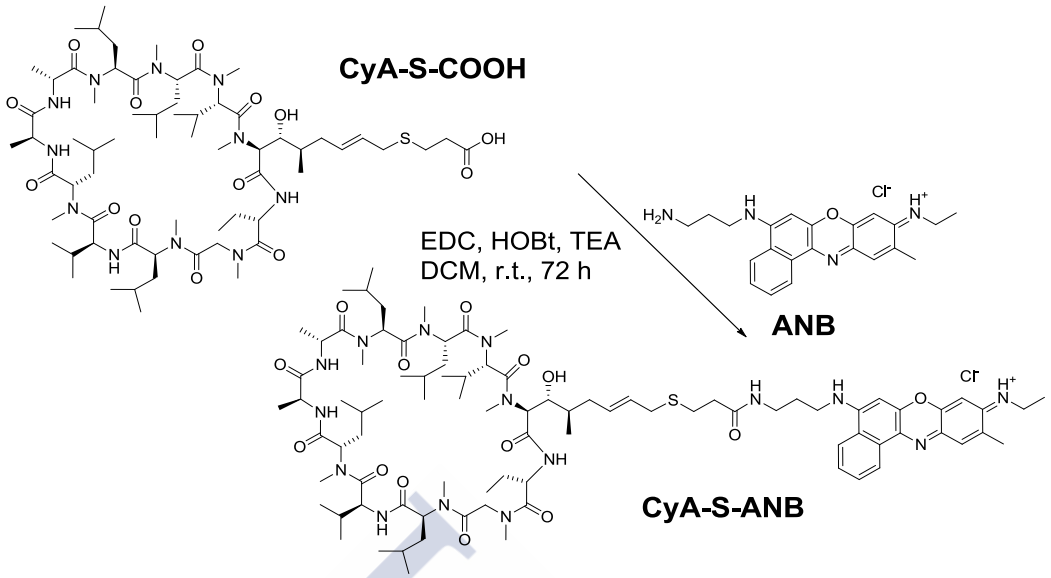


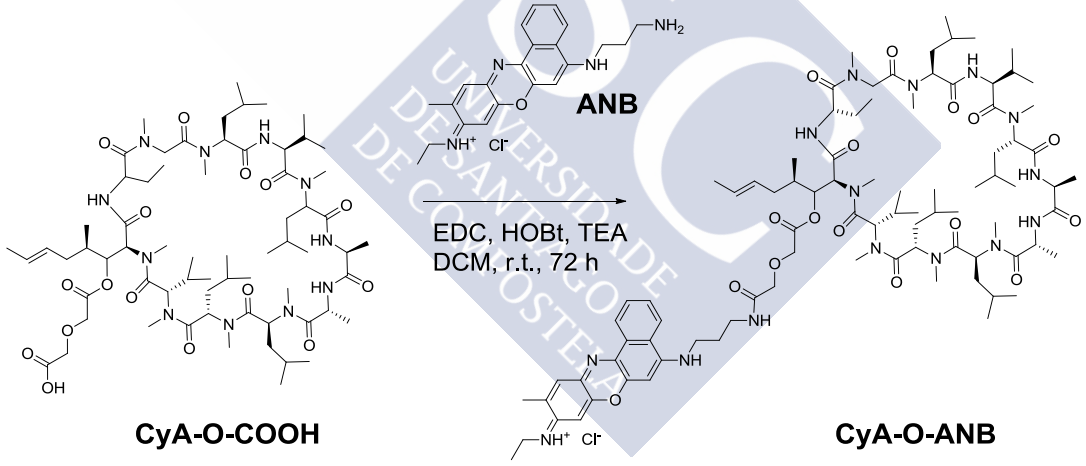
Figure 45. Evolution of the emission spectra of ANB (right) and Cy7 (left) in ethanol before (black line) and after (red line) 20 h of irradiation (λ_{em} =635 nm).

3.3.3. Coupling of CyA-COOH with Amino Nile Blue

CyA-O-COOH (Scheme 24) and CyA-S-COOH (Scheme 23) were also conjugated to ANB. The coupling reaction between CyA-X-COOH (where X is S or O) and ANB was carried out following the method described in section 3.1. The coupling agents EDC/HOBt were used to form an amide bond between the carboxylic group of the CyA derivatives and the ω-amine group of ANB. DCM was used as solvent and TEA was added to dissolve the cationic dye ANB. The reaction was stirred at room temperature under argon during 72 h. After this time, the crude product was examined by TCL and reveled with bromocresol green for the detection of carboxylic acids: no -COOH was detected. The conjugates were purified by extraction with slightly acidic water and then with brine and dichloromethane obtaining the pure product in > 55% yield in both cases.



Scheme 23. Synthesis of the fluorescent CyA-S-ANB derivative.



Scheme 24. Synthesis of the fluorescent CyA-O-ANB derivative.

The fluorescent CyA-S-ANB and CyA-O-ANB were characterized by mass spectrometry, ^{13}C-NMR, ^{1}H-NMR and UV-Vis spectroscopies.

In case of CyA-S-ANB, the ^{13}C-NMR (176 MHz) signals were very weak, due to the low quantity of product available and its high molecular weight. It was not possible to identify the new amide bond resulting from the coupling between CyA-S-COOH and ANB. However, the 175 to 169 ppm reveals differences in the signal shifts compared to the

starting carboxylic acid, and between 130 and 100 ppm it is possible to appreciate the signals corresponding to the aromatic carbons of ANB.

The ^{13}C-NMR of CyA-O-ANB was made in deuterated benzene with the aim of improving the resolution with respect to CyA-S-ANB. In this case, again, it was very difficult to notice the presence of a new amide group. The multitude of C=O groups in this molecule complicates the proper identification and sometimes the signals even overlapped.

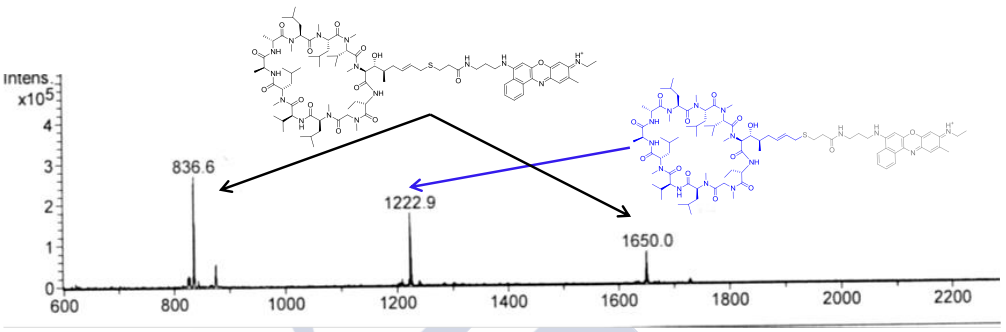


Figure 46. Mass spectrum of CyA-S-ANB by electrospray ionization in positive detection mode; $[M]^+$ calculated for $[C_{87}H_{138}N_{15}O_{14}S]^+$ 1650.2 found 1650.0, and doubly charged ion at 836.6 m/z (black structure). The peak at m/z 1222.9 corresponds to the blue fragment.

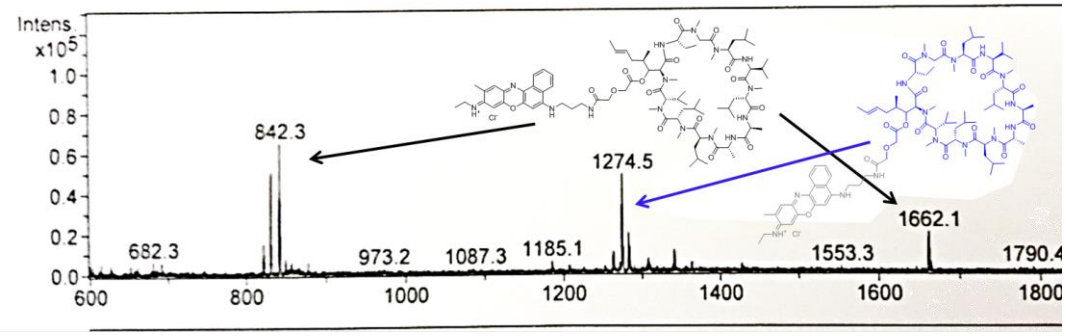
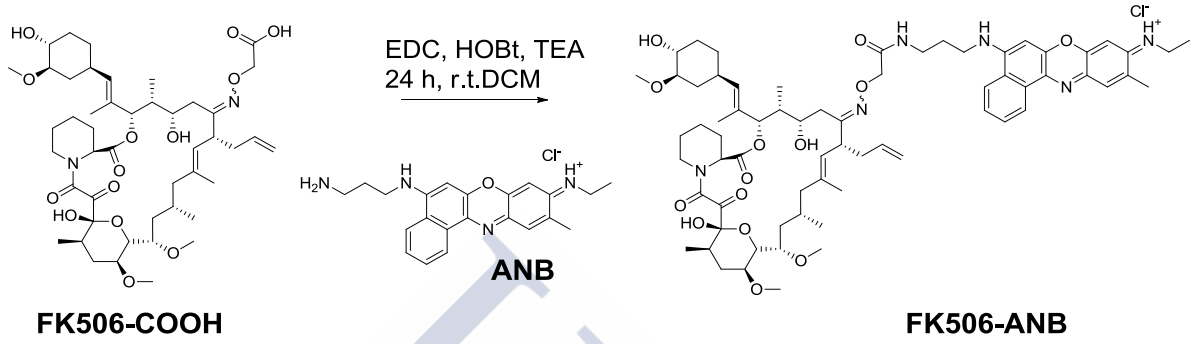


Figure 47. Mass spectrum of CyA-O-ANB by electrospray ionization in positive detection mode; m/z $[M]^+$ calculated for $[C_{88}H_{138}N_{15}O_{16}]^+$ 1662.1, found 1662.1, and the doubly charged ion at 842.5 m/z (black structure) The peak at m/z 1274.5 corresponds to the blue fragment.

In this regard, the characterization by MS was essential. CyA-S-ANB and CyA-O-ANB were analyzed by ESI and FAB. For both compounds, in the ESI (+) spectrum the main peak observed arises from the doubly charged ions at 836.6 m/z for CyA-S-ANB (Figure 46) and 842.3 m/z for CyA-O-ANB (Figure 47). It is also possible to observe

fragmentations corresponding to the structures marked in blue in Figure 46 and 21. The expected molecular ions for $[M]^+$: $[C_{87}H_{138}N_{15}O_{14}S]^+$ and $[C_{88}H_{138}N_{15}O_{16}]^+$ were also found at 1650.0 m/z (CyA-S-ANB) and 1662.1 m/z (CyA-O-ANB), respectively.

3.3.4. Coupling of FK506-COOH with Amino Nile Blue



Scheme 25. Conjugation of FK56-COOH to ANB.

FK506-COOH was also conjugated to ANB following the same method described for CyA-X-COOH (Scheme 25): EDC/HOBt were used as activating agents, TEA as base and DCM as solvent. The product FK506-ANB was obtained with a remarkable yield of >80%. The fluorescent immunosuppressive derivative was characterized by UV-Vis absorption and fluorescence spectroscopies.

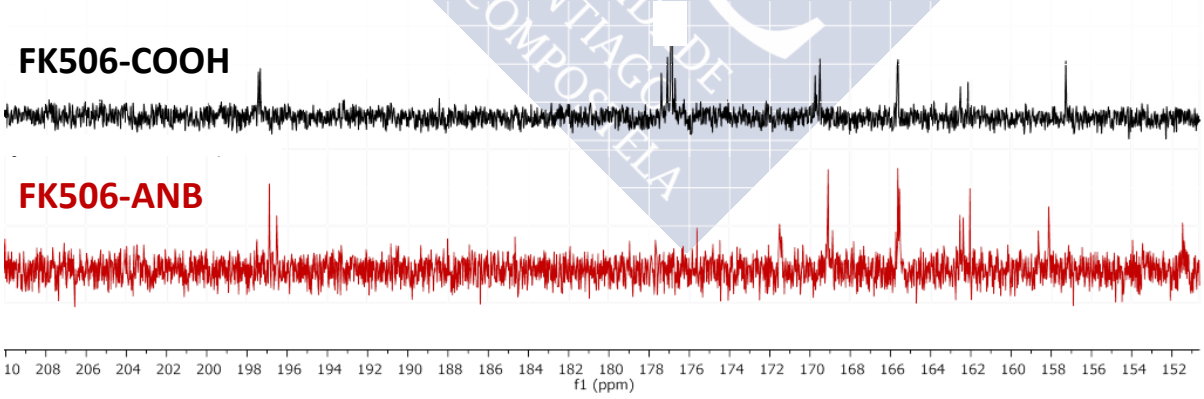


Figure 48. Comparison between ^{13}C-NMR spectra of FK506-COOH (black) and FK506-ANB the starting (commercial) FK506 (176 MHz, in $CDCl_3$).

After ANB labeling, the characteristic signals at 177 ppm of the –COOH function disappear, indicating an effective coupling between ANB and FK506-COOH. At the same

time, a new signal appears at 171.51 ppm for FK506-ANB, corresponding to the new C=O amide group (Figure 48). As in the case of FK506-COOH most signals are multiple.

In the mass spectrometry (ESI+) the peak corresponding to $[M]^+$ was found (Figure 49).

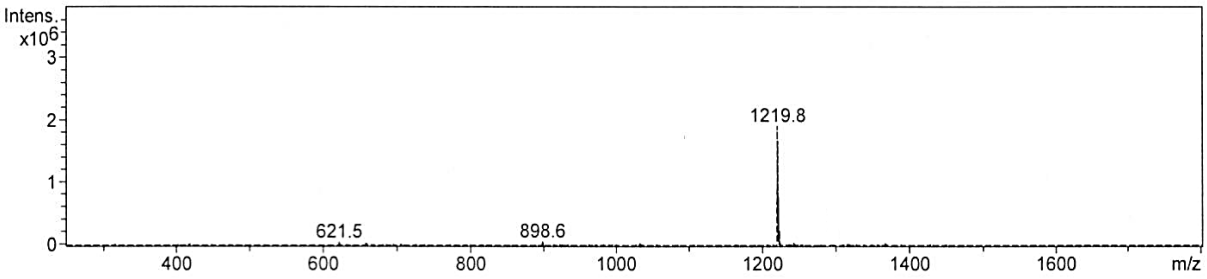
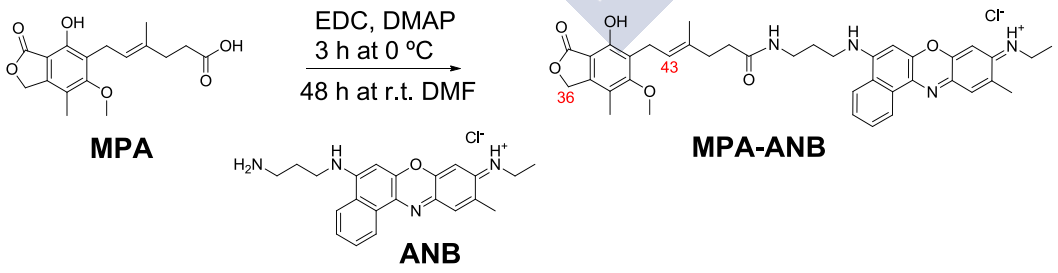


Figure 49. Mass spectrum of FK506-ANB by electrospray ionization in positive detection mode; m/z $[M]^+$ calculated for $[C_{68}H_{95}N_6O_{14}]^+$ 1219.7, found 1219.8.

3.3.5. Coupling of MPA to Amino Nile Blue

The conjugation reaction between MPA and ANB was optimized by testing three different synthetic conditions: a) using EDC in the presence of DMAP (Scheme 26); b) with EDC/HOBt and DMPA, or c) using acetyl chloride, KOH and TEA. In the case c) many subproducts were formed and the method was discarded. Both reactions performed with EDC provided good yields. Finally method a) was chosen for the conjugation.[166] The crude product was isolated by liquid-liquid extraction with H_2O and dichloromethane (yield > 80 %).



Scheme 26. Synthesis of MPA-ANB.

[166] D. Iwaszkiewicz-Grzes G. Cholewinski, A. Kot–Wasik, P. Trzonkowski , K. Dzierzbicka., *Eur. J. Med. Chem.*, **2013**, *69*, 863–871.

The fluorescent MPA-ANB conjugate was characterized by ^{1}H-NMR, mass spectrometry and UV-Vis and fluorescence spectroscopies (λ_{abs} / λ_{em} = 630 / 655 nm in phosphate buffer, pH 7.4) (Figure 51, right). The fluorescence quantum yield was also determined. The ^{1}H-NMR was performed in deuterated methanol, where the aromatic signals of the ANB chromophore can be observed. Around 5 ppm the signals corresponding to protons in the C36 and C43 (Scheme 26) can be found. The [M$^+$] detected by MS (ESI+) confirmed the formation of the conjugate (see annex part).

3.3.6. Comparison of the spectroscopy data of the different immunosuppressants labeled with ANB

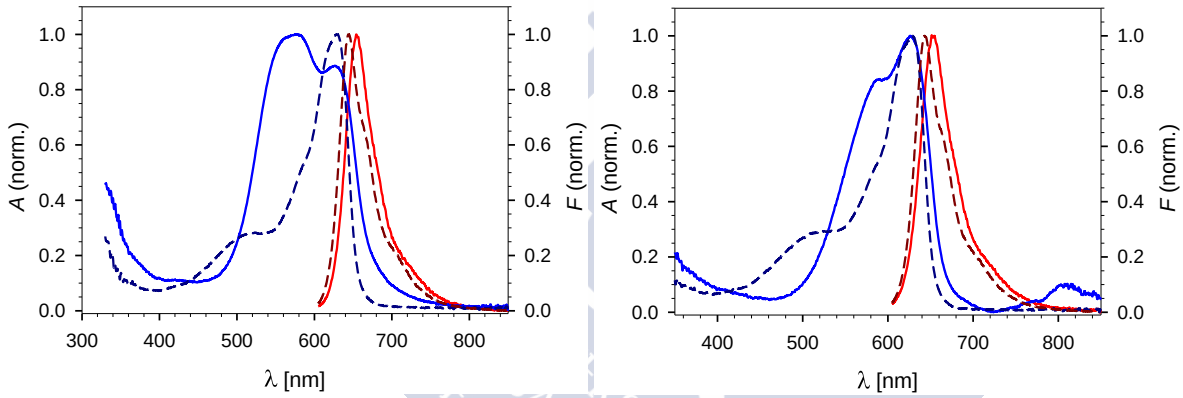


Figure 50. Normalized absorption (blue) and emission (red) spectra for CyA- S-ANB (left) and of CyA-O-ANB (right) in ethanol (dashed line) and in PBS pH 7.4, 100 mM (solid line), λ_{ex} = 600 nm.

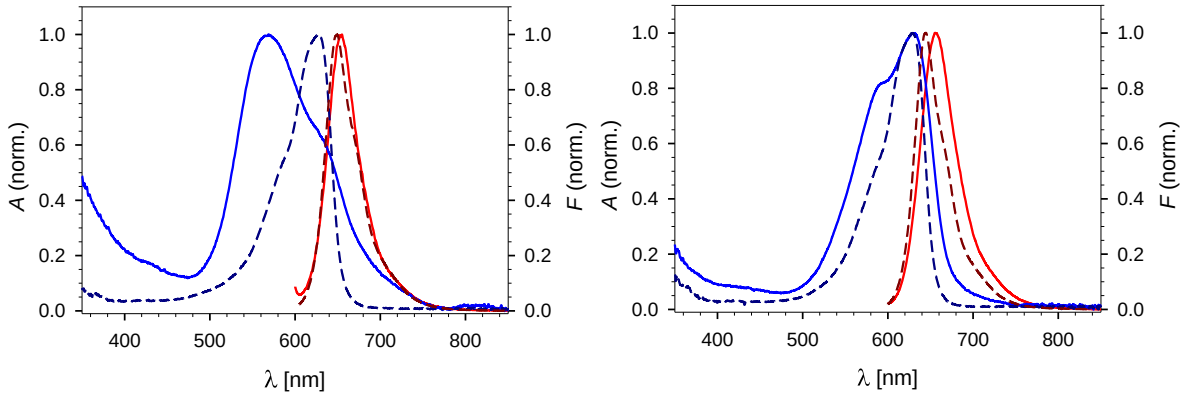


Figure 51. Normalized absorption (blue) and emission (red) spectra for FK506-ANB (left) and MPA-ANB (right) in ethanol (dashed line) and PBS pH = 7.4, 100 mM (solid line), λ_{ex} = 590 nm.

Absorption and emission spectra of the labeled immunosuppressants (ISs-ANB) are shown on Figure 51 and Figure 51, in both, organic media (ethanol) and 100% aqueous phosphate buffer solution at physiological pH. The absorption and emission maxima are summarized in Table 5 together with the values of the fluorescence lifetimes. The characterization in phosphate buffer of the labeled ISs was also studied because it is the best medium that simulates the physiological conditions. The results obtained for the labeled ISs are in agreement to those obtained for the free ANB label (Table 5). This implies that the optical properties of ANB are not importantly modified upon conjugation to the ISs. Absorption and emission maxima of ISs-ANB remain centered at ca. 630 and 645 nm in EtOH, respectively. The shape of the normalized absorption and emission spectra of ISs-ANB in both solvents displays a good match indicating that the fluorescent label is not prone to aggregation in water at micromolar concentrations. Good solubility is an important feature for performing reproducible bioassays in aqueous media, since NIR dyes are normally large, planar, hydrophobic molecules prone to aggregation in water (see introduction). Exceptions are the absorption of CyA-S-ANB and FK506-ANB in PBS. In the case of the fluorescent cyclosporine, the absorption spectrum shows a maximum at ca. 550 nm, with a shoulder at the expected 640 nm. For the FK506-ANB the ratio between the intensity of the absorption band at 550/640 nm in PBS media is even higher than in the case of CyA-S-ANB. The band at 550 nm is indicative of a shift in the protonation/deprotonation equilibrium of ANB toward the deprotonated (neutral) form. It can be stressed that in the absorption spectrum of CyA-S-ANB in PBS the equilibrium between the protonated and deprotonated form of the ANB is shifted towards the deprotonated one; whereas in this case of labeled tacrolimus the neutral form of ANB prevails. This behavior must be related to the local environment around the fluorescent tag in those two cases.[167] Probably, the deprotonated form of ANB is stabilized in aqueous solution when encapsulated inside the hydrophobic cycle of the immunosuppressant. Nevertheless this behavior does not affect the emission properties of all the ISs because they have the same emission maximum, something very important for the application of the labeled ISs.

[167] J. Madsen, I. Canton, N. J. Warren, E. Themistou, A. Blanazs, B. Ustbas, X. Tian, R. Pearson, G. Battaglia, A. L. Lewis, S. P. Armes, *J. Am. Chem. Soc.,* **2013**, *135*, 14863–14870.

Table 5. Maxima of absorption and emission and fluorescence lifetimes in ethanol and PBS of the labeled immunosuppressants and comparison with the free ANB fluorophore.

	Ethanol			*PBS pH 7.4, 100 mM*		
Compound	λ_{abs} [nm]	λ_{em} [nm]	τ [ns][a]	λ_{abs} [nm]	λ_{em} [nm]	τ [ns] [a]
ANB	625	641	3.60	627	641	2.14
FK506-ANB	627	646	3.57	*569*	655	2.59
MPA-ANB	629	646	3.24	630	655	1.90
CyA-O-ANB	629	643	3.58	626	652	2.38
CyA-S-ANB	630	644	3.61	*579*	654	2.65

[a]The goodness-of-the-fit (χ^2) is always ≤ 1.4 and the uncertainty of the τ values is 2%.

The emission quantum yield for the MPA-ANB was also measured, its value is remarkable in ethanol solution (Φ_f = 0.48 ± 0.05) and somewhat lower in aqueous PBS (Φ_f = 0.16 ± 0.02), yet the fluorescence is still strong enough to allow a sensitive detection (i.e. in bioanalytical applications). The results obtained for MPA-ANB are in agreement with those of ANB (see section 3.3.2) this is another evidence that the properties of ANB are not modified when it is conjugated whit ISs.

Also in the case of fluorescence lifetime, considering the uncertainty of the τ values (2%), the values acquired for the ANB-labeled immunosuppressants comply with those of the free ANB (Table 5). Figure 52 shows the fluorescence decay for FK506-ANB, it can be observed that in water PBS buffer the fluorescence decay is accelerated (shorter fluorescence lifetime in water than in ethanol).

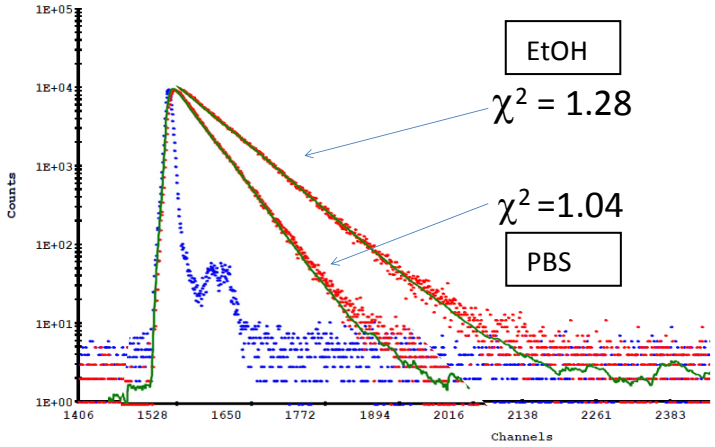


Figure 52. Decay of FK506-ANB in ethanol (large, χ^2 = 1.28) and in PBS pH7.4, 100 mM, (short, χ^2 = 1.04). Excitation with Horiba NanoLED-635L laser diode, peak at 640-nm (250-ps pulses, slit 1 nm) λ_{em} = 665 nm.

4. Binding analysis of IS-ANB labels with Human Serum Albumin with fluorescence polarization

4.1. Free fraction of ISs

The free drug concentration is the quantity of the drug that is not bound to proteins in the body. In the case of ISs, the free fraction is the one able of crossing the plasma membrane and binding the corresponding receptor, having a therapeutic effect. Therefore, the ISs free fraction provides a better correlation with the clinical efficacy of the drug.[168] As already described in the Introduction part, one of the main complications, when analyzing ISs in a blood sample, is the high tendency of these drugs to bind plasma protein, such as the Human Serum Albumin (HSA).[169] The free drug concentration is better quantified as the "free fraction" of a drug or "α", and represents the relationship between the free and total drug concentrations (Eq. 1).

$$\alpha = {}^{\text{free drug concentration}}/_{\text{total drug concentration}} \qquad (1)$$

The total drug concentration is the bound plus the free drug concentration. The free fraction α does not vary with the total drug concentration because the protein-binding sites usually exceed the number of drug molecules present.

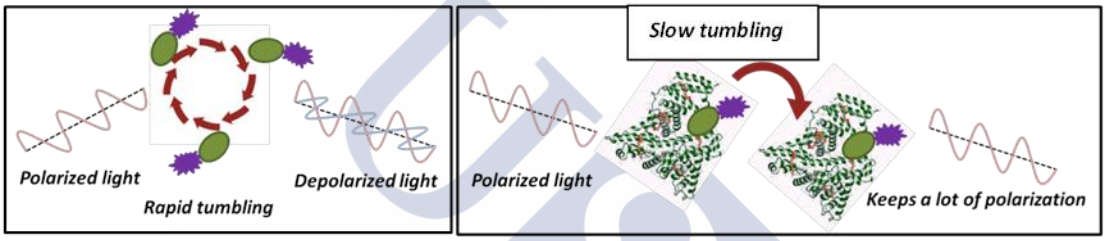
Normally in therapeutic drug monitoring, the free fraction is not taken into consideration because of the technical difficulties to find a routine procedure in clinical

[168] T. Bohnert, L. S. Gan, *J. Pharm. Sci.*, **2013**, *102*, 2953-2994.
[169] D. M. Jameson, J. A. Ross, *Chem. Rev.*, **2010**, *110*, 2685–2708.

laboratories for its determination.[170] However, it is proved that, there is a significant difference in the free fraction of ISs between stable transplant recipients and those experiencing rejection. Despite no statistically significant, a difference is usually observed in trough blood ISs concentration. These findings suggest the need for monitoring unbound concentration of immunosuppressants over the post-transplantation phase.[171]

Here we suggest the use of fluorescent polarization-based techniques for the estimation of ISs free fraction levels. These measurements can be employed for monitoring binding of a small molecule (the IS) to a macromolecule (a protein) as explained in Section 4.2.

4.2. Fluorescence polarization technique



Scheme 27. Comparison between the rotational diffusion rate of a free small fluorophore (left) and when the fluorophore is bound to a macromolecule (right) and the influence in the degree of polarization of the emitted light when excited with polarized radiation. When the dye is free to rotate in solution, its fluorescence polarization is close to zero (left). However, FP increases when the dye is bound to a large macromolecule such as a protein that greatly slows down its rotation (right).

A free fluorescent labeled molecule (in the absence of proteins), exited with polarized light, will emit a strongly depolarized light because its rotational diffusion rate is high, and the molecule rotates before emission of a photon. However if the small fluorophore is bound to a molecule of a high molecular weight (typically >10 kDa), its rate of rotation decreases and the polarization of the radiation used for excitation is preserved in the emission. The degree of polarization is inversely proportional to the rate of molecular rotation. Therefore fluorescence polarization provides a basis for binding assays examining the interactions of a small labeled ligand with a larger protein, with the advantage (vs methods based on intensity of fluorescence changes) that the signal output is independent of dye concentration, dye photobleaching or fluctuation of intensity of excitation light.

[170] A. Dasgupta, *Clin. Chim. Acta*, **2007**, *377*, 1–13.
[171] H. Zahir, A. J. McLachlan, A. Nelson, G. McCaughan, M. Gleeson, F. Akhlaghi, *Ther. Drug. Monit.*, **2005**, *27*, 422–430.

The advantages of FP technique are manifold, small amount of reagents are needed and the assays based on FP are very reproducible. One of the most useful advantages is that it does not require the physical separation between bound and free ligand,**Errore. Il segnalibro non è definito.** and with this, washing steps are not necessary. In his first studies in 1952 D. J. R. Laurence demonstrated that a binding isotherm could be obtained without separation of the free and bound components.[172] In fact, FP permits acquisition of data under conditions of thermodynamic equilibrium without the need of using separation techniques such as ultrafiltration, chromatography sedimentation or centrifugation.

4.3. How to obtain the free fraction α from the dissociation constant K_D

Here the ANB labeled immunosuppressants were employed to study the interaction between the drugs and the Human Serum Albumin (HSA) taking advantage of the fluorescence polarization (FP) technique. The dissociation constant K_D and the free fraction α for each IS will be obtained.

In the next section (4.5) it is shown in more detail how the concentration of the free drugs can be determined. Here for simplicity it is shown just how to calculate the free fraction for cyclosporine A, but the same stating can be made for the others immunosuppressants (or drugs in general) examined in this thesis: tacrolimus and mycophenolic acid and of course for the labeled ISs (ISs-ANB).

$$\mathrm{CyA} + \mathrm{HSA} \rightleftarrows \mathrm{CyAHSA} \tag{2}$$

The latter (Equation 2) is the equilibrium which describes the interaction between the cyclosporine A, the ISs, and the protein HSA. Here the equilibrium dissociation constant is chosen to describe the affinity between the immunosuppressant CyA and the HSA.

$$K_D = \frac{[\mathrm{CyA}][\mathrm{HSA}]}{[\mathrm{CyAHSA}]} \tag{3}$$

In Equation 3 concentrations refer, of course, to the free concentrations of CyA and HSA, but as they associate to form CyAHSA, their free concentrations must decrease. If the concentration of one reactant massively exceeds that of the other (HSA >> CyA), their association will significantly affect the free concentration of only the less concentrated reactant (CyA in this case). It can be assumed that the HSA concentration after the formation of CyAHSA is not changed. This latter sentence implies that

$$[\mathrm{CyA}]_{\mathrm{free}} = [\mathrm{CyA}]_{\mathrm{tot}} - [\mathrm{CyAHSA}] \tag{4}$$

And consequently Equation 4 can be rearranged as:

[172] D. J. R., Laurence, *Biochem. J.*, **1952**, *51*, 168–172.

$$K_D = \frac{([\mathrm{CyA}]_{\mathrm{tot}} - [\mathrm{CyAHSA}])[HSA]}{[\mathrm{CyAHSA}]} \quad (5)$$

$$[\mathrm{CyA}]_{\mathrm{tot}} - [\mathrm{CyAHSA}] = \frac{K_D\,[CyAHSA]}{[HSA]} \quad (6)$$

Substituting Equation (4) in Equation (6) it is possible to calculate the free concentration of the immunosuppressant drug:

$$[\mathrm{CyA}]_{\mathrm{free}} = \frac{K_D\,[CyAHSA]}{[HSA]} \quad (7)$$

Equation (6) can also be expressed as follow:

$$[\mathrm{CyA}]_{\mathrm{tot}} = [\mathrm{CyAHSA}] + \left(\frac{K_D\,[CyAHSA]}{[HSA]}\right) \quad (8)$$

Equation (8) is equivalent to:

$$[\mathrm{CyA}]_{\mathrm{tot}} = \frac{[CyAHSA]\,(HSA + K_D)}{[HSA]} \quad (9)$$

Therefore, combining Equation (7) with Equation (9), Equation (1) can also be expressed as the following equation:

$$\alpha = \frac{[\mathrm{CyA}]_{\mathrm{free}}}{[\mathrm{CyA}]_{\mathrm{tot}}} = \left(\frac{K_D\,[CyAHSA]}{[HSA]}\right)\left(\frac{[HSA]}{[CyAHSA]\,(HSA + K_D)}\right) \quad (10)$$

$$\alpha = \frac{K_D}{HSA + K_D} \quad (11)$$

It is demonstrated that it is possible to calculate the free concentration of the immunosuppressant drugs and its free fraction α knowing the K_D.[173]

It can be stressed that HSA is not the only protein present in the plasma blood, the estimation of free concentration is rough but reliable. Nevertheless albumin was selected because is the most abundant protein in the blood plasma and has a high general binding capacity.[174] However many works demonstrated that tacrolimus and cyclosporine A have higher affinity to lipoprotein than albumin (80% lipoprotein, 20% other proteins). Therefore the association constant, K_A (where $K_A = 1/K_D$) for FK506 or CyA bound to lipoprotein is higher than the K_A related to the binding with others plasma proteins. But in any of these works there was not any study of the affinity constant in a

[173] A. M Rossi, C. W Taylor, *Nat. Protoc.*, **2011**, *3*, 365–387.
[174] H. Zahir, G. McCaughan, M. Gleeson, A. J. McLachlan, *J. Clin. Pharmacol*. **2003**, *57*, 298–309.

sample with both albumin and lipoproteins. Moreover as lipoprotein are not so abundant as the albumin its contribution can be not considered.[175,176,177]

4.4. Optimization of the condition for the FP binding assay

4.4.1. Fluorescent emission of IS-ANB in the presence of HSA

It is of particular significance that the binding process is not accompanied by alterations in the quantum yield of fluorescence or emission maximum of the probe, because this could alter the outcome of the FPIA based analysis. For example, in a study carried out by O. Cañadas et al.[147] it was noted that, in the presence of a protein, a labeled IS (FK506 labelled with a dansyl fluorophore) showed changes in the spectral properties, such as blue or red shift in the maxima of emission or an increase in the intensity of fluorescence emission. Such increase means that the fluorescent IS bound to the protein has higher fluorescence quantum yield than the free fluorescent IS, so that it makes a different contribution to the measured anisotropy. To correct for this bias, O. Cañadas et al.[147] weighted the anisotropy with a correction factor. In order to check whether such optical changes are also present in the case of the ANB labeled immunosuppressants, a similar study was performed with CyA-S-ANB and HSA.

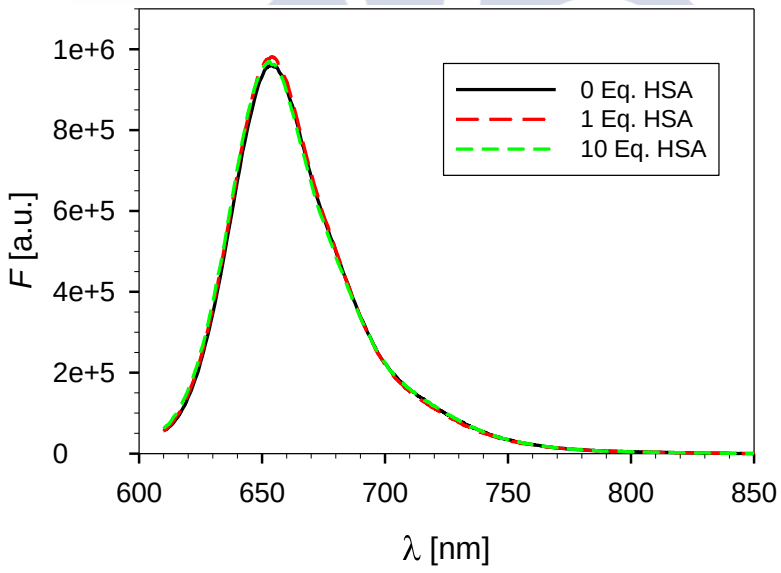


Figure 53. Emission spectra of CyA-S-ANB 0.5 µM in water with 1% of ethanol in the presence of 0 (black), 1 (red) and 10 (green) equivalents of HSA, λ_{ex} = 600 nm, slits 5-5 nm.

[175] F. Akhlaghi A. K. Trull, *Clin. Pharmacokinet,* **2002**, *41*, 615–637.
[176] I. Zaghloul, R. J. Ptachcinski, G. J. Burckart, D. Van Thiel, T. E. Starzel, R. Venhataramanan, *J. Clinical Pharmacol.*, **1987**; *27*, 240–242.
[177] K. Nagase, K. Iwasaki, K. Nozaki, K. Noda, *J. Pharm. Pharmacol.,* **1994**, *46*, 113–117.

As shown in Figure 53, the addition of several equivalents of the protein HSA to an aqueous solution (containing 1% of ethanol) of the CyA-S-ANB fluorophore did not induce any change on the emission properties of the dye, contrary to what O. Cañadas et al. observed for the dansyl-FK506 derivative.[147] In our case, there is no need for including a correction factor in the anisotropy measurements. Moreover the lack of changes in the spectral properties of CyA-S-ANB in the presence of the protein allowed us to infer that fluorescent IS binds to HSA by the CyA moiety and not by the ANB fluorophore part.

4.4.2. Concentration of the labeled immunosuppressant

For the purpose of obtaining the most trustworthy binding curve for K_D determination, it is important to establish the concentration of the labeled immunosuppressant. Three different concentrations (100 nM, 1 μM and 2 μM) of CyA-S-ANB were tested and for each concentration of IS-ANB three different concentrations of HSA were used: 0 equivalent, 1 equivalent and 20 equivalents. The polarization (mP) was measured after 30 minutes of incubation at 25 °C. The 100 nM CyA-S-ANB concentration was discarded for further experiments because these measurements provided higher noise and less difference between the signal for 0 and 20 equivalents of HSA (Figure 54).

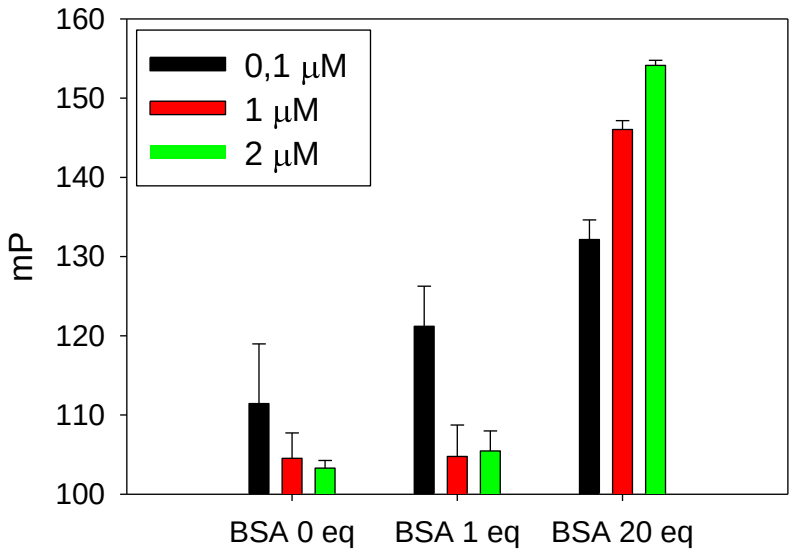


Figure 54. Fluorescence polarization (FP) values obtained for three different concentrations of CyA-S-ANB: 100 nM (black), 1 μM (red) and 2 μM (green). The measurements were performed in a 96 well microtiter plate, with a P590-50 excitation filter, an LP639 dichroic filter, and a P675-50 emission filter.

On the other hand, the experiment described in Figure 55 helped us to determine the CyA-S-ANB concentration interval where the relationship between emission intensity and IS-ANB concentration was linear, indicating that there are no aggregation issues of the fluorescent marker within 0.3 μM to 1.6 μM range. According to the results obtained in Figure 55, 0.83 μM was chosen as proper concentration of IS-ANB to be used in the saturation binding assays, because it stays in the lower linear range, allowing minimizing the amount of reagents needed for the assay, still, it has a good response in terms of signal-to-noise ratio.

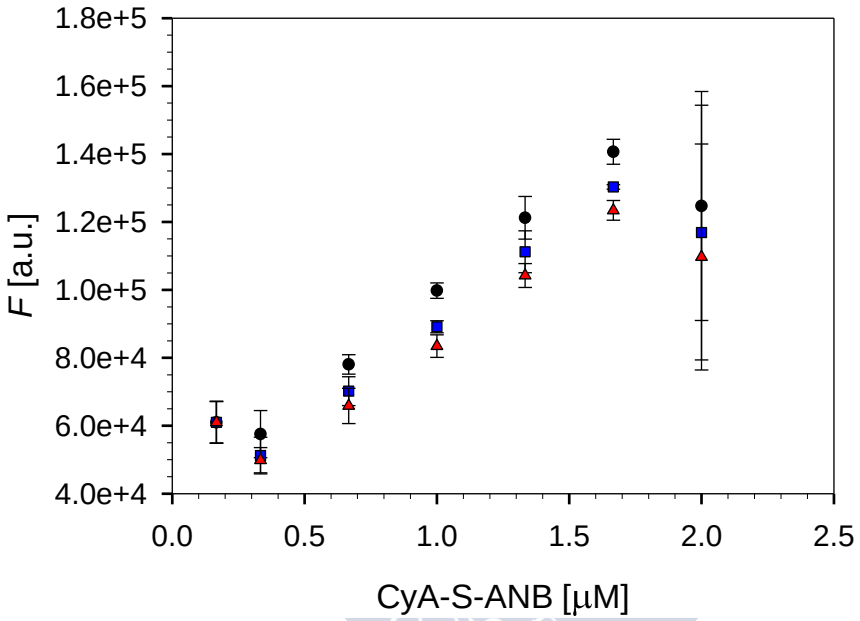


Figure 55. Variation of the fluorescence intensity in function of the concentration of a CyA-S-ANB (*c* = 0.166 μM to 2.0 μM). The measurements were performed in triplicate in a 96 well microtiter plate, with λ_{ex} = 585 nm, λ_{em} = 654 nm and a dichroic filter at 619.5 nm.

4.4.3. Preliminary FP binding assay with BSA

A preliminary binding assay was made in a microplate reader from BMG CLARIOstar® using bovine serum albumin (BSA) instead of HSA. The experimental conditions are described in the Experimental Part. A constant amount of CyA-S-ANB (1 μM in ethanol) was incubated 30 minutes at 25 °C with increasing amounts of BSA in PBS 100 mM at pH =7.4. After that time, the FP of the solution was recorded. It was observed that the FP value considerably increases when the fluorescent IS is bound to BSA (Figure 56). The dissociation constant (K_D) can be obtained by the fitting the experimental data to the Hill

equation (Eq. 12), where b is the so-called Hill coefficient and x in this case is the micromolar concentration of BSA.

$$f(x) = \frac{\mathrm{a}x^b}{K_{\mathrm{D}}^b + x^b} \tag{12}$$

The total (specific and non-specific) binding constant obtained was K_D = 0.0164 mM.

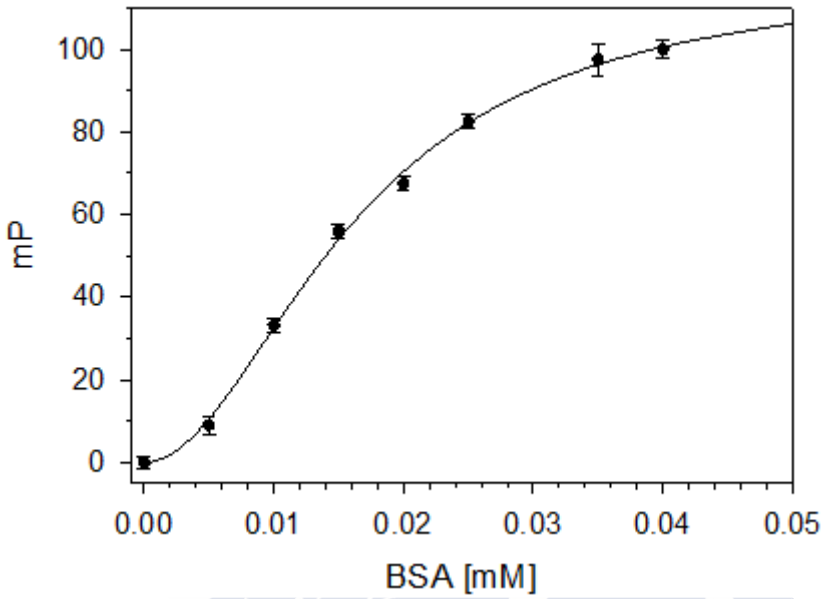


Figure 56. Binding curve for CyA-S-ANB with BSA obtained by fluorescence polarization.

An increment of anisotropy was observed as the amount of protein increased. This behavior is due to the reduced mobility of the labeled immunosuppressant caused by the binding to the protein. This confirms the suitability of the assay for determining binding of IS-ANB molecules to macromolecules. In the next section, the FP binding assay was applied to study the interaction between the three different IS-ANBs: MPA-ANB, CyA-ANB and FK506-ANB, with the human serum albumin protein and to determine the corresponding K_D and the free fraction α in PBS.

4.5. Biding assay for CyA-S-ANB, FK506-ANB and MPA-ANB

The binding assay was performed taking inspiration from the work published by A. M Rossi and C. W. Taylor.[173] The microplate was prepared as it is shown in the Scheme 28. A more detailed description is given in the Experimental part.

	1	2	3	4	5	6	7	8	9	10	11	12	
IS-ANB HSA To obtain A_M	R1	R2	R3	R4	R5	R6	R7	R8	R9	R10	R11	R12	A
	12 increasing concentrations of HSA ---------->												B
	Constant concentration of IS-ANB												C
IS-ANB HSA [IS] saturating To obtain A_I	R1	R2	R3	R4	R5	R6	R7	R8	R9	R10	R11	R12	D
	12 increasing concentrations of HSA ---------->												E
	Constant concentration of IS-ANB												F
	Constant saturating concertation of unlabeled IS												
	Ad*r			Ad*									G
Blank	R1	R2	R3	R4	R5	R6	R7	R8	R9	R10	R11	R12	H

Scheme 28. Graphic representation of the microplate used for the binding assay. A_M A_I Ad*r and Ad* are defined in the Equations (15), (16) ad (17).

A 96 well microlplate was used for each immunosuppressant. A different concentration of HSA was added in each column; this amount is increasing along the same row. The concentration of the labeled immunosuppressant is kept constant at 0.83 μM.

In the first three rows (A, B, C) it is possible to obtain the "measured anisotropy" A_M. The value of A_M is directly provided by the microplate reader as:

$$A_M = (I_{II} - I_{\perp}) / (I_{II} + 2I_{\perp}) \quad (13)$$

Where I_{II} is the intensity of the light emitted in parallel and $I_{\perp}$ is the light emitted in perpendicular plane with respect to the polarized light used for excitation. It is necessary to titrate the labeled IS with an unlabeled competitor and to demonstrate that the FP decreases with respect to the value of A_M with the purpose of establishing the specificity of the assay. The "gold standard" for specificity is the unlabeled IS. A_I is measured in rows D, E, F. A_I is the anisotropy obtained for each protein concentration in the presence of a saturating concentration of the IS (I). The IS (I) competes with the labeled immunosuppressant (named D* in the equations) to occupy the binding sites of the protein. A_I is necessary to calculate the anisotropy due to nonspecific binding (A_{NS}).

The specific anisotropy is calculated subtracting the A_{NS} to the measured anisotropy A_M:

$$A_{specific} = A_{measured} - A_{no\ specific} \quad (14)$$

that is $$A_S = A_M - A_{NS} \quad (15)$$

where $$A_{NS} = (A_I - A_{D^*})(1 - F_B) \quad (16)$$

And $$F_B = (A_M M - A_{D^*}) \Big/ (A_{D^*R} - A_{D^*}) \quad (17)$$

A_{D^*} is the anisotropy of the free IS-ANB, F_B is the fraction of D* bound both specifically and non-specifically, and A_{D^*R} is the anisotropy at saturating concentration of HSA. The blank (PBS and HSA at the corresponding concentration), in row H, is subtracted manually a posteriori. The dissociation constant $K_{D\ TOT}$ is obtained from Eq. (12) after plotting A_M *vs.* the concentration of HSA as depicted in Figure 30.

The BMG CLARIOstar® plate reader was used firstly in Fluorescence Intensity (FI) mode. In this way it was possible to observe if the intensity of all the samples was reproducible. The samples were exited at 585 nm and the emission intensity was monitored at 654 nm. It was found that the standard deviation in the mean fluorescence intensity in the 96 wells plate was 7.4% for cyclosporine A, 3.9% for tacrolimus and 9.5% for mycophenolic acid, demonstrating that the variations in the emission intensity were negligible. The next step was the microplate reader was set into the Fluorescence Polarization (FP) mode for the determination of the IS-HAS binding constants. Before each measurement, the samples were incubated for 30 minutes at 25 °C and shaken with double orbital mode for 60 seconds. The next combination of filters was used: excitation filter of 590 nm (P590-50), long-pass dichroic filter of 639 nm (LP639), and an emission filter of 675 nm (P675-50).

The binding curves obtained for the labelled mycophenolic acid, cyclosporine A and tacrolimus in phosphate buffer are depicted in Figure 57 to Figure **59**.

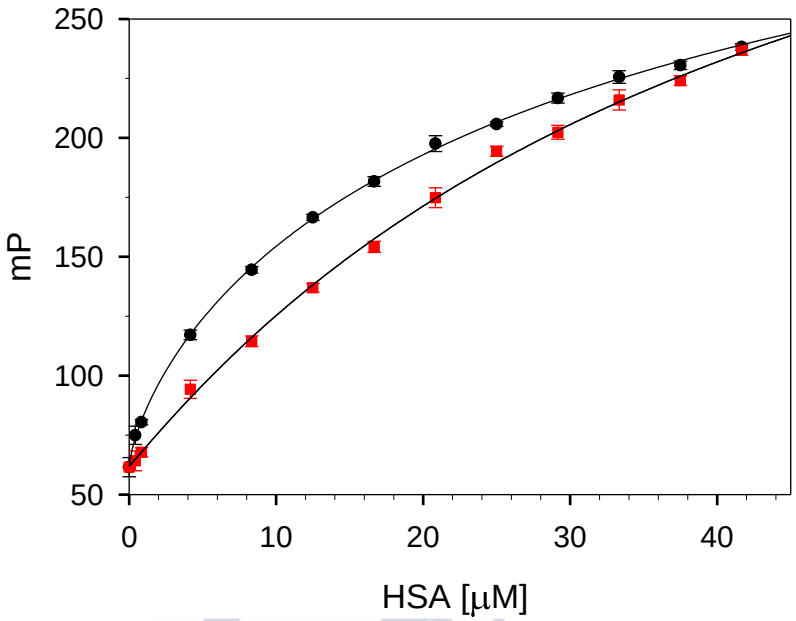


Figure 57. Total binding (black) and specific binding (red) curves for MPA-ANB and HSA.

For MPA the total dissociation constant is $K_{D\ TOT}$ = (3.95 ± 0.61) x 10^{-5} M (Figure 57, black) and the specific dissociation constant is $K_{D\ S}$ = (4.70 ± 0.96) x 10^{-5} M (Figure 57, red). In this case considering the error it can be assumed that $K_{D\ TOT}$ and $K_{D\ S}$ have the same value. The free fraction (obtained using the K_D Svalue) is α = 0.069.

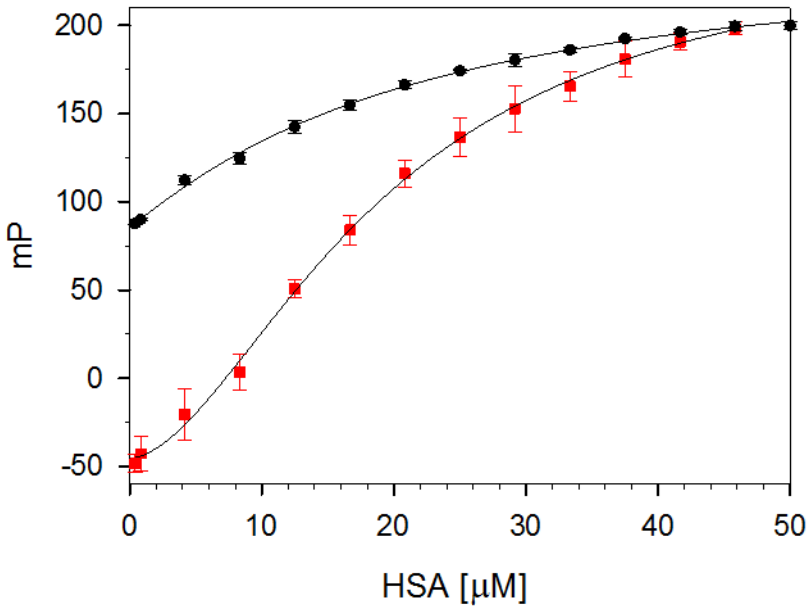


Figure 58. Total binding (black) and specific binding (red) curves for CyA-S-ANB and HSA.

For CyA the total dissociation constant is $K_{D\ TOT}$ = (2.16 ± 0.30) x 10^{-5} M (Figure 58, black) and the specific dissociation constant is $K_{D\ S}$ = (1.95 ± 0.11) x 10^{-5} M (Figure 58, red). In this case $K_{D\ TOT} = K_{D\ S}$ and α = 0.030.

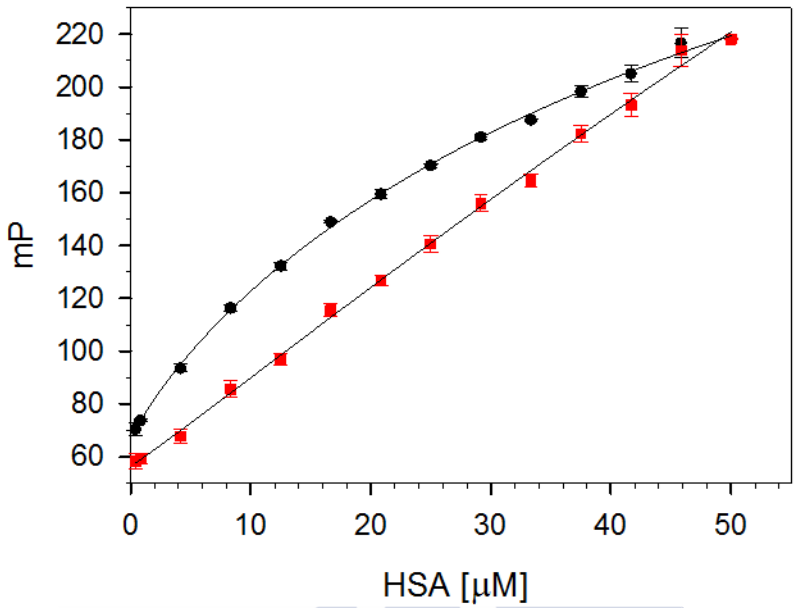


Figure 59. Total binding (black) and specific binding (red) curves for FK506-ANB and HSA.

For FK506 the total dissociation constant is $K_{D\ TOT}$ = (6.92 ± 0.28) x 10^{-5} M (Figure 59, balck) and the specific dissociation constant is $K_{D\ S}$ = (3.26 ± 0.61) x 10^{-4} M (Figure 59, red). In this case $K_{D\ TOT} < K_{D\ S}$ and α = 0.338.

Table 6. Values of K_D (total and specific), K_A (total and specific), and drug free fraction (α) measured for the ANB-labelled immunosuppressants.

	$K_{D\ TOT}$ [μM]	$K_{A\ TOT}$ [mM^{-1}]	$K_{D\ S}$ [μM]	$K_{A\ S}$ [mM^{-1}]	α
MPA-ANB	39.5 ± 6.1	25.3 ± 3.9	47.0 ± 9.6	21.3 ± 4.3	0.069 ± 0.011
CyA-ANB	21.6 ± 3.0	46.3 ± 6.4	19.5 ± 1.1	51.3 ± 2.9	0.030 ± 0.0042
FK506-ANB	69.2 ± 2.8	14.5 ± 0.6	326 ± 61	3.1 ± 0.6	0.338 ± 0.014

The goodness of the fit using the Hill equation is high: R^2 = 0.99 for every binding assay.

According to the calculated values (Table 6), (labelled) cyclosporine A displays the highest affinity for HSA while (labelled) tacrolimus shows the lowest. As a consequence,

the (labelled) tacrolimus free fraction is the largest. The dissociation constants obtained for the (labelled) drug-HSA complexes are comparable to those reported in literature for similar systems. [178,179] except for tacrolimus. The results for tacrolimus are significantly different to those recently described in the literature, where the reported tacrolimus free fraction is lower than 3% of the overall amount in blood plasma (determined by ultrafiltration).[180] In a different work, other authors have reported free tacrolimus concentrations as high as 43–56% after incubation with HSA (determined by ultracentrifugation).[181,182] These differences show that the data reported in literature for ISs binding are ambiguous due to the lack of a validated technique to determine the drug free fraction. We propose that, if properly validated, immunosuppressants labelling together with fluorescence polarization measurements might be a fast, simple and reproducible method for determining the drug free fraction.

It must be emphasized that this is a just model to highlight the potentiality of FP in TDM because we are not considering the real equilibrium of the drugs in the physiological conditions of a just transplanted patient. Additionally, the same experiment should be carried out with a different fluorescent marker, to confirm that the fluorophore used for labelling is not affecting the IS-HAS binding equilibrium, and the same binding constant values are obtained.

5. Applications of the synthetized immunosuppressant derivatives

5.1. Fluorescence polarization immunoassay (FPIA)

The labeled MPA-ANB molecule was used for developing a new fluorescence polarization immunoassay (FPIA) for the rapid analysis of free mycophenolic acid (MPA) in plasma of transplanted patients. This was a part of a doctoral thesis developed by Ana Bettina Glahn Martinez in our research group (GSOLFA). The approach is based on a fluorescence competitive assay between the target immunosuppressant (MPA) and MPA-ANB, for the binding sites of an anti-MPA antibody. The sample, containing the free mycophenolic acid, was incubated for 20 min with 5 µg/mL of anti-MPA antibody and 1 nM of MPA-ANB before the measurements. The developed FPIA displays a limit of detection of 0.8 ng/mL (10% binding inhibition) and a dynamic range of 1.7–39 ng/mL (20–80% binding inhibition) in PBS buffer, fitting the therapeutic requirements. The

[178] I. Nowak, L. M. Shaw, *Clin. Chem.*, **1995**, *7*, 1011–1017.
[179] P. Kuzmi, M. L. Moss, J. L. Kofron, D. H. Rich, *Anal. Biochem.*, **1992**, *205*, 65–69.
[180] N. A. Stienstra, M. A. Sikma, A. van Dapperen, D. W. de Lange, E. M. van Maarseveen, *Ther. Drug Monit.*, **2016**, *26*, 506–515.
[181] W. Plekoszewskl, W. J. Jusk, *J. Pharm. Sci.* **1993**, *82*, 340–341.
[182] H. Zahir, G . Mccaughan, M. Gleeson, *Ther. Drug Monit.*, **2004**, *26*, 506–515.

immunoassay selectivity was evaluated by measuring the cross-reactivity to other immunosuppressive drugs administered in combination with MPA (cyclosporin A and tacrolimus), as well as for the metabolite MPA glucuronide. The assay has been successfully applied to the analysis of free MPA in the blood of a heart transplanted patient after oral administration of both mycophenolate mofetil (MMF) and tacrolimus and the results have been validated by rapid-resolution liquid chromatography with diode array detection (RRLC-DAD).[183]

5.2. Collaborations with the NANODEM EU Project Partners

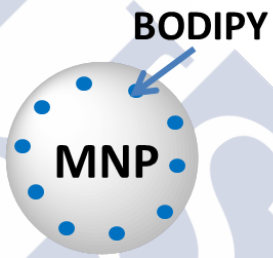
The derivatized ISs, CyA-S-COOH, CyA-O-COOH, CyA-N-COOH, FK506-COOH and the fluorescently labelled CyA-ANB, FK506-ANB, MPA-ANB compounds, were sent to two of the NANODEM Project partners: the group of Prof. Dr. G. Gauglitz of the Optical Spectroscopy group at the University of Tübingen (EKUT) and the group of Dr. F. Baldini of the Chemical and Biochemical Optical Sensor Group at the Consiglio Nazionale delle Ricerche of Florence (IFAC-CNR), for developing competitive FIAs in different formats for the three immunosuppressants.

[183] B. Glahn-Martínez, E. Benito-Peña, F. Salis, A B. Descalzo, G. Orellana, María C. Moreno-Bondi, *Anal. Chem.*, **2018**, *90*, 5459–5465.

Fluorescent nanoparticles as markers for sensitive immunoassays

1. Introduction

Fluorescence immunoassays display limitations in biological samples due to strong absorption of light, background fluorescence from matrix components, or light scattering by the biomacromolecules. A powerful strategy to overcome these problems is introduced here by using fluorescent magnetic nanobeads doped with two boron-dipyrromethane (BODIPY) dyes displaying intense emission in the visible and near-infrared region. The synthesis of fluorescent BODIPY dyes and their spectroscopically characterization, together with the characterization of magnetic nanoparticles doped with BODIPYs (Scheme 29) are the aims of this chapter.



Scheme 29. Encapsulation of BODIPY dyes in a magnetic nanoparticle.

Our work has addressed the following issues:

1) Good separation of absorption and emission wavelengths through a large *virtual* Stokes shift will be achieved through a **Förster Resonance Energy Transfer** (FRET) intraparticle system.[184] The FRET is briefly described below.

> Resonance Energy Transfer (RET),[185] a non-radiative transfer of excited state energy, is a thermodynamic process which obeys energy conservation rule and requires the coupling by a dipole–dipole between donor (D) and acceptor (A). RET is not the result of emission from the donor being absorbed by the acceptor (radiative or "trivial" energy transfer) and there is no intermediate photon in RET. Energy transfer can result from different interaction mechanisms.

[184] a) L. Wang, W. Tan, *Nano Lett.*, **2006**, *6*, 84–88; b) J. Xu, J. Liang, J. Li, W.Yang, *Langmuir,* **2010**, *26*, 15722–15725.

[185] a) V. Balzani, A. Credi, M. Venturi, *Molecular Devices and Machines - A journey into the Nano World*, WILEY-VCH, Weinheim, **2003**, 21–32; b) B. Valeur, *Molecular fluorescence principles and applications*, WILEY-VCH, **2001**, 113–124.

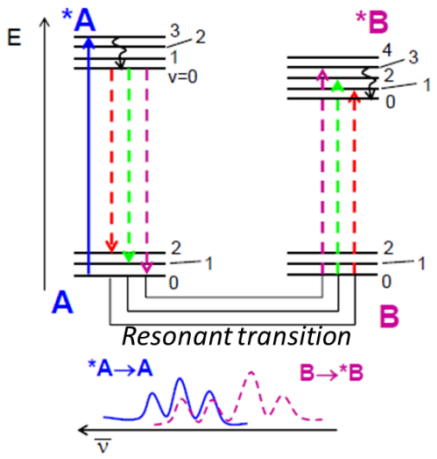
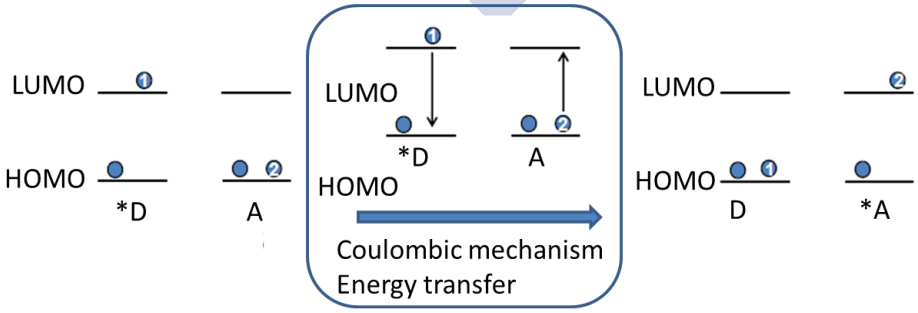


Figure 60. Schematic representation of resonant energy transfer. After excitation and internal conversion, the donor molecule reaches the vibration ground level of the first exited state S1. Through FRET it can pass on its excitation energy to an acceptor that in turn becomes excited. Conservation of energy implies a spectral overlap between the donor emission and the acceptor absorbance.

These interactions may be Coulombic or Dexter-type. The two mechanisms depend differently on the parameters of the system (i.e. spin of ground and excited states, donor-acceptor distance, etc.) and each can become predominant depending on the specific system and experimental conditions.

Coulombic interactions consist of long-range dipole–dipole interaction (**Förster mechanism**) that does not require physical contact between donor and acceptor. The orbital aspects of the Förster mechanism are represented schematically in **Scheme 30**. The donor *D, in its excited state, "gives" its energy, through the so-called Förster mechanism, to the acceptor A. Acquiring this energy, A "jumps" to its excited state. If A is a fluorophore its emission will be observed.



Scheme 30. Schematic representation of **Förster** Resonant Energy Transfer mechanism.

The rate constant for the dipole-dipole Coulombic energy transfer (k_{et}) can be expressed as a function of the spectroscopic and photophysical properties of the two molecular components:

$$k_{et}(\lambda) \propto \frac{\kappa\, \Phi_{*A}}{n^4 \tau^0_{*A} r^6_{AB}}\, J(\lambda) \qquad (1)$$

where κ is an orientation factor which takes into account the directional nature of the dipole-dipole interaction, Φ and τ are, respectively, the luminescence quantum yield and lifetime of the donor, n is the solvent refractive index, r^6_{AB} is the distance (in Å) between donor and acceptor, and $J(\lambda)$ is the Förster overlap integral of the luminescence spectrum of the donor and the absorption spectrum of the acceptor. With good spectral overlap integral and appropriate photophysical properties, the $1/r^6_{AB}$ distance dependence enables energy transfer to occur efficiently over distances substantially exceeding the molecular diameters (i.e. up to 80-100 Å).

FRET may occur between two BODIPY dyes with appropriate spectral overlap, displaying in this way a larger *virtual* Stokes shift. This is an elegant strategy to avoid perturbation of the analytical signal by the scattering of the excitation light from the NPs and, in this way, to decrease the background level of the detected fluorescence, obtaining a better limit of detection in the assay. This is particularly relevant to the design of immunoassays on chip platforms, a format that usually employs laser excitation sources and plastic materials.

2) **BODIPY dyes** were selected as fluorophores because of their high fluorescence quantum yields and high absorption coefficients that will provide a strong analytical signal. The simplest BODIPY dye displays absorption and emission bands centered at ca. 500 and 510 nm respectively, with fluorescence quantum yields approaching unity, and absorption coefficients (ε) close to 10^5 L mol^{-1} cm^{-1}.[186]

3) The chosen fluorophores should **emit in the NIR region** of the spectrum to decrease interference of the background fluorescence on the analytical signal. In this regard, BODIPY dyes are very appropriate. Indeed another advantage of BODIPY dyes is their versatile chemistry that allows introduction of additional π-conjugated units, causing a bathochromic shift in their absorption and emission while maintaining its strong fluorescence. This is an important feature to prepare fluorescent labels that operate in the near infrared region of the electromagnetic spectrum (650–900 nm), where

[186] a) G. Ulrich, R. Ziessel, A. Harriman, *Angew. Chem. Int. Ed.*, **2008**, *47*, 1184–1201; b) A. Loudet, K. Burgess, *Chem. Rev.*, **2007**, *107*, 4891–4932; c) N. Boens, B. Verbelen, W. Dehaen, *Eur. J. Org. Chem.*, **2015**, *30*, 6577–6761.

interference from the light scattering is at its lowest.[187,] In addition, BODIPY dyes are largely insensitive to solvent polarity and pH (unless they bear ad-hoc substituents), display sharp excitation and emission peaks contributing to increase their brightness, have a significant photochemical stability, and possess good solubility in many organic solvents.

4) The synthesized BODIPYs will be encapsulated in a **nanoparticle** to enhance the analytical signal. Therefore, protocols to prepare polymeric nanoparticles will be studied. Dye-doped NPs will be prepared using different non-light absorbing materials. Apt candidates are silica and polystyrene NPs.

Silica-based nanoparticles can be readily obtained by the Stöber method.[188] Doping of silica NPs with luminescent dyes has become a popular approach due to the versatility of the covalent attachment of the label after derivatization of the NP surface with functionalized alkoxysilane groups. Alternatively, the dye can be silanized to tether it to the NP surface. Moreover, introduction of functional groups onto the silica surface for further (bio)functionalization (i.e. coupling with antibodies) can also be achieved by silanization procedures.

Nano/micro-polystyrene NPs can be prepared by emulsion polymerization or are commercially available. Due to their high hydrophobicity, BODIPY dyes are best suitable for doping polystyrene beads through simple encapsulation into the polystyrene (latex) matrix by swelling-shrinking in an organic solvent.[189,190] Polystyrene NPs are available with $-NH_2$ or –COOH surface groups to avoid aggregation in aqueous media.

5) Fluorescent **magnetic nanoparticles** (FMNs) significantly simplify competitive immunoassays when permanent magnets or electromagnets are used to (i) *mix* the antibody-labelled nanoparticles during incubation with the analyte; (ii) *concentrate* the nanoparticles in the detector region during interrogation of their fluorescence, and (iii) *facilitate washing* of the analyte-bound nanoparticles with blocking buffers or buffer media. Despite the magnetic nature of the nanobeads, they must still be strongly fluorescent.

---

[187] a) K. Rurack, M. Kollmannsberger, J. Daub, *New. J. Chem.,* **2001**, *25*, 289–292; b) Y.-H. Yu, A. B. Descalzo, Z. Shen, H. Röhr, Q. Liu, Y.-W. Wang, M. Spieles, Y.-Z. Li, K. Rurack, X.-Z. You, *Chem. Asian. J.,* **2006**, *1*, 176–187; c) K. Umezawa, Y. Nakamura, H. Makino, D. Citterio, K. Suzuki, *J. Am. Chem. Soc.,* **2008**, *130*, 1550–1551; d) Y. Hayashi, N. Obata, M. Tamaru, S. Yamaguchi, Y. Matsuo, A. Saeki, S. Seki, Y. Kureishi, S. Saito, S. Yamaguchi, H. Shinokubo, *Org. Lett.,* **2012**, *14*, 866–869; e) Y. Ni, W. Zeng, K.-W. Huang, J. Wu, *Chem. Commun.,* **2013**, *49*, 1217–1219; f) M. Hecht, T. Fischer, P. Diedritch, W. Kraus, A. B. Descalzo, W.E.S. Unger, K. Rurack, *Chem. Open*, **2013**, *2*, 25–38; g) Y. Ni, J. Wu, *Org. Biomol. Chem.,* **2014**, *12*, 3774–3791.

[188] W. Stober, A. Fink, E. Bohn, *J. Colloid Interface Sci.*, **1968**, *26*, 62–69.

[189] A. B. Descalzo, H.-J. Xu, Z.-L Xue, K. Hoffmann, Z. Shen, M.G. Weller, X.-Z. You, K. Rurack, *Org. Lett.,* **2008**, *10*, 1581–1584.

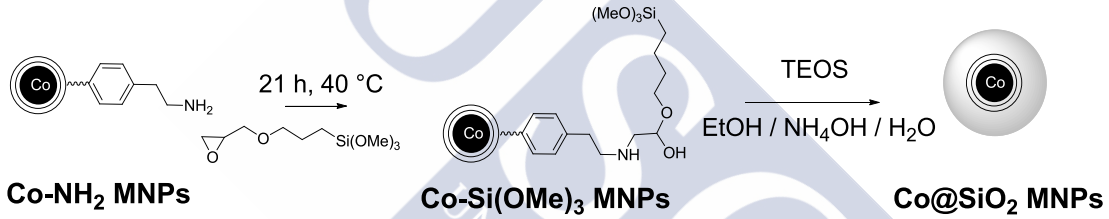
[190] T. Behnke, C. Würth, K. Hoffmann, M. Hübner, U. Panne, U. Resch-Genger, *J. Fluoresc.*, **2011**, 21, 937–944.

2. Cobalt core magnetic NPs

Firstly, commercial cobalt NPs (TurboBeads®) were chosen as magnetic core due to their superior magnetic properties compared with other ferromagnetic materials,[191] such as saturation magnetization of 158 A m^2 kg^{-2}, leading to a rate > 30 g h^{-1}. A carbon (graphene, as per the manufacturer specs) outermost shell provides stability under air and at temperatures up to 190 °C, and the possibility of introducing organic functions.[192] In order to allow fluorescent doping, a further polymeric shell (silica or polystyrene) was grown.

2.1. $Co@SiO_2$ MNPs

The first requirement that magnetic nanoparticles (MNPs) have to meet is the presence, on its surface, of suitable groups that allow silica condensation. To this end, commercial TurboBeads® with aliphatic amino functionalization (Co-NH_2 NPs) were chosen.



Scheme 31. Preparation of MNPs consisting of a Co nucleus and a silica shell.

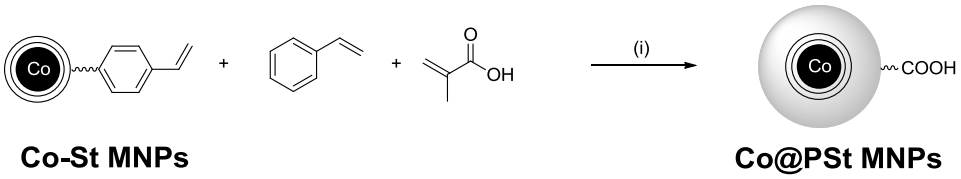
The Co-NH_2 NPs are allowed to react, through a S_N2 reaction, by opening the epoxide of 3-(glycidoxypropyl)trimethoxysilane to provide Co-Si$(OMe)_3$ NPs as shown in Scheme 31. The latter were then used to grow a silica layer via a classical Stöber reaction. Synthesized $Co@SiO_2$ MNPs showed a silica shell of 50-100 nm by transmission electron microscopy (TEM) (see section 3.2 in the Annex part).[193]

2.1.1. Co@PSt MNPs

The growth of a polystyrene shell on magnetic nanoparticles was carried out with TurboBeads® functionalized with vinyl groups as starting material (Co-St MNPs). The free radical polymerization is initiated by potassium persulfate (KPS) or 2,2'-azobis(2,4-

[191] R. Fuhrer, E. K. Athanassiou, N. A. Luechinger, and W. J. Stark, *Small,* **2009**, *5*, 383–388.
[192] C. G. Tan, R. N. Grass, *Angew. Chem. Int. Ed.,* **2007**, *46,* 4909–4912.
[193] a) J. Fuhrer, E. K. Athanassiou, N. A. Luechinger, W. J. Stark, *Small*, **2009**, *5*, 383–388. b) D. K. Yi, S. S. Lee, J.Y. Ying, *Chem. Mater*., **2006**, *10*, 2459–2461. c) H. Lu, G. Yi, S. Zhao, D. Chen, L.H. Guo, J. Cheng, *J. Mater. Chem*., **2004**, *14*, 1336–1341.

dimethylvaleronitrile) (ABDVN) and it is performed in water or acetonitrile in the presence of methacrylic acid to provide polystyrene shell with carboxylic external groups (Scheme 32).



Scheme 32. Preparation of core-shell nanoparticle. The shell is made with polystyrene, with external carboxylic functionalities, and the core is the Co-graphene material of TurboBeads®. (i) Conditions for the different synthetic protocols followed: a) AIBN/SDS, H_2O, 8 h, 50 °C; b) KPS, H_2O, 8 h, 75 °C; c) AIBN, MeCN, 8 h, 50 °C; d) ABDV, MeCN, 2 h, 50 °C.

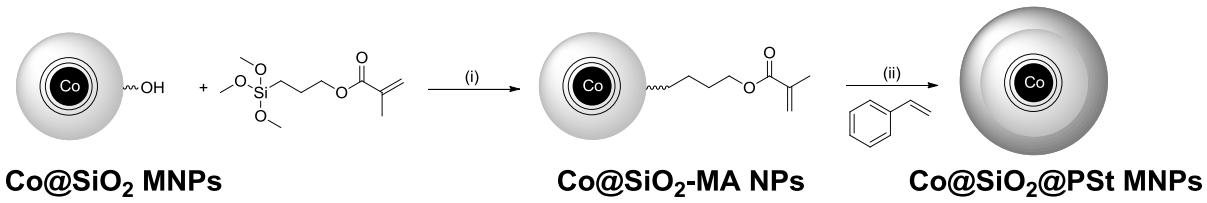
Different synthetic protocols were followed, namely: a) a quasi-surfactant-free emulsion polymerization[194] using AIBN as initiator and sodium dodecyl sulfate (SDS) as surfactant, H_2O, 8 h, 50 °C; or surfactant-free emulsion polymerization;[195] b) $K_2S_2O_8$ (KPS), H_2O, 8 h, 75 °C; c) AIBN, MeCN, 8 h, 50 °C; d) AIBN, MeCN, 2 h, 50 °C.

The polystyrene shell could not be observed by TEM. The starting NPs were also sent to a TEM analysis and it was discovered that the NPs did not present any graphene shell. Moreover, the FTIR of the starting material differs from that one published by the supplier. The MNPs did not meet the provider specifications from TurboBeads®. Despite the suppliers were repeatedly contacted for clarification, no response was obtained.

2.2. Co@SiO_2@PSt magnetic NPs

Taking into account the difficulty met with the commercial Co-St TurboBeads®, a different approach was followed. The synthesized Co@SiO_2 MNPs were taken as a template to grow a polystyrene shell via a 2-step reaction: firstly, by silanization of the silica shell with 3-(trimethoxysilyl)propyl methacrylate; then, the methacrylate groups on the NPs's surface were used as seed for starting a radical polymerization with styrene (Scheme 33).

[194] P. D. Stevens, J. Fan, H. M. R. Gardimalla, M. Yen, Y. Gao, *Org. Lett.*, **2005**, *7, 11*, 2085−2088.
[195] S. Xu, W.-F. Ma, L.-J. You, J.-M. Li, J. G., J. J. Hu, C.-C. Wang, *Langmuir*, **2012**, *28*, 3271−3278.



Scheme 33. Projected growth of a layer of polystyrene on a methacrylate-silica shell of TurboBeads®.

Unfortunately, the FTIR and TEM results did not give a clear-cut evidence of the presence of a polystyrene layer. From the TEM images it can be inferred that the majority of styrene has polymerized separately from the silica NPs (Figure 61); moreover, due to the inhomogeneity of the starting NPs, it was very difficult to assess the presence of a new polystyrene layer around the silica shell.

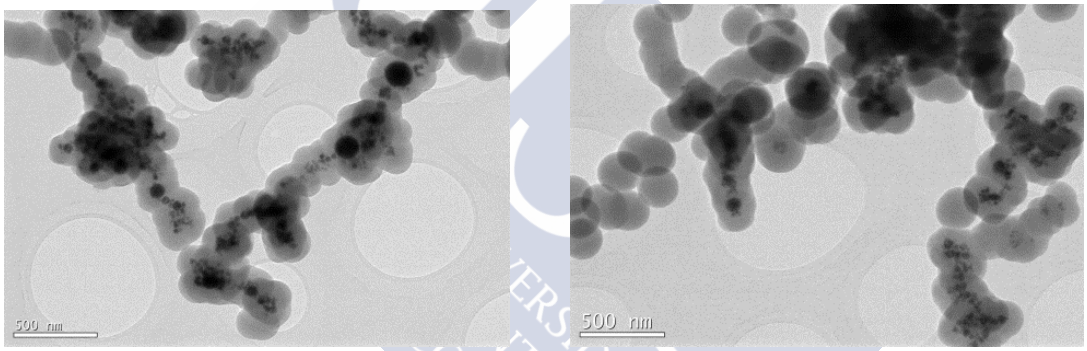
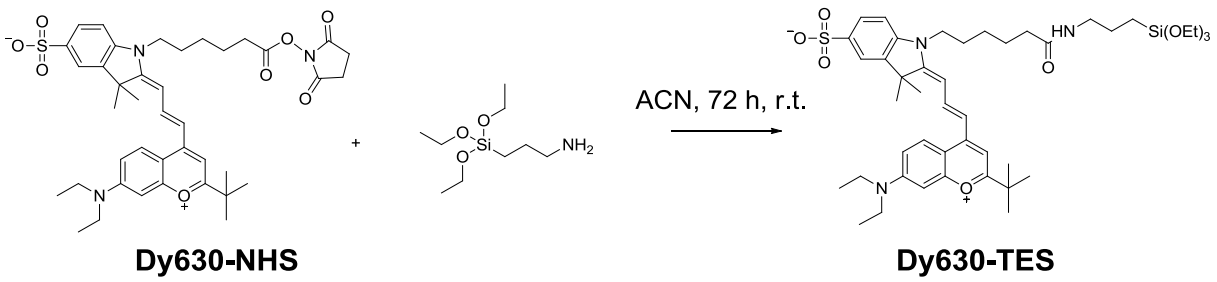


Figure 61. TEM images of Co@SiO_2@PSt NPs.

2.2.1. Fluorescent doping of Co@SiO_2 NPs

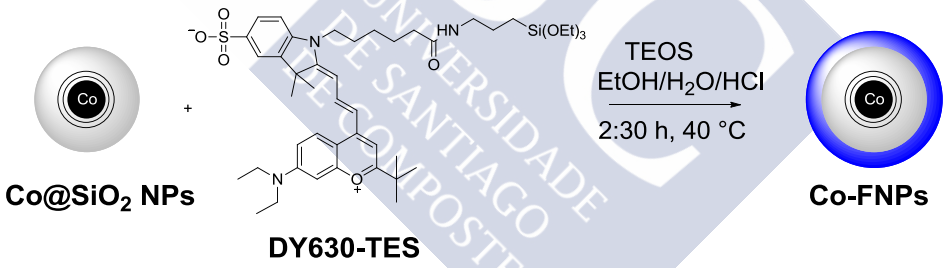
The commercial dye DY630-NHS-ester was purchased from Dyomics GmbH. It has similar spectroscopic characteristics to PFB-641 (see section 3.2 Synthesis of PFB-515 and PFB-641 BODIPY dyes) but it has lower fluorescence quantum yield, less photostability and a rather "prohibitive" price.



Scheme 34. Synthesis of the triethoxysilane derivative Dy630-TES.

DY630-NHS-ester was derivatized with (3-aminopropyl)triethoxysilane (APTES) with a coupling reaction for forming an amide. In this way the dye was modified with triethoxysilane groups as shown in Scheme 34. Due to de very small amount available, DY630-TES could only be characterized by mass spectrometry that confirmed the success of the amide coupling reaction.

The derivative DY630-TES was employed to covalently dope the home-made $Co@SiO_2$ MNPs.



Scheme 35. Preparation of fluorescent silica magnetic NPs based on a Co core.

In this case the classical Stöber synthesis under basic conditions cannot be followed because it could lead to dye decomposition and acidic medium had to be employed.[196,197] Thus, the $Co@SiO_2$ MNPs stored in ethanol were dried. DY630-TES, acetic acid, and TEOS were mixed in a flask. The fluorescent magnetic NPs were prepared in two batches each one with different concentrations of dye (37 μmol/mg and 149 μmol/mg, respectively).

[196] E. Rampazzo, S. Bonacchi, R. Juris, M. Montalti, D. Genovese, N. Zaccheroni, L. Prodi, D. C. Rambaldi, A. Zattoni, P. Reschiglian, *J. Phys. Chem., B* **2010**, *114*, 14605–14613.
[197] S. Zanarini, E. Rampazzo, S. Bonacchi, R. Juris, M. Marcaccio, M. Montalti, F. Paolucci, L. Prodi, *J. Am. Chem. Soc.*, **2009**, *131*, 14208–14209.

The NPs were shaken during 2 h at 40 °C. After this time the cobalt fluorescent magnetic NPs (Co-FMNPs) were washed with water and finally stored in 5 mL of absolute ethanol. During the washing process some leaching of the dye was observed, indicating an incomplete covalent binding of the fluorophore to the silica. A loss of dye was observed, indicating that the dye was not fully bound.

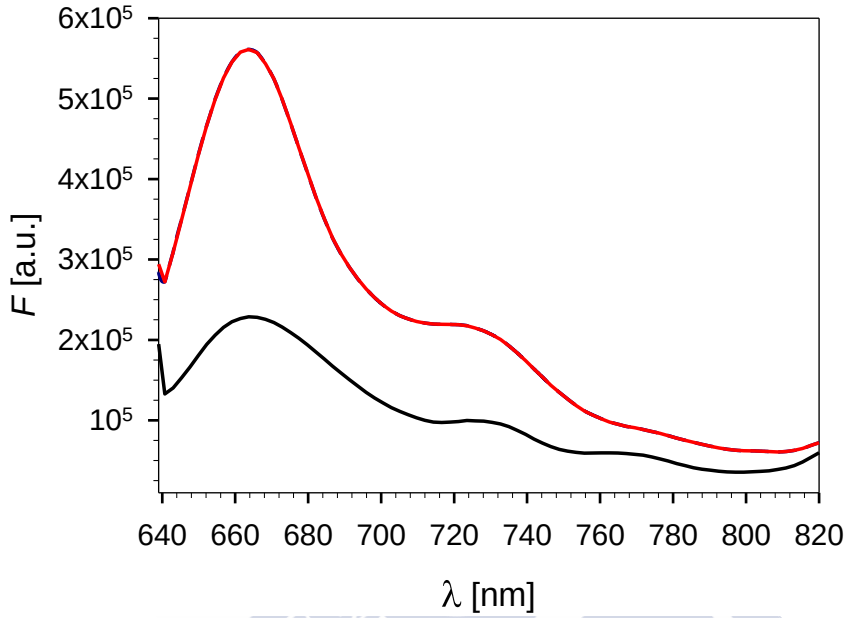


Figure 62. Emission spectra of magnetic core-silica shell NPs doped with DY630-TES. λ_{ex} = 610 nm cut off filter at 590 nm. In black NPs doped with 37 µmol/mg and in red NPs doped with 149 µmol/mg of DY630-TES.

The Co FNPs were characterized by TEM, UV-Vis. From the TEM images it was complicated to determine the real growth of the silica shell after the doping due to the heterogeneous diameter of the starting Co-silica NPs. Despite the loss of dye, the doped cobalt NPs still showed emission at 663 nm as depicted in Figure 62. The nanoparticles were also characterized by dynamic light scattering and nanoparticles of about 200 nm in diameter were found, together with aggregates of around 400-500 nm (data not shown).

An ethanol suspension of magnetic core-silica shell NPs doped with DY630-TES was sent to the NANODEM project partner IFAC-CNR. However, partial release of the dye after the nanoparticles centrifugation was observed by measuring the supernatant fluorescence.

Despite all the synthetic efforts described above, the Co-silica NPs were finally discarded for the immobilization of NIR dyes, for two main reasons: i) the co-polymerization of a silane derivative of the NIR dyes could not be performed by the classic Stöber synthesis under basic conditions because it provoked dye degradation; ii) alternatively, covalent

attachment of the silane derivative of a commercial NIR dye (Dyomics DY-636) to silica NPs surface did not properly work and a progressive leaching of the dye in aqueous solution was observed.

Moreover, in spite of the excellent magnetic properties of cobalt-core nanoparticles and all the efforts made to provide them a suitable shell to attach fluorophores TurboBeads®, the Co NPs were also discarded due to three important reasons: (i) the wide polydispersity of particle sizes around the nominal value (30 nm), much larger than that that specified by the vendor (Turbobeads LLC, CH) (Figure 63); (ii) their strong tendency to aggregate; (iii) the very thin (1-2 nm) graphene layer, that protects the Co core, is destroyed by organic solvents; (iv) some of the TurboBeads® types did ot meet the vendor specification (i.e the Co-St NPs).

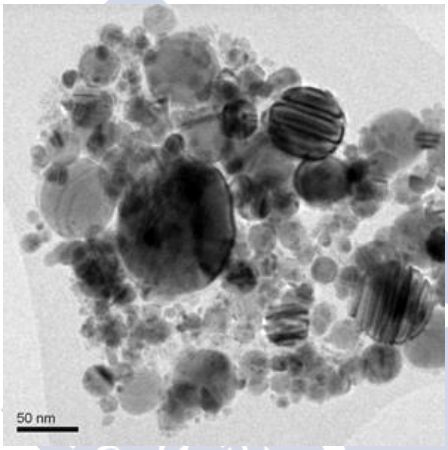


Figure 63. TEM image of commercial TurboBeads® NPs.

3. Ferrite-decorated polystyrene NPs

As alternative to the TurboBeads® NPs, carboxylated magnetic nanospheres from Merck Millipore (Estapor®), of 300 nm diameter (as per dynamic light scattering measurements from the manufacturer), were selected as nanoparticle platform. NPs of 300 nm were chosen as a compromise between large enough particles for a significant magnetic attraction, but small enough to keep a good surface-to-volume ratio. The commercial Estapor® polystyrene nanospheres are decorated with *ca*. 55% (by weight) of ferrite nanograins (ca. 8-10 nm size, as shown by transmission electron microscopy, Figure 64) that confer them *superparamagnetic* properties. Carboxylic functionalization of the NPs surface (148 μeq COOH/g) was chosen to allow facile bioconjugation with the detection antibodies (see 4.1 Coupling of capture antibodies to the fluoromagnetic

nanoparticles). Doping of this type of NPs with lipophilic BODIPY dyes is described in the next section.

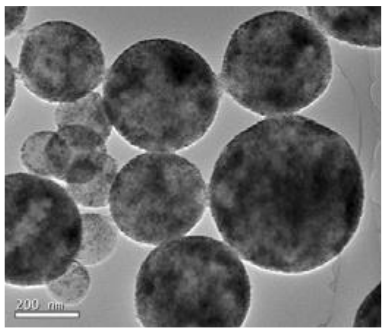
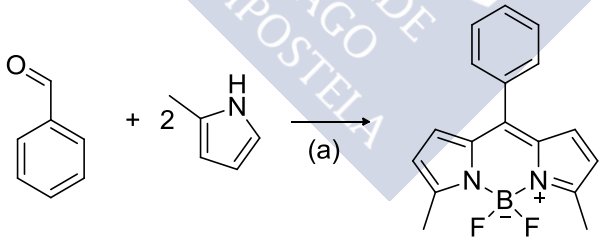


Figure 64. TEM image of commercial Estapor® polystyrene nanospheres.

3.1. Synthesis and characterization of BODIPY dyes

BODIPY dyes can be prepared by an acid-catalyzed condensation of commercially available pyrroles with acid chlorides, or with benzaldehyde derivatives.[198] This route requires an oxidation step; usually, the oxidant used is *p*-chloranil (2,3,5,6-tetrachloro-*p*-benzoquinone) or DDQ (2,3-dichloro-5,6-dicyano-*p*-benzoquinone) (Scheme 36). Possible byproducts, especially from the oxidation step, have to be removed after the complexation with the boron trifluoride diethyl etherate.[199] It is relatively easy to produce a variety of symmetrically substituted BODIPY dyes whit this direct method.

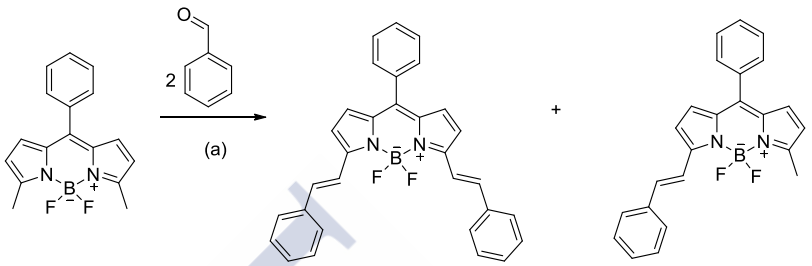


Scheme 36. General synthesis of a BODIPY dye. (a) i) TFA, CH_2Cl_2, Ar, rt; ii) chloranil, CH_2Cl_2, rt; iii) $BF_3{\cdot}OEt_2$, Et_3N, CH_2Cl_2, rt.

Asymmetric BODIPYs can be achieved by using of ketopyrrole intermediates, followed by a Lewis acid-mediated condensation of the latter with another pyrrole fragment.[200]

[198] R. W. Wagner; J. S. Lindsey, *Pure Appl. Chem.,* **1996**, *68*, 1373–1380.
[199] N. Boens, V. Leen, W. Dehaen, *Chem. Soc. Rev.,* **2012**, *41*, 1130–1172.
[200] A. Loudet, K. Burgess, *Chem. Rev.*, **2007**, *107*, 4891–4932.

The 3,5-methyl substituents on BODIPY are sufficiently acidic to participate in Knoevenagel reactions with aromatic aldehydes to form C=C double bonds (Scheme 37). These reactions normally take place under basic conditions.[201] Usually they yield a mixture of the mono- and di-styryl derivatives. The latter can be obtained as major product with longer reaction times. This condensation provides BODIPY dyes with red-shifted fluorescence properties due to their extended π-conjugated system.



Scheme 37. Introduction of π-conjugated units in the BODIPY core. (a) Piperidine, toluene, reflux.

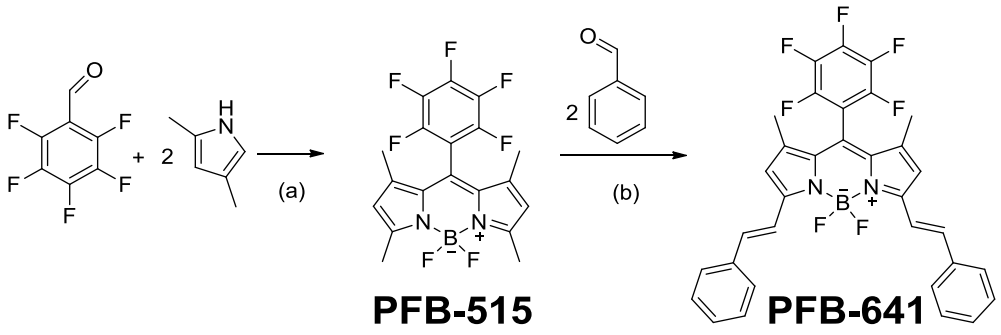
The red shift is more noticeable in polar solvents indicating that excitation of the dyes leads to more polarized excited states. As a consequence of the free rotation of the aryl group, a decrease of the fluorescence quantum yields, is observed because there is an energy loss via non-radiative pathways from the excited state.[202]

It is demonstrated that molecular constraints such as the presence of a pentafluorophenyl moiety in the *meso* position, confers to BODIPY dyes a higher fluorescence quantum yield, longer emission lifetime, and bathochromic shifts in absorption and emission maxima with respect to the parent derivatives without substituent in the *meso* position.[203]

3.2. Synthesis of PFB-515 and PFB-641 BODIPY dyes

Taking into account their very apt properties discussed above, two BODIPY dyes were designed for intra-particle FRET (Scheme 38): a donor (D), with absorption around 500 nm, and an acceptor (A) with a π-extended scaffold, for emission in the NIR region of the spectra.

[201] X. Zhang, Y. Xiao, J. Qi, J. Qu, B. Kim, X. Yue, K. D. Belfield, *J. Org. Chem.* **2013**, *78*, 9153–9160.
[202] A. Burghart, H. Kim, M. B. Welch, L. H. Thoresen, J. Reibenspies, K. Burgess, F. Bergstrom, L. B-A. Johansson, *J. Org. Chem.,* **1999**, *64*, 7813–7819.
[203] M. Hecht, T. Fischer, P. Dietrich, W. Kraus, A. B. Descalzo, W. E. S. Unger, K. Rurack, *Chem. Open,* **2013**, *2*, 25–38.



Scheme 38. Synthesis of (a) PFB-515 and (b) PFB-641. (a) i) TFA, CH_2Cl_2, Ar, rt; ii) chloranil, CH_2Cl_2, rt; iii) $BF_3{\cdot}OEt_2$, Et_3N, CH_2Cl_2, rt, and, (b) piperidine, toluene, reflux.

The synthesized BODIPY dyes were abbreviated as PFB-515 and PFB-641, where PFB stands for pentafluoro-BODIPY and the number that follows represents their maximum absorption in ethanol.

The fluorescence molecular probes PFB-515 and PFB-641 were synthesized following a similar procedure to that described by Vives et al. and shown on Scheme 38.[204] The reaction consisted in a condensation of the pentafluoro aldehyde with 3-ethyl-2,4-dimethylpyrrole in the presence of trifluoroacetic acid (TFA), followed by oxidation with *p*-chloranil, and finally the complexation with $BF_3{\cdot}OEt_2$. The more conjugated BODIPY was obtained by a Knoevenagel-type condensation in the presence of piperidine under anhydrous conditions. The donor (D) and acceptor (A) dyes incorporate a pentafluorophenyl substituent in the *meso* position. Such highly electron withdrawing unit confers, as described above (see section 3.1) superior spectroscopic characteristics.[203,205,] Moreover, to accomplish an efficient FRET process, we also have to keep in mind that the selected dyes must display the largest possible spectral overlap between the emission of D and the absorption of A.

3.3. Spectroscopic characterization of PFB-515 and PFB-641

After chromatographic purification, the dyes were spectroscopically characterized to verify their fitness-to-purpose. The absorption and emission spectra of the two synthesized BODIPY dyes are illustrated in Figure 65. The typical π-π* absorption and emission maximums of BODIPY dyes appear at 515 and 525 nm, respectively, for PFB-

[204] a) O. Galangau, C. Dumas-Verdes, R. Méallet-Renault, G. Clavier, *Org. Biomol. Chem*. **2010**, *8*, 4546–4553. b) G. Vives, G. Giansante, R. Bofinger, G. Raffy, A. del Guerzo, B. Kauffmann, P. Batat, G. Jonusauskas, N.D. McClenaghan, *Chem. Commun*., **2011**, *47*, 10425–10427.

[205] M. A. H. Alamiry, A. C. Benniston, J. Hagon, T. P. L. Winstanley, H. Lemmetyinen, N. V. Tkachenko, *RSC Adv.*, **2012**, *2*, 4944–4950.

515 in ethanol, with a remarkable fluorescence quantum yield (Φ_f = 0.87) and a rather long decay time (6.2 ns) for this type of dyes due to the electron-withdrawing effect of the perfluorinated phenyl ring. In the same solvent, PFB-641 in ethanol shows maximums at 641 nm (absorption) and 657 nm (emission), and a Φ_f of 0.73, with a fluorescence lifetime of 4.0 ns, a lower value than that of PFB-515 due to the effect of the excited state–ground state energy gap law. Table 7 shows the spectroscopic features of the compounds investigated by absorption as well as steady state and time-resolved fluorescence spectroscopy.

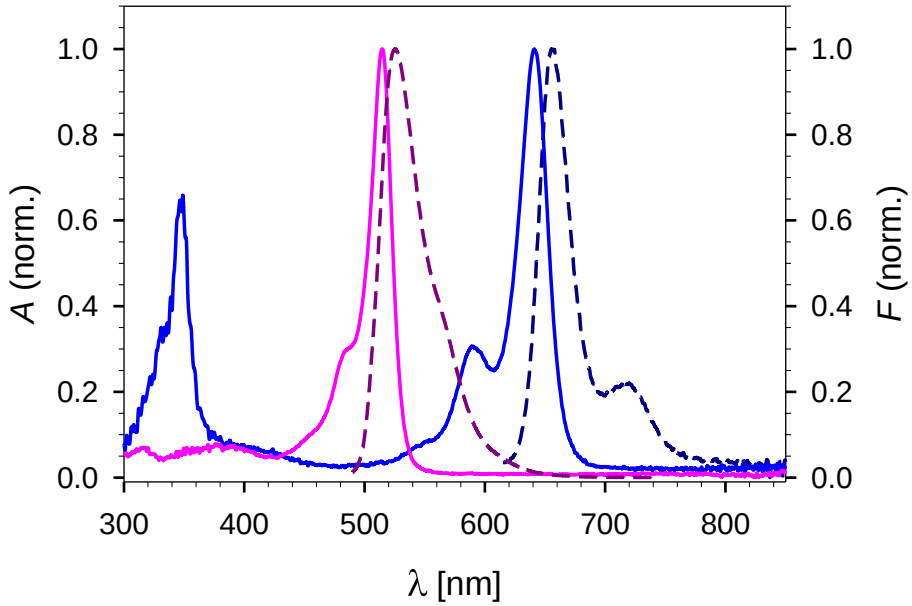


Figure 65. Normalized absorption and emission spectra of PFB-515 (pink, λ_{ex} = 485 nm) and PFB-641 (blue, λ_{ex} = 610 nm) in ethanol.

Table 7. Photophysical data of the BODIPY dyes (1 μM) in air-equilibrated ethanol at 25 °C.

Dye	λ_{abs}^{max} [nm][a)]	ε_{max} [M^{-1} cm^{-1}]	λ_{em}^{max} [nm][a)]	Φ_f[d)]	τ [ns][e)]
PFB-515	515	6.0 x 10^4 [b)]	525	0.87	6.2
PFB-641	641	9.4 x 10^4 [c)]	657	0.73	4.0

[a)] λ ± 0.5 nm; [b)] ε ± 3000 M^{-1} cm^{-1}; [c)] ε ± 12000 M^{-1} cm^{-1}; [d)]Fluorescence quantum yields determined for PFB-515 and PFB-641 dyes using rhodamine 123 (Φ_f = 0.90 in EtOH, λ_{ex} = 485 nm)[206] and oxazine 170 (Φ_f = 0.579 in EtOH, λ_{ex} = 610 nm)[207] as reference dyes, respectively; the uncertainty in the Φ_f determination is around 5%; [e)] ± 0.1 ns.

In Figure 66 the mono-exponential fluorescence decays of PFB-515 and PFB-641 dyes are shown.

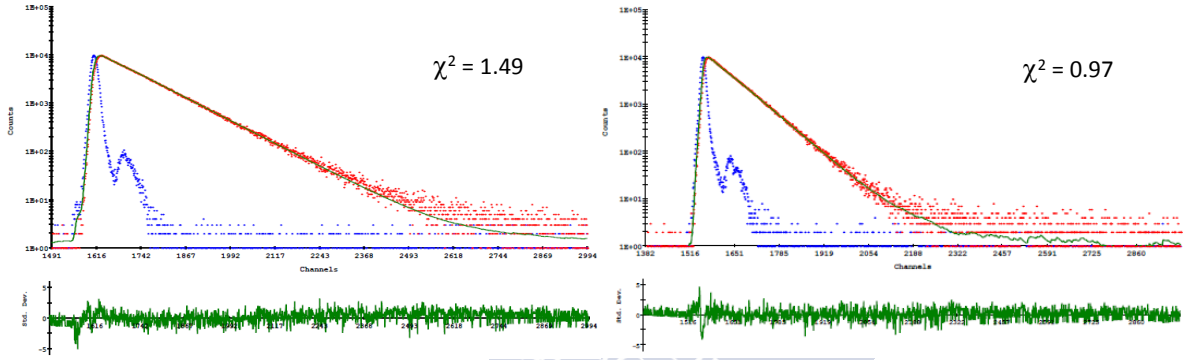


Figure 66. Left: PFB-515 fluorescence decay, upon excitation with 463-nm laser diode (1-ns pulses filtered through a 475 nm and 495 nm band-pass filters); λ_{em} = 550 nm. Right: PFB-641 fluorescence decay, upon excitation with 640-nm laser diode (250-ps pulses filtered through a 665 nm band-pass filter); λ_{em} = 680 nm.

[206] R. F. Kubin, A. N. Fletcher, *J. Lumin.*, **1982**, *27*, 455–462.
[207] K. Rurack, M. Spieles, *Anal. Chem.*, **2011**, *83*, 1232–1242.

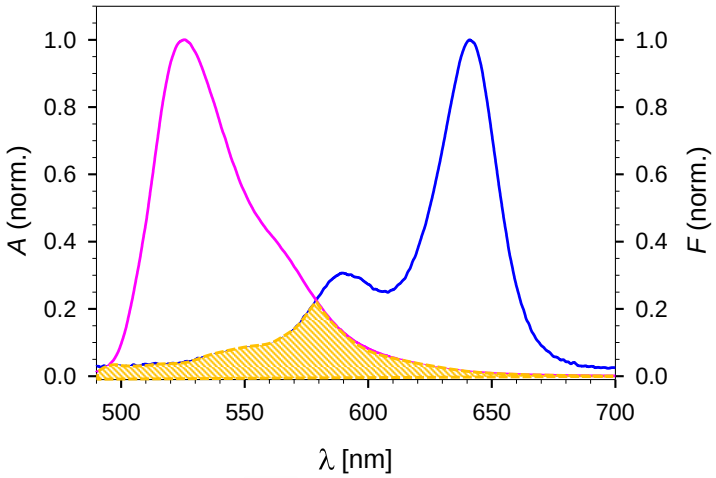


Figure 67. In pink, normalized emission spectrum of PFB-515 and, in blue, normalized absorption spectrum of PFB-641. In yellow, the spectral overlap between them is shown.

Figure 67 demonstrates the significant spectral overlap between the emission of PFB-515 and the absorption of PFB-641. In order to calculate the overlap and, in this way, how effective the FRET process could result, the spectral overlap integral $J(\lambda)$ and the Förster distance (R_0, also called "critical quenching radius", namely, the donor–acceptor distance at which the probability of the excited donor to fluoresce is equal to the probability of energy transfer to the acceptor) were determined using Equation (2) and (3).[208]

$$J(\lambda) = \int_0^\infty F_D(\lambda)\varepsilon_A(\lambda)\lambda^4 d\lambda = \frac{\int_0^\infty F_D(\lambda)\varepsilon_A(\lambda)\lambda^4 d\lambda}{\int_0^\infty F_D(\lambda)d\lambda} \quad (2)$$

$$R_0/\mathrm{nm} = 2.108 \times 10^{-2} \left\{ \kappa^2 \Phi_D^0 n^{-4} \int_0^\infty F_D(\lambda)[\varepsilon_A(\lambda)/\mathrm{dm^3 mol^{-1} cm^{-1}}](\lambda/\mathrm{nm})^{-4} d\lambda \right\}^{1/6} \quad (3)$$

In calculating $J(\lambda)$ one should use the corrected emission spectrum with its area normalized to unity (Eq. 2,middle), or normalize the calculated value of $J(\lambda)$ by the area (Eq. 2, right).

In Eq 3, κ is the is the dipole orientation factor (which is usually assumed to be equal to $(2/3)^{1/2}$ for randomly oriented transition dipole moments of the dyes), Φ_D^0 is the

[208] a) S. E. Braslavsky, *IUPAC* **2007**, *79*, 293; b) I. Medintz, N. Hildebrandt (Eds.), *FRET - Förster Resonance Energy Transfer: From Theory to Applications*, Wiley-VCH **2014**.

fluorescence quantum yield of the donor in the absence of acceptor, N is the Avogadro's number, n is the average refractive index of the medium in the wavelength range where spectral overlap occurs, $F_D(\lambda)$ is the normalized spectral fluorescence radiant intensity of the donor so that $\int_0^\infty F_D(\lambda)d\lambda = 1$, and $\varepsilon_A(\lambda)$ is the molar decadic absorption coefficient of the acceptor at λ. The calculated overlap integral for our D/A pair in ethanol (n = 1.3611)[209] is 1.35 × 10^{15} M^{-1} cm^{-1} nm^4, yielding a Förster distance of 5.2 nm, a similar value for instance to those reported for the popular fluorescein isothiocyanate-tetramethylrhodamine (FITC-TMR) pair (4.9–5.4 nm).[210] The energy transfer rate, $k_T(r)$, is given by $1/\tau_D$ when the D-to-A distance (r) is equal to R_0. Therefore, when the energy transfer efficiency is 50%, k_T amounts to 1.6 x 10^8 s^{-1}.

The photostability of PFB-641 was evaluated in the same way as that of ANB (see Chapter 1 of Results and discussion part) with cyanine-7 (Cy-7) for comparison, as this dye shows a similar spectral profile (λ_{abs} = 650 nm in EtOH) to that of PFB-641 (λ_{abs} = 641 nm in EtOH). The absorption of the dyes at the excitation wavelength (635 nm) was adjusted to the same value (0.12 a.u. Figure 68, left) in order to have the same optical density. An EtOH solution of the dye was irradiated continuously during 20 h with a 5 mW red laser (λ_{em} = 635 nm) (Figure 68, right). Emission spectra before and after the irradiation were also collected (Figure 69).

PFB-641 shows an excellent photostability; its emission intensity only decreases less than 5% over 20 h. Therefore, it may be repeatedly used (i.e. in immunoassay) without losing sensitivity in their analytical applications.

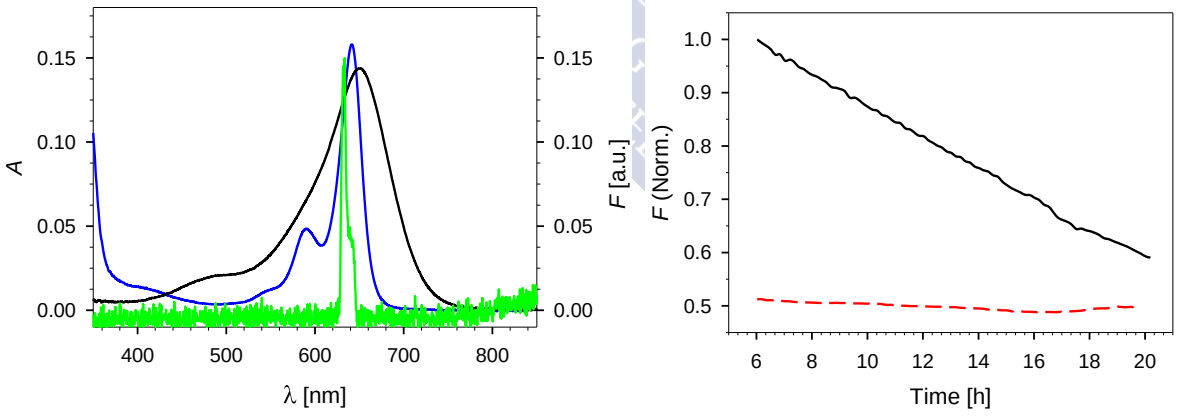


Figure 68. Left: Absorption spectra of PFB-641 (blue) and cyanine-7 in ethanol. In green, the normalized emission spectrum of the red laser diode (635 nm, 5 mW, Picotronic) used for irradiation. Right: Changes in the emission intensity of PFB-641 (red) and cyanine-7 (black) under the red laser illumination.

[209] D. R. Lide (Ed.) *Handbook of Chemistry and Physics* 89th ed., CRC Press, **2008–2009**.
[210] P. Wu, L. Brand, *Anal. Biochem.*, **1994**, *218*, 1–13.

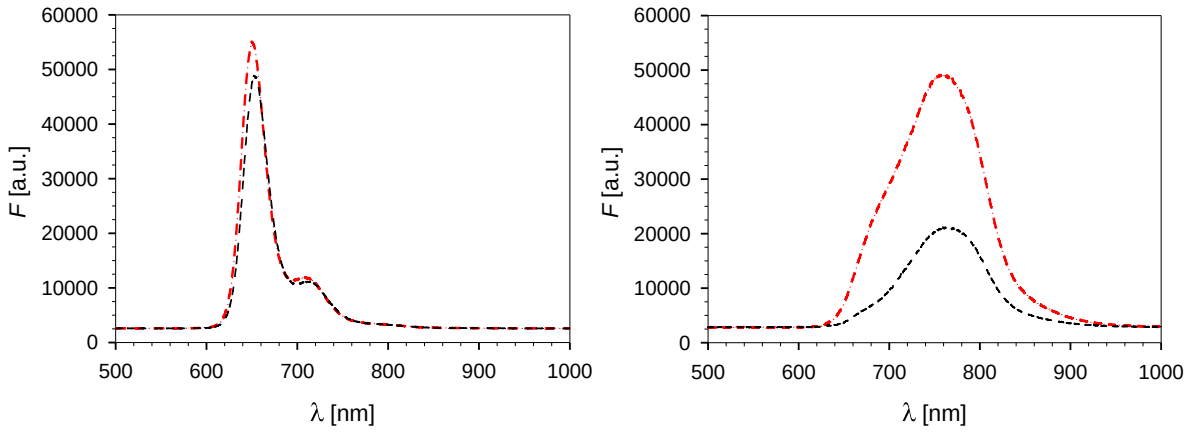


Figure 69. Evolution of the emission spectra of PFB-641 (left) and cyanine-7 (right) in ethanol. Black line, before, and red line, after, 20 h irradiation with the red laser diode (635 nm, 5 mW, Picotronic).

BODIPY dyes are not water soluble but this can be overcame by their incorporation inside a *nanocarrier*. As it is shown in Figure 70, PFB-641 has a fluorescence emission nearly cero in neat water. However, in the presence of surfactant (Tween®) micelles, a strong increase in the fluorescence of the PFB-641 dye is observed due to its encapsulation into the hydrophobic core of the micelles.

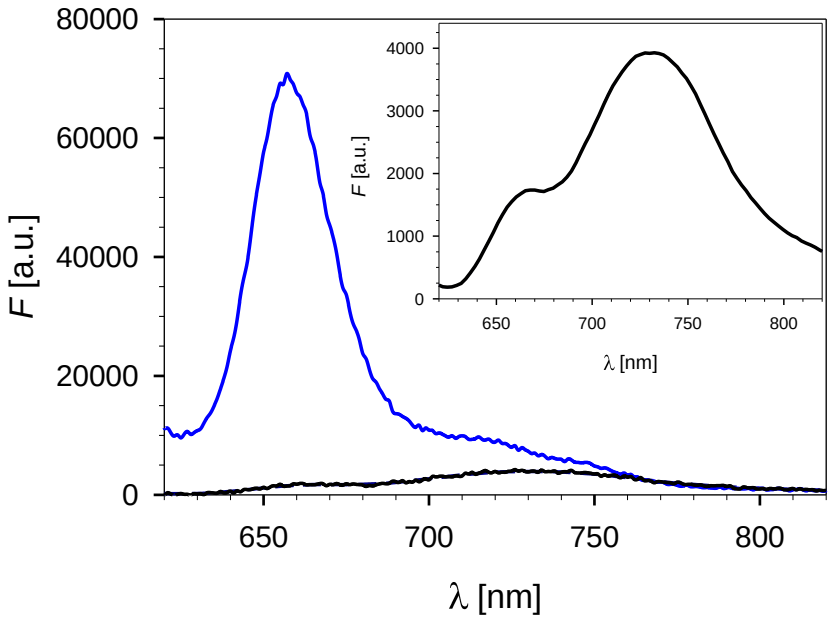
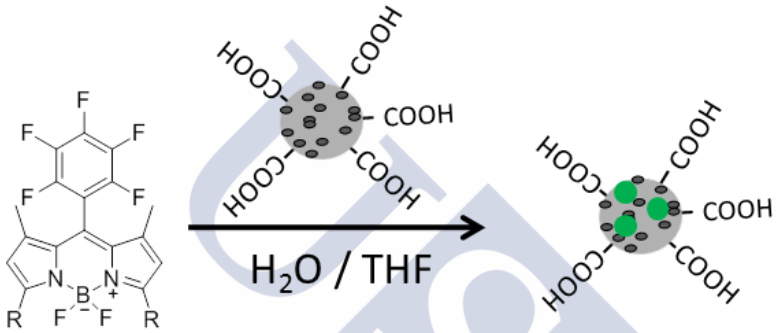


Figure 70. Emission spectra of PFB-641 in H_2O (black line and inset) and after adding 1% Tween® (w/v) (blue line). (λ_{em} = 590 nm, slits 3/3 nm, cut-off filter at 590 nm).

3.4. Protocol for doping polystyrene Estapor® NPs with BODIPY dyes

To test the performance of PFBs in bead-based applications, the synthesized BODIPY dyes were incorporated in the polystyrene Estapor® magnetic nanoparticles functionalized on the surface with carboxylic groups for further bioconjugation (MNPs-COOH). In this way, BODIPY dyes can be used in aqueous media. Firstly, for the fluorescent doping, optimization of dye loading was evaluated. The magnetic beads were loaded with either PFB-515 or PFB-641, and different batches were prepared by increasing the concentration of each dye in the loading solution.



Scheme 39. Swelling procedure for doping MNPs-COOH with BODIPY dyes. where R = H for PFB-515 or R = styryl for PFB-641.

According to the method that has been developed for loading dyes into the PS nanoparticles (Scheme 39), the commercial aqueous suspension of magnetic particles is firstly diluted with water, and then THF is added for swelling the polystyrene. Swelling allows easy diffusion of the hydrophobic dyes into the polystyrene network. Immediately after, the corresponding amount of a solution of the BODIPY dye in THF is added. After vortex stirring, the particles are thoroughly washed with water with the aid of a neodymium magnet, and re-suspended in the same solvent. Although the amount of PFB dye was varied for different batches, the total amount of THF was always kept at 250 μL per mL water in order to ensure a reproducible swelling of the polystyrene fluoromagnetic nanoparticles (FMNPs).

3.5. Spectroscopic characterization of NPs doped with BODIPY dyes (FMNPs)

Excitation and emission spectra and lifetime in water, for particles doped with PFB-515 or PFB-641 were measured.

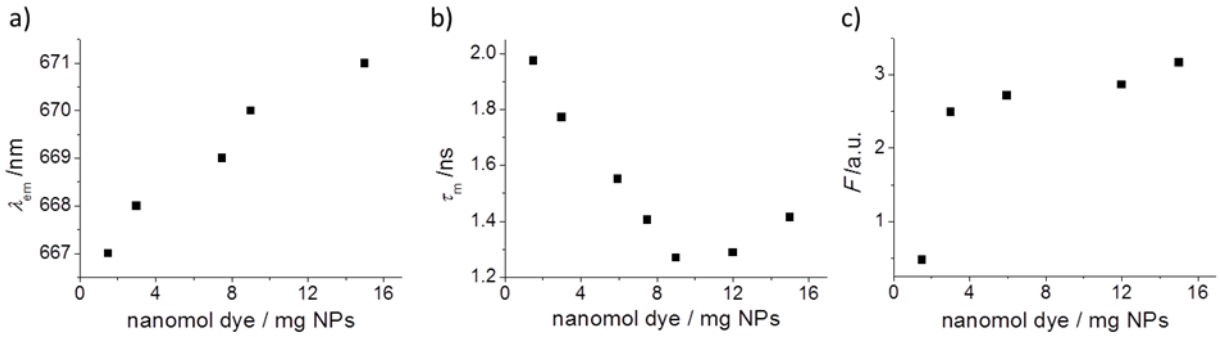


Figure 71. Variation of different properties of FMNPs in aqueous suspension (c_{NPs} = 10 mg mL^{-1}) as a function of the amount of PFB-641 dye employed during the doping procedure. a) Emission maximum; b) pre-exponentially weighted emission lifetime (see Table 8 for its calculation); c) area under the fluorescence spectrum. For steady-state measurements: λ_{ex} = 583 nm and a 590 nm cut-off filter in the emission channel; for time resolved measurements, λ_{ex} = 640 nm and λ_{em} = 680 nm.

As shown in Figure 71, for FMNPs containing PFB-641 (this study was only performed with the acceptor dye), an increase of dye loading yields a small red shift of its emission maximum, together with a decrease of the fluorescence lifetime. The emission red shift might be attributed to the fact that an increase in the number of molecules of dye per FMNP leads to larger inner-filter effect due to the small Stokes shift of the dye, apparently shifting the fluorescence maximum. The same effect is observed when increasing the dye concentration in solution.[211] The fluorescence intensity of the FMNPs levels off at ca. 5 nmol of PFB-641 per mg of MNPs (Figure 71c).

Table 8 shows the emission lifetimes measured for different batches of fluorescent NPs in aqueous suspension. Although the emission decay of the free dyes in ethanol is exponential (Figure 66), the fluorescence decay of the NPs always obeyed multi-exponential kinetics. To be able to compare the different systems, we calculated the so-called pre-exponentially weighted fluorescence lifetimes (τ_m, Table 2).[212] Calculation of τ_m allows a more robust comparison of heavily non-exponential decays, as it removes the uncertainty of the parameters of the fit (pre-exponential factors and lifetimes) caused by their important covariance.[213] The robustness of τ_m lies on the fact that it is also equal to the area under the decay curve divided by the *y*-intercept, so that it is independent of any fit.[214]

[211] M. J. Mayoral, P. Ovejero, M. Cano, G. Orellana, *Dalton Trans.,* **2011**, *40*, 377–383.
[212] E. R. Carraway, J. N. Demas, B. A. DeGraff, *Anal. Chem.,* **1991**, *63*, 332–336.
[213] J. N. Demas, *Excited State Lifetime Measurements*, Academic Press, New York **1983**.
[214] G. Orellana, in *Optical Chemical Sensors* (Eds. F. Baldini, A. N. Chester, J. Homola, S. Martellucci), NATO Sci. Ser. II, vol. 224, Springer (Germany) **2006**; 99–116.

The τ_m of the FMNPs doped with PFB-641 (λ_{ex} = 640 nm; λ_{em} = 680 nm) decreases from 1.97 to 1.29 ns as the concentration of the fluorophore increases (Table 2), being those values always lower than the emission lifetime of the free dye in ethanol (4.0 ns). The same effect is also evident in the case of the FMNPs loaded with PFB-515 (λ_{ex} = 463 nm; λ_{em} = 550 nm): τ_m decreases from 2.16 to 1.85 ns upon an increase of the immobilized dye concentration (6.2 ns for the dye in solution). The emission lifetime drop after immobilization and upon increasing the immobilized dye concentration is in agreement to the changes observed by other authors: when a large number of fluorophores are encapsulated into a NP, the high local concentration of dyes favors formation of poorly emitting aggregates.[215] Moreover, the observed concentration quenching might be due to the Fe_3O_4 grains embedded into the polystyrene surface. It has been demonstrated that nanoparticulated Fe_3O_4 is an efficient quencher of the BODIPY fluorescence by photoinduced electron transfer from the excited state of the latter to an unfilled d orbital of the Fe^{III} atoms of the metal oxide.[216] Therefore, the higher the concentration of surface-embedded dye, together with the large number of molecules next to the surface Fe_3O_4 nanograins, are leading to the observed fluorescence lifetime quenching.

[215] D. Genovese, E. Rampazzo, S. Bonacchi, M. Montalti, N. Zaccheroni, L. Prodi, *Nanoscale,* **2014**, *6*, 3022
[216] C.-J. Yu, S.-M. Wu, W.-L. Tseng, *Anal. Chem.,* **2013**, *85*, 8559–8565.

Table 8. Fluorescence lifetimes of different batches of dye-loaded magnetic nanoparticles in aqueous suspension at (25 ± 1) °C.

Batch	PFB-515/-641 [10^{-9} mol[a)]]	$\lambda_{ex}/\lambda_{em}$ [nm]	τ_1 [ns] (%B_1) [b)]	τ_2 [ns] (%B_2) [b)]	τ_3 (B_3) [ns] [b)]	τ_m [ns][b]
FMNP-641a	-/1.5	640/680	0.61 (34.7)	2.60 (62.4)	4.86 (2.9)	1.98
FMNP-641b	-/3.0	640/680	0.87 (50.6)	2.66 (49.0)	7.67 (0.4)	1.77
FMNP-641c	-/6.0	640/680	0.44 (36.7)	1.69 (41.6)	3.16 (21.7)	1.55
FMNP-641d	-/7.5	640/680	0.45 (39.0)	1.72 (49.6)	3.30 (11.3)	1.40
FMNP-641e	-/9.0	640/680	0.47 (52.8)	1.94 (41.5)	3.84 (5.8)	1.27
FMNP-641f	-/12	640/680	0.42 (43.5)	1.69 (47.4)	3.37 (9.1)	1.29
FMNP-641g	-/15	640/680	0.43 (37.4)	1.73 (51.7)	3.31 (10.9)	1.41
FMNP-515a	3.2/-	463/550	0.93 (59.8)	3.81 (39.6)	15.7 (0.6)	2.16
FMNP-515b	4.8/-	463/550	0.68 (64.7)	3.57 (32.8)	9.61 (2.5)	1.85

[a)] Moles of dye per mg of MNPs (dry weight). [b)] $\boldsymbol{I_f(t) = A + \sum_1^3 B_i \exp(-t/\tau_i)}$, where $\%\boldsymbol{B_i = B_i \times 100/\sum_1^3 B_i}$. [c)] $\boldsymbol{\tau_m = \sum_1^3 B_i \tau_i / 100}$.

Excitation and emission spectra in water, for particles loaded with PFB-515 or PFB-641 are shown in Figure 72; excitation spectra are given instead of absorption because scattering of the suspensions was too strong. As discussed above by comparison to the free dyes in diluted ethanol solution (Table 7), the spectral maxima of the FMNPs are considerably red shifted in all cases. For example, $\lambda_{abs}/\lambda_{em}$ are 515/525 nm for PFB-515 in ethanol but 521/535 nm for the FMNPs doped with PFB-515 at 6.4 nmol/mg MNPs; $\lambda_{abs}/\lambda_{em}$ are 641/657 nm for PFB-641 in ethanol but 653/668 nm for FMNPs doped with PFB-641 at 3.0 nmol/mg MNPs. Because the absorption and emission maxima are red shifted synchronously upon immobilization, the D-A spectral overlap is also large for an efficient FRET into the dye-doped NPs. Therefore, we should observe sensitized emission of PFB-641 at λ > 650 nm by exciting the donor PFB-515 around 500 nm. In this way, a virtual Stokes shift larger than 150 nm can be achieved, so that suppression

of the disturbing scattering effects and, consequently, enhancement of the immunoassay sensitivity should be feasible. In order to confirm these predictions, MNPs-COOH doped with mixtures of PFB-515 and PFB-641 were prepared. It is important to mention that both dyes are readily co-encapsulated into the polystyrene matrix because they have similar polarity.

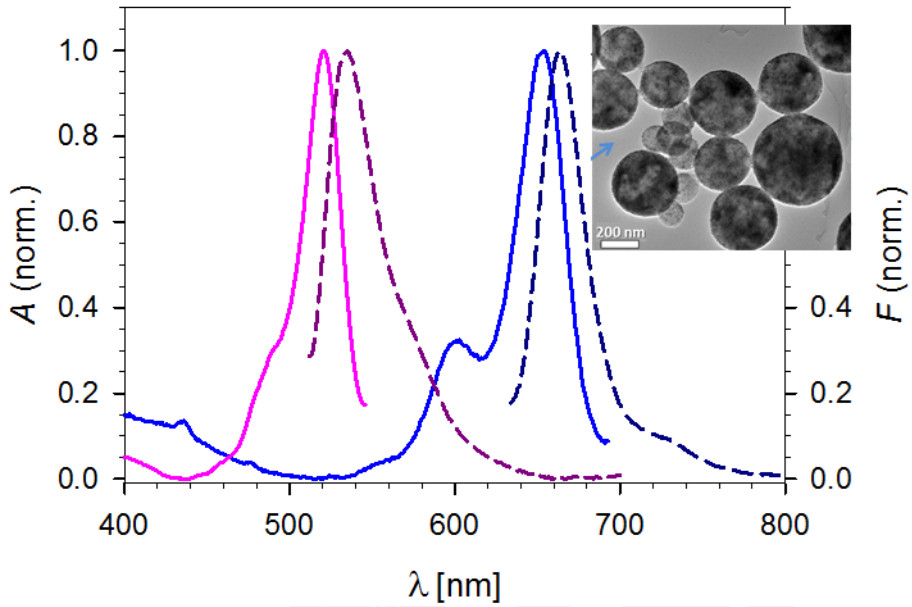


Figure 72. Excitation and emission spectra of suspensions of magnetic particles doped with PFB-515 (3.2 nmol/mg NPs), (λ_{em} = 570 nm, λ_{ex} = 495 nm, in pink) and PFB-641, (3.0 nmol/mg NPs, λ_{em} = 715 nm, λ_{ex} = 590 nm, in blue) in water. The inset shows a TEM micrograph of the PFB-641-doped magnetic nanoparticles (batch "b" of Table 9).

3.6. Intra-particle Förster resonance energy transfer

The Estapor® magnetic nanoparticles were simultaneously doped with PFB-515 and PFB-641 for obtaining the sought intra-particle FRET label. The proper acceptor dye concentration was determined as described above for the PFB-641-doped FMNPs (*ca*. 5 nmol dye per mg NPs provided the maximum emission intensity). Keeping constant the total amount of immobilized dye molecules at ca. 10 nmol/mg MNPs, the PFB-515 to PFB-641 mole ratio was varied from 1:1 to 2:1 in order to investigate the effect of the relative amount of A with respect to D; the results are shown in Figure 73 and Table 9. In spite of the smaller number of A molecules, we can observe that an increase of the D/A ratio leads to higher fluorescence from the acceptor dye, meaning that the FRET process is improved due to the presence of more "antennas". This enhancement is confirmed in the excitation spectra (Figure 73) and in the study of the fluorescence lifetimes.

Therefore, a 2:1 D/A mole ratio was chosen for preparation of the optimized FRET-based MNPs that were finally used for the bioconjugation.

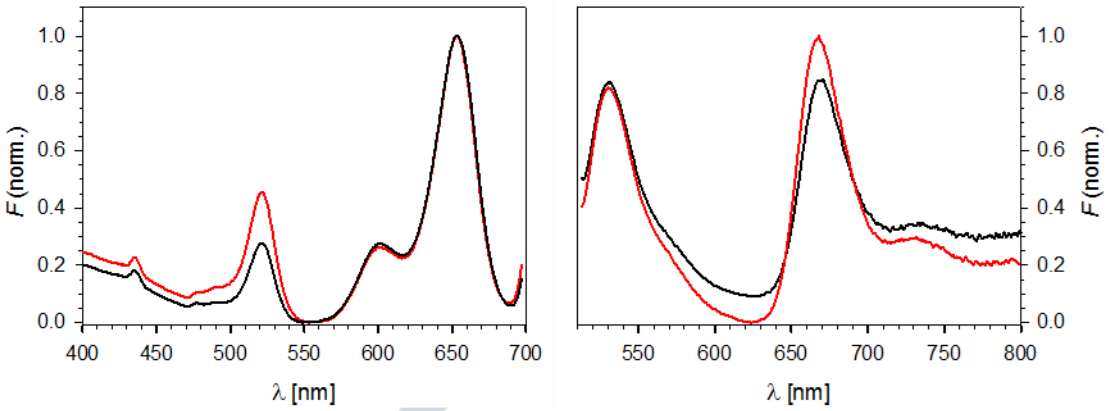


Figure 73. Normalized excitation and emission spectra of a suspension in water of two different FRET-based FMNPs. Left: excitation spectra monitored at the PFB-641 acceptor emission (715 nm); right: emission spectra of the FRET-based FMNPs excited at the donor PFB-515 absorption (495 nm). Black curves: FMNPs doped with a 1:1 donor/acceptor mole ratio; red curves: FMNPs doped with a 2:1 donor/acceptor mole ratio.

Next, two D/A ratios were tested to confirm the improved FRET efficiency in the FMNPs (Table 9). To determine the emission lifetimes of the latter, the same excitation wavelength was always employed (463 nm, absorption of the donor), while the fluorescence was monitored at two different wavelengths (550 nm emission from D, or 680 nm emission from A).

Table 9. Fluorescence lifetimes of different batches of dye-loaded magnetic nanoparticles in aqueous suspension at (25 ± 1) °C.

Batch	PFB-515/-641 [10^{-9} mol[a)]]	$\lambda_{ex}/\lambda_{em}$ [nm]	τ_1 [ns] (%B_1) [b)]	τ_2 [ns] (%B_2) [b)]	τ_3 [ns] (%B_3) [b)]	τ_m [ns][b]
FMNP-ETa	4.8/4.8	463/550	0.53 (85.6)	4.43 (13.8)	17.2 (0.5)	1.16
FMNP-ETa	4.8/4.8	463/680	1.02 (52.1)	2.79 (47.7)	16.1 (0.2)	1.89
FMNP-ETb	6.4/3.2	463/550	0.67 (84.2)	4.30 (15.2)	16.1 (0.6)	1.32
FMNP-ETb	6.4/3.2	463/680	1.27 (45.1)	3.01 (54.7)	18.4 (0.2)	2.25

[a)] Moles of dye per mg of MNPs (dry weight). [b)] $I_f(t) = A + \sum_1^3 B_i \exp(-t/\tau_i)$, where $\%B_i = B_i \times 100/\sum_1^3 B_i$. [c)] $\tau_m = \sum_1^3 B_i \tau_i/100$.

In every case, and although the fluorescence lifetime of PFB-641 is shorter than that of PFB-515 (4.0 and 6.2, respectively), the lifetimes measured at 680 nm (1.89 and 2.25 ns for D/A 1:1 and 2:1, respectively) are longer than those measured at 550 nm (1.16 and 1.32 ns for D/A 1:1 and 2:1, respectively) (Table 9), indicating the occurrence of the FRET process. These results confirm that a higher relative amount of donor dye (D/A 2:1 *vs* 1:1) leads to a longer-lived acceptor species, suggesting a more efficient FRET quenching and lending support to the results of the fluorescent intensity measurements discussed above.

3.7. Magnetic characterization of the fluoromagnetic nanoparticles (INESC-MS)

The magnetic moment for the Estapor®, Merck Millipore nanoparticles doped with both PFB-515 and PFB-641 (FMNP-ETb Table 9), was also measured at INESC-MS. The results are shown in Figure 77. As it can be observed, the magnetic moment of the FMNPs does not change after introducing the fluorophores, demonstrating that the ferrite decoration is not modified during the dyes immobilization procedure.

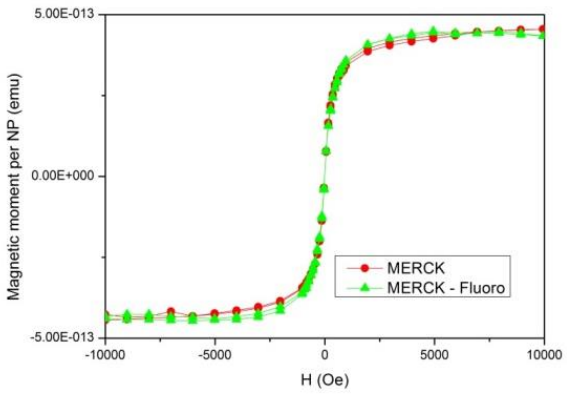


Figure 74. Comparison of the magnetic moment of Estapor®, Merck Millipore nanoparticles of 300 nm (red) *vs* the same particles after doping with both PFB-515 and PFB-641 (green), as a function of an external magnetic field.

4. Application of the FRET NPs: Heterogeneous immunoassay for tacrolimus

The novel FRET NPs are employed as labels for quantification of the tacrolimus immunosuppressive drug to illustrate their usefulness to increase the sensitivity of fluorescence immunoassays.

4.1. Coupling of capture antibodies to the fluoromagnetic nanoparticles

The selected FRET-based fluoromagnetic nanoparticles (FMNP-ETb, those doped with a 2:1 PFB-515/PFB-641 mole ratio) were conjugated to different capture antibodies after

activation of the former with the classical EDC/sulfo-NHS combination in MES buffer (Figure 75). Then, they were washed with PBSSDS and incubated in the same buffer with the required capture antibody to tacrolimus.

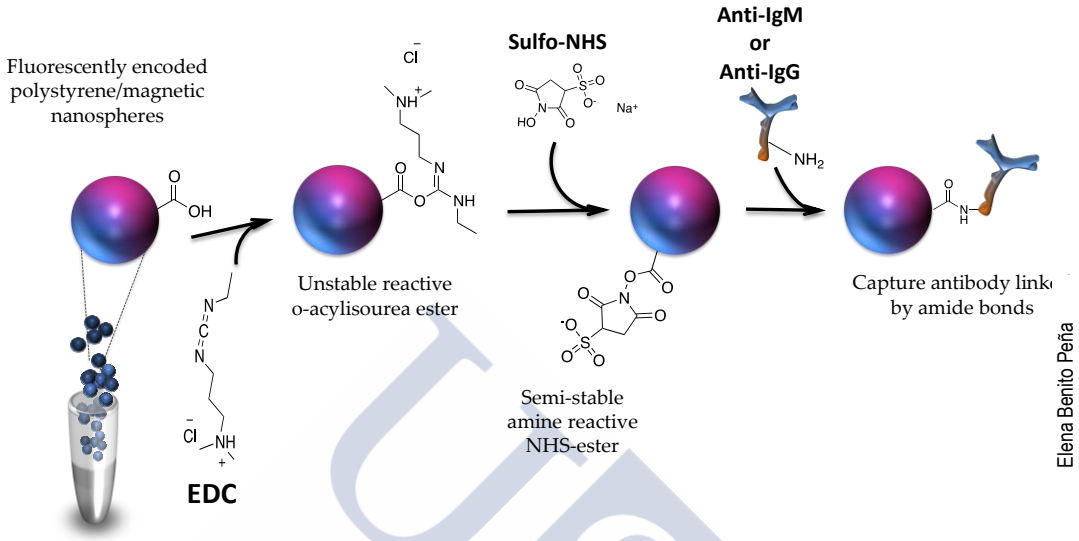


Figure 75. Workflow of the protocol followed to couple the carboxylated fluorescent magnetic nanoparticles to the detection antibodies using the EDC/sulfo-NHS method.

Additionally, some FMNPs were functionalized with neutravidin to be used as positive or negative control in the immunoassays. Efficient conjugation of the IgG anti-IgM antibodies to the fluoromagnetic NPs was confirmed by a magnetic bead-based enzymatic assay,[217] using a microplate fluorescence reader, HRP-labeled anti-IgG, and the commercial Amplex® Red Hydrogen Peroxide/Peroxidase Assay Kit (Figure 76). The very small response obtained for FMNPs coated with neutravidin (negative control) confirms the selectivity of the assay.

[217] D. M. Rissin, C. W. Kan, T. G. Campbell, S. C. Howes, D. R. Fournier, L. Song, T.Piech, P. P. Patel, L. Chang, A. J. Rivnak, E. P. Ferrell, J. D. Randall, G. K. Provuncher, D. R. Walt, D. C. Duffy, *Nat. Biotech.,* **2010**, *28*, 595–599.

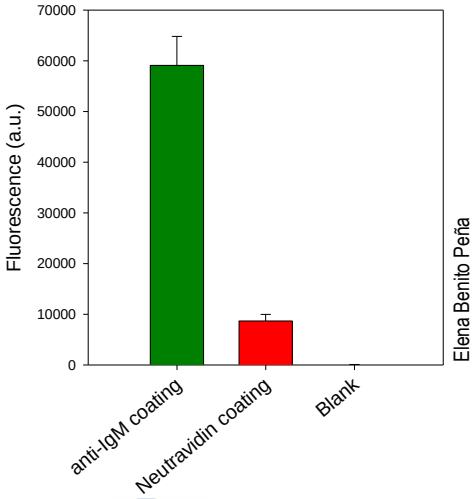


Figure 76. Responses obtained using (a) a suspension of 3 µg mL-1 of FMNP-ETb decorated with antibodies (monkey IgG anti-IgM) (green), or neutravidin (red). The blank signal corresponds to the response of non-decorated particles.

4.2. FMNPs-based competitive immunoassay for Tacrolimus

Determination of the immunosuppressant used to test the FRET-based fluoromagnetic nanoparticles is based on a competitive (inhibition) assay between a suitable derivative of Tacrolimus (FK506-COOH) immobilized onto the glass bottom surface of the microwells, and Tacrolimus present in the sample, for a limited number of antibody (Ab) binding sites (Figure 77).

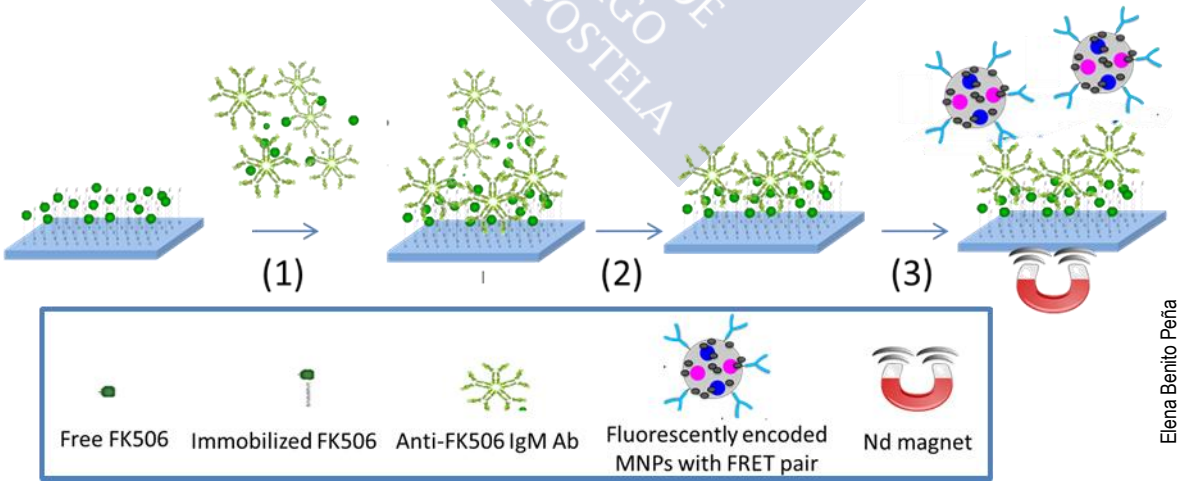


Figure 77. Tacrolimus immunoassay protocol summary: (1) mixing and incubation of sample and IgM anti-FK506 antibody into (FK506-COOH)-bound microwell; (2) wash out of the bioreagents excess; (3) incubation with PSE FMNP-ETb functionalized with the detection IgG anti-IgM antibody, second wash and fluorescence measurement.

In order to achieve a defined and sufficiently high density of immobilized haptens without loss of their biological activity, the glass wells were functionalized with either 3-aminopropyltriethoxysilane (APTES) or poly-L-lysine. Figure 78 shows that the latter provides significantly lower background, (measured in the absence of anti-FK506 antibody) while the fluorescence is high and reproducible, so that it was selected for further experiments.[218]

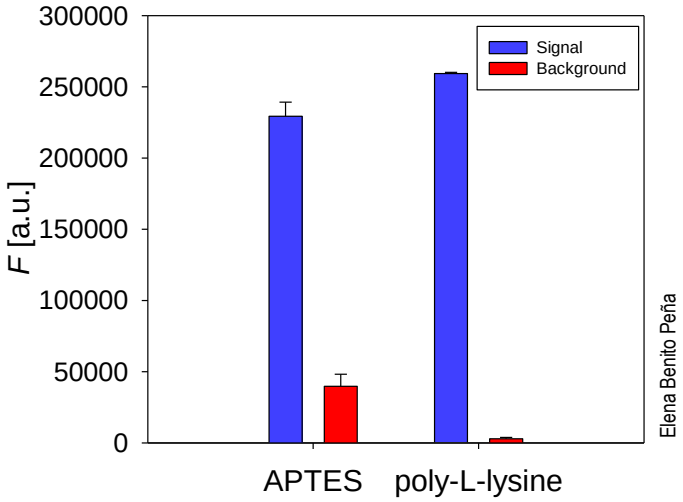


Figure 78. Responses obtained using different immobilization procedures: (a) covalently FK506-COOH linked to amino groups of APTES; (b) covalently FK506-COOH linked to amino groups of poly-L-lysine.

The fluorescence data were plotted as the B (fluorescence signal in the presence of FK506) to B_0 (fluorescence signal in the absence of the analyte) ratio against the FK506 concentration on a logarithmic scale (Figure 79). The experimental points are fitted (Systat Sigma Plot v.12) to a four-parameter sigmoidal logistic equation (Equation 4),[219]

$$\frac{B}{B_0} = \frac{A_{max} - A_{min}}{1 + \left(\frac{[FK506]}{IC_{50}}\right)^b} + B_{min} \qquad (4)$$

where A_{max} and A_{min} are the asymptotic maximum and minimum of the normalized signal, respectively, b represents the slope of the curve at the inflection point, and IC_{50} is the concentration of analyte at the inflection point (concentration giving 50% inhibition of A_{max}). The limit of detection (LOD) was calculated as the analyte concentration for

[218] W. Kusnezow, J. D. Hoheisel, *J. Mol. Recognit.,* **2003,** *16*, 165–176.

[219] R. F. Masseyeff, W. H. Albert, N. A. Staines, *Methods of Immunological Analysis*, Wiley-VCH, New York, 1st edn, **1992**, 655–671.

which the tracer binding to the antibody is inhibited by 10%, and the dynamic range (DR) of the method corresponds to the analyte concentrations that produce a normalized response in the 20–80% range. Figure 79 shows the competitive inhibition curves obtained using FK506 standard solutions in the 0.01 – 7500 ng mL^{-1} range. When the signal was acquired in the *FRET mode*, i.e. upon excitation at the donor absorption wavelength (525 nm) and monitoring the sensitized emission of the acceptor at 680 nm, the LOD and IC_{50} values obtained were 0.08 and 0.47 ng mL^{-1}, respectively, with a dynamic range of 0.15 to 2.0 ng mL^{-1} However, when the *direct excitation mode* was used, i.e. by illuminating at the acceptor absorption (638 nm) and monitoring its fluorescence at 680 nm (without any FRET), the signal background was found to be significantly higher. Thus, both the LOD (0.27 ng mL^{-1}) and the IC_{50} value (23 ng mL^{-1}) were higher, with a dynamic range between 4.1 and 130 ng mL^{-1}.

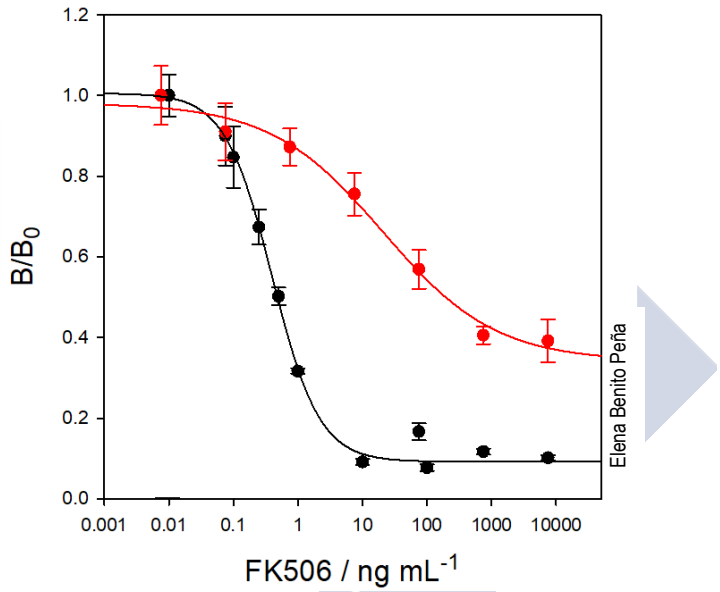


Figure 79. Competitive immunoassay calibration curve. The plate was assayed with FK506 (0, and 0.010 to 7500 ng mL^{-1}) in the presence of 2.5 µg mL^{-1} of anti-FK506 and 2.5 µg mL^{-1} of anti-biotin (positive control) antibodies. Tracer solution is a mixture of 3 µg mL^{-1} of fluorescently-encoded magnetic nanospheres decorated with either anti-IgM or anti-IgG (positive control) (*n* = 3). Results obtained when the FMNPs were excited at the 525 nm donor absorption (in black), or when the PSE FMNPs were directly excited at the 638 nm FPB-641 absorption (in red). In both cases, fluorescence was monitored at 680 nm.

The last recommendation of a panel of European experts on tacrolimus is the development of analytical methods featuring a limit of quantification up to 1 ng mL^{-1} in

order to provide reliable concentrations during low-dose tacrolimus therapy.[220] In this context, the proposed system would be sensitive enough to quantify tacrolimus in real samples given its insensitivity to the sample fluorescence background. Even more, compared to previously reported fluoroimmunoassays for tacrolimus, the novel FRET-based fluoromagnetic nanoparticles showed similar[221] or superior[222] performance in terms of sensitivity.

4.3. Stability of the FMNPs in the presence of surfactant

The presence of a surfactant, such as the one used in the protocol for antibody conjugation to the magnetic nanoparticles (Tween® 20), might cause partial desorption and re-dissolution of the outermost physisorbed/entrapped BODIPY dyes from the fluorescent-magnetic FRET NPs nanoparticles (FMNPs). For this reason a stability tests of the loaded dye were carried out. FMNPs functionalized with antibodies were tested in buffer in the presence of the surfactant. The protocol for the conjugation of the antibodies to the NPs surface required the use of 0.05% Tween® 20 in PBS 10 mM. This concentration of surfactant in PBS is lower than its critical micelle concentration (CMC).

As it is shown in Figure 80, there was no fluorescence increase of the FMNPs functionalized with antibodies, after washing with 0.05% Tween® 20 (lower concentration than CMC) in PBS 10 mM with respect to the unwashed FMNPs. Instead when the same NPs were previously washed with 0.1% Tween® 20 (higher concentration than its CMC), in PBS 10 mM, an increased fluorescence was observed with respect to FMNPs suspended in surfactant-free buffer (Figure 80). This result can be explained if (partial) desorption of BODIPY dyes from the surface of the FMNPs and successively encapsulation into the Tween® 20 micelles has occurred. This phenomenon has been confirmed by observing the typical emission of PFB-641 at 660 nm in the (filtered) supernatant after washing the FMNPs with Tween® 20. This behavior is the same that was observed when in a water suspension of free BODIPY was added a surfactant (Figure 70)

Therefore, some desorption of the loaded dye can be observed when the NPs are washed with surfactants at concentration higher than the CMC. Nevertheless no changes in the emission were observed when the NPs were washed with a proper concentration (lower than CMC) of surfactant.

---

[220] P. Wallemacq, V. W Armstrong, M. Brunet, V. Haufroid, D. W. Holt, A. Johnston, D. Kuypers, Y. Le Meur, P. Marquet, M. Oellerich, E. Thervet, B. Toenshoff, N. Undre, L. T. Weber, I. S Westley, M. Mourad, *Ther. Drug Monit.,* **2009**, *31*,139–152.

[221] M. Menotta, S. Biagiotti, L. Streppa, L. Rossi, M. Magnani, *Anal. Chem. Acta,* **2015**, *884*, 90–96.

[222] C. Berrettoni, S. Berneschi, R. Bernini, A. Giannetti, I. A. Grimaldi, G. Persichetti, G. Testa, S. Tombelli, C.Trono, F.Baldini, *Procedia Engineer*. **2014**, *87*, 392–395.

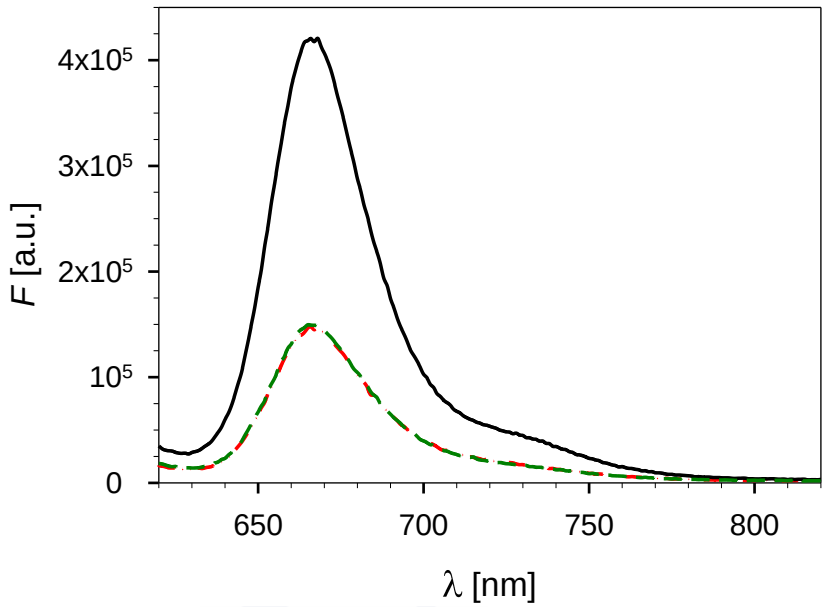
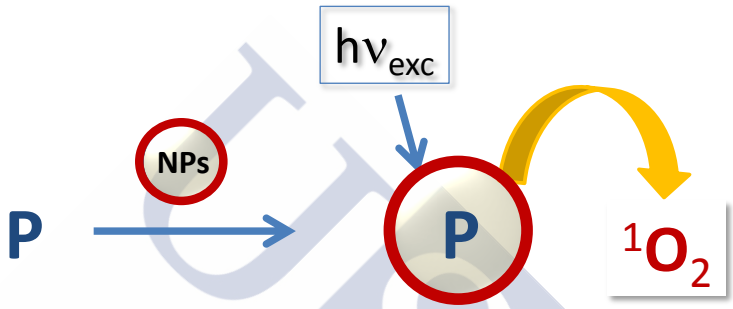


Figure 80. Fluorescence spectra of aqueous suspensions of FMNPs conjugated with antibodies (λ_{ex} = 590 nm, slits 3-3 nm, cut off 590 nm). Green dashed curve: FMNPs not washed with Tween® 20. Red curve: FMNPs after being washed with 0.05% Tween® 20 in PBS. Black curve: FMNPs after being washed with 0.1% Tween® 20 in PBS.

Photosensitizing nanoparticles for singlet oxygen production

1. Objective

The aim of this section is the doping of polystyrene and magnetic NPs with photosensitizers for the production of singlet oxygen (**Scheme 40**). It is expected that the encapsulation into nanoparticles, which allows a higher concentration of photosensitizer, will enhance the singlet oxygen production with respect to the photosensitizers in solution.



Scheme 40. Encapsulation of photosensitizers (P) in nanoparticles (NPs). $^1O_2$ is produced when the photosensitizing nanoparticles are excited with the appropriate light.

Actually, these nanoparticles were prepared with the more ambitious goal as donor nanoparticles for the proximity assay (see introduction section). Unfortunately the study on this assay has not been completed due to the lack of time. In fact, the synthesis of $^1O_2$ acceptor NPs has not been carried out, so that it was not possible to check how the chemiluminescence was produced after the oxidation of the dioxene dopant (singlet acceptor molecule) by singlet oxygen. Therefore this is an occasion to pass the baton to other group member to successfully finish the started work and fining tune the conditions for the proximity assays.

In addition to the proximity assay, the NPs described in this chapter can be used for other purposes, for example as photosensitizers for photodynamic therapy.[223] Some examples reported in the literature show the advantages of the photosensitizers encapsulation in NPs.[224,225] Furthermore it is known that singlet oxygen can be used as a

[223] A. V. Silva, A. Lopez-Sanchez, H. C. Junqueira, L. Rivas, M. S. Baptista, G. Orellana, *Tetrahedron*, **2015**, *71*, 457-462.
[224] M. J. Moreno, E. Monson, Ra. G. Reddy, A. Rehemtulla, B. D. Ross, M. Philbert, R. J. Schneiderd, R. Kopelman, *Sens. Actuator B-Chem.*, **2003**, *90*, 82–89.
[225] G. Boeuf, G. V. Roullin, J. Moreau, L. Van Gulick, N. Z. Pineda, C. Terryn, D. Ploton, M. C. Andry, F.A. Chuburu, M. Molinari, G. Lemercier, *Chem. Plus Chem.*, **2014**, *79*, 171–180.

reagent in organic chemistry. So that encapsulation of photosensitizer into particles would facilitate their removal after completion of the oxidant process.

The objective of producing NPs for generation of singlet oxygen will be reached through the following steps:

1) Selection of an appropriate Ru(II) complex for the doping of polystyrene NPs.

2) Synthesis of photosensitizers based on iodinated BODIPYs with high singlet oxygen production quantum yield Φ_{Δ}.

3) Optimization of protocols for doping both magnetic and non-magnetic polystyrene nanobeads with Ru(II) complexes.

4) Doping of NPs with the synthesized photosensitizers based on iodinated BODIPY using the method used for FRET NPs (see Chapter 2 of "Results and discussion").

5) Once the NPs are prepared, their photophysical and photochemical characterization will be carried out.

6) A method to evaluate the singlet oxygen production quantum yield (Φ_{Δ}) in NPs will be developed.

2. Ruthenium complexes as photosensitizer dyes

Singlet oxygen is produced by photosensitization involving energy transfer from the triplet excited state of a photosensitizer dye. The above photosensitizer is a chemical entity which produces reactive oxygen species (ROS) upon irradiation with light.

Ruthenium complexes hold most of the properties that a good photosensitizer should exhibit:[226,227,228] a) relatively strong absorption in the visible spectrum (blue-green); b) a triplet excited state of suitable energy (>95 kJ mol^{-1}); c) intersystem crossing quantum yields as close to unity as possible; d) relatively long triplet state lifetimes; e) high $^1O_2$ generation quantum yield (Φ_{Δ}) (>0.5), and f) high photo and thermal stability.[229] Another important advantage of the Ru(II) complexes is that they can be immobilized (by adsorption, electrostatically or covalently) on different polymers depending on the nature of the coordinating polypyridyl ligand. Actually, many of the photosensitizers based on ruthenium complexes display a quantum yield of singlet oxygen production higher than the well-studied methylene blue or the rose Bengal.[230]

[226] F. Manjón, L. Villén, D. García-Fresnadillo, G. Orellana, *Environ. Sci. Technol*. **2008**, *42*, 301–307.
[227] D. García-Fresnadillo, Y. Georgiadou, G. Orellana , A. M. Braun, E. Oliveros, *Helv. Chim. Acta*, **1996**, *79*, 1222–1238.
[228] G. Orellana, C. Alvarez-Ibarra , M. L. Quiroga, *Bull. Soc.Chim.Belg.*, **1988**, *97*, 731–741.
[229] M. C. DeRosa, R. J. Crutchley, *Coordination Chemistry Reviews*, **2002**, *233–234*, 351–371.
[230] G. Orellana, A. M. Braun, *Helv. Chim. Acta* **1996,** *79,* 1222–1238.

The tris(4,7-diphenyl-1,10-phenanthroline)ruthenium(II) complex (RD3) (Figure 81) was chosen as photosensitizer to dope $^1O_2$ generating NPs. It has high hydrophobicity and thus it can be readily encapsulated into polystyrene NPs by simple entrapment. Moreover, it has a very high quantum yield of singlet oxygen production (0.97 in methanol).[230] The complex belongs to a large library of ruthenium complexes available in our research group and its synthesis was not performed. RD3 had been prepared using established methods described by G. Orellana and co-workers.[230,231]

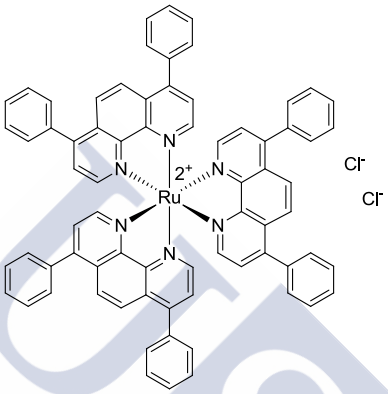


Figure 81. Chemical structure of [tris(4,7-diphenyl-1,10-phenanthroline)ruthenium(II)] dichloride (RD3).

Table 10 collects the spectroscopic features of RD3 reported in the literature.[230]

Table 10. Relevant spectroscopic characteristics of RD3 in solution.[230]

RD3 $[Ru(dip)_3]^{2+}$	**λ_{abs} [nm]**	**ε [$M^{-1}cm^{-1}$]**	**λ_{em} [nm]**	**Φ_Δ**	**τ_{Ar} [ns]**	**τ_{Air} [ns]**	**τ_{O_2} [ns]**
CH_3OH	462	29450	619				
H_2O	460	29500	632				
CD_3OD				0.97	5944	241	52
D_2O			638	0.42	5287	949	211

[231] G. Orellana, C. Alvarez-Ibarra, M. L. Quiroga, *Bull. Soc. Chim. Belg.,* **1988,** *97*, 73–81.

3. BODIPY dyes as photosensitizer

To overcome the scarcity of photostable photosensitizing dyes with absorption in the yellow-red region, a new class of sensitizer based on the BODIPYs scaffold has been developed in the last few years. BODIPY dyes have generally a very high fluorescence; they are highly photostable and show a poor quantum yield of triplet formation. In order to transform them in productive photosensitizer dyes, a spin-orbit perturbation must be introduced. This goal can be achieved by incorporating in the BODIPY core heavy atoms that promote intersystem crossing (ISC).[232, 233]

3.1. Electrophilic substitution reactions: halogenation

The 2- and 6-positions of the BODIPY core carry the least positive charge, as follows from the study of the structures contributing to the BODIPY core resonance; consequently these positions are the most reactive to electrophilic attack (Figure 82).[234]

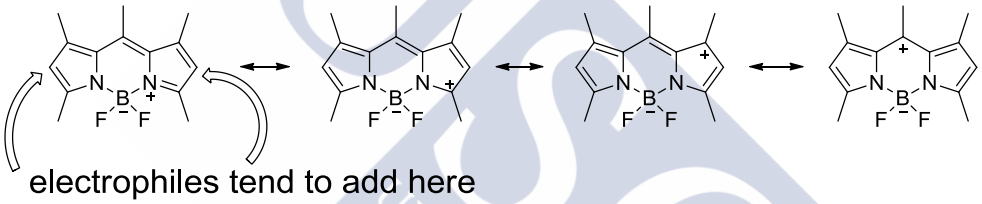
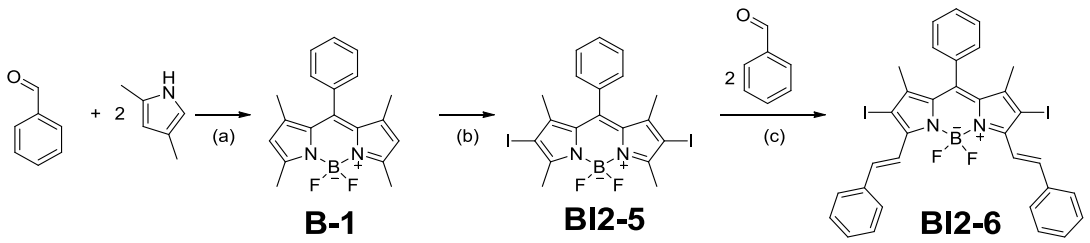


Figure 82. Mesomeric structures of BODIPY.

Bromination or iodination provide the dihalogenated product with the Br or I in positions 2 and 6.[235,232] Predictably, introduction of halogen substituents causes the quenching of the BODIPY fluorescence due to the heavy atom effect and a red shift in the absorption and emission maximums due to their electronic effect. Brominated or iodinated BODIPYs are efficient photosensitizers and show better photostability than Rose Bengal because the BODIPY core has a more positive oxidation potential.[233]

The target photosensitizers were prepared following synthetic protocols described in the literature.[232236,237,235] In this work iodinated BODIPY dyes were prepared with a similar chemical structure to those BODIPYs used for the FRET NPs (Scheme 41 and Chapter 2).

[232] Y. Gabe, Y. Urano, K. Kikuchi, H. Kojima, T. Nagano, *J. Am. Chem. Soc*., **2004**, *126*, 3357–3367.
[233] T. Yogo, Y. Urano, Y. Ishitsuka, F. Maniwa, T. Nagano, *J. Am. Chem. Soc.* **2005**, *127*, 12162–12163.
[234] S. Banfi, G. Nasini, S. Zaza, E. Caruso, *Tetrahedron*, **2013**, *69*,4845–4856.
[235] T. Yogo, Y. Urano, Y. Ishitsuka, F. Maniwa, T. Nagano, *J. Am.Chem. Soc.*, **2005**, *127*, 12162–1263.
[236] L. Huang, J. Zhao, S. Guo, C. Zhang, J. Ma, *J. Org. Chem.* **2013**, *78*, 5627–5637.
[237] W. Wu, H. Guo, W. Wu, S. Ji, J. Zhao, *J. Org. Chem*., **2011**, *76*, 7056–7064.



Scheme 41. Scheme of the synthesis of photosensitizing BODIPYs. (a) Condensation of the aldehyde followed by oxidation with *p*-chloranil, and finally the complexation with $BF_3{\cdot}OEt_2$ in DCM, under Ar atmosphere, at r.t. during 18 h. (b) *N*-Iodosuccinimide (NIS), anhydrous DCM under Ar atmosphere, at r.t. during 1 h. (c) Knoevenagel-type condensation of BI2-5 in anhydrous conditions, with toluene reflux, 24 h.

The synthesis starts with the condensation of benzaldehyde with 2,4-dimethylpyrrole in the presence of trifluoroacetic acid (TFA), followed by oxidation with *p*-chloranil, and final complexation with $BF_3{\cdot}OEt_2$ in order to coordinate the boron to the pyrrolic nitrogen atom. The B-1 BODIPY obtained is then iodinated by electrophilic halogenation in positions 2- and 6- of the BODIPY core by *N*-iodosuccinimide (NIS). Finally, the more extended conjugated BI2-6 BODIPY is obtained by a Knoevenagel-type condensation of BI2-5 BODIPY with benzaldehyde in the presence of piperidine under anhydrous conditions.

The B-1, BI2-5 and BI2-6 dye were carefully purified by column chromatography and characterized by mass spectrometry and ^{1}H-NMR. The results were in agreement to those already published.[238,236,236] The reaction yields for compounds B-1 and BI2-5 are comparable to those published, while for the BI2-6 the yield obtained with reflux (20%) is lower than that already reported by L. Huang et al.[239] (42%), which used MW. After purification, the photophysical characterization of BI2-5 and BI2-6 was carried out (Figure 83) and the results compared to those reported in the literature.

[238] W. Wu, H. Guo, W. Wu, S Ji, J. ZhaoJ., *Org. Chem*., **2011**, *76*, 7056–7064.
[239] Y. Chen, J. Zhao, H. Guo, L. Xie, *J. Org. Chem.*, **2012**, *77*, 2192–2206.

Table 11. Photophysical characteristics of BODIPY dyes B-1, BI2-5 and BI2-6.

Dye	*Solvent*	λ_{abs} [nm]	ε x 10^5 [$M^{-1}cm^{-1}$]	λ_{em} [nm]	Φ_f[a]	Φ_Δ[b]	τ_f [ns][c]	τ_T [μs][d]	*Ref*
B-1	ACN	503	0.82	515	0.712		3.86	0.02	237
B-1	$PhCH_3$	504	0.94	516	0.852		3.4		240
B-1	DCM	501	0.87	513					240
B-1	MeOH	498	0.88	509					240
B-1	DMSO	502		517	0.55				241
BI2-5	EtOH	532	0.46	548	0.040[e]				Tw[f]
BI2-5	ACN	529	0.89	552	0.023		0.13	57.1	237
BI2-5	ACN	529	0.85	548	0.027	0.79		84.6	236
BI2-5	DMF/H_2O					0.30			242
BI2-6	EtOH	634	1.47	650					Tw[f]
BI2-6	$PhCH_3$	643	1.03	663	0.1				243
BI2-6	DCM	637	0.94	660	0.1	0.62			243
BI2-6	ACN	629	0.90	655	0.1				243
BI2-6	$PhCH_3$				0.3[g]				Tw[f]
BI2-6	ACN	630	0.77	654	0.05	0.69		1.8	236
BI2-6	DMF/H_2O					0.21			242

a) Fluorescence quantum yield. b) Singlet oxygen generating quantum yield with Rose Bengal (RB) as the standard (Φ_Δ = 0.8 in methanol) at 22 °C. c) Fluorescence lifetime. d) Triplet state lifetimes, measured by transient absorption spectra. e) Rhodamine 123 was used as standard (Φ_f = 0.90 in ethanol). f) This work. g) Oxazine 170 was used as standard (Φ_f = 0.58 in ethanol).

[240] Y. Chen, J. Zhao, H. Guo, L. Xie, *J. Org. Chem.*, **2012**, *77*, 2192−2206.
[241] A. Vázquez-Romero, N. Kielland, M. J. Arévalo, S. Preciado, R. J. Mellanby,Y. Feng, R. Lavilla, M. Vendrell, *J. Am. Chem. Soc.*, **2013**, *135*, 16018−16021.
[242] W. Wu, Y. Geng, W. Fan, Z. Li, L. Zhan, X. Wu, J. Zheng, J. Zhao, M. Wu, *RSC Adv.*, **2014**, *4*, 51349−51352.
[243] J. Ma, X. Yuan, B. Küçüköz, S. Li, C. Zhang, P. Majumdar, A. Karatay, X. Li, H. G. Yaglioglu, A. Elmali, J. Zhao, M. Hayval, *J. Mater. Chem. C*, **2014**, *2*, 3900−3913.

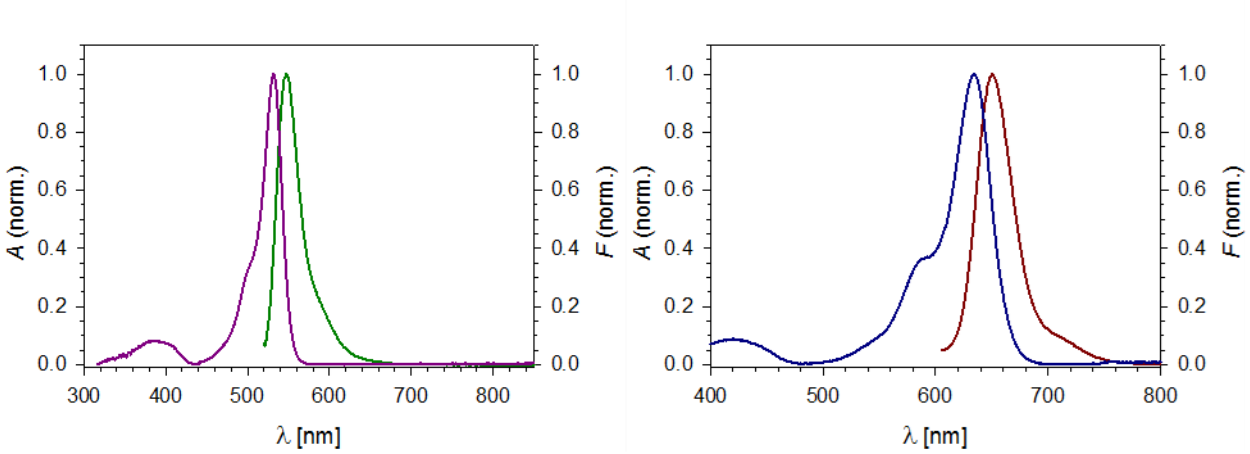


Figure 83. Left: normalized absorption (purple) and emission (green) spectra of BI2-5 in ethanol (λ_{ex}= 513 nm). Right: normalized absorption (blue) and emission (red) spectra of BI2-6 in ethanol (λ_{ex} = 600 nm).

It can be seen that the Φ_f decreases by an order of magnitude once the BODIPY dyes has been functionalized with iodine. The values obtained in this thesis are slightly higher than those reported in literature; this could be due to the presence of a small amount of monoiodinated BODIPY in the sample of the reported value. BI2-5 and BI2-6 are good photosensitizers as they display high Φ_Δ. In the presence of H_2O the singlet oxygen production quantum yield considerably decreases; however, these values are still high.

4. Doping of NPs with the BODIPY photosensitizing dyes

The commercial polystyrene NPs provided by Bangs Laboratories® functionalized with carboxylic groups on the surface and with a diameter of of 390 nm (by dynamic light scattering, from the provider) were doped with the iodinated BODIPY photosensitizers. The commercial carboxylated magnetic nanospheres (Estapor®, Merck Millipore) of 300 nm diameter were also doped. Both commercial NPs suspension have a solid content of 10 mg/mL.

The protocol optimized for the BODIPY dyes was followed (see Chapter 2 of "Results and discussion").

The commercial NPs were diluted in H_2O, and then a THF stock solution of ***BI2-6*** was added. The volume of THF was kept at 25% of the total volume (H_2O) and the concentration of photosensitizer was 40 nmol/mg NPs. After 3 h of swelling, the NPs were washed three times with water. Two different batches of 390 nm polystyrene NPs from Bangs (**92A** and **92B**) were prepared. Likewise, the two batches **M92C** and **M92D** were synthesized with 300 nm Estapor® MNPs.

It must be taken into account that in every doping procedure a small amount of nanoparticles is lost during the washing steps. In order to have a fast tool for determining the concentration of NPs in an aqueous suspension after washing, calibration curves of absorption vs. concentration of NPs (in mg/mL) were built. A very good (linear) correlation was found between the measured absorption at 600 nm (due to the scattering of the red light) and the NPs concentration.

Taking into account the dilution used, is then possible to know the exact concentration of the NPs (mg/mL) in the water suspension using the equation built in the calibration. The calibration curves are reported in the Experimental part in section 13.

The equations obtained for the 390 nm polystyrene NPs (Bangs) and for the 300 nm Estapor® magnetic NPs are respectively:

$$y = 7.4\,x \quad (1)$$

$$y = 10.7\,x \quad (2)$$

Where y is the absorbance at 600 nm and x is the concentration of NPs in mg/mL. The concentration mg/mL of the NPs doped with BODIPY photosensitizer are summarized in Table 12.

Table 12. Concentration of the NPs suspension doped BI2-6 and the total amount of photosensitizer per mg of NPs.

Sample	***NPs* [mg/mL]**	***BI2-6 per mg NPs* [nmol][a]**
92a	1.44	40
92b	1.41	40
M92c	3.33	40
M92d	3.59	40

a) Calculated knowing the volume added (0.5 mL) of the BI2-6 stock solution (0.159 mM) and the quantity of PSt-COOH of 300 nm NPs in the sample (2 mg).

Emission and excitation spectra were recorded for each sample of NPs. The excitation instead of absorption spectra are measured because scattering of the suspensions was too strong to yield meaningful spectra. The normalized spectra of BI2-6 doped NPs (92a) and the normalized spectra of with Estapor® MNPs of 300 nm (M92c) are shown in Figure 84 and Figure 85, respectively.

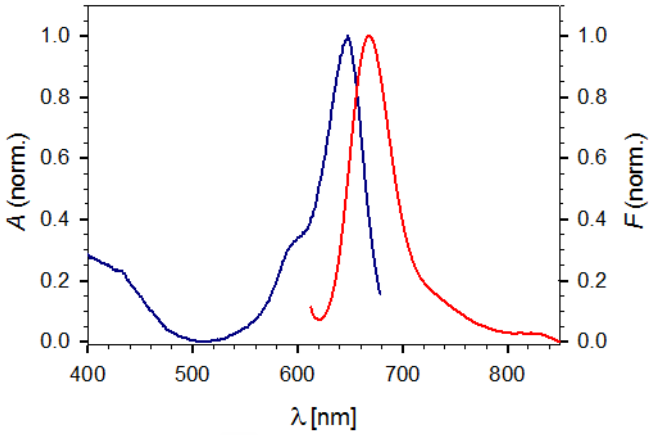


Figure 84. Normalized excitation (blue, λ_{em} = 690 nm, slits 5-5 nm, 20 µL of sample in 3 mL H_2O) and emission (red, λ_{ex} = 590 nm, slits 5-5 nm, 20 µL of sample in 3 mL H_2O) spectra of 390 nm PSt-COOH NPs doped with BI2-6.

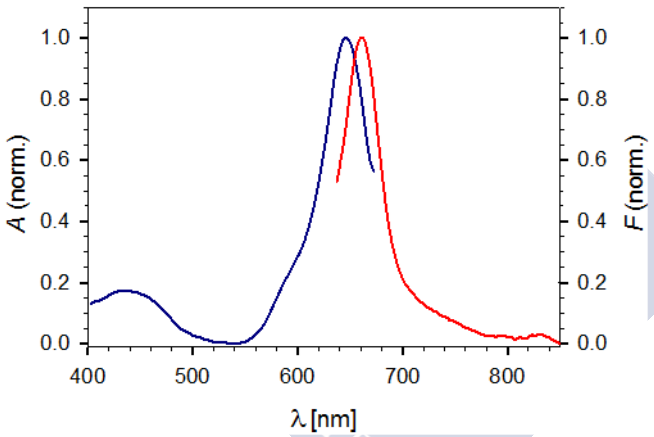


Figure 85. Normalized excitation (blue, λ_{em} = 690 nm, slits 5-5 nm, 20 µL of sample in 3 mL H_2O) and emission (red, λ_{ex} = 590 nm, slits 5-5 nm, 20 µL of sample in 3 mL H_2O) spectra of 300 nm Estapor® MNPs doped with BI2-6.

The fluorescence of the doped polystyrene NPs was compared to that of MNPs. It was calculated as the area under the curve and, in this case, it was necessary to normalize the intensity for 1 mg of NPs because each sample has a different concentration (mg/mL) of NPs (Table 12 and Figure 86). The samples were prepared in duplicate using the same BI2-6 stock solution and performing the swelling at the same time, using an Eppendorf adapter as vortex accessory in order to have a more accurate comparison and to be sure that 1 mg of the two types of NPs contain the same amount of dye. The MNPs presents a very low emission intensity in comparison with the non-magnetic NPs probably because quenching and/or absorption of the incident light by the ferrite nanograins.

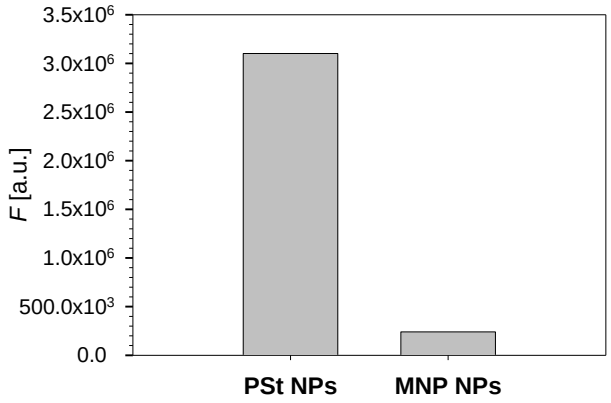


Figure 86. Comparison between the magnetic (MNPs) and non-magnetic (PSt) NPs emission intensity (for 1 mg of NPs) in aqueous suspension of BI2-6 doped NPs.

Emission spectra were also recorded at λ_{ex} = 532 nm because this is the wavelength of the excitation light used for the experiment with laser kinetic spectrometry to detect the decay of singlet oxygen (Figure 87). In these conditions, the MNPs did not emit.

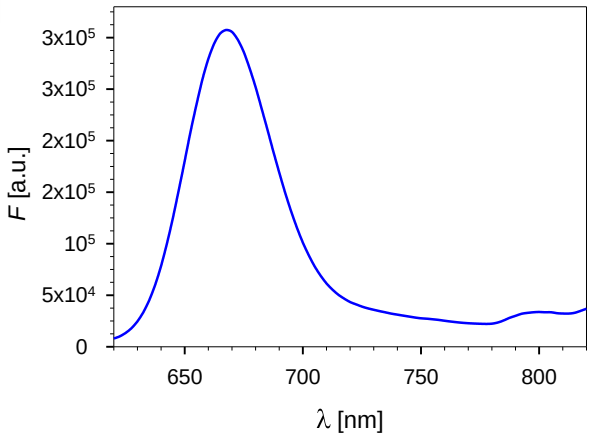


Figure 87. Corrected emission spectra of the non-magnetic NPs doped with BI2-6 (λ_{ex} = 532 nm, slits 5-5 nm, 20 μL of sample in 3 mL H_2O).

As it was observed for the NPs doped with PFB-515 and PFB-641 (see Chapter 2 of "Results and discussion") there is a considerable red shift in the fluorescence maxima compared to the free photosensitizer in toluene: the absorption and emission maxima of the BI2-6 dye in toluene are 634 and 650 nm respectively, while the corresponding maxima for the fluorescent nanoparticles (92a/b) doped with BI2-6 are 646 and 666 nm, respectively (Table 13).

Table 13. Spectroscopic characteristics of water suspensions of NPs doped with BI2-6 and of the free photosensitizer BI2-6 in ethanol.

Sample	λ_{abs} **[nm]**	λ_{em} **[nm]**
NPs 92a&b	646	666
BI2-6	634	650

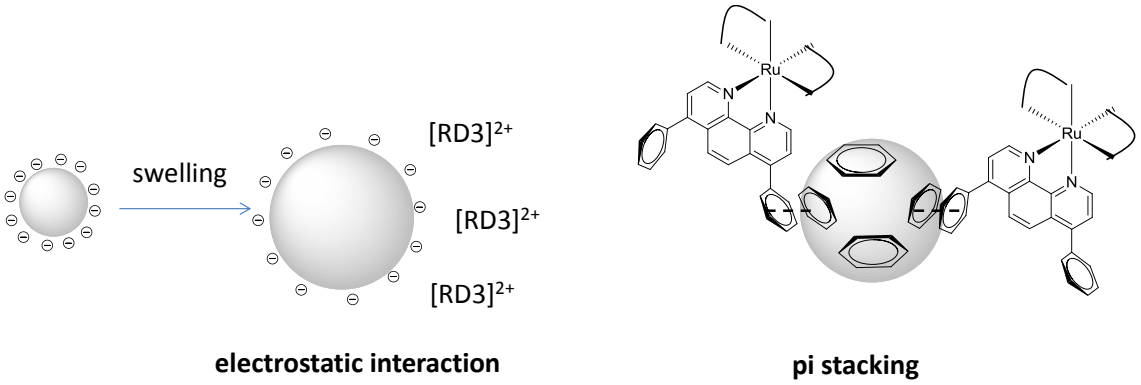
5. Doping of polystyrene NPs with the ruthenium photosensitizing dyes

In this section it will be described how another photosensitizer will be encapsulated into the nanoparticles in order to evaluate the production of singlet oxygen. The protocol already developed for the BODIPY dyes (see Chapter 2 of "Results and discussion") could not be applied for the ruthenium complex because it is not soluble in THF. The procedure for preparing these new NPs is discussed below. Moreover, characterization of the NPs has been carried out in order to choose the best NP in terms of the amount of photosensitizer per nanoparticle that can be encapsulated. With this feature in mind, the NPs with the highest emission signal should correspond to those with the highest singlet oxygen generation yield as well.

5.1. Polystyrene carboxylated nanoparticle (PSt-COOH NPs) doped with RD3

The same commercial polystyrene NPs used for the doping with BODIPY photosensitizers were also used for encapsulating RD3 (see section 2). NPs of different sizes (20 nm, 200 nm and 390 nm diameter by dynamic light scattering, as per the supplier) were tested and finally used for different purposes.

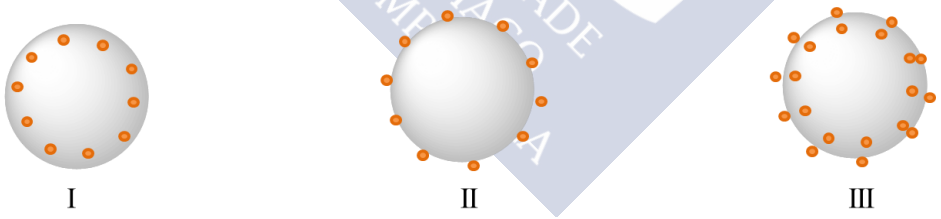
The polymeric matrix of the selected commercial PSt-COOH NPs has to be swollen. In this way, the external carboxylic groups should become more separated and the polymeric structure of the NPs will be less compact.



Scheme 42. Left: the NP swelling makes the negative charges of carboxylic groups accessible to a higher number of RD3 dye molecules. Right: π-π-stacking interactions between the aromatic rings of the complexes and the polystyrene surface (probably, with both phenyl substituents).

There are three possible ways in which the RD3 will interact with the NPs: a) by π-π stacking between the aromatic rings of the complexes and the polystyrene surface of the NPs; b) became entangled into the swollen polymeric matrix; or c) associate through electrostatic interaction between the positive charge of the complex and the negative charge of the carboxylic functional group of the NPs (Scheme 42).

Hence the RD3 photosensitizer can be found inside the NPs if it permeates the polystyrene surface, just in onto the surface of NPs in the case of electrostatic interactions (including π–π-stacking), or in both positions simultaneously (Scheme 43).



Scheme 43. Possible location of RD3 in the NPs.

5.1.1. Nanoparticles swelling with different solvents

The mandatory requirement is that the swelling solvent has to exhibit miscibility with water, because the nanoparticles are used in aqueous suspension. Furthermore, it must be able to dissolve the photosensitizer dye.

In order to load the PSt-COOH NPs with RD3, different solvents were tested, namely acetonitrile (ACN), 1,4-dioxane, tetrahydrofuran (THF) with 2% MeOH, dimethylformamide (DMF), dimethyl sulfoxide (DMSO). Therefore, tests for loading the dye were made for each solvent. The solvent in which the Ru complex is better dissolved was acetonitrile.

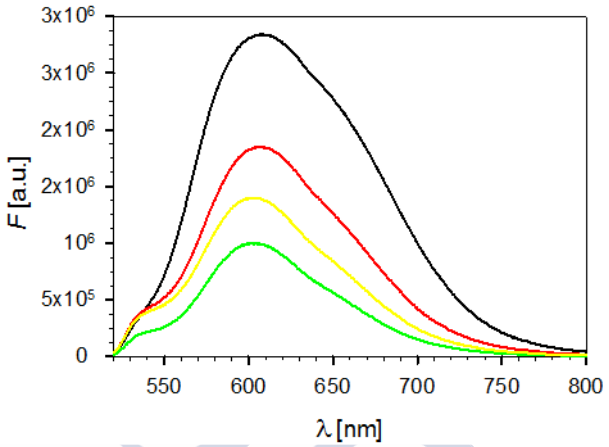
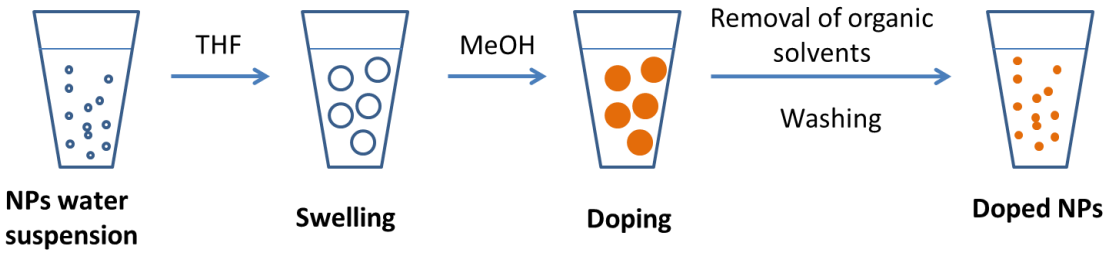


Figure 88. Emission spectra of polystyrene NPs doped with RD3 (λ_{ex} = 450 nm, slits 5-5 nm, cut off filter at 515 nm 100 μL of doped NPs in 2.5 mL of H_2O). ACN (black line), DMF (red line), THF (green line) 1,4-dioxane (yellow line).

As it is shown in Figure 88, the doped NPs show higher emission intensity when the swelling is made with ACN. However we noticed that the NPs precipitate and aggregate when swollen in this solvent. In DMSO, the NPs collapse. In DMF and 1,4-dioxane, leakage of the photosensitizer after some weeks was noticed. Therefore, finally THF with 2% methanol was selected as swelling solvent. As described for the NPs doped with BODIPY, THF it is the best solvent for swelling polystyrene nanoparticles. Unfortunately RD3 is not soluble in this solvent, so that a mixture of THF-MeOH was needed. RD3 is highly soluble in MeOH, and MeOH is also miscible with THF and H_2O.

5.1.2. Study of the swelling with different methanol-THF mixture

The dye loading protocol is summarize in Scheme 44. Polystyrene NPs of 390 nm were used.



Scheme 44. Procedure for doping the PSt-COOH NPs with RD3.

The composition of the solvent mixture for swelling the NPs was optimized using varying percentages of THF, MeOH and H_2O, but keeping constant the amount of RD3. Stock solutions of RD3 in methanol with different concentrations were prepared. The detailed protocol, for doping the NPs is described in the Experimental part. Suspended PSt-COOH NPs were diluted with H_2O, then the corresponding amount of THF was added and the NPs were kept shaken for 30 min. Thus a RD3 stock solution in methanol was mixed in the suspension (Table 14). Finally the NPs were re-suspended in water protected from light and stored at 4 °C. Eight different volume ratios of H_2O/THF/MeOH were tested: 1/0.1/0.025; 1/0.075/0.05; 1/0.025/0.1; 1/0.05/0.15; 1/0.2/0.05; 1/0.15/0.1; 1/0.1/0.15; 1/0.225/0.025 (Table 14). NPs prepared with 1/0.1/0.025; 1/0.075/0.05 and /0.225/0.025 solvent mixture aggregate immediately and were discarded.

Table 14. Final NPs concentrations after loading the RD3 dye in the specific solvent mixture used for the swelling and concentration of RD3 stock solutions employed in each solvent mixture.

Mixture (by volume) ***H_2O/THF/MeOH***	***NPs concentration*** **[mg/mL]**	***RD3 SS in*** ***MeOH*** **[mM]**
1/0.025/0.1	3.65	0.23
1/0.05/0.15	2.45	0.15
1/0.2/0.05	2.37	0.46
1/0.15/0.1[a)]	**2.57**	**0.23**
1/0.1/0.15	4.68	0.15

a) Strongest emission per mg of NPs achieved.

The luminescence for each batch of NPs was calculated as the area under the emission curve. To select the best solvent mixture it was necessary to normalize the emission to 1 mg of NPs because, as it is reported in the Table 4, the concentration mg/mL of NPs is

different for each sample. The highest degree of doping, as assessed by the strongest emission per mg of NPs it was achieved using the proportion of H_2O/THF/MeOH 1/0.15/0.1 (Figure 89). For this reason this mixture of solvents was then used always for the preparation of particles.

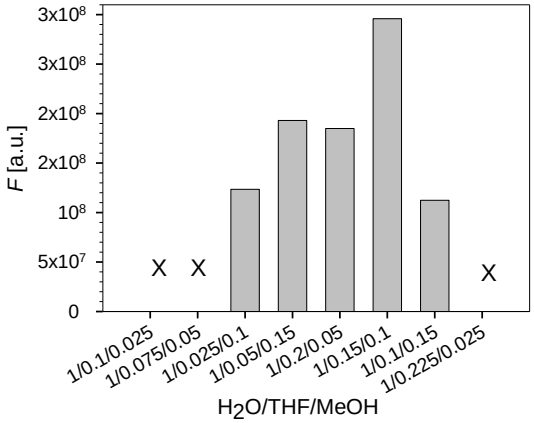


Figure 89. Emission (calculated as the area under the curve of each emission spectrum) of 10 mg of RD3 doped 390 nm PSt-COOH NPs as a function of the solvent mixture used during the swelling process.

5.1.3. Study of the dye leaching

In order to check that the RD3 complex was not leaching out from the NPs, the dye-doped NPs were suspended in pH 2 buffer and washed several times with water. Leaching of the dye was ruled out because the supernatant did not show any measurable luminescence at 620 nm in any of the washing steps (Figure 90), the emission maximum of RD3. The small signal at 530 nm is the Raman band of the water.

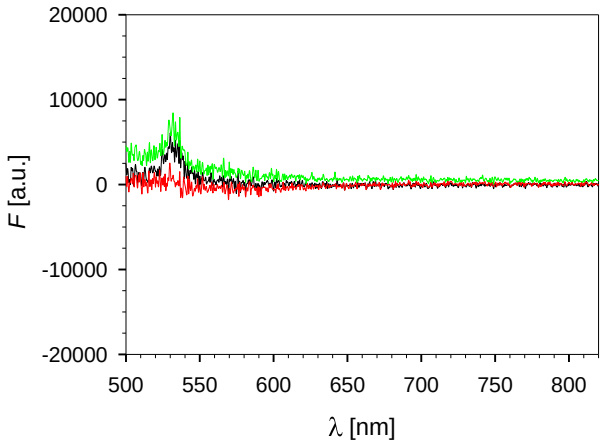


Figure 90. Luminescence of the filtered NPs supernatant obtained after each of three washing steps. (λ_{ex} = 420 nm, slits 5-5).

5.1.4. Optimum loading of the RD3 photosensitizer in 390 nm PSt-COOH NPs

Once the mixture of solvents for the best loading was optimized, the procedure was further refined. This time the amount of methanol was kept constant and the amount of ruthenium complex per mg of NPs was increased. Table 15 summarize the concentration of each sample.

During the washing steps a large amount of NPs was lost because many NPs are stuck to the centrifugation tubes walls that were not previously blocked with buffer. The final concentration of the NPs was calculated measuring the absorbance in H_2O at 600 nm of an aliquot of the RD3 doped NPs, according to Equation (1).

Table 15. RD3 loading and concentration of the 390 nm NPs suspended in water after the washing process.

Sample code	RD3 SS in MeOH [mM]	RD3 per 1 mg of NPs [nmol] [a)]	NPs concentration [mg/mL][b)]
17a	0.228	4.56	2.09
17b	0.459	9.18	1.16
17c	0.895	17.00	0.67
21a	1.04	20.78	1.53
21b	1.30	26.00	1.16
21c	1.80	35.92	0.96

a) Assuming all the RD3 added during the loading procedure has attached to the NPs. b) Calculated according to equation (1).

In order to know which batch shows the highest photosensitizer loading, their emission spectra were recorded (Figure 91). The overall luminescence was calculated as the area under the curve and normalized to 1 mg of NPs because each sample has a different concentration (mg/mL) (Figure 92).

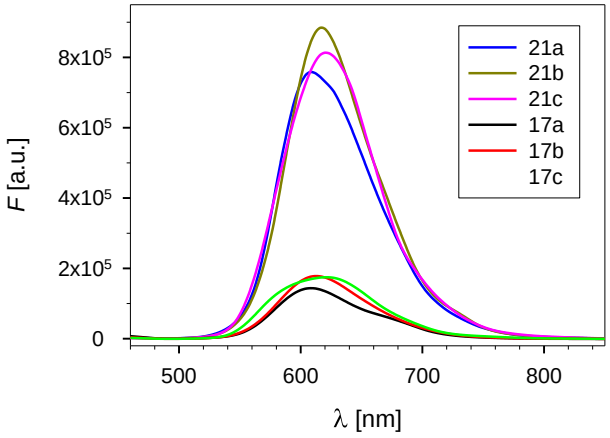


Figure 91. Emission spectra of 20 µL of 390 nm PSt-COOH NPs doped with different amount of RD3 (**Table 15**) in 3000 µL of H_2O (λ_{ex} = 450 nm, cut off filter of 515 nm, slits 3-3 nm).

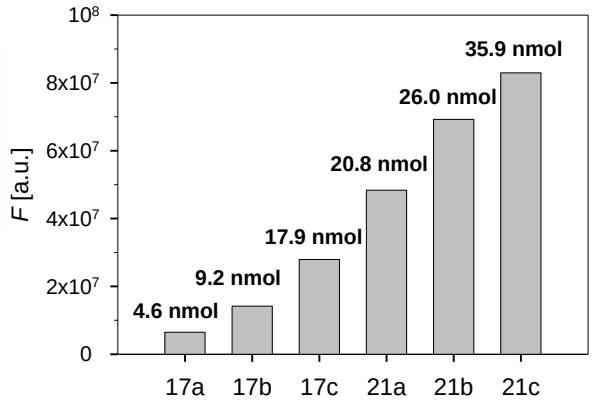


Figure 92. Emission intensity of aqueous suspensions of RD3-doped PSt-COOH NPs OF 390 nm as a function of the RD3 amount used for loading (assuming all the RD3 used has bound to the NPs as in the supernatant any measurable luminescence at 620 nm was observed as shown in Figure 90).

The selected loading of RD3 was 20.8 nmol per mg of NPs (sample 21a). Batch 21b and 21c were discarded because aggregation was observed just one week after their preparation.

5.1.5. Preparation of 200 nm PSt-COOH NPs

Bang Labs® NPs of 200 nm diameter were also tested. The beads were doped using the same protocol optimized for the 390 nm NPs. Two batches were prepared with much higher doping of RD3 (504 nmol and 358 nmol of RD3 per mg of NPs) than the optimized concentration found for the 390 nm NPs (20.8 nmol of RD3 per mg of NPs). The smaller beads were prepared with a different purpose than the "proximity assay" (Introduction) and thus the aggregation of the beads is not so important. The excitation

and emission spectra of the RD3 doped PSt-COOH NPs mirror the corresponding spectra of the free RD3 in solution (Figure 93).

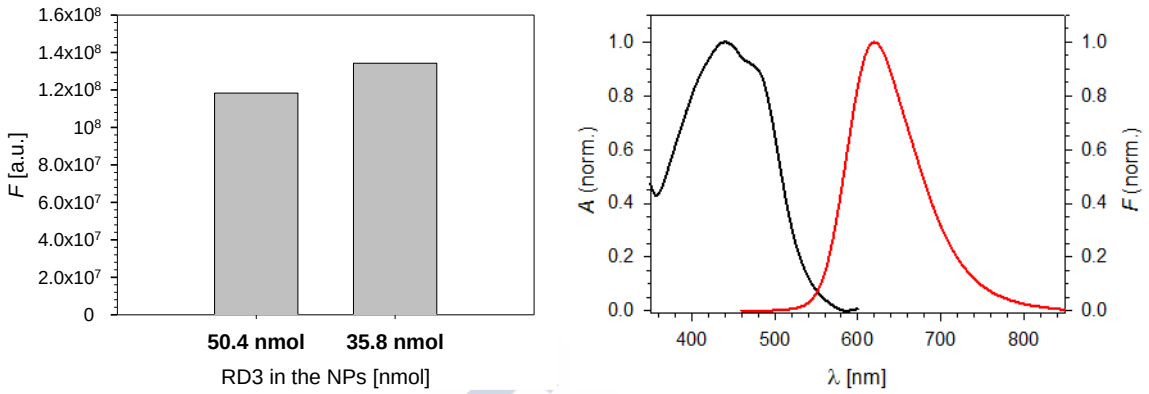


Figure 93. Left: emission intensity (calculated as the area under the emission spectrum) for mg of 200 nm PSt-COOH NPs doped with RD3. Right: normalized excitation (black, λ_{em} = 620 nm, slits 5-5 nm) and emission (red, λ_{ex} = 450 nm, 515 nm cut-off filter, slits 3-3 nm) spectra of 200 nm PSt-COOH NPs doped with RD3.

The final concentration of the washed NPs was calculated with Equation (3) built in the calibration procedural (see Experimental Part) were y is the absorbance at 600 nm and x is the concentration of the NPs in mg/mL.

$$y = 3.2\,x \tag{3}$$

Table 16. RD3 loading and concentration of the 200 nm NPs suspended in water after the washing process.

Sample code	RD3 SS in MeOH [mM]	RD3 per mg of NPs [nmol][a)]	NPs concentration [mg/mL][b)]
146A	1.26	50.4	2.3
146B	0.90	35.8	2.2

a) Moles of dye per mg of PSt-COOH NPs (dry weight). b) Assuming all the RD3 added during the loading procedure has attached to the NPs. c) Calculated according to equation (3).

5.1.6. Preparation of doped RD3 26 nm PSt-COOH NPs

RD3 PSt-COOH NPs of 26 nm diameter (Bang Labs®) were also prepared. The NPs were doped with the optimized protocol for the RD3 390 nm PSt-COOH NPs. For these 26 nm NPs of the washing step was carried out by dialysis because they are too small to be

centrifuged. The following mixture was prepared: 3800 μL of H_2O, 200 μL 26 nm PSt-COOH NPs stock (suspended in water), 600 μL of THF, 400 μL of RD3 stock solution in methanol with the required concentration, (see In order to know which sample shows the optimum photosensitizer load, emission spectra for these batches were recorded. The emission intensity was calculated as the area under the curve and, in this case, it was also necessary to normalize the intensity for 1 mg of NPs (like those of the 390 nm and 200 nm NPs) because each sample has a different NPs concentration (Figure 94, right).

Table 17 for the exact concentration of stoke solution for each NPs batch). The dialysis bag containing the NPs batch suspension was immersed in a 250 mL beaker full of water. The water was changed four times during 25 h. Leaching of the dye into the dialysate was not observed. When the dialysis process was finished, the NPs suspension was transferred to a glass vial and the final volume was measured therefore the final concentration mg/mL of the doped NPs batches could be determined (In order to know which sample shows the optimum photosensitizer load, emission spectra for these batches were recorded. The emission intensity was calculated as the area under the curve and, in this case, it was also necessary to normalize the intensity for 1 mg of NPs (like those of the 390 nm and 200 nm NPs) because each sample has a different NPs concentration (Figure 94, right).

Table 17). Five batches were prepared with different RD3 concentration from 4.5 to 22.4 nmol of RD3 per mg of NPs.

In order to know which sample shows the optimum photosensitizer load, emission spectra for these batches were recorded. The emission intensity was calculated as the area under the curve and, in this case, it was also necessary to normalize the intensity for 1 mg of NPs (like those of the 390 nm and 200 nm NPs) because each sample has a different NPs concentration (Figure 94, right).

Table 17. RD3 loading and concentration of the 20 nm NPs after the washing process.

Sample code	RD3 SS in MeOH [mM]	RD3 per mg of NPs [nmol][a)]	Final volume [mL]	NPs concentration [mg/mL][b)]
14-1	0.22	4.48	4.95	4.04
14-2	0.44	8.94	5.77	3.47
14.3	0.67	13.42	5.58	3.58
14.4	0.90	17.90	5.05	3.96
14-5	1.11	22.38	4.55	4.40

a) Assuming all the RD3 added during the loading procedure has attached to the NPs. c) Calculated dividing 20 mg per the final volume of NPs.

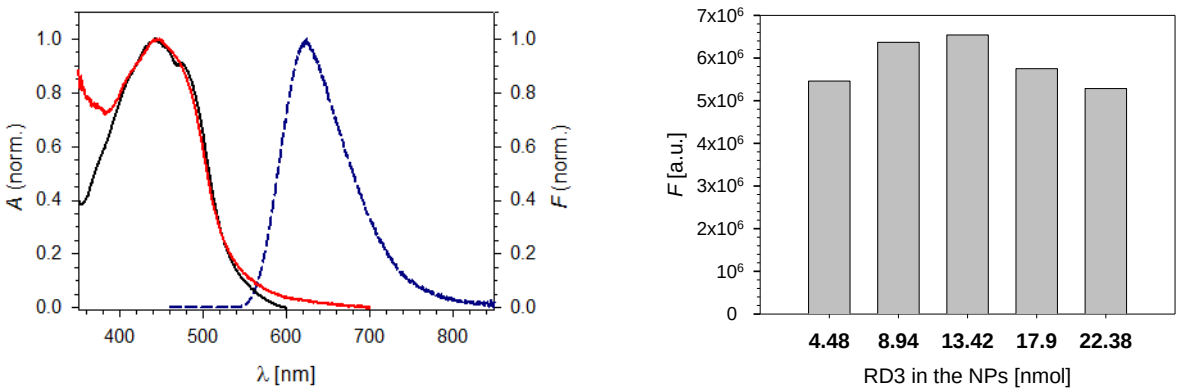


Figure 94. Left: normalized, absorption (black), excitation (red) and emission (blue) spectra in H_2O of the 26 nm NPs doped with RD3. Right: emission intensity of aqueous suspensions of RD3 doped PSt-COOH NPs as a function of the RD3 concentration.

The absorption, emission and excitation spectra of the 26 nm RD3-doped PSt-COOH NPs are depicted in the Figure 94, left. The spectra of the doped NPs possess the typical fingerprint of ruthenium polypyridyl complexes: a broad (black) absorption and (blue) emission corresponding to an allowed ^{3}MLCT transition.

In this case the best loading was found with 13.4 nmol of RD3 per mg of NPs. This concentration is significantly lower than the one found for the best loading in the 390 m NPs, a reasonable result taking into account the smaller size of the beads. The optimum NPs doped with RD3 were then used to measure the singlet oxygen production quantum yield.

6. Magnetic nanoparticles (MNPs-COOH) doped with RD3

Commercial carboxylated magnetic nanospheres (Estapor®, Merck Millipore) of 300 nm diameter (the same NPs doped with BODIPY dyes PFB-515 and PFB-641) were also doped with RD3. The protocol developed for the RD3 doped 390 nm PSt-COOH NPs was used. In this case, after the swelling process, it was not necessary to wash the NPs by centrifugation but the supernatant was removed while the MNPs-COOH were being held on the bottom with the aid of a Nd magnet. Two batches with different RD3 concentrations were prepared. When suspended in H_2O, the MNPs-COOH have a comparable emission intensity to the non-magnetic under the same conditions (Figure 95) in spite of their dark color due to the ferrite nanograins.

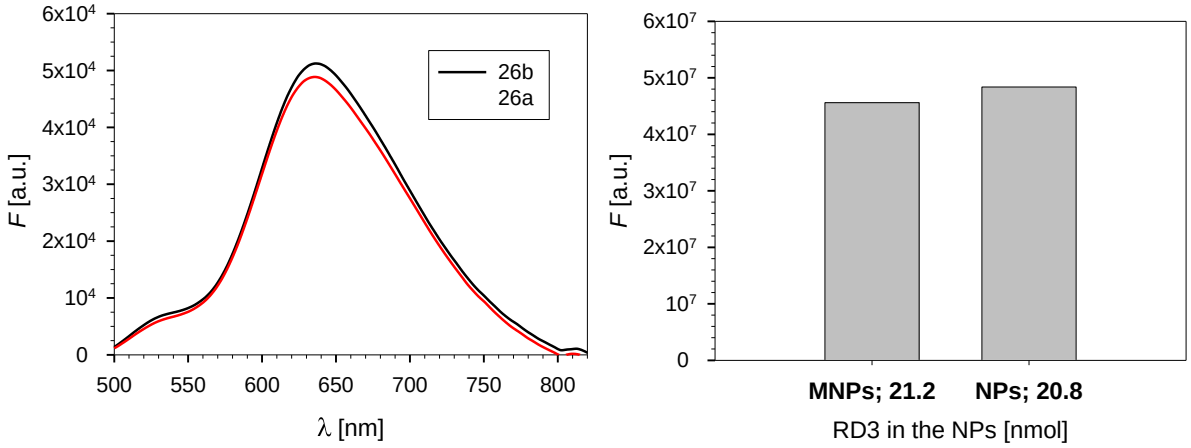


Figure 95. Left: corrected emission spectra of two batches of the magnetic NPs doped with RD3 (120 µL of sample in 3 mL H_2O, λ_{ex} = 450 nm, 515 nm cut-off, slits 3-3 nm). Right: comparison between the emission intensity of the magnetic nanoparticles of 300 nm and non-magnetic NPs of 390 nm doped with a similar amount of RD3 per mg of NPs.

7. Phosphorescence kinetics of 390 nm PSt-COOH NPs doped with RD3

Emission lifetime of the 390 nm RD3-doped PSt-COOH NPs was measured at different O_2 concentrations in suspension (0%, 21% and 100%). Measurements were performed by laser kinetic spectrometry upon excitation at 532 nm and monitoring at 620 nm (maximum of the RD3 emission) in water. A notch filter at 532 nm was used to avoid the effect of the strong scattering due the particles in suspension, and a 590 nm cut-off filter was also used in front of the monochromator. The emission lifetimes can be used to provide information on the environment around the sensitizer dye. Consequently, it is possible to know whether the singlet oxygen is being produced in the NPs surface or deeper into the polystyrene matrix.

RD3-doped PSt-COOH NPs of 390 nm showed a bi-exponential phosphorescence decay. This is probably due to the presence of two populations of RD3 (III in Scheme 43, pag. 140), for dyes doped NPs such behavior is not unusual.[244] The photosensitizer molecules that display the shortest lifetime are close to the water, interacting probably by coulombic attraction to the carboxylic groups of the nanoparticles surface. The RD3 population with longer lifetime is probably attached to the polystyrene surface by π-stacking interactions. This concept is also confirmed because τ_{RD3} in NPs is higher than in solution (water is a good quencher of the ^{3}MLCT excited state of Ru (II) polypyridyls by a charge-transfer-to-solvent (CTTS) mechanism)[230].

[244] N. S. Singha, R. S. Ningthoujamb, M. N. Luwangc, S. D. Singha, R. K. Vatsa, *Chem. Phys. Lett.*, **2009**, *480(4-6)*, 237–242.

Table 18. Luminescence lifetime of RD3-doped PSt-COOH NPs of 390 nm suspended in water containing different concentrations of dissolved O_2.

	***RD3 in Sample* [nmol]**[a]	τ_1 [μs]	B_1 [b]	τ_2 [μs]	B_2 [b]	τ_m [c] [μs]	τ RD3 [μs]
0% O_2	4.6	4.88	90.1	0.92	9.9	4.48	**2.68**
	9.2	4.18	86.7	0.77	13.3	3.73	
	17.9	3.95	85.9	0.74	14.1	3.50	
	20.8	3.57	82.5	0.66	17.5	3.06	
	26.0	4.10	84.1	0.76	15.9	3.57	
	35.9	4.21	83.8	0.75	16.2	3.65	
21% O_2	4.6	4.43	89.2	0.90	10.8	4.05	**0.73**
	9.2	3.05	89.6	0.39	10.4	2.77	
	17.9	2.90	88.7	0.40	11.3	2.61	
	20.8	2.53	87	0.32	13	2.24	
	26.0	2.82	87.4	0.47	12.6	2.52	
	35.9	2.78	87.2	0.45	12.8	2.48	
100% O_2	4.6	3.47	91.6	0.60	8.4	3.22	**0.21**
	9.2	3.03	89.8	0.51	10.2	2.77	
	17.9	2.90	89.7	0.48	10.3	2.65	
	20.8	2.57	87.2	0.46	12.8	2.30	
	26.0	2.91	89	0.49	11	2.64	
	35.9	2.46	87.5	0.45	12.5	2.21	

The uncertainty of the τ_i values is 2%; the O_2 % (by volume) are those in the O_2/N_2 mixtures sparged in the solution a) The RD3 nmoles correspond to 1 mg of NPs.

b) $\% = B_i\tau_i / \sum_i^2 B_i\tau_i$ and c) $\tau_m = \sum_1^3 B_i\tau_i / 100$

It is possible that the initial decrease of the *Ru^{II} complex lifetime, also observed in the absence of the quencher (the oxygen), is due to a triplet self-quenching. When the concentration of the RD3 in the NPs increases, the molecules are forced to stay in close proximity to other RD3 molecules. In this way, an efficient energy migration between photosensitizer molecules adsorbed on the polystyrene surface is proposed to be an important excited state deactivation pathway for high RD3 concentration, in the absence

of oxygen. We think that this explanation is reasonable since a similar behavior was already observed for the RD3 complex in silicone films.[245] While the concentration of RD3 increases further, the emission lifetime rises again probably because the photosensitizer is now forced to go deeper into the NPs.

The multi-exponential emission decay profile observed in the presence of molecular oxygen, cannot be explained just by the fact that the RD3 molecules are located at different positions, where O_2 might have different accessibility. Such a situation would imply a single-exponential decay in the absence of O_2. Therefore, the bi-exponential emission decay must be also a consequence of the intrinsic heterogeneity of the dye distribution within the NPs.

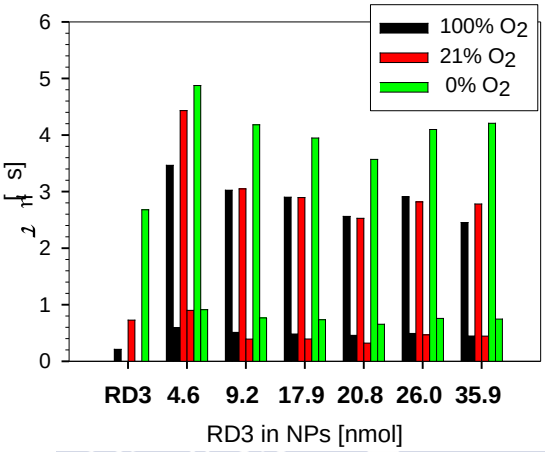


Figure 96. Luminescence lifetime comparison between the different RD3 doped PSt-COOH NPs of 390 nm changing the oxygen concentration ($P_{atm.}$= 711 Torr). Each batch shows two components one longer lifetime (τ_1) and one for shorter lifetime (τ_2).

Figure 97, Figure 98, and Figure 99 depict the decays of the RD3-doped PSt-COOH NPs of 390 nm from samples 17a to 21c, and the lifetimes τ_1 and τ_2 obtained for each different oxygen concentration.

[245] J. Lopez-Gejo, D. Haigh, G. Orellana, *Langmuir*, **2010**, *26 (3)*, 2144–2150.

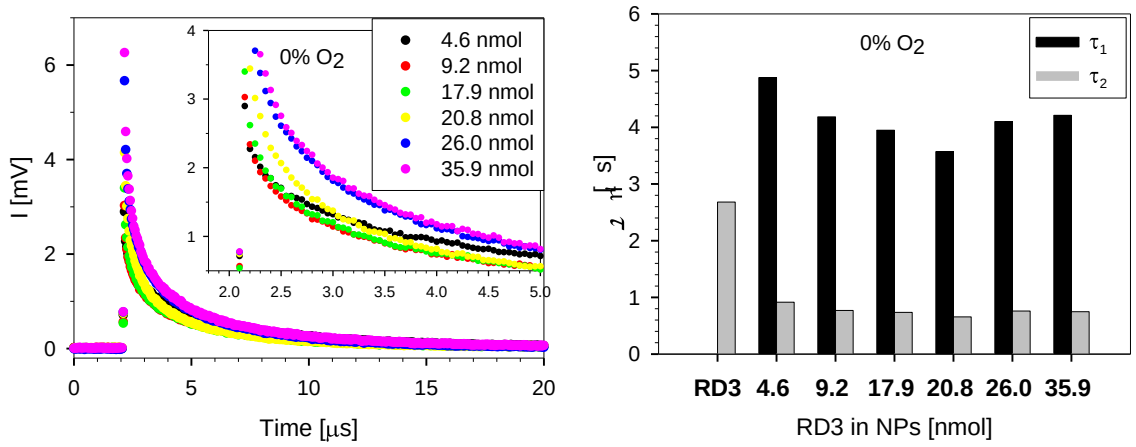


Figure 97. Left: emission decays of RD3 in NPs in H_2O with argon (λ_{ex}= 532 nm; λ_{em}= 620 nm, 590 nm cut-off filter, notch filter at 532 nm). Right: lifetimes τ_1 (black bar) and τ_2 (grey bar) obtained for each batch under argon.

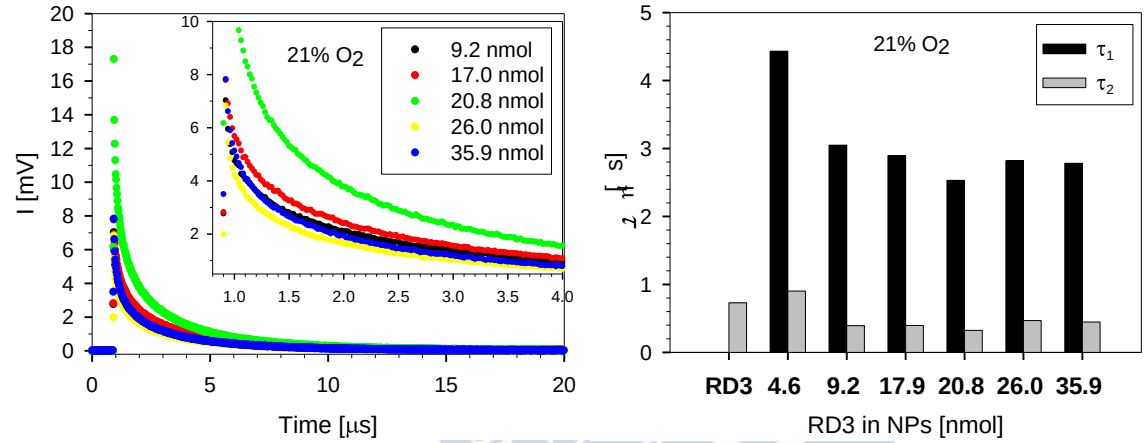


Figure 98. Left: emission decays of RD3 in NPs in H_2O with air (λ_{ex}= 532 nm; λ_{em}= 620 nm, 590 nm cut-off filter, notch filter at 532 nm). Right: lifetimes τ_1 (black bar) and τ_2 (grey bar) obtained for each batch under air.

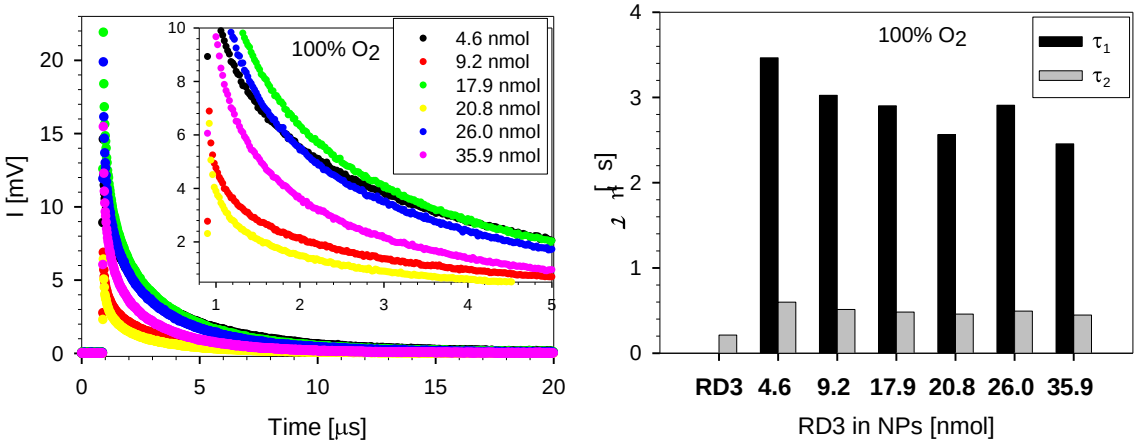


Figure 99. Left: emission decays of RD3 in NPs in H_2O with argon (λ_{ex}= 532 nm; λ_{em}= 620 nm, 590 nm cut-off filter, notch filter at 532 nm). Right: lifetimes τ_1 (black bar) and τ_2 (grey bar) obtained for each batch under oxygen.

The τ_m obtained (Table 18) for the PSt-COOH NPs of 390 nm doped with RD3 was plotted against the oxygen concentration (Figure 100). The samples from 9.2 to 35.9 nmol of RD3, with a high RD3 loading in the NPs, show a clear non-linear Stern-Volmer plot indicating the presence of different environments around the photosensitizer and that one fraction of the photosensitizer is more easily accessible by oxygen than the other. Such behavior is not unusual for complex systems.[246] The linearity is only observed for the NPs with the lowest concentration of RD3, probably due to homogenous distribution of RD3 in the PSt-COOH NPs.

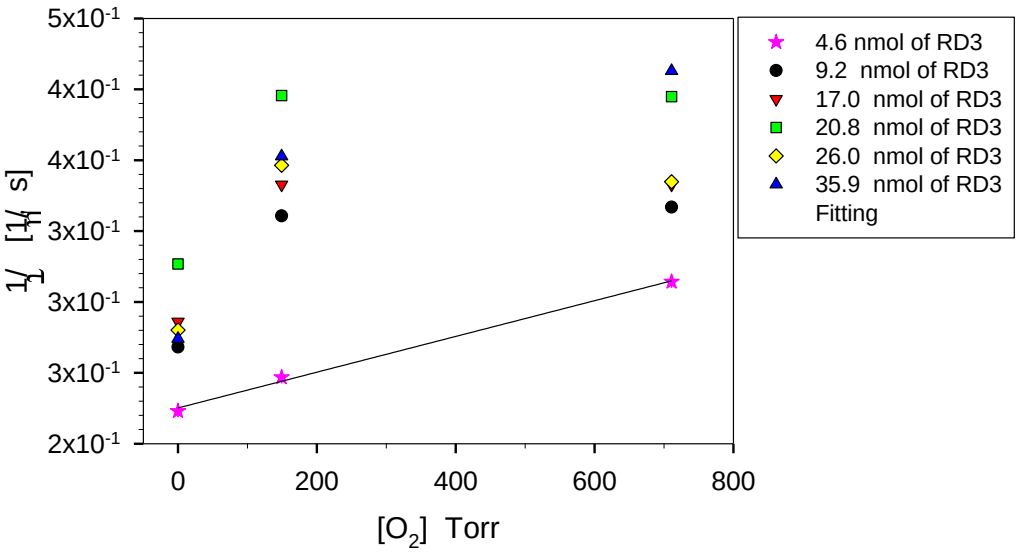


Figure 100. Stern–Volmer plot for τ_m (see Table 18) of RD3 doped PSt-COOH NPs of 390 nm.

8. Quantum yield of singlet oxygen production of the RD3-doped NPs

The Ru (II) polypyridyl complexes have a very large emission band, so that it is possible to observe the tail of the luminescence of the ^{3}MLCT state also at 1270 nm, which is the emission maximum of the singlet oxygen phosphorescence. This is a disadvantage when measuring the production of singlet oxygen by PSt-COOH NPs doped with RD3. Therefore, to facilitate the measurements, some precautions were adopted. For instance, we decided to measure the $^1O_2$ generation quantum yield (Φ_Δ) in deuterated water because in this solvent the singlet oxygen emission is stronger.[230] Moreover, the sample was sparged with oxygen for 30 min in order to fully quench the emission of the RD3 due to the higher concentration of oxygen. Many attempts to measure the quantum yield of singlet oxygen production in NPs were made.[247]

[246] K. Koren, R. I. Dmitriev, S. M. Borisov, D.B. Papkovsky, I. Klimant, *ChemBioChem*, **2012**, *13*, 1184–1190.
[247] S. Nonell, S. E. Braslavsky, *Methods Enzymol.*, **2000**, *319*, 37–49.

Polystyrene nanoparticles of 26 nm doped with RD3 (see section 5.1.6 pag 146) were lyophilized and then re-suspended in D_2O. However, scattering was observed even with so small NPs (26 nm). The lyophilization process probably causes aggregation.

To avoid lyophilization, nanoparticles of 390 nm were also used. In this case, the NPs were centrifuged to exchange the D_2O for H_2O. Unfortunately, it was impossible to make more than one centrifugation process because the density of the NPs is 1.06 g/mL and that of D_2O is 1.1 g/mL. Φ_Δ measurements were attempted, but there was too much scattering so that it was impossible to correlate the energy of the laser with the initial intensity of the decays curves.

Therefore, the suspension of 26 nm NPs of PSt-COOH with optimized RD3 loading ("14-3" NPs with 13.4 nmol of RD3 per mg/mL of NPs) were dialyzed against D_2O. To that end, 1 mL of NPs suspension in H_2O was dialyzed against 100 mL of D_2O. Three additional changes of D_2O with 50 mL D_2O after 2, 18 and 21 h were made. The dialysis was finished after 25 h.

After the dialysis, there were 800 μL of NPs suspension in D_2O, which was supplemented with 200 μL of D_2O directly added into the spectroscopic cell. The latter (10 x 4 mm optical pathlength) was equipped with a septum needed for the oxygen sparging. The longer path of the cell is used for the laser excitation while the singlet oxygen phosphorescence was collected always in the short path. Oxygen was sparged for 30 min immediately before the measurements.

The standard used is the $[Ru(dpds)_3]^{4-}$ complex, which has a Φ_Δ of 0.43 in D_2O.[230] The absorption of the sample and of the standard were measured before and after the singlet oxygen measurements to check if there was photobleaching caused by the repeated excitation of the sample with the powerful Nd-YAG laser (Figure 101).

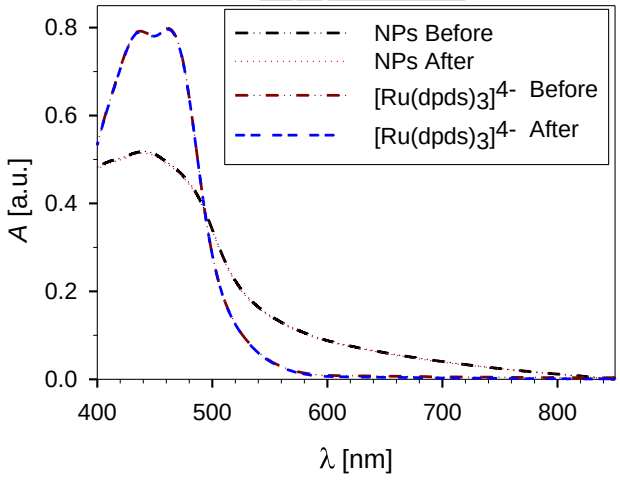


Figure 101. Absorption spectra of $[Ru(dpds)_3]^{4-}$ and of 14-3 NPs before and after the measurement of $^1O_2$ phosphorescence.

The standard and the sample were measured exactly under the same conditions: First of all the emission lifetimes of singlet oxygen and of RuL_3 (were L stand for ligand) were measured by recording the decay at λ_{em} 1270 nm (Table 19).

Table 19. Luminescence lifetimes of Ru(II) complexes and of $^1O_2$ in O_2-saturated D_2O.

	τRuL_3 [μs]	τ^1O_2 [μs]
PSt- COOH NPs doped with RD3	3.2	42.5
$[Ru(dpds)_3]^{4-}$	0.27	64.3

The *Ru-complex quenching by O_2 is observed in the shorter lifetime measured in comparison to aerated D_2O.[227] However, quenching of *RD3 in the NPs is less efficient due to the protection that the NPs surface provide, hindering the approach of the O_2 molecules.

The lifetime of singlet oxygen in PSt-COOH NPs of 26 nm is shorter than that reported in the literature for the singlet oxygen in deuterated water (62 μs). [227] This result may be due to the presence of residual H_2O in the NPs. We determined that the addition of 50 μL of H_2O lowered the τ $^1O_2$ for the standard in D_2O by ca. 20 μs. Therefore 100 μL of H_2O were added to the standard. Under these conditions the observed lifetime of singlet oxygen is 42.0 μs.

Finally, we reached a situation where scattering was tolerable, the lifetime of singlet oxygen in the sample and in the standard were close enough, and the variation of the area under of the decay follows the laser energy. After all these precautions, it was possible to proceed with the measurements of the singlet oxygen generation quantum yield.

Five singlet oxygen measurements for the sample (Figure 102) and three measurements for the reference were carried out (Figure 103).

For the time-resolved detection at 1270 nm of the $^1O_2$ luminescence, the decays were measured with the laser kinetic spectrometer upon excitation at 532 nm (see Experimental Part). Each decay was collected using different laser energies. To obtain the singlet oxygen production quantum yield it is necessary to process the experimental decay data in the following way:

1) The decay traces were fitted to a 2-exp decay function. It is possible to extract information from the fitting such as (i) the emission lifetime of the Ru complex ^{3}MLCT (τ_f), (ii) the emission lifetime of $^1O_2$ (τ_Δ), (iii) their contribution to the overall decay (B in mV), and (iv) the weighed residuals and autocorrelation function that were employed to estimate the quality of the fits.

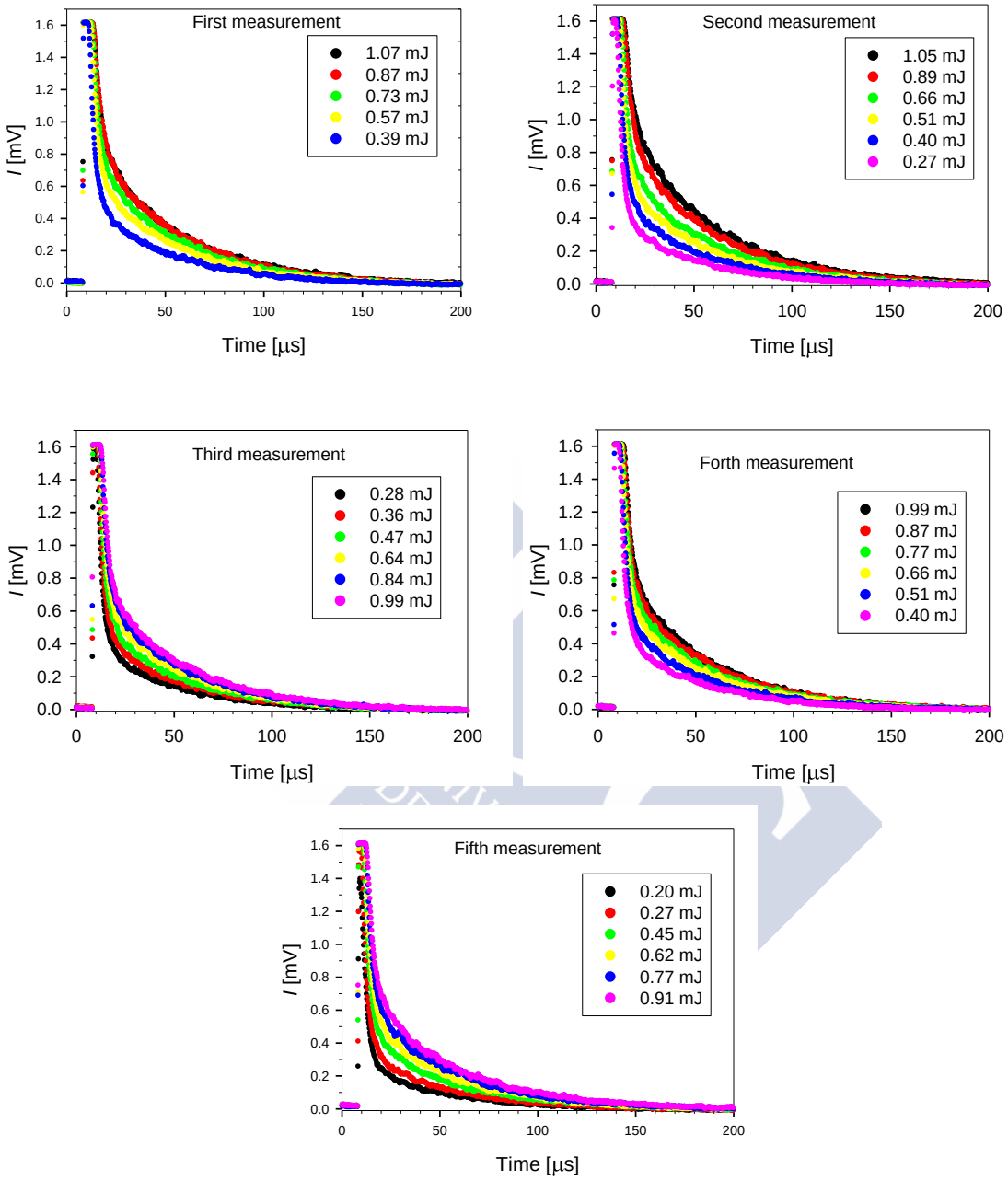


Figure 102. Measurements of the singlet oxygen decay generated by PSt-COOH NPs doped with RD3 in D_2O/O_2 (satd.) at different laser energies. λ_{ex} = 532 nm, λ_{em} = 1270 nm, slits 1.92/2.00 nm.

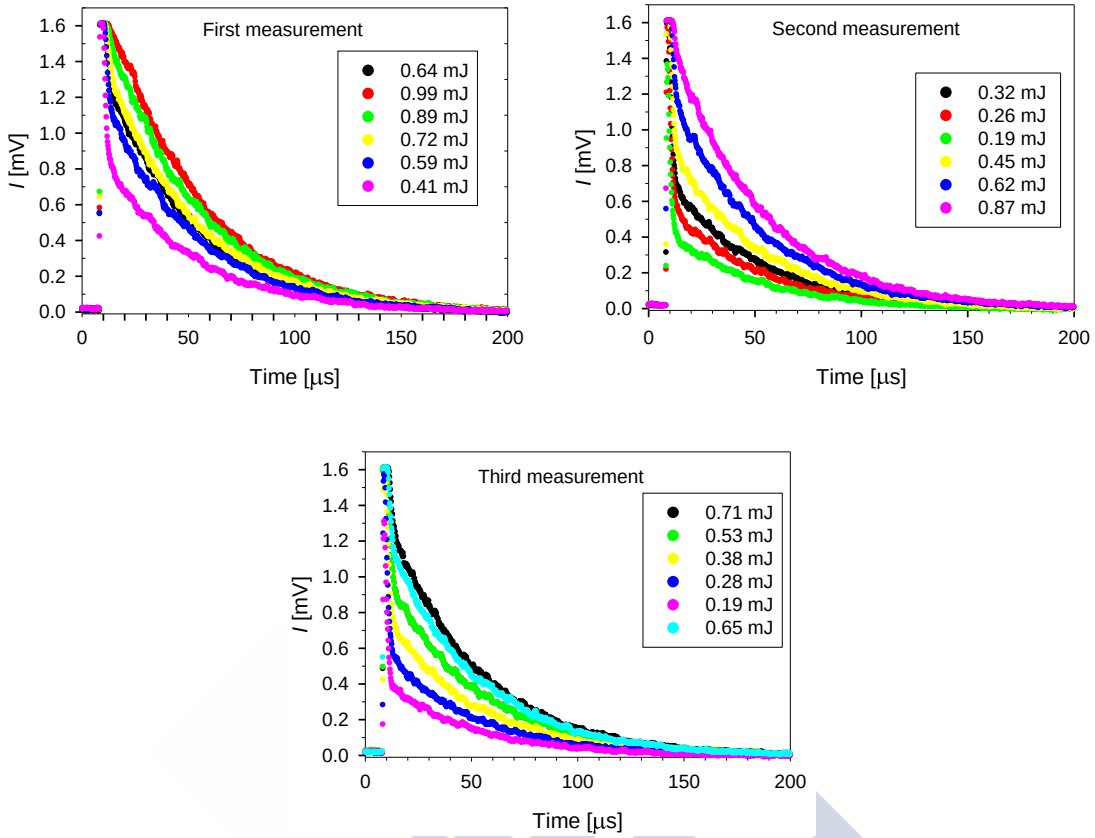


Figure 103. Measurements of the singlet oxygen decays generated by $[Ru(dpds)_3]^{4-}$ in D_2O/O_2 (satd.) at different laser energies. λ_{ex} = 532 nm, λ_{em} = 1270 nm, slits 1.92/2.00 nm.

2) All the decays are bi-exponential but it is important to exclude the contribution of the Ru(II) photosensitizer ^{3}MLCT phosphorescence. This is done by calculating just the area under the decay curve that corresponds to the singlet oxygen emission. The exponential decay that corresponds only to the singlet oxygen was mathematical obtained with the following formula

$$y = B\, e^{(x/\tau_\Delta)} \qquad (4)$$

where B (mV) gives the weight of the contribution of the τ_Δ lifetime to the overall decay, x is the time abscissa, and τ_Δ is the lifetime of singlet oxygen that is obtained after each fit. So from every experimental decay, a single-exponential decay corresponding to $^1O_2$ emission is obtained (Figure 104 and Figure 105).

3) The areas under the decays obtained in the point 2 were calculated.

4) Then a plot of the area vs the laser energy was built (Figure 106 for the NPs and Figure 107 for the standard).

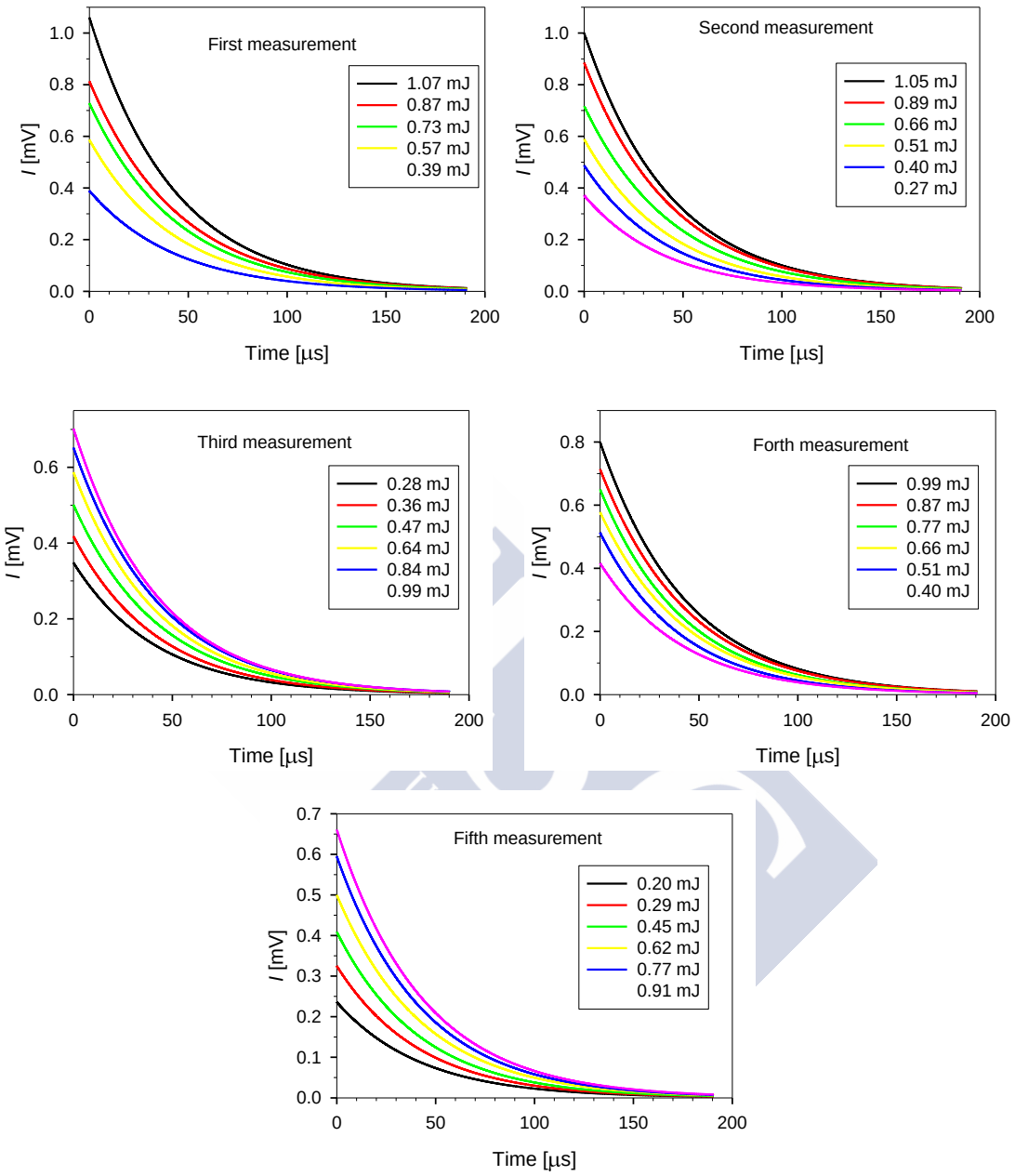


Figure 104. Calculated single-exponential decays of the $^1O_2$ photogenerated by PSt-COOH NPs doped with RD3, in D_2O/O_2 (satd.).

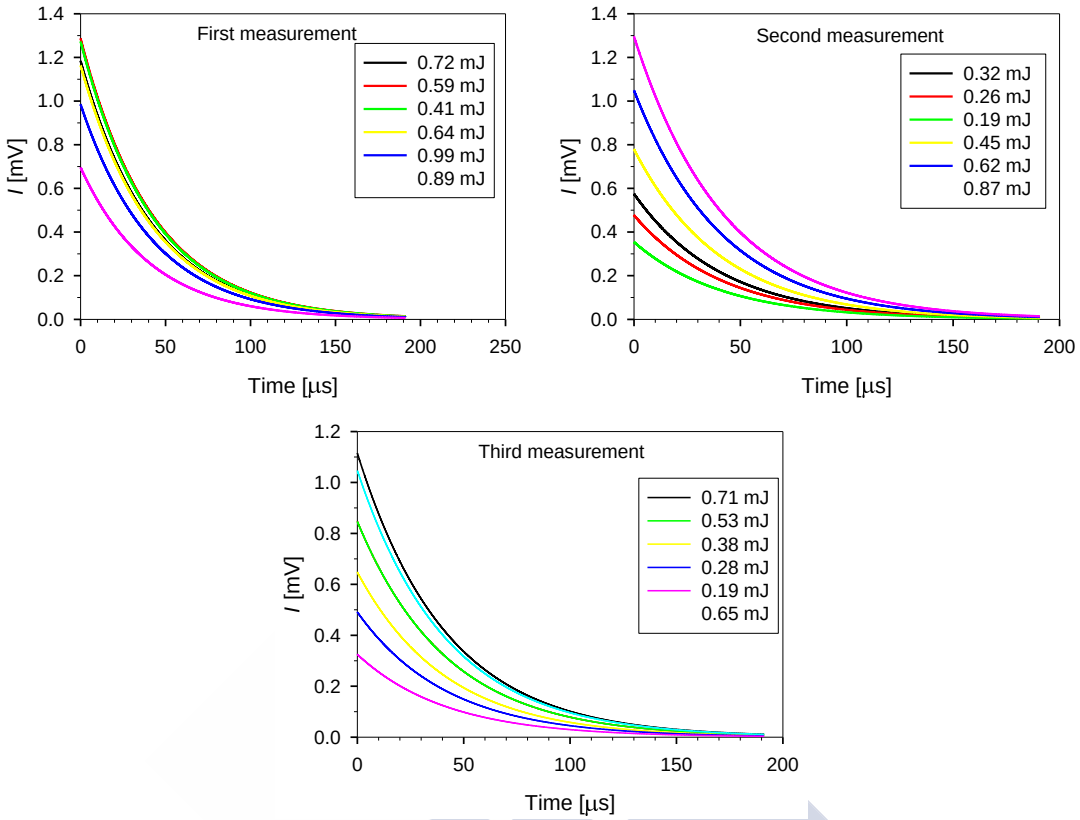


Figure 105. Calculated mono-exponential decays for the $^1O_2$ photogenerated by $[Ru(dpds)_3]^{4-}$ in D_2O/O_2 (satd.).

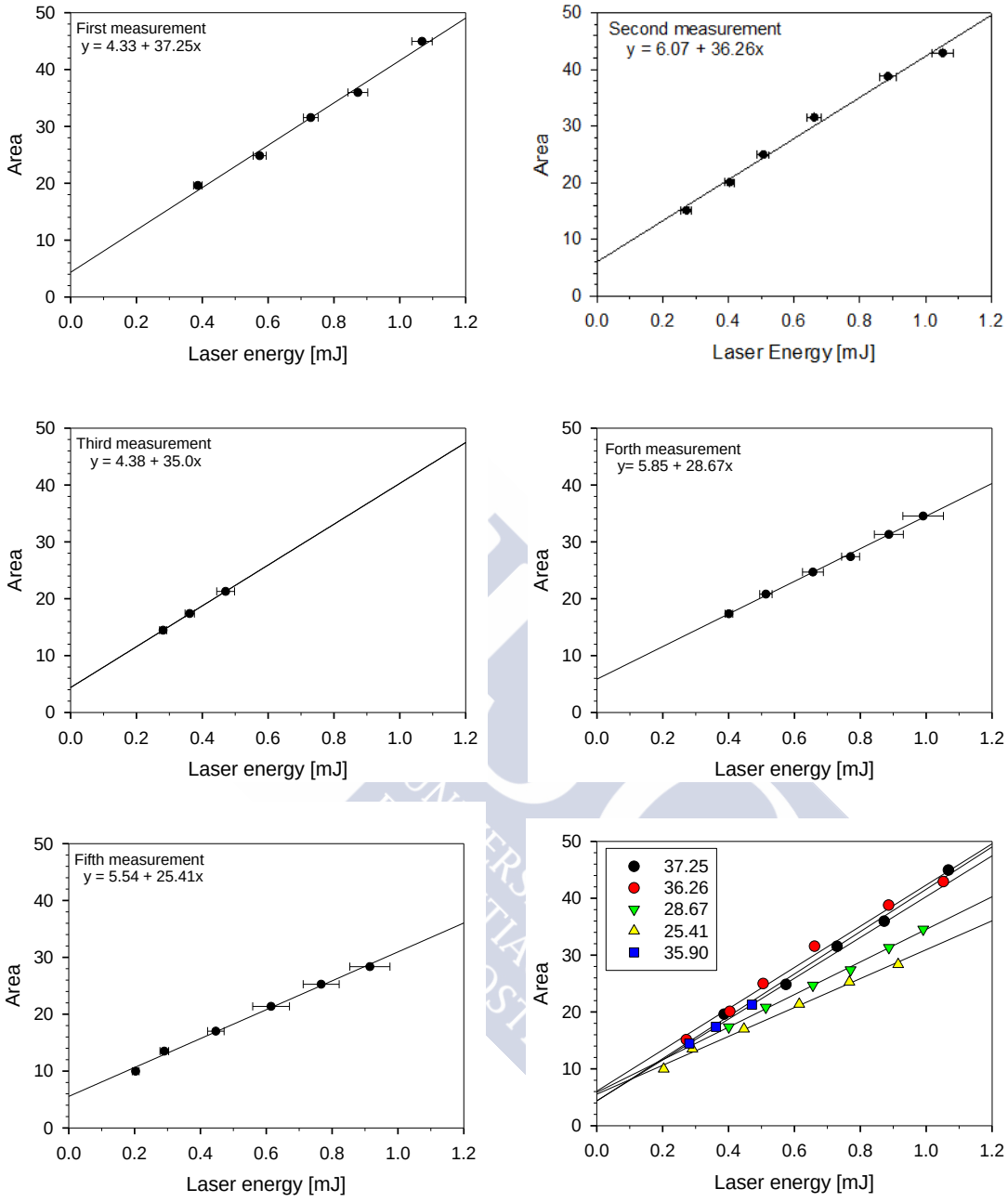


Figure 106. Emission of $^1O_2$ (as from the areas under the decay of its emission at 1270 nm) as a function of the laser pulse energy for PSt-COOH NPs doped with RD3, in D_2O/O_2 (satd.) for the five replicas of Figure 102 and Figure 104. The solid lines represent the best fit of the experimental points to the eq. shown within each graph.

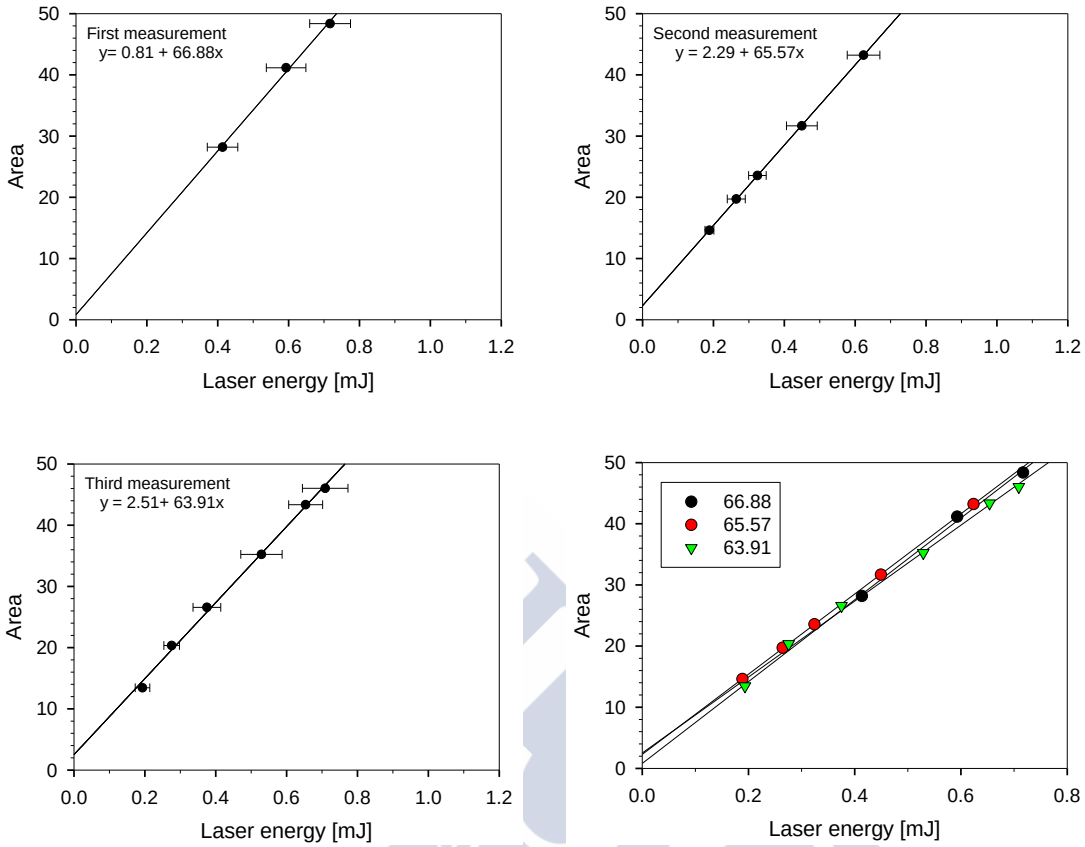


Figure 107. Emission of $^1O_2$ (as from the areas under the decay of its emission at 1270 nm) as a function of laser pulse for $[Ru(dpds)_3]^{4-}$, in D_2O/O_2 (satd.), for the three replicas of **Figure 103** and **Figure 104**. The solid lines represent the best fit of the experimental points to the eq. shown within each graph.

5) Moreover, graphs of B (in mV) vs the laser energy were also obtained (Figure 108).

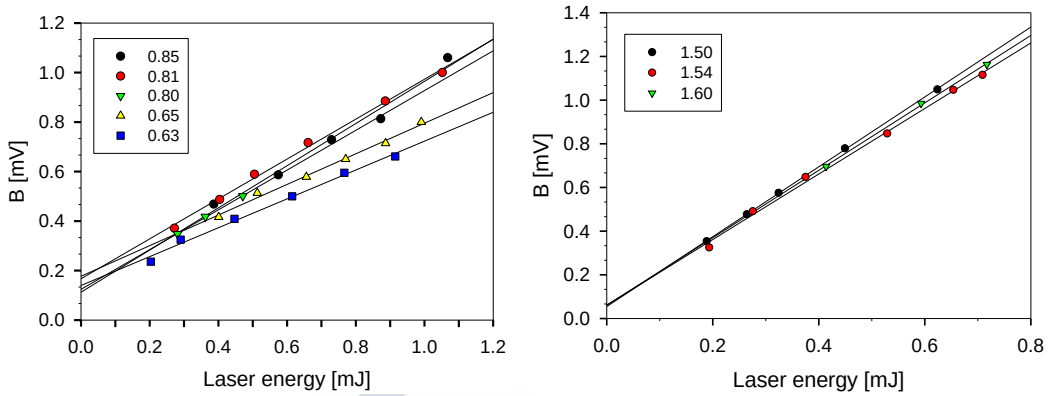


Figure 108. Plot of B (Eq. 3) vs the laser energy. Left: PSt-COOH NPs doped with RD3; right: $[Ru(dpds)_3]^{4-}$.

6) The graphs were fitted with a linear regression and the slopes (Table 20) were used for the next calculations.

7) A graph of B in mV versus the laser energy was also obtained.

Table 20. Slopes obtained from the linear fit of the experimental points to eq. 3. Sample: PSt-COOH NPs doped with RD3, standard $[Ru(dpds)_3]^{4-}$.

Slope sample [mV]	***Slope sample [area]***	***Slope reference [mV]***	***Slope reference [area]***
0.85	37.25	1.60	66.88
0.81	36.26	1.50	65.57
0.80	35.90	1.54	63.91
0.65	28.68		
0.63	25.41		
Mean	**0.75 ± 0.10**	**32.7 ± 5.3**	**1.55 ± 0.05**	**65.5 ± 1.5**

8) Sample and reference were optically matched at the laser excitation wavelength (532 nm). However it was impossible to perform a meaningful matching of the absorbances because even with 20 nm NPs, the suspension displayed significant scattering (Figure 109).

9) Finally the scattering contribution was mathematically calculated and then subtracted from the experimental absorption spectrum. In this way, the difference at 532 nm between the normalized absorption of NPs (***A_{norm}***) and the normalized scattering spectrum $y = (x)^{-4}$ (***Sc_{norm}***) was calculated. The actual contribution of the scattering at 532 nm (***Sc_{532}***) was then calculated as

$$Sc_{532}\% = A_{norm} x\ 100/Sc_{norm} \quad (4)$$

$$Sc_{532}\% = 0.35\ x\ 100/0.28 = 81\%$$

$$A^{532}_{real\ NPs} = \left(A^{532}_{NPs}(100 - Sc_{532}\%)\right)/100) \quad (5)$$

$$A^{532}_{real\ NPs} = (0.18\ x\ 19\%/100) = 0.035$$

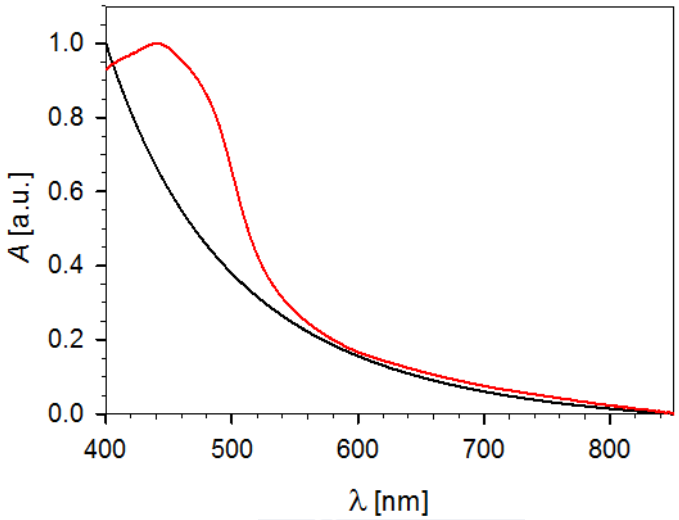


Figure 109. Normalized absorption spectra of the scattering (black line) and of the NPs (red line).

10) Finally, the quantum yield of singlet oxygen production of was obtained.

$$\Phi_{\Delta\ NPs} = \Phi_{\Delta\ ref}\ \frac{A^{532}_{ref}}{A^{532}_{real\ NPs}}\ \frac{S_{NPs}}{S_{ref}} \quad (6)$$

If the slope used in the formula is obtained from the initial intensity of the $^1O_2$ decay, the singlet oxygen production quantum yield for the NPs suspension is:

$$\Phi_{\Delta\,NPs} = 0.43\ \frac{0.0795}{0.0346}\ \frac{0.7486}{1.5482} = \mathbf{0.49} \qquad (7)$$

If the slope used in the formula is obtained from the area of the $^1O_2$ emission decay, the singlet oxygen production quantum yield for the NPs suspension is:

$$\Phi_{\Delta\,NPs} = 0.43\ \frac{0.0795}{0.346}\ \frac{32.7012}{65.4558} = \mathbf{0.51} \qquad (8)$$

The quantum yield of $^1O_2$ production, Φ_Δ, is defined as the number of $^1O_2$ molecules formed per absorbed photon. Its value is determined by three factors, as shown in equation (9),[248]

$$\Phi_\Delta = \Phi_T P_{O_2}^T f_\Delta^T \qquad (9)$$

where $P_{O_2}^T$ is the proportion of triplet excited states quenched by O_2 and reflects the fact that energy transfer from ^3M ($^3RD3$ in this case) to O_2 ($^3\Sigma_g^-$) is a collisional process (Dexter mechanism) that requires the formation of encounter complexes between both entities within the lifetime of ^3M, f_Δ^T is the fraction of excited triplet sates quenched by O_2 yielding $^1O_2$, and Φ_T is the quantum yield of triplet excited state formation (intersystem crossing). The latter is considered to be equal to one for the complex studied.[249]

Among the methods to determine the singlet oxygen quantum yield, there is the trapping. This method consists in monitoring the photobleaching of a singlet oxygen scavenger, resulting in the progressive decrease of its absorbance.[250] Among the most common singlet oxygen scavenger, there are: 1,3-diphenylisobenzofuran (DPBF) which strongly absorbs light at 412 nm, very close to the λ_{max}^{abs} of RD3; moreover, DPBF is not soluble in water; 9,10-anthracenedipropionic acid (ADPA) is an alternative water-soluble singlet oxygen scavenger which has characteristic absorption maxima in the 350–400 nm, also unsuitable when RD3 is used as photosensitizer;[251] Sensor Green, a

[248] A. Hergueta-Bravo, M. E. Jimenez-Hernandez, F. Montero,E. Oliveros, G. Orellana, *J. Phys. Chem. B*, **2002**, *106*, 4010–4017.
[249] S. Nonell, S. E. Braslavsky, *Methods Enzymol.*, **2000**, *319*, 37–49.
[250] S. J. Chadwick, D. Salah, P. M. Livesey, M. Brust, M. Volk, *J. Phys. Chem. C*, **2016**, *120*, 10647–10657.
[251] S. M. Mooi, B. Heyne, *Photochem. Photobiol.*, **2014**, *90*, 85–91.

dyad made of fluorescein and anthracene moieties, where its fluorescence (500– 600 nm) is monitored, also incompatible with λ_{max}^{em} of RD3.[252,253]

Therefore, due to the broad absorption (ca. from 350 nm to 500 nm in ethanol) and emission spectra (ca. from 550 nm to 800 nm in ethanol) of RD3, it was not possible take advantage of the straightforward method of trapping for determining the Φ_Δ. Consequently, due to the impossibility of employing the trapping method for the determination of the singlet oxygen production quantum yield, and since only a few reports in the literature comment on the Φ_Δ in a nanoparticle system,[250,251] we develop the method described above. We believe that this method is accurate enough because we are taking into account the scattered light when calculating the $\Phi_{\Delta\, NPs}$.

We monitor the $^1O_2$ lifetime decays at its phosphorescence emission peak (1270 nm), employing a reference method. In this approach, the singlet oxygen production quantum yield of the photosensitizer, $\Phi_{\Delta\,\mathrm{NPs}}$, can be determined by calibration against a reference photosensitizer with a known singlet oxygen production quantum yield, $\Phi_{\Delta\,\mathrm{ref}}$.

The value of singlet oxygen production quantum yield obtained for the PSt-COOH NPs doped with RD3 is higher than the $\Phi_{\Delta\,\mathrm{RD3}}$ in the same solvent (D_2O), $\Phi_{\Delta\,\mathrm{NPs}} = 0.50 > \Phi_{\Delta\,\mathrm{RD3}} = 0.42$.[230] This result indicates that the singlet oxygen generated by the Ru photosensitizer immobilized in the polystyrene matrix diffuses efficiently through the solution.

This result is in agreement with recent work published, in which it was observed an increase of singlet oxygen production quantum yield after immobilization of a photosensitizer in silica NPs. [254]

Another interesting result has been reported by Mafukidze et al.,[255] which used a phthalocyaninato indium(III) complex as photosensitizer immobilized onto a polystyrene film functionalized with –COOH groups. In this case, it was observed an increase of Φ_Δ from 0.43 (DMSO) for the free photosensitizer, to $\Phi_\Delta = 0.63$ (DMSO) for the photosensitizer immobilized in the PSt.

Following to Chadwick et al.,[250] who observe an increase of $\Phi_{\Delta\,\mathrm{NPs}}$ by ca. 40%, raising the size of the spherical NPs from 15 to 46 nm, we expect a higher $\Phi_{\Delta\,\mathrm{NPs}}$ for the PSt-COOH NPs of 390 nm than those of 26 nm used here for the determination of singlet oxygen quantum production quantum yield. In conclusion, it has been demonstrated that PSt-COOH NPs when combined with RD3 photosensitizer can improve efficiently the $^1O_2$ formation.

[252] S. Clement, M. Sobhan, W. Deng, E. Camilleri, E. M. Goldys, *J. Photochem. Photobiol. A*, **2017**, *332*, 66–71.
[253] S. Kim, M. Fujitsuka, T. Majima, *J. Phys. Chem. B*, **2013**, *117,* 13985–13992.
[254] L. M. Rossi, P. R. Silva, L. L. R. Vono, A. U. Fernandes, D. B. Tada, M. S. Baptista, *Langmuir*, **2008**, *24*, 12534–12538.
[255] D. M. Mafukidze, P. Mashazi, T. Nyokong, Polymer, **2016**, *105*, 203–213.

Experimental part

1. Materials and instrumentations

Reagents and solvents used in this thesis were purchased as high-grade commercial products from industrial suppliers (Sigma-Aldrich, Acros Organics, Fluorochem, Scharlab, Alfa Aesar, Panreac Quimica, Fisher Scientific, Thermo Scientific, Riedel-de Haën) and used as received, unless stated otherwise. The immunosuppressive drugs tacrolimus, cyclosporine A and mycophenolic acid were provided by Sinoway Ind. Co. (China). Antibodies were supplied by Santa Cruz Biotechnology or Jackson ImmunoResearch. Anhydrous dichloromethane was obtained by distillation from calcium hydride. Water was purified with a Direct-Q3-UV system (Merck Millipore).

Nanoparticles. The magnetic cobalt nanoparticles **TurboBeads®** were supplied as aqueous suspension with a solid content of 3% by weight (30 mg/mL). They have an average particle size of 30 nm (manufacturer value obtained by TEM), functional loading of –COOH onto the surface higher than 0.1 mmol/g and saturation magnetization higher than 150 emu/g. The magnetic nanospheres **Estapor®**, (Merck Millipore), were supplied as aqueous suspension with a solid content of 10% by weight. They have a mean diameter of 301 nm (manufacturer value obtained by dynamic light scattering), a magnetite content of 54.1% *w/w* (dry weight), and a concentration of –COOH surface groups of 148 μeq g^{-1}. The polystyrene NPs were provided by **Bangs Laboratories®**. They are functionalized with carboxylic groups onto the surface. Different diameter sizes 26 nm, 200 nm and 390 nm (manufacturer value obtained by dynamic light scattering) were tested depending on the final purpose. The **Bangs NPs with 26 nm** have a solid content of 9.97 mg/mL (9.97 wt. %), 528.7 –COOH μeq/g, density: 1.06 g/mL, number of particles per gram of dry solid: 1.025 x 10^{17}, surface area: 2.177 x 10^{14} μm^2/g, parking area 68.4 A^2/surface group, number of microspheres per mL 1.028 x 10^{16}. The **Bangs NPs with 200 nm** have a solid content of 10 wt. % (10 mg/mL 159.0 –COOH μeq/g, density: 1.06 g/mL, number of particles per gram of dry solid: 2.393 x 10^{14}, surface area: 2.888 x 10^{13} μm^2/g, parking area 30.2 A^2/surface group, number of microspheres per mL 2.443 x 10^{13}. The **Bangs NPs with 390 mm** have a solid content of 10 wt % (10 mg/mL), 235.0 –COOH μeq/g, density: 1.06 g/mL, number of particles per gram of dry solid: 2.815 x 10^{13}, surface area: 1.415 x 10^{13} μm^2/g, parking area 10 A^2/surface group, number of microspheres per mL 2.868 x 10^{12}.

Analytical thin-layer chromatography (TLC) was performed using aluminum coated Merck Kieselgel aluminium oxide 60 neutral F254 and silica gel 60 F254. Detection was made with UV-light (λ = 254 or 365nm), I_2 vapor, or Bromocresol Green Stain prepared as follows: 0.04 g of bromocresol green were added to 100 mL of absolute ethanol. Then a 0.1 M solution of aqueous NaOH was added dropwise until the solution turned blue.

Flash column chromatography was performed using silica gel (230-400 mesh) or neutral aluminium oxide.

High performance liquid chromatography (HPLC) was carried out in an Agilent 1100 series chromatograph with a 1100 quaternary pump, automatic injector and fraction collector. The type of column and eluents were changed according to circumstances.

Microwave reactor. A Biotage® Initiator+ reactor was used with a temperature range of 40–300 °C. Temperature increase was typically 2–5 °C/s depending on solvent and power applied. Typically, most reactions of this thesis did not require more than 2 hours. Pressure range was within 0–302 bar (3 MPa; 435 psi), power range 0–400 W from magnetron at 2.45 GHz. Reaction volumes used were 4 or 5 mL of solvent. Magnetic stirring variable: magnetic stirrer (300–900 rpm). The microwave is equipped with a cooling pressurized air supply: > 60 L/min (2.1 cubic feet/min) and a touch screen of 10.4".

Nuclear Magnetic Resonance (NMR) spectra were recorded on a Bruker Avance III 700 MHz (^{1}H, 700 MHz; ^{13}C, 175 MHz), or Bruker DPX 300MHz (^{1}H, 300 MHz; ^{13}C, 75 MHz, ^{19}F, 282 MHz) at "UCM NMR Central Instrumentation Facilities, CIF". All spectra were processed by the software "MestReNova-9.0.1-13254" and calibrated to meet the solvent shifts as reported in the same software. Chemical shifts (δ) are expressed in parts per million relative to internal tetramethylsilane; coupling constants (J) are in hertz (Hz). The following abbreviations are used to describe peak patterns when appropriate: s (singlet), d (doublet), t (triplet), q (quartet), quint (quintet), m (multiplet), dd (double doublet), td (tripled doublet) and br (broad).

Fourier transform infrared (FTIR) spectra were carried out using a Bruker TENSOR 27 spectrophotometer FTIR instrument. Samples were prepared with KBr disk. Frequencies (ν) are expressed in cm^{-1}.

Mass spectra were obtained with a Bruker HCT Ultra (ESI), with a MALDI-TOF/TOF Bruker ULTRAFLEX, or with a MAT 95 XP of high resolution (FAB) spectrometers at "UCM's mass spectrometry central facility".

Transmission electron microscopy measurements were carried out with a JEOL JEM 2100 (200 kV) at the *Centro Nacional de Microscopía Electronica* (CNME).

UV-VIS absorption spectra were recorded with a double beam Varian Cary 3-Bio spectrophotometer.

Steady-state and lifetime emission measurements were carried out on a Horiba Fluoromax-4TCSPC spectrofluorometer equipped with a 150-W xenon lamp for the steady-state spectral recordings. For time-resolved fluorescence determinations, either a Horiba Fluoromax-4TCSPC instrument or a FLS980 fluorescence spectrometer (Edinburgh Instruments, with double monochromator in the emission channel) were employed. In both cases, a Horiba NanoLED-470LH laser diode (peak at 463 nm, 1 ns pulses) and Horiba NanoLED-635L laser diode (peak at 640 nm, 250 ps pulses) were used. Fluorescence decays were measured with a 50-, 100- or 200-ns window (4096

channels), after accumulating at least 20,000 counts in the peak channel, with a repetition rate of 500 kHz. Emission lifetimes were extracted from the exponential curve fittings using the proprietary Horiba hybrid algorithm (with deconvolution of the instrumental response function). Any observed decay component equal to or below the laser pulse width was discarded. The goodness-of-the-fit of the exponential decays was judged by visual inspection and the reduced chi-squared parameter ($\chi_R^2 < 1.5$) of the residuals. All emission measurements were carried out using optically diluted samples ($A_{max} < 0.1$).

Fluorescence quantum yield. Fluorescence quantum yield vales were determined using a relative method, with a standard. The standard used has to show some specific characteristic as: absorption and emission in the same spectral region of the investigated sample; its Φ_{em} has to be not sensitive to O_2; its concentration has to be constant in solution. After measuring the absorption and emission spectra of the standard and the sample (diluted solution, A < 0.1 in the maximum, in triplicate), the next formula (1) was applied for the calculation:

$$\Phi_x = \Phi_s \frac{A_s}{A_x} \frac{I_x}{I_s} \frac{\eta^2_x}{\eta^2_s} \qquad (1)$$

Were **A** is the absorbance at the λ_{ex}; **I** is the area underneath the emission spectrum; **η** is the solvent refractive index, the subindex "x" and "s" make reference to the sample and the standard respectively.

Oxazine 170 (Φ_f = 0.579 in EtOH)[256] was used as standard for the determination of the fluorescence quantum yield in ethanol of Dy636 (4.1), ANB (section 4.2.3), PFB-641 (section 7.2) and BI2-6 (10.3), and for Dy636 (section 4.1) and ANB (section 4.2.3) in PBS 100 mM at pH = 7.4

Rhodamine 123 (Φ_f =0.90 in EtOH)[257] was used as standard for the determination of fluorescence quantum yield in ethanol of PFB- 515 (section 7.1) and BI2-5 (section 10.2).

B-1 (section 10.1) (Φ_f = 0.72 in THF)[258] was used as standard for the determination of fluorescence quantum yield of BI2-5 (section 10.2) in acetonitrile.

Microplate reader. A CLARIOstar (BMG Labtech, Germany) was employed; instrument control and data processing were performed with the manufacturer´s original software

[256] K. Rurack, M. Spieles, *Anal. Chem*., **2011**, *83*, 1232–1242.
[257] R. F. Kubin, A.N. Fletcher, *J. Lumin.*, **1982**, *4*, 455–462.
[258] L. Huang, J. Zhao, S. Guo, C. Zhang, J. Ma, *J. Org. Chem.,* **2013**, *78*, 5627–5637.

(MARS). A microplate PACKARD HTRF 96 was used. For the **polarization assay** (see section 5…) a P590-50 excitation filter was used, a LP639 dichroic filter and a P675-50 emission filter. For **intensity based measurements** for the determination of the binding constants (see chapter…) the excitation and emission wavelengths were set at 585 and 654 nm, respectively. For the determination of tacrolimus beads-based fluorescent immunoassay using the **FRET-based fluoromagnetic nanoparticles** (see section 9.3) the excitation and emission wavelengths for measurements using the FRET mode were set at 500 and 680 nm, respectively. The excitation and emission wavelengths for measurements in the absence of the FRET mode were set at 638 and 680 nm, respectively.

Photostability study of ANB and PFB-641 was carried out with a fiber-optic Maya® Pro Spectrometer (Ocean Optics). A 5-mW 632-nm red laser diode from Picotronic was used as excitation source. The laser was connected to the cuvette holder with a homemade piece built with a Velleman 3D printer. A fiber optic carries the emitted light from the sample to the detector.

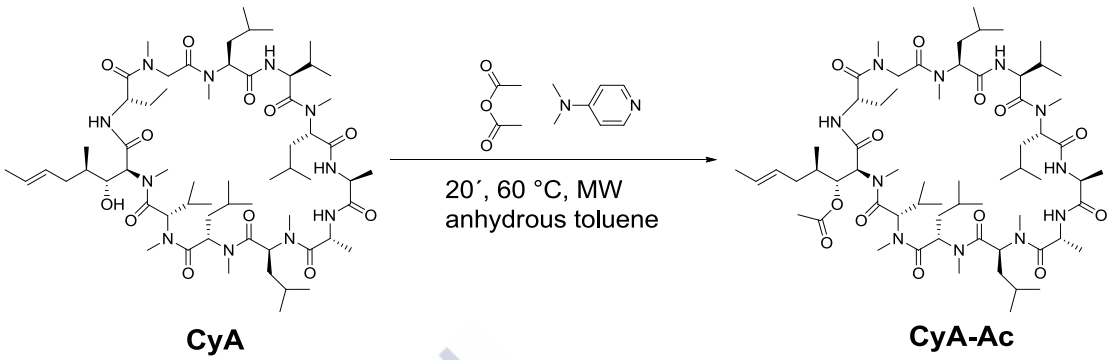
Time-resolved detection of $^1O_2$ luminescence at 1270 nm was performed with single a photon counting (SPC) laser kinetic spectrometer system from Edinburgh Instruments (UK) LP-900 equipped with a Hamamatsu H10330-45 NIR PMT detector. For excitation the 532 nm line of a Nd:YAG laser was used (Minilite II, Continuum, CA). The decay traces obtained were deconvoluted for the instrumental response and fitted to a double exponential function using the nonlinear Marquardt algorithm included in the Edinburgh Analytical Instruments original software package. The reduced χ^2 weighed residuals and autocorrelation function were employed to estimate the quality of the fits. The energy of the laser can be measured with an energy detector, GENTEC-EO. The detector is directly plugged into a PC and it can be controlled easily by integrated software.

2. Synthesis of cyclosporine A[259] derivatives

Three different CyA-COOH derivatives were synthetized and unambiguously characterized by ^{1}H-NMR, ^{13}C-NMR and mass spectrometry. Due to the presence of a large number of aliphatic protons, the ^{1}H-NMR spectra of the cyclosporine derivatives will be given only at ca. $\delta > 3$ ppm, were the most relevant protons of the new derivatives show up.

[259] Cyclo[L-alanyl-D-alanyl-N-methyl-L-leucyl-N-methyl-L-leucyl-N-methyl-L-valyl-(3R,4R,6E)-6,7-didehydro-3-hydroxy-N,4-dimethyl-L-2-aminooctanoyl-L-2-aminobutanoyl-N-methylglycyl-N-methyl-L-leucyl-L-valyl-N-methyl-L-leucyl]

2.1. Synthesis of Cyclosporine A acetate (CyA-Ac) for the synthesis of CyA-S-COOH and CyA-N-COOH



Scheme 45. Protection of the hydroxyl group of CyA with acetic anhydride.

Acylation of the CyA hydroxyl group. CyA (301 mg, 0.245 mmol) and 4-dimethylamino-pyridine (DMAP) (93 mg, 0.76 mmol) were added in a 5 mL microwave-proof reaction tube. Anhydrous toluene (4 mL) and acetic anhydride (150 μL, 1.6 mmol) were added with a syringe once the vial was sealed and purged with argon. The mixture was irradiated into a laboratory microwave reactor for 20 min at 60 °C. The solvent was evaporated and the crude product was obtained as a pale yellow oil. The crude product was washed with brine and extracted with dichloromethane. The excess of DMAP and of acetic acid were eliminated in water. The organic phase was concentrated under reduced pressure to give CyA-Ac as pale yellow solid in 97% yield.

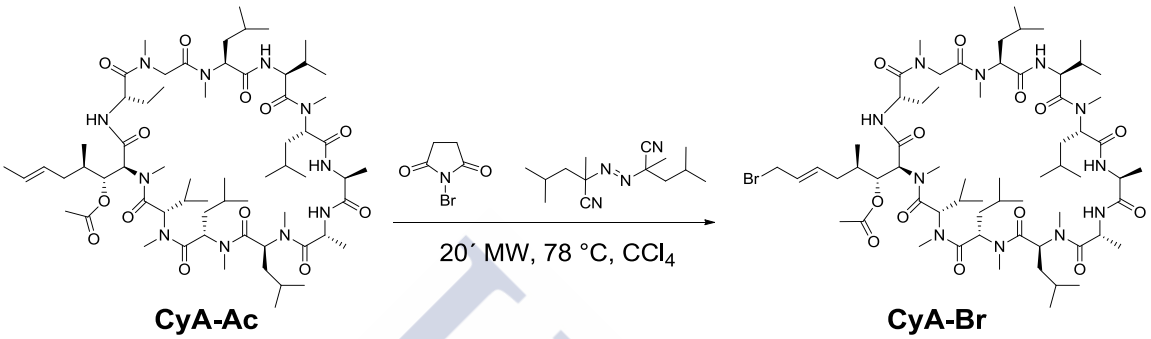
^{1}H-NMR (300 MHz, $CDCl_3$) δ: δ 8.51 (d, J = 9.7 Hz, 1H, CON*H*), 7.99 (d, J = 6.9 Hz, 1H, CON*H*), 7.43 (m, J = 12.7, 8.4 Hz, 2H, CON*H*), 5.67 – 5.56 (m, 1H, CH_{alkene}), 5.46 (s, 2H), 5.38 – 5.28 (m, 1H, CH_{alkene}), 5.25 (s, 2H, NCH_2), 5.24 – 5.03 (m, 3H, NC*H*), 4.96 – 4.87 (m, 2H, NC*H*), 4.78 (t, J = 7.2 Hz, 1H, C*H*Ac), 4.71 (t, J = 9.6 Hz, 1H, NC*H*), 4.59 (d, J = 13.7 Hz, 1H, NC*H*), 4.35 (t, J = 7.0 Hz, 1H, NC*H*), 3.40 (s, 3H, NCH_3), 3.20 (s, 3H, NCH_3), 3.18 (s, 3H, NCH_3), 3.15 (s, 3H, NCH_3), 3.09 (d, J = 4.1 Hz, 1H), 3.04 (s, 3H, NCH_3), 2.62 (s, 3H, NCH_3), 2.59 (s, 3H, NCH_3).

^{13}C-NMR (75 MHz, $CDCl_3$) δ: 173.86, 173.48, 173.00, 172.91, 171.60, 171.37, 170.96, 170.90, 170.62, 170.41, 169.98, 168.15, 129.27, 126.42, 77.16, 77.16, 73.37 (CHOAc), 58.40, 57.39, 56.29, 55.31, 54.82, 54.44, 53.54, 50.12, 48.85, 48.41, 48.01, 44.78, 41.13, 39.36, 37.13, 35.96, 33.83, 33.16, 32.39, 31.79, 31.45, 30.28, 29.98, 29.80, 29.59, 25.12, 24.87, 24.62, 24.31, 23.88, 23.67, 23.62, 21.95, 21.56, 21.36, 21.28, 20.84, 20.57, 19.75, 18.77, 18.27, 17.99, 17.81, 17.76, 15.16, 10.02.

MS (FAB +): m/z $[M+H]^+$ calculated for $C_{64}H_{114}N_{11}O_{13}^+$ 1244.8, found 1245.2.

2.2. Synthesis of CyA-S-COOH

2.2.1. Synthesis of Cyclosporine A 6-bromo-2-methylhex-4-en-1-yl acetate (CyA-Br)



Scheme 46. Allylic bromination of CyA-Ac using N-bromosuccinimide and a radical initiator.

Wohl-Ziegler reaction. CyA-Ac (212 mg, 0.117 mmol), N-bromosuccinimide (107 mg, 0.60 mmol) and a catalytic amount of azobisvaleronitrile (1 mg) were placed into a 5 mL microwave tube. Once the vial was closed and was purged with argon, 4 mL of CCl_4 were added. The mixture was irradiated with microwaves for 20 minutes at 78 °C. The crude product was obtained as a brown solid. It was isolated by liquid-liquid extraction into ethyl acetate by washing first with brine, evaporated with reduced pressure and then washed again with $CHCl_3$. The organic phase was concentrated under reduced pressure to give CyA-Br as light brown-orange solid in 70% yield.

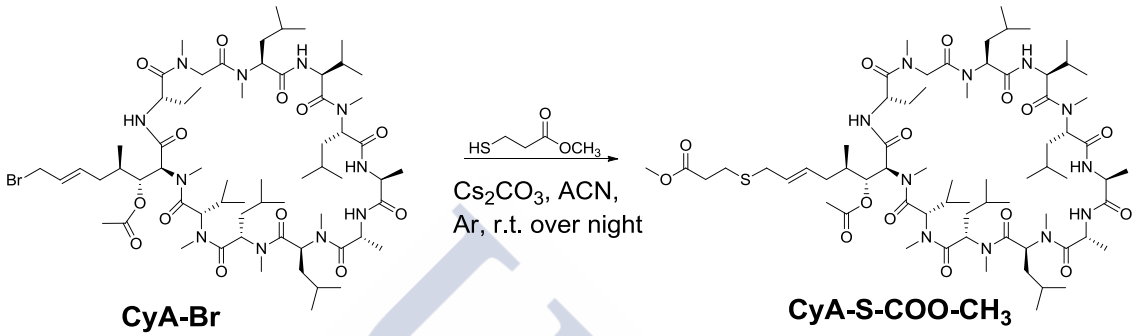
^{1}H-NMR (300 MHz, $CDCl_3$) δ: δ 8.64 – 8.46 (m, 1H, CON*H*), 8.09 – 7.92 (m, 1H, CON*H*), 7.69 – 7.50 (m, 1H, CON*H*), 7.49 – 7.33 (m, 1H, CON*H*), 5.67 – 5.55 (m, 2H, CH_{alkene}), 5.49 – 5.44 (m, 1H), 5.26 (s, 2H, NC*H*$_2$), 5.12 – 5.01 (m, 2H), 4.93 (t, J = 11.2, 3.2 Hz, 3H), 4.85 – 4.72 (m, 2H), 4.72 – 4.53 (m, 2H), 4.44 – 4.28 (m, 2H), 4.05 (q, J = 7.1 Hz, 2H, C*H*$_2$Br).

^{13}C-NMR (75 MHz, $CDCl_3$) δ: 174.15, 173.77, 173.53, 173.47, 173.27, 173.16, 172.96, 172.79, 171.23, 171.21, 171.16, 171.05, 170.88, 170.81, 170.61, 170.53, 170.48, 170.43, 170.35, 170.13, 167.97, 167.90, 134.95, 134.13, 128.80, 128.53, 72.96, 72.83, 71.97, 71.78, 60.41, 58.32, 57.29, 56.03, 55.28, 54.88, 54.25, 54.00, 53.50, 50.06, 48.75, 48.25, 48.16, 47.87, 46.43, 44.70, 44.66, 41.01, 40.69, 39.58, 39.23, 38.06, 37.14, 36.14, 35.93, 35.67, 33.67, 32.90, 32.34, 31.93, 31.69, 31.41, 31.13, 30.19, 30.12, 29.88, 29.70, 29.66, 29.50, 29.36, 24.95, 24.76, 24.67, 24.41, 24.26, 24.09, 23.77, 23.54, 23.39, 23.35, 22.70, 21.82, 21.28, 21.08, 20.74, 20.49, 19.93, 19.73, 18.64, 18.08, 17.95, 17.69, 15.08, 14.23, 14.16, 9.91.

MS (ESI -): m/z $[M–H]^-$ calculated for $C_{64}H_{111}BrN_{11}O_{13}^-$ 1322.8 found 1322.6, (the di-bromine derivative was also found at 1400.5 m/z).

MS (FAB +): m/z $[M+H]^+$ calculated for $C_{64}H_{113}BrN_{11}O_{13}^+$ 1324.8 found 1325.3, (the di- and tri- bromine derivative were also found at 1403.1 m/z for $C_{64}H_{113}Br_2N_{11}O_{13}^+$, 1483.0 for $C_{64}H_{113}Br_3N_{11}O_{13}^+$m/z).

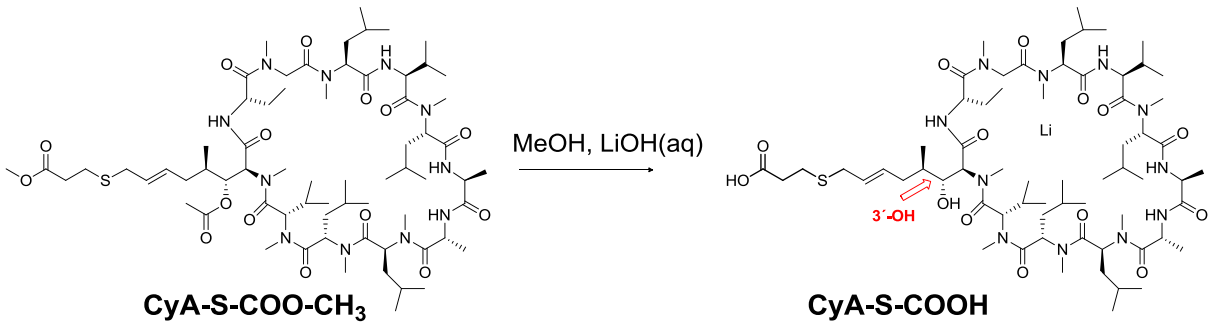
2.2.2. Synthesis of Cyclosporine-6-acetoxy-thiopropanoate



Scheme 47. Nucleophilic substitution in CyA-Br with a ω-thiolated carboxylic ester.

Nucleophilic substitution of Br^- in CyA-Br with a mercaptan. In a 25 mL two-necked flask, CyA-Br (170 mg, 0.128 mmol) was dissolved in 3 mL of acetonitrile under argon atmosphere. Then cesium carbonate (98 mg, 0.289 mmol) and methyl 3-mercaptopropionate (30 μL, 0.27 mmol) were added into the flask. The reaction mixture was stirred overnight. The crude product was obtained as a turbid brown solution, washed with brine and extracted with dichloromethane. The organic phase was concentrated under reduced pressure to give CyA-S-ester as light brown solid in 90% yield. The product purity was confirmed by thin-layer chromatography with silica (CH_2Cl_2:MeOH 10/1 *v/v*) and used without further treatment for the next step.

2.2.3. Synthesis of Cyclosporine A thiopropanoic acid (CyA-S-COOH)



Scheme 48. Final step (alkaline hydrolysis) in the preparation of the target derivative CyA-S-COOH.

Alkaline hydrolysis of the ester group of CyA-S-COOCH$_3$. The precursor CyA-S-COOCH$_3$ (113 mg, 0.103 mmol) was dissolved in a mixture of methanol (5 mL) and an aqueous solution of LiOH (7 mL, 0.2 M). The reaction mixture was kept stirring overnight at room temperature with vigorous stirring. Then the solvent was evaporated under reduced pressure and the crude product was washed by liquid-liquid extraction H^{2}O/CHCl$_3$. The organic phase was concentrated under reduced pressure to give CyA-S-COOH as a light brown solid in 71% yield. The pure product was characterized by ^{13}C-NMR (75 MHz, CDCl$_3$), ^{1}H-NMR (300 MHz, CDCl$_3$) and mass spectrometry.

^{1}H-NMR (300 MHz, CDCl$_3$) δ: 8.24 (d, J = 9.8 Hz, 1H, CON*H*), 7.91 (d, J = 7.2 Hz, 1H, CON*H*), 7.51 (d, J = 8.5 Hz, 1H, CON*H*), 7.34 (d, J = 7.9 Hz, 1H, CON*H*), 6.14 – 5.97 (m, 2H), 5.73 – 5.55 (m, 4H), 5.18 – 5.02 (m, 5H), 4.88 – 4.76 (m, 2H), 4.70 (t, J = 10.8 Hz, 3H), 4.53 – 4.38 (m, 3H), 3.84(s b, 1H, OH), 3.47 (s, 3H, NC*H$_3$*), 3.39 (s, 3H, NC*H$_3$*), 3.29 (s, 3H, NC*H$_3$*), 3.13 (s, 3H, NC*H$_3$*), 3.04 (s, 3H, NC*H$_3$*), 2.68 (s, 3H, NC*H$_3$*), 2.67 (s, 3H, NC*H$_3$*).

^{13}C-NMR (75 MHz, CDCl$_3$) δ: 173.99, 173.83, 173.69, 171.66, 171.24, 171.01, 170.76, 170.27, 170.14, 169.81, 137.35, 132.82, 77.36, 73.54, 60.02, 58.06, 57.40, 55.47, 55.20, 54.62, 50.22, 48.79, 48.55, 48.10, 45.00, 40.85, 39.48, 39.27, 37.97, 37.60, 36.15, 33.55, 32.04, 31.45, 31.38, 31.34, 30.20, 29.94, 29.81, 29.75, 29.63, 24.98, 24.81, 24.58, 23.97, 23.84, 23.77, 23.59, 23.51, 23.41, 22.80, 22.00, 21.69, 21.36, 20.46, 19.88, 18.77, 18.44, 18.03, 15.65, 14.23, 10.05, 9.98.

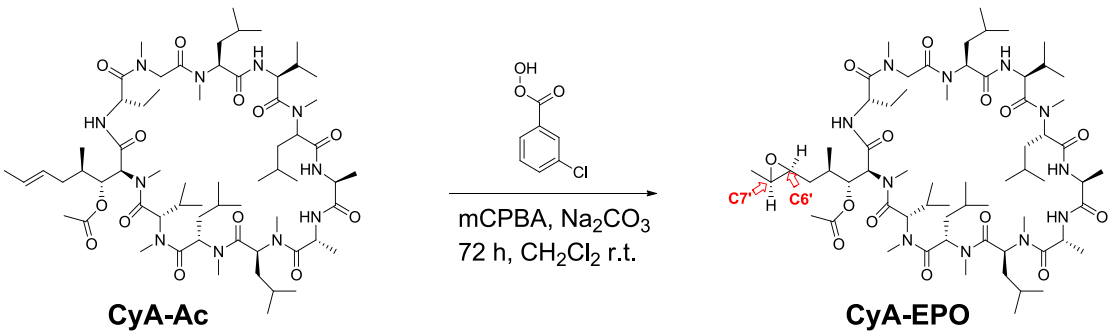
MS (ESI -): m/z [M–H]$^-$ calculated for $C_{65}H_{114}N_{11}O_{14}S^-$1304.8, found 1304.7.

MS (FAB +): m/z [M+H]$^+$ calculated for $C_{65}H_{116}N_{11}O_{14}S^+$ 1306.8, found 1307.2.

(MALDI TOF +): m/z [M+Li]$^+$ calculated for $C_{65}H_{115}LiN_{11}O_{14}S^+$ 1312.9, found 1312.9 and m/z [M+Na]$^+$ calculated for $C_{65}H_{115}N_{11}NaO_{14}S^+$ 1328.8, found 1328.9.

2.3. Synthesis of CyA-N-COOH

2.3.1. Synthesis of Epoxy Cyclosporine A (CyA-EPO)



Scheme 49. Synthetic route for preparation of epoxy-Cyclosporine A.

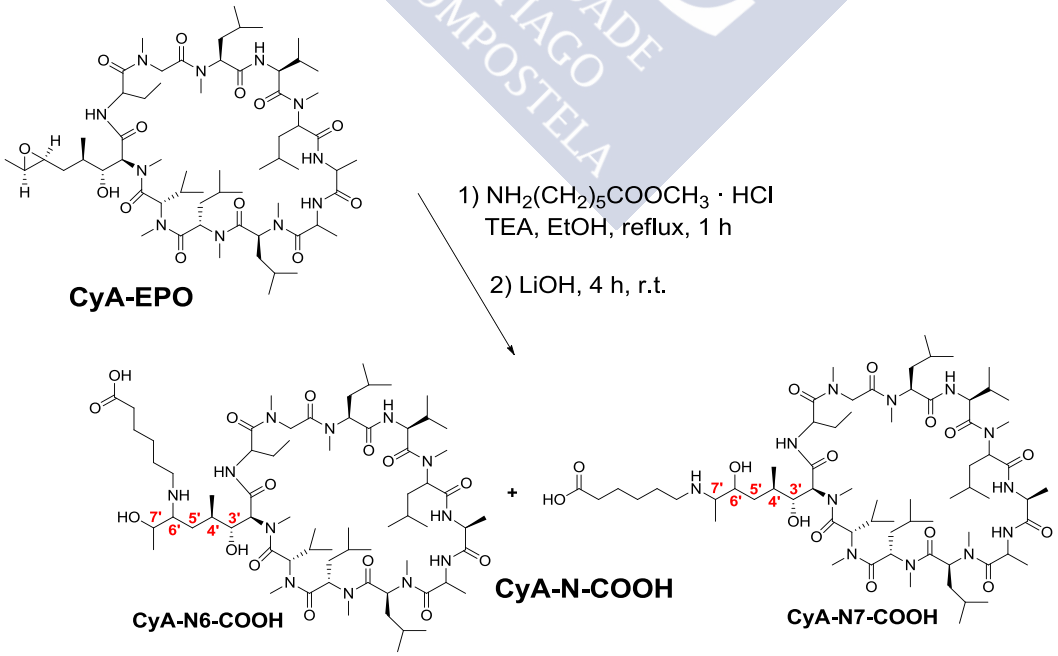
Epoxidation of the C=C bond of CyA-Ac. To a solution of CyA-Ac (283 mg, 0.287 mmol) in dichloromethane (9 mL), 3-chloroperoxibenzoic acid (mCPBA) (139 mg, 0.81 mmol) and sodium carbonate (29.3 mg, 3.61 mmol) were added. The mixture was stirred for 72 h at room temperature. The crude product was extracted into CH_2Cl_2 and washed with $NaHCO_3$(aq) 20% (w/v). The organic phase was concentrated under reduced pressure to give CyA-EPO as a white solid in 78% yield. The pure product was characterized by ^{13}C-NMR (75 MHz, $CDCl_3$), ^{1}H-NMR (300 MHz, $CDCl_3$) and mass spectrometry.

^{1}H-NMR (300 MHz, $CDCl_3$) δ: δ 8.03 – 7.91 (m, 1H, CON*H*), 7.43 (m, 2H, CON*H*), 8.59 (d, J = 9.7 Hz, 1H, CON*H*), 5.60 (dd, J = 11.2, 4.1 Hz, 1H), 5.46 (s, 2H), 5.42 – 5.19 (m, 2H), 5.18 – 5.02 (m, 2H), 4.98 – 4.86 (m, 2H), 4.84 – 4.67 (m, 2H), 4.59 (d, J = 13.8 Hz, 1H), 4.45 – 4.28 (m, 1H), 3.40 (s, 3H), 3.32 – 3.23 (m, 3H), 3.21 (d, J = 2.9 Hz, 3H), 3.15 (s, 4H), 3.03 (d, J = 4.2 Hz, 3H), 2.61 (s, 3H), 2.58 (s, 3H).

^{13}C-NMR (75 MHz, $CDCl_3$) δ: 173.76, 173.40, 172.99, 172.66, 171.68, 171.30, 171.08, 170.81, 170.47, 170.39, 169.72, 167.95, 77.58, 73.20, 58.32, 57.79, 57.62 (C-epoxy), 57.28, 56.10, 55.69 (C-epoxy), 55.13, 54.75, 54.38, 53.97, 53.47, 50.04, 48.78, 48.28, 47.88, 44.69, 40.99, 39.21, 36.84, 35.80, 32.98, 32.27, 31.74, 31.44, 30.19, 29.89, 29.70, 29.50, 25.06, 24.77, 24.52, 24.12, 23.81, 23.61, 23.54, 21.84, 21.34, 21.29, 20.68, 20.50, 19.64, 18.67, 18.37, 18.22, 18.10, 17.71, 17.50, 15.07, 9.93.

MS (ESI -): m/z $[M-H]^-$ calculated for $C_{64}H_{112}N_{11}O_{14}^-$ 1258.9, found 1258.8.

2.3.2. Synthesis of Cyclosporine A ((2-yl)amino)hexanoic acid (CyA-N-COOH)



Scheme 50. Synthetic route for preparation of the target carboxy-Cyclosporine A (II).

Epoxide opening by an ω-aminoester. In a 25 mL flask, methyl-6-aminohexanoate hydrochloride (50 mg, 0.28 mmol) was dissolved in 4 mL of absolute ethanol containing an excess (0.5 mL) of triethylamine. Then CyA-Epo (169 mg, 0.134 mmol) was added to the solution and the reaction mixture was kept under reflux overnight. After the evaporation of the EtOH by rotavap, the crude product was purified by liquid-liquid extraction (dichloromethane/brine). The organic phase was concentrated under reduced pressure to give CyA-N-ester as a white solid in 77% yield. The product was confirmed by thin-layer chromatography and mass spectrometry and used for the next step without further treatment.

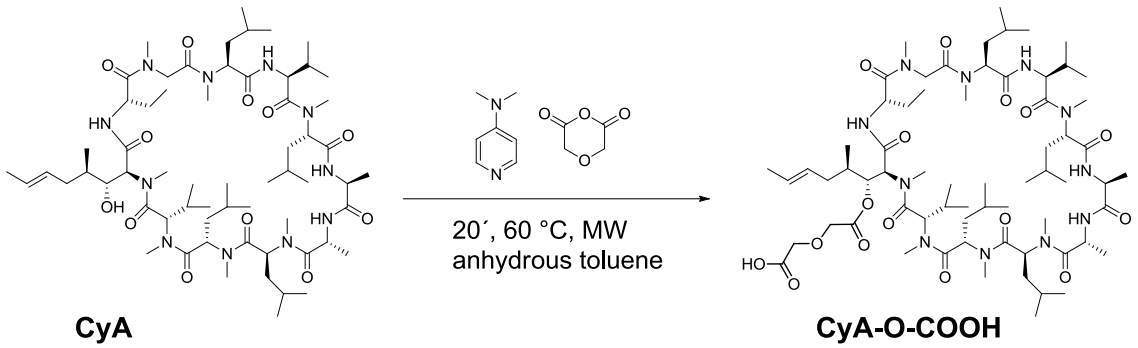
Alkaline hydrolysis of the ester. The intermediate CyA-N-ester (147 mg, 0.103 mmol) was dissolved in mixture of methanol (5 mL) and LiOH(aq) (7 mL, 0.2 M). The reaction mixture was kept overnight at room temperature with vigorous stirring. Then the solvent was evaporated under reduced pressure and the crude product was dissolved in chloroform and filtered. The organic phase was concentrated under reduced pressure to provide CyA-N-COOH as white solid in 81% yield. The product was obtained as a mixture of isomers (Nu- addiction at the 6' and 7' C) as shown by the complex 1H and ^{13}C NMR.

^{1}H-NMR (300 MHz, $CDCl_3$) δ: δ 8.51 – 8.37 (m, 1H, CON*H*), 8.08 (d, J = 9.9 Hz, 1H, CON*H*), 7.97 (d, J = 7.3 Hz, 1H, CON*H*), 7.65 (t, J = 9.3 Hz, 1H, CON*H*), 7.53 (d, J = 8.1 Hz, 1H, CON*H*), 7.20 – 7.11 (m, 2H, CON*H*), 7.07 (d, J = 8.1 Hz, 1H, CON*H*), 5.75 – 5.56 (m, 3H), 5.41 (d, J = 4.3 Hz, 1H), 5.30 – 5.09 (m, 7H), 5.09 – 4.97 (m, 2H), 4.94 (t, J = 7.3 Hz, 2H), 4.87 – 4.57 (m, 3H), 4.53 – 4.39 (m, 2H), 4.20 – 4.08 (m, 2H), 3.98 (d, 2H), 3.84 (br, 2H, CHO*H*), 3.70 – 3.61 (m, 2H), 3.47 (s, 2H), 3.34 (d, J = 5.5 Hz, 3H), 3.27 (d, J = 3.2 Hz, 7H), 3.22 (s, 2H), 3.18 (s, 4H), 3.12 (d, J = 3.4 Hz, 3H), 3.06 (s, 6H, CH_3), 2.92 (s, 3H, CH_3), 2.72 (d, J = 3.5 Hz, 2H), 2.69 (s, 2H), 2.66 (d, J = 3.0 Hz, 9H).

^{13}C-NMR (75 MHz, $CDCl_3$) δ: 174.07, 173.95, 173.55, 173.44, 172.95, 172.78, 172.75, 171.90, 171.40, 171.28, 171.26, 171.04, 170.92, 170.79, 170.57, 170.50, 170.32, 170.30, 169.42, 169.27, 168.45, 85.63 (C-O*H*), 82.99 (C-O*H*), 82.65 (C-O*H*), 67.31, 67.03, 59.99, 58.12, 57.74, 57.50, 57.38, 57.24, 55.32, 55.22, 54.73, 54.60, 54.37, 50.17, 49.52, 48.96, 48.87, 48.49, 48.31, 48.00, 44.98, 44.87, 41.23, 40.23, 39.40, 38.40, 37.47, 36.27, 36.17, 35.84, 35.74, 33.47, 32.84, 31.75, 31.53, 31.37, 31.32, 31.28, 31.16, 31.05, 30.80, 30.59, 30.14, 30.11, 30.04, 30.02, 29.91, 29.87, 29.82, 29.76, 29.74, 29.70, 29.57, 29.40, 29.13, 28.04, 27.92, 25.79, 25.07, 24.98, 24.77, 24.73, 24.21, 24.10, 24.03, 23.93, 23.86, 23.69, 23.49, 23.39, 22.99, 22.90, 22.76, 22.56, 22.27, 22.17, 22.07, 21.88, 21.72, 21.27, 21.08, 20.65, 20.60, 20.46, 19.62, 19.36, 19.27, 19.04, 18.90, 18.79, 18.73, 18.56, 18.52, 18.44, 18.36, 18.15, 17.99, 17.87, 17.69, 15.48, 9.74.

MS (FAB +): m/z $[M + Li]^+$ calculated for $C_{68}H_{124}LiN_{12}O_{15}^+$ 1355.9, found 1355.2.

2.4. Synthesis of Cyclosporine A (2-oxoethoxy) acetic acid (CyA-O-COOH)



Scheme 51. Synthesis of the CyA-O-COOH from diglycolic anhydride.

CyA (261 mg, 0.217 mmol), diglycolic anhydride (253 mg, 2.17 mmol,) and dimethylaminopyridine (DMAP, 83 mg, 0.679 mmol,) were dissolved in 4 mL of anhydrous toluene, in a 5 mL MW glass vial. The reaction mixture was irradiated with MW for 20 minutes at 60 °C and the solvent then removed by vacuum evaporation. The crude product was purified by liquid-liquid extraction (dichloromethane/brine). The organic phase was concentrated under reduced pressure to give CyA-O-COOH as a white solid in 84% yield. The purity of the product was confirmed by mass, ^{13}C-NMR (75 MHz, $CDCl_3$) and ^{1}H-NMR (300 MHz, $CDCl_3$).

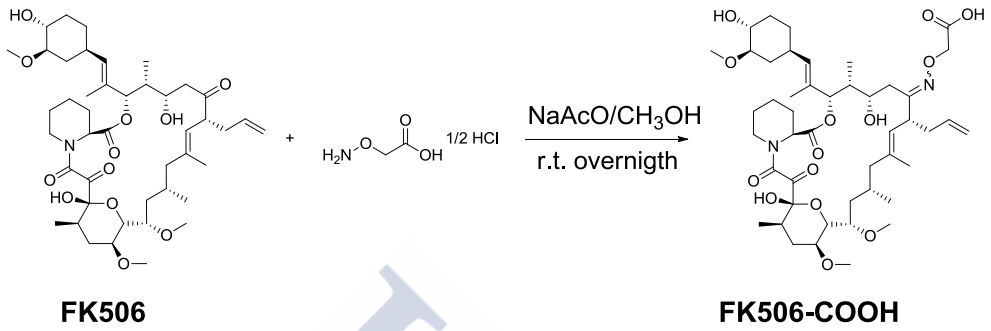
^{1}H-NMR (300 MHz, $CDCl_3$) δ: 8.60 – 8.48 (m, 1H), 8.20 (d, 1H), 8.01 (t, J = 7.7 Hz, 1H), 7.57 – 7.40 (m, 2H), 6.73 (d, 1H), 5.75 – 5.44 (m, 4H), 5.35 (dd, J = 11.8, 3.9 Hz, 1H), 5.29 – 5.16 (m, 1H), 5.17 – 5.04 (m, 1H), 4.96 – 4.69 (m, 3H), 4.63 (d, J = 13.8 Hz, 1H), 4.44 – 4.26 (m, 2H), 4.25 – 4.17 (m, 3H), 3.76 (d, J = 3.1 Hz, 1H).

^{13}C-NMR (75 MHz, $CDCl_3$) δ: 173.92, 173.82, 173.55, 173.50, 173.10, 173.05, 172.88, 172.81, 171.39, 171.22, 171.02, 170.66, 168.03, 160.48, 128.74, 126.86, 77.16, 71.18, 69.49, 68.48, 58.52, 57.53, 55.95, 55.32, 54.82, 54.35, 52.24, 50.17, 48.88, 48.38, 48.08, 44.75, 40.88, 39.35, 37.10, 35.88, 34.31, 33.72, 33.27, 32.96, 32.36, 31.82, 31.41, 29.97, 29.76, 29.43, 24.84, 24.64, 24.35, 24.25, 23.87, 23.62, 21.87, 21.31, 21.15, 20.77, 20.57, 19.68, 18.69, 18.43, 18.23, 17.75, 17.57, 15.14, 9.97.

MS (FAB +): m/z $[M+H]^+$ calculated for $C_{66}H_{116}N_{11}O_{16}^+$ 1318.85, found 1319.28.

3. Synthesis of tacrolimus derivatives

3.1. Synthesis of carboxylated tacrolimus (FK506-COOH)



Scheme 52. Synthesis of a carboxy derivative of tacrolimus.

Carboxylated Tacrolimus (FK506-COOH) was prepared according to Cañadas *et al*..[260] by reaction of commercial tacrolimus (423.80 mg, 0.53mmol) with carboxymethoxylamine hemichlorhydrate (109.3mg, 2.7mmol) in anhydrous methanol, in the presence of sodium acetate (82.03mg, 3.96 mmol). The reaction mixture was kept stirring overnight. The crude product was purified by liquid-liquid extraction with H_2O-$CHCl_3$. FK506-COOH was obtained as a white solid with 82% yield. Confirmation of the correct functionalization of tacrolimus was provided by comparison of the corresponding ^{13}C NMR spectra as well as from the mass spectrum of the carboxylated tacrolimus with those previously reported.

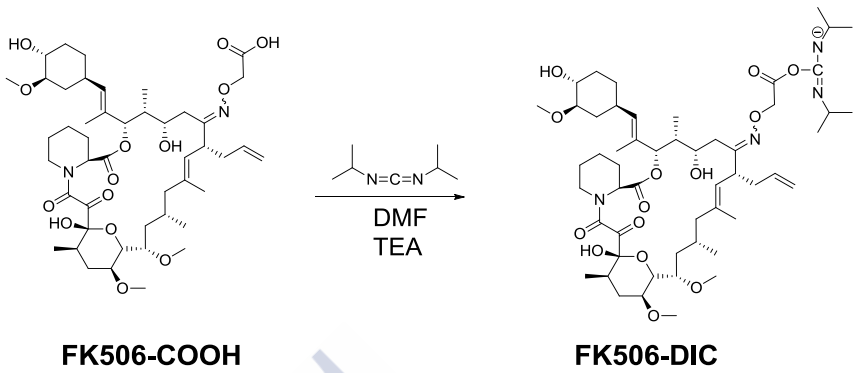
^{1}H-NMR (300 MHz, $CDCl_3$, δ): 6.78 (s,), 5.82 – 5.65 (m, 1H), 5.44 (d, J = 12.4 Hz, 1H), 5.11 – 4.96 (m, 5H), 4.64 (s, 1H), 4.60 – 4.52 (m, 1H), 4.49 (s, 1H), 4.40 (s, 2H), 4.28 (s, 1H), 4.12 (s, 1H), 3.96 (s, 1H), 3.54 – 3.43 (m, 5H), 3.42 – 3.38 (m, 3H), 3.37 – 3.31 (m, 3H), 3.13 – 3.01 (m, 2H).

^{13}C-NMR (75 MHz, $CDCl_3$) δ: 197.08, 196.98, 177.04,76.73, 176.54, 176.35, 169.39, 169.15, 165.27, 162.17, 161.79, 156.92, 138.57, 138.03, 136.24, 135.81, 132.91, 132.36, 125.40, 116.36, 116.01, 97.54, 96.79, 84.00, 77.43, 77.20, 77.00, 76.58, 73.87, 73.43, 71.11, 70.20, 56.81, 56.68, 56.58, 56.54, 56.48, 56.33, 56.25, 43.88, 40.03, 39.83, 39.03, 38.50, 34.95, 34.72, 34.48, 33.36, 31.24, 30.63, 27.23, 24.23, 21.59, 21.27, 21.19, 20.85, 16.05, 15.79, 15.74, 15.28, 15.17, 14.54, 14.20, 9.84, 9.17.

MS (ESI -): m/z [M] calculated for for $[C_{46}H_{72}N_2O_{14} - H]^-$, 875.5; found, 875.2.

[260] O. Cañadas, Al. Sáenz, G. Orellana, C. Casals, *Anal. Biochem*. **2005**, *340*, 57–65.

3.2. Synthesis of Diisopropylcarbodiimide Tacrolimus (FK506-DIC)



Scheme 53. Synthesis of FK506-DIC.

The FK506-COOH (50.10 mg, 0.057 mmol) and diisopropylcarbodiimide (DIC) (10 μL, 0.065 mmol) were dissolved in 200 μL of anhydrous DMF at room temperature under argon atmosphere. The reaction was kept stirring overnight. The crude product was washed with ethylacetate. The purity of the product was confirmed by mass spectrometry.

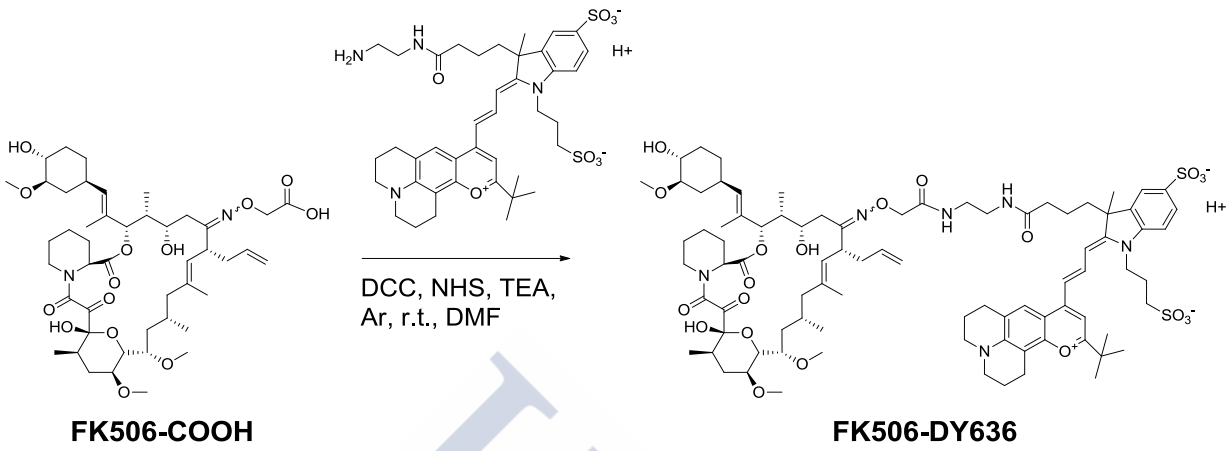
MS (ESI -): m/z $[M]^-$ calculated for $[C_{53}H_{85}N_4O_{14}]^-$ 1001.61, found 1001.61.

4. Synthesis of fluorescent conjugate of immunosuppressive drugs

The coupling reaction between the corresponding –COOH immunosuppressant and an aminated fluorescent label was carried out with the coupling agents EDC/HOBt (N-(3-dimethylaminopropyl)-N′-ethylcarbodiimide hydrochloride/1-hydroxybenzotriazole) to form an amide bond. The conjugates were obtained in > 55% yield in all cases.

The emission lifetimes, absorption and emission spectra, were determine for each immunosuppressive drug labeled with ANB in ethanol and phosphate buffer (PBS, pH 7.4, 100 mM).

4.1. Labeling of tacrolimus with Dy636-NH_2 (FK506-DY-636)



Scheme 54. Synthesis of FK506-DY636.

FK506-COOH (4.14 mg, 0.0047 mmol) and DY-636 by Dyomics GmbH (1.62 mg, 0.0021 mmol) were added in 2 mL DMF with N,N'-dicicloesilcarbodiimmide (DCC) (11.52 mg, 0.056 mmol), N-hydroxysuccinimide (NHS) (8.86 mg, 0.077 mmol) and 65 µL triethylamine (TEA). The reaction was kept 72 h at room temperature under argon atmosphere. The DMF was removed under reduced pressure and the crude product was kept in a vacuum oven during 18 h at 40°C. The crude product was washed with brine and extracted with chloroform. The pure product was obtained with very low reaction yield (< 10%) and was characterized by mass spectrometry.

MS (MALDI TOF +): m/z $[M+H]^+$ calculated for $C_{86}H_{113}N_6O_{21}S_2^+$ 1639.81, found 1639.60.

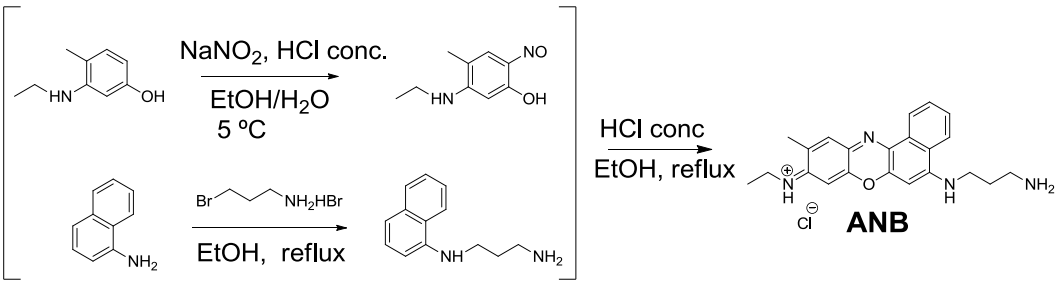
UV-VIS: λ_{abs} = 636 nm (EtOH).

4.2. Synthesis of Amino Nile Blue (ANB)

[(Z)-N-(5-((3-aminopropyl)amino)-10-methyl-9H-benzo[a]phenoxazin-9-ylidene)ethanaminium]

For the synthesis of ANB, nitration of commercially available 3-(ethylamino)-*p*-cresol and aminoalkylation of the naphthylamine are necessary. The ANB is produced by the condensation of the two intermediates, by reflux in acidic ethanol (64% yield).[261]

[261] V. H. J. Frade, M. Sameiro, T. Gonçalves, J.C.V.P. Moura., *Tetrahedron Lett.* **2006**, *47*, 8567–8570.



Scheme 55. Synthesis of propylamino Nile Blue.

4.2.1. Synthesis of 5-ethylamino-4-mathyl-2-nitrosophenol.

To a cold solution (0 °C) of 3-(ethylamino)-4-methylphenol (1.002 g, 6.63 mmol) in 100 mL of an aqueous solution of $NaNO_2$ 2.15 M, was added drop by drop a concentrated HCl solution (6 M, 16.4 mL). The mixture was stirred at 0 °C for 1 h. The solution acquired a very intense brown-orange color. The reaction was followed by TLC in silica gel (AcOEt:EtOH 10:1, v/v). The crude product was purified by precipitation by adding a solution of NaOH (pH 11). The precipitate was filtered off, washed with cold 1 M HCl and dried in vacuum. The pure product was obtained as a brown solid (0.56 g, 47% yield).

^{1}H-NMR (300 MHz, $CDCl_3$) δ: 6.93 (s, 1H), 5.61 (s, 1H), 5.31 (br, 1H, $NHCH_2CH_3$), 3.34 (quint, J = 7.2 Hz, 2H, $NHCH_2CH_3$), 2.15 (s, 3H) 1.36 (t, J = 7.3 Hz, 3H, $NHCH_2CH_3$).

^{13}C-NMR (75 MHz, CD_3OD) δ: 168.71, 166.19, 145.92, 132.77, 122.20, 41.46, 17.21, 14.00.

MS (ESI +): m/z $[M+H]^+$ calculated for $C_9H_{13}N_2O_2^+$ 181.1, found 181.0, the m/z $[M+Na]^+$ was also found at 203.1.

4.2.2. Synthesis of N^1-1-naphthalenyl-1,3-propanediamine

The N^1-1-naphthalenyl-1,3-propanediamine was synthetized with the following procedure. 1-naftilamine (1.013 g, 7.07 mmol) was dissolved in 10 mL of ethanol and then 3-bromopropylamine hydrobromide (1.694 g, 7.74 mmol) was added in the mixture. The reaction was kept under reflux for 8 h and monitoring by TLC (silica-gel CH_2Cl_2:MeOH 10:1 *v/v*).

^{1}H-NMR (300 MHz, CD_3OD) δ: 6.57 (d, J = 8.5 Hz, 1H), 6.46 – 6.35 (m, 2H), 6.17 – 6.00 (m, 3H), 5.98 (t, J = 4.1 Hz, 1H), 2.17 – 2.06 (m, 2H), 1.51 (t, J = 7.7 Hz, 2H), 0.77 – 0.59 (m, 2H).

^{13}C-NMR (75 MHz, CD_3OD) δ: 135.95, 132.86, 130.41, 130.23, 129.09, 128.41, 126.71, 126.45, 126.32, 121.60, 37.99, 25.58.

MS (ESI +): m/z $[M+H]^+$ calculated for $C_{13}H_{17}N_2^+$ 201.1, found 202.0

4.2.3. Synthesis propylamino Nile Blue (ANB)

N[1]-(naphtalen-1-yl)propane-1,3-diamine (0.42 g, 1.8 mmol) and 12 M HCl (5.0×10^{-2} mL) were added to a cold solution of 5-ethylamino-4-methyl-2-nitrosophenol (0.37 g, 1.8 mmol) in ethanol (6 mL). The mixture was refluxed for 1.5 h while monitored by silica TLC (dichloromethane-methanol 9:1 *v/v*), and the crude product was purified by recrystallization in ethanol. ANB was obtained as blue-green crystals (0.46 g, 64%).

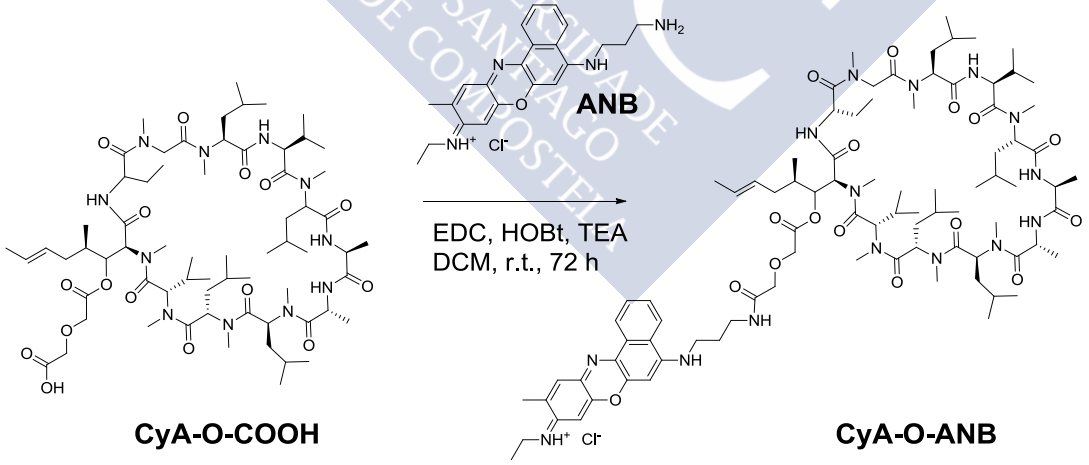
^{1}H-NMR (300 MHz, CD_3OD) δ: 8.92 (d, J = 8.0 Hz, 1H), 8.41 (d, J = 8.3 Hz, 1H), 7.92 (t, J = 7.6 Hz, 1H), 7.82 (t, J = 7.5 Hz, 1H), 7.71 (s, 1H), 7.05 (s, 1H), 6.88 (s, 1H), 3.85 (t, J = 7.2 Hz, 2H), 3.56 (q, J = 7.0 Hz, 2H), 3.17 (t, J = 7.7 Hz, 2H), 2.35 (s, 3H), 2.23 (t, J = 7.5 Hz, 2H), 1.38 (t, J = 7.1 Hz, 3H).

^{13}C-NMR (75 MHz, CD_3OD) δ: 157.81, 156.70, 152.06, 148.92, 133.28, 132.56, 132.53, 132.19, 131.74, 130.49, 129.08, 125.08, 124.10, 124.00, 94.44, 94.03, 39.91, 38.48, 27.61, 24.21, 18.01, 14.22.

MS (ESI +): m/z $[M]^+$ calculated for $[C_{22}H_{25}N_4O]^+$ 361.2, found 361.2.

UV-VIS: λ_{abs} = 630 nm (EtOH), λ_{abs} = 627 nm (PBS pH 7.4, 100 mM).

4.3. Synthesis of Cyclosporne A-(oxoethoxy)(acetamido)(propylamino)-NileBlue (CyA-O-ANB)



Scheme 56. Preparation of the fluorescent CyA-O-ANB.

CyA-O-COOH (32.1 mg, 0.024 mmol), ANB (20.2 mg, 0.051 mmol), EDC (10.6 mg, 0.068 mmol), and HOBt (12.3 mg, 0.091 mmol) were dissolved in 40 mL dichloromethane, in a 100 mL flask. For solubilizing ANB^+Cl^- salt in CH_2Cl_2 addition of triethylamine (500 µL) was necessary. The reaction was kept stirring in an ice bath for 1 h and then at room

temperture overnight, protected from light. The crude product was purified by liquid-liquid extractions (HCl(aq), pH ca. 5.5 and CH_2Cl_2). Then the organic phase was concentrated under reduced pressure to yield CyA-O-ANB as a shiny blue solid. The pure fluorescent product was confirmed by mass spectrometry and characterized by UV-VIS absorption and fluorescence spectroscopy and ^{13}C-NMR (700 MHz, C_6D_6), ^{1}H-NMR (700 MHz, C_6D_6).

^{1}H-NMR (700 MHz, C_6D_6) δ: δ 8.77 – 8.69 (m, 1H, CH_{Ar}), 8.41 – 8.25 (m, 1H, CH_{Ar}), 8.06 – 7.95 (m, 1H, CH_{Ar}), 7.84 – 7.73 (m, 1H, CH_{Ar}), 7.58 – 7.45 (m, 1H, CH_{Ar}), 7.29 – 7.22 (m, 1H, C=N*H*), 7.01 – 6.92 (m, 1H, CH_{Ar}), 6.89 – 6.78 (m, 1H, CH_{Ar}), 6.11 – 5.99 (m, 1H), 5.96 – 5.79 (m, 2H), 5.67 – 5.61 (m, 1H), 5.58 – 5.50 (m, 1H), 5.49 – 5.34 (m, 2H), 5.21 (s, 2H), 5.09 – 4.89 (m, 3H), 4.85 – 4.71 (m, 1H), 4.60 – 4.47 (m, 2H), 4.11 – 3.97 (m, 1H).

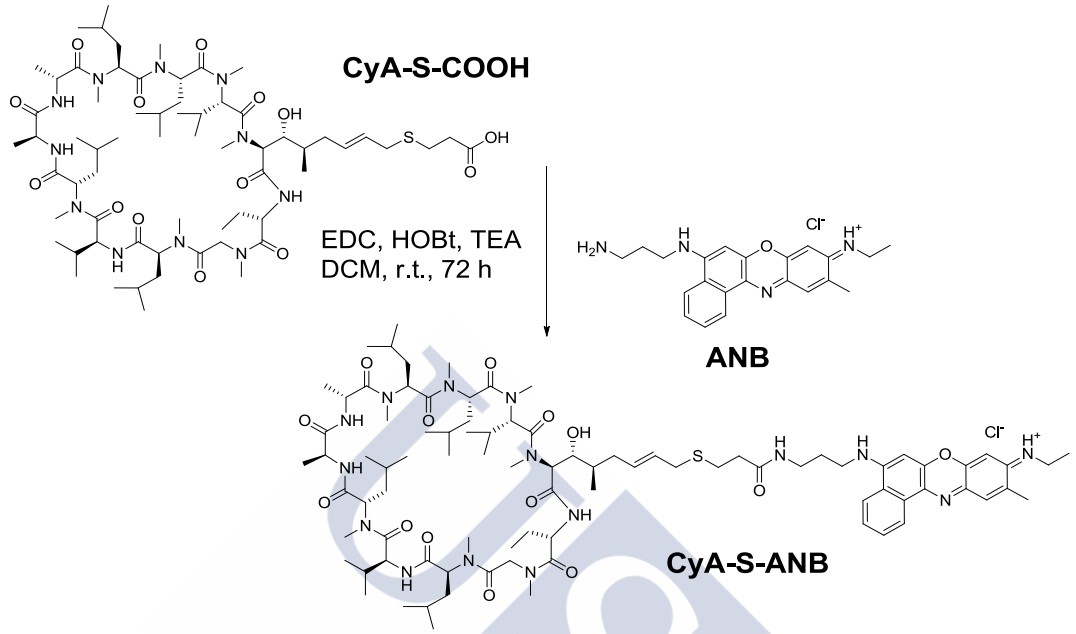
^{13}C-NMR (176 MHz, C_6D_6) δ: 174.25, 173.54, 173.01, 172.69, 172.63, 171.25, 171.22, 171.11, 171.05, 170.85, 170.47, 170.12, 169.32, 167.99, 143.55, 124.41, 120.16, 108.95, 84.65, 73.94, 67.18, 58.72, 57.55, 56.21, 55.06, 54.47, 49.02, 48.66, 48.61, 48.21, 48.10, 47.82, 44.61, 44.55, 40.49, 39.55, 38.65, 37.31, 35.89, 34.62, 33.40, 32.84, 32.13, 31.99, 31.84, 31.74, 31.15, 31.11, 30.64, 30.49, 30.41, 29.86, 29.79, 29.75, 29.49, 29.34, 29.23, 25.17, 24.79, 24.71, 24.58, 24.54, 23.92, 23.88, 23.64, 23.44, 22.78, 21.69, 21.64, 21.28, 20.99, 20.12, 19.84, 19.59, 18.75, 18.39, 18.19, 17.97, 17.63, 17.18, 17.14, 15.01, 14.97, 14.04, 9.82, 1.06.

MS (ESI +): m/z $[M]^+$ calculated for $[C_{88}H_{138}N_{15}O_{16}]^+$ 1662.1, found 1662.1, also the peak $[(M+Na)/2]^+$ at 842.3was found.

MS (FAB +): m/z $[M]^+$ calculated $[C_{88}H_{138}N_{15}O_{16}]^+$ 1662.1, found 1662.2.

UV-VIS: λ_{abs} = 629 nm (EtOH), λ_{abs} = 626 nm (PBS pH 7.4, 100 mM).

4.4. Synthesis of Cyclosporine A(thio)(propanamido)(propylamino)-Nile Blue (CyA-S-ANB)



Scheme 57. Preparation of the fluorescent CyA-S-ANB.

CyA-S-COOH (30.62 mg, 0.023 mmol), ANB (13.6 mg, 0.034 mmol), EDC (17.45 mg, 0.11 mmol), HOBt (8.95 mg, 0.066 mmol) and TEA (150 μL) were dissolved in dichloromethane, in a 100 mL flask. The reaction was protected from light and kept stirring in an ice bath for 1 h and then at room temperature for additional 18 h. The crude product was purified by liquid-liquid extractions (HCl(aq), pH ca. 5.5 and CH_2Cl_2). Finally the organic phase was concentrated under reduced pressure to yield CyA-S-ANB as a shiny blue solid.

^{1}H-NMR (700 MHz $CDCl_3$) δ: 9.27 – 9.14 (m, 1H), 8.83 (s, 1H), 8.26 (d, J = 9.8 Hz, 1H), 7.90 – 7.73 (m, 3H), 7.61 – 7.49 (m, 2H), 7.37 – 7.32 (m, 1H), 7.23 – 7.04 (m, 1H), 6.60 (d, J = 7.6 Hz, 1H), 6.51 – 6.40 (m, 1H), 6.12 – 6.01 (m, 1H), 5.72 – 5.66 (m, 1H), 5.61 (dd, J = 14.4, 6.8 Hz, 1H), 5.51 (m, 1H), 5.44 (d, J = 6.6 Hz, 1H), 5.37 – 5.28 (m, 1H), 5.26 (d, J = 8.1 Hz, 1H), 5.19 (dd, J = 11.3, 4.1 Hz, 1H), 5.16 (d, J = 11.0 Hz, 1H), 5.13 – 5.03 (m, 2H), 5.03 – 4.97 (m, 2H), 4.87 – 4.78 (m, 2H), 4.74 – 4.62 (m, 2H), 4.53 – 4.44 (m, 1H), 3.99 – 3.80 (m, 3H, CO*H,* NH*CH_2*).

^{13}C-NMR (176 MHz, $CDCl_3$) δ: 173.82, 173.67, 173.50, 171.49, 171.06, 170.89, 170.55, 170.08, 169.95, 169.65, 158.22, 153.25, 151.35, 146.67, 137.16. 134.40, 132.66, 132.13, 131.40, 130.69, 129.76, 127.94, 127.49, 125.22, 124.33, 115.98, 109.26, 93.59, 73.38, 71.75, 69.17, 59.89, 57.86, 57.21, 55.28, 55.04, 54.44, 50.03, 48.58, 48.35, 47.88, 46.36,

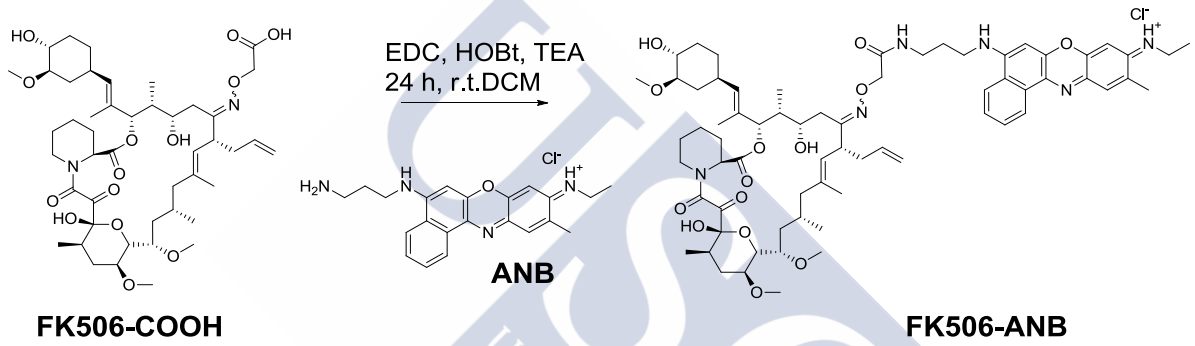
44.80, 40.66, 39.36, 39.05, 38.73, 37.79, 37.44, 35.96, 33.43, 31.88, 31.29, 31.20, 30.01, 29.84, 29.78, 29.65, 29.57, 29.52, 29.32, 28.09, 26.40, 25.18, 24.95, 24.83, 24.80, 24.78, 24.62, 24.37, 23.80, 23.69, 23.43, 22.65, 21.83, 21.47, 21.17, 20.33, 19.76, 18.65, 18.60, 18.25, 17.87, 15.82, 15.46, 14.07, 9.89.

MS (ESI +): m/z $[M]^+$ calculated for $[C_{87}H_{138}N_{15}O_{14}S]^+$ 1650.2 found 1650.0, also the peak $[(M+Na)/2]^+$ at 836.6 was found.

MS (FAB +): m/z $[M]^+$ calculated for $[C_{87}H_{138}N_{15}O_{14}S]^+$ 1650.2 found 1649.3.

UV-VIS: λ_{abs} = 630 nm (EtOH), λ_{abs} = 579 nm, 628 nm (PBS pH 7.4, 100 mM).

4.5. Synthesis of Tacrolimus-propylamino Nile Blue (FK506-ANB)



Scheme 58. Synthesis of a fluorescent derivative of tacrolimus (FK506-ANB).

FK506-COOH (8.65 mg, 9.86 μmol), ANB (6.6 mg, 0.017 mmol), EDC (5.18 mg, 0.027 mmol), HOBt (2.85 mg, 0.021 mmol) and TEA (3 μL) were dissolved in 20 mL dichloromethane. The reaction was kept stirring at 0 °C for 1 h and successively at room temperature overnight protected from light. The crude product was purified by extractions (HCl(aq), pH ca. 5.5 and CH_2Cl_2) and washed with H_2O. Then the organic phase was concentrated under reduced pressure to yield FK506-ANB as a shiny blue solid with 82% yield.

^{1}H-NMR (700 MHz, $CDCl_3$) δ: 9.10 – 8.60 (m, 3H), 7.82 (s, 2H), 7.59 – 7.30 (m, 1H), 6.66 – 6.38 (m, 2H), 5.88 – 5.60 (m, 1H), 5.58 – 5.21 (m, 1H), 5.15 – 4.91 (m, 5H), 4.74 – 4.56 (m, 2H), 4.48 – 4.29 (m, 2H), 4.03 – 3.57 (m, 2H), 3.45 – 3.37 (m, 5H), 3.37 – 3.31 (m, 4H), 3.31 – 3.24 (m, 3H), 3.06 – 2.88 (m, 1H), 2.82 – 2.41 (m, 3H), 2.38 – 2.24 (m, 5H), 2.23 – 2.12 (m, 1H), 2.11 – 1.93 (m, 3H), 1.82 – 1.67 (m, 4H), 1.66 – 1.53 (m, 7H), 1.45 – 1.36 (m, 4H), 1.35 – 1.18 (m, 22H), 1.03 – 0.95 (m, 4H), 0.93 – 0.78 (m, 7H).

^{13}C-NMR (176 MHz, $CDCl_3$) δ: 196.71, 196.52, 171.51, 168.92, 165.45, 161.86, 157.94, 146.68, 137.71, 136.62, 136.05, 132.98, 130.74, 128.80, 125.86, 125.69, 124.32, 116.20, 97.45, 96.97, 96.07, 84.15, 84.10, 77.16, 76.98, 76.80, 75.74, 75.57, 74.20, 74.12, 74.01,

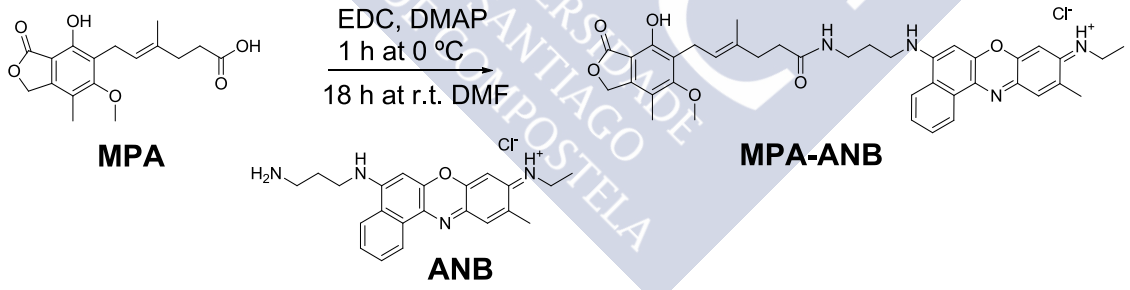
73.59, 73.55, 72.58, 71.76, 70.23, 64.92, 56.81, 56.61, 56.48, 56.29, 48.85, 48.42, 43.97, 39.06, 38.95, 38.74, 38.10, 36.94, 36.31, 35.89, 34.95, 34.78, 34.69, 34.50, 34.13, 32.54, 32.40, 31.90, 31.40, 31.14, 30.70, 30.28, 30.15, 29.67, 29.63, 29.57, 29.49, 29.34, 29.22, 29.10, 28.55, 27.96, 27.62, 27.22, 26.99, 25.87, 25.14, 24.89, 24.34, 22.67, 21.35, 21.11, 19.13, 17.44, 17.28, 16.17, 15.88, 15.78, 15.40, 15.22, 14.79, 14.11, 10.03, 9.86, 9.45, 0.99.

^{13}C-NMR (176 MHz, MeOD) δ: 283.84, 173.81, 171.43, 169.33, 164.88, 162.05, 158.58, 156.75, 156.65, 152.93, 152.66, 149.40, 149.20, 134.49, 134.36, 133.54, 133.21, 133.12, 132.84, 132.68, 132.51, 132.39, 132.23, 131.72, 130.98, 130.77, 130.66, 129.88, 128.85, 128.42, 126.63, 126.47, 125.53, 124.74, 124.59, 124.08, 123.75, 97.21, 94.53, 94.48, 93.98, 85.22, 76.45, 75.80, 74.63, 73.64, 72.13, 70.61, 66.99, 64.28, 57.46, 56.04, 54.82, 49.49, 49.36, 49.24, 49.12, 49.00, 48.88, 48.76, 48.63, 42.98, 40.41, 39.73, 39.68, 37.76, 37.67, 37.54, 37.00, 36.97, 34.29, 33.23, 33.07, 31.67, 30.75, 30.47, 30.42, 29.53, 29.22, 27.89, 27.47, 27.20, 27.01, 26.53, 26.04, 24.05, 23.74, 20.29, 19.41, 19.30, 17.72, 14.45, 14.17, 11.76.

MS (ESI +): m/z $[M]^+$ calculated for $[C_{68}H_{95}N_6O_{14}]^+$ 1219.7, found 1219.8.

UV-VIS: λ_{abs} = 627 nm (EtOH), λ_{abs} = 569 nm (PBS pH 7.4, 100 mM).

4.6. Synthesis of Mycophenolic propylamino Nile Blue (MPA-ANB)



Scheme 59. Synthesis of MPA-ANB.

Mycophenolic acid (2.88 mg, 0.009 mmol), ANB (4.53 mg, 0.011 mmol), EDC (2.30 mg, 0.012 mmol) and DMAP (2.13 mg, 0.017 mmol) were dissolved in 8 mL of dry DMF in a 25 mL round-bottom flask. The mixture was protected from light and kept in an ice bath with stirring for 3 h, and then at room temperature for additional 48 h. After this time, DMF was eliminated by reduced pressure and the crude product was extracted into CH_2Cl_2 and washed with NH_4Cl(aq). MPA-ANB was obtained as a shiny blue solid in 85% yield. The fluorescent MPA-AO was characterized by ^{1}H-NMR, mass spectrometry and UV-VIS spectroscopy.

^{1}H-NMR (300 MHz, CD_3OD): δ/ppm 8.94 (d, *J* = 8.1 Hz, 1H), 8.29 (d, *J* = 8.2 Hz, 1H), 7.92 (t, *J* = 7.5 Hz, 1H), 7.86 (t, *J* = 7.5 Hz, 1H), 7.73 (s, 1H), 6.86 (s, 1H), 6.81 (s, 1H), 5.36 (t, *J* = 3.6 Hz, 1H), 4.92 (s, 2H), 3.76 (s, 3H), 3.63 (m, 2H), 3.54 (q, *J* = 7.2 Hz, 2H), 3.42 – 3.34 (m, 2H), 3.16 – 3.12 (m, 2H), 2.40 (s, 3H), 2.36 (s, 4H), 2.27 (t, *J* = 7.4 Hz, 2H) 2.16 (s, 3H), 1.88 (s, 3H), 1.39 (t, *J* = 7.2 Hz, 3H).

MS (ESI +): m/z $[M]^+$ calculated for calculated for: $[C_{39}H_{43}N_4O_6]^+$ 663,3 found 663.4.

UV-VIS: λ_{abs}^{max} = 629 nm in EtOH and in 0.1 M PBS pH 7.4.

5. Binding assay with immunosuppressant using fluorescence polarization

5.1. Preparation of stock solutions

Stock solutions of CyA, FK506, MPA, CyA-S-ANB, FK506-ANB, MPA-ANB, and Human Serum Albumin (HSA) were prepared as described in Table 21. The immunosuppressants and the labeled immunosuppressants were dissolved in absolute ethanol; HSA was dissolved in PBS (100 mM).

Table 21. Concentration of the stock solutions used for the fluorescent polarization assay.

Sample	*MW [g/mol]*	*[mg]*	*[μmol]*	*Volume [mL]*	*Molarity [M]*
CyA	1202.61	12.76	10.61	2.120[a]	5 x 10 $^{-3}$
FK506	804.02	15.01	18.66	3.734 [a]	5 x 10 $^{-3}$
MPA	320.34	5.01	15.64	3.130 [a]	5 x 10 $^{-3}$
CyA-S-ANB	1685.6	0.66	0.39	07.830 [a]	5 x 10 $^{-5}$
FK506-ANB	1255.97	0.19	0.15	2.970 [a]	5 x 10 $^{-5}$
MPA-ANB	699.23	0.67	0.95	19.069 [a]	5 x 10 $^{-5}$
HSA	66478	166.1	2.50	50.000 [b]	5 x 10 $^{-5}$

[a] absolute ethanol; [b] PBS aqueous buffer 0.1 M.

5.2. Filling of a 96 wells microplate for the FP binding assay

The corresponding labeled immunosuppressant was added in the wells of a microplate PACKARD HTRF 96 (96 wells) with a constant concentration of 0.83 μM.

HSA was added in increasing concentrations along each row: from 0.5 to 50 equivalents of labeled immunosuppressant. In this way, in each column of the microplate there is a different concentration of the receptor (HSA). In rows A, B, C the labeled immunosuppressant is mixed with HSA and diluted with PBS when needed, in order to have the same volume in each well (300 μl). Rows D, E, F are filled exactly in the same

way as rows A, B and C but adding the corresponding free immunosuppressant in a saturated concentration. In row G there are three wells with the labeled immunosuppressant without HSA, and in another three wells the labeled immunosuppressant is added in the presence of a saturating concentration of HSA. There are six wells free for eventual errors during the previous adding. The H row is used for the blank (HSA + PBS). This scheme allows the measurement of fluorescent polarization in triplicate. The details are shown in Table 22.

Fluorescence intensity was measured before the measurement of the fluorescence polarization for each well. The conditions employed were: 40 flashes per well, λ_{ex} = 585 nm, λ_{em} = 654 nm, excitation and emission bandwidths 10 nm, both. A dichroic filter of 619.5 nm was used.

For the measurement of fluorescence polarization the number of flashes per well were 200. The filters used were: for the excitation a P590-50, a dichroic filter LP639 and for the emission a P675-50. The plate was shaken with a double orbital mode 60 s before plate reading.

USC UNIVERSIDADE DE SANTIAGO DE COMPOSTELA

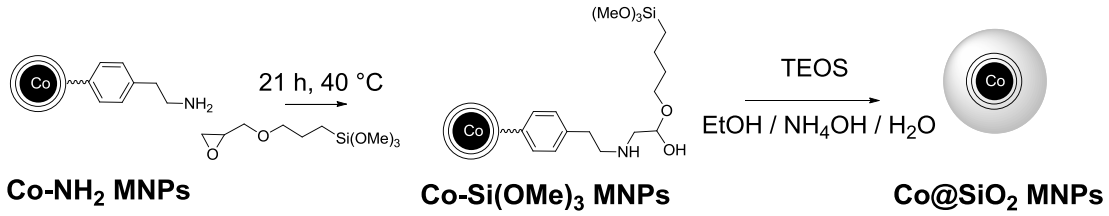
Table 22. Representative scheme of the filling of a microplate (96 wells) for performing a fluorescent polarization binding assay for the CyA-HSA complex. The plate for FK506 and MPA were prepared following the same protocol.

		1	2	3	4	5	6	7	8	9	10	11	12
		[µL]	[µL]	[µL]	[µL]	[µL]	[µL]	[µL]	[µL]	[µL]	[µL]	[µL]	[µL]
A	CyA-S-ANB[a]	5	5	5	5	5	5	5	5	5	5	5	5
	HSA[a]	2.5	5	25	50	75	100	125	150	175	200	225	250
	PBS	292.5	290	270	245	220	195	170	145	120	95	70	45
B	CyA-S-ANB[a]	5	5	5	5	5	5	5	5	5	5	5	5
	HSA[a]	2.5	5	25	50	75	100	125	150	175	200	225	250
	PBS	292.5	290	270	245	220	195	170	145	120	95	70	45
C	CyA-S-ANB[a]	5	5	5	5	5	5	5	5	5	5	5	5
	HSA[a]	2.5	5	25	50	75	100	125	150	175	200	225	250
	PBS	292.5	290	270	245	220	195	170	145	120	95	70	45
D	CyA-S-ANB[a]	5	5	5	5	5	5	5	5	5	5	5	5
	HSA[a]	2.5	5	25	50	75	100	125	150	175	200	225	250
	PBS µL	287.5	285	265	240	215	190	165	140	115	90	65	40
	CyA[b]	5	5	5	5	5	5	5	5	5	5	5	5
E	CyA-S-ANB[a]	5	5	5	5	5	5	5	5	5	5	5	5
	HSA[a]	2.5	5	25	50	75	100	125	150	175	200	225	250
	PBS	287.5	285	265	240	215	190	165	140	115	90	65	40
	CyA[b]	5	5	5	5	5	5	5	5	5	5	5	5
F	CyA-S-ANB[a]	5	5	5	5	5	5	5	5	5	5	5	5
	HSA[a]L	2.5	5	25	50	75	100	125	150	175	200	225	250
	PBS	287.5	285	265	240	215	190	165	140	115	90	65	40
	CyA[b]	5	5	5	5	5	5	5	5	5	5	5	5
G	CyA-S-ANB[a]	5	5	5	5	5	5						
	HSA[a]	300	300	300	0	0	0						
	PBS	0	0	0	295	295	295						
	CyA[b]	0	0	0	0	0	0						
H	HSA[a]	2.5	5	25	50	75	100	125	150	175	200	225	250
	PBS	297.5	295	275	250	225	200	175	150	125	100	75	50

[a] 5×10^{-5} M, [b] 5×10^{-3} M.

6. Cobalt core magnetic nanoparticles

6.1. Synthesis of $Co@SiO_2$ MNPs



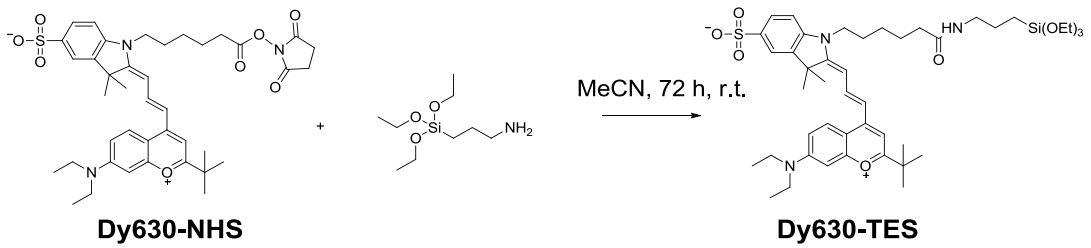
Scheme 60. Preparation of core-shell magnetic silica nanoparticles.

TurboBeads® with aliphatic primary amino group Co-NH_2 MNPs (1 mL, 30 mg/L, the concentration of the $-NH_2$ groups is 0.15 mmol/g that correspond to 4.5 μmol) were sonicated during 5 minutes and washed three time with absolute ethanol. After each washing the NPs were sonicated for 2 minutes. Then the washed NPs were sonicated for 30 additional minutes and the 3-(glycidyloxypropyl)trimethoxy silane (15 μL, 67.5 μmol) was added. The Co-NH_2 MNPs were mixed during 21 hours at 40 °C at 250 rpm. After this time the Co-$Si(OMe)_3$ NPs were washed with ethanol three times with the help of a magnet and finally stored in 1 mL of EtOH. Successively 40 mL of 2-propanol, 3.75 mL of H_2O, 4.5 mL of NH_3 at 28%, 400 μL of MNPs Co-$Si(OMe)_3$ NPs, and finally 50 μL of TEOS were added in this order in a Erlenmeyer. The mixture was sonicated for 30 minutes, and then shaked at 200 rpm at 40 °C for 2 hours. The $Co@SiO_2$ NPs were washed three times with ethanol and finally stored in 50 mL of EtOH (final concentration of NP 0.6 mg/L). The synthesized $Co@SiO_2$ nanoparticles were characterized by TEM microscopy and FTIR (see figure x in Annex part).

FTIR: Wavenumber, cm^{-1}: 3424.29, 2924.30, 1635.90, 1384.24, 1094.58, 958.96, 799.46, 469.37.

6.2. Fluorescent doping of $Co@SiO_2$ NPs

6.2.1. Synthesis of Dy630-TES



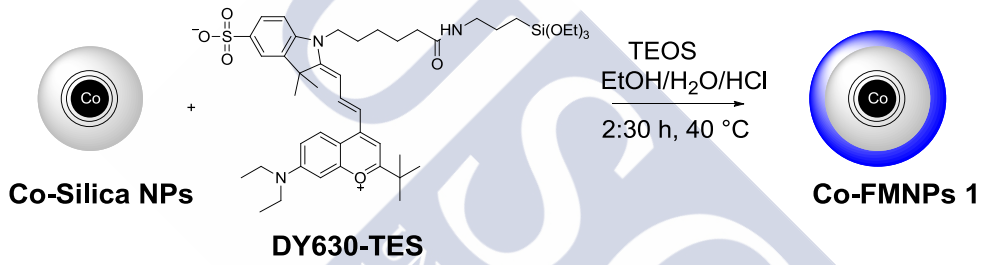
Scheme 61. Synthesis of the triethoxisilane derivative Dy630-TES.

The commercial dye (Dyomics GmbH), DY630-NHS-ester (1 mg, 0.0014 mmol) and (3-aminopropyl)triethoxysilane (APTES) (130 µL of a stock solution in acetonitrile 0.043 M) were added in 0.5 mL of acetonitrile, in a 1.5 mL eppendorf. The reaction was kept stirring at room temperature during 72 h, protected from light. The reaction progress was followed by TLC silica gel (ethyl acetate-methanol 10:3 *v/v*). The crude product was dried and washed with chloroform (yield 45%).

MS (ESI-): m/z $[M-H]^-$ calculated for $C_{45}H_{67}N_3O_8SSi$, 836.4, found: 836.2.

6.2.2. Doping of Co@SiO_2 NPs with Dy630-TES

Doping of Co@SiO_2 nanoparticles is achieved by covalent attachment of alkoxysilane derivatized fluorescent label Dy630-TES by acid-catalized condensation in aqueous media.



Scheme 62. Preparation of fluorescent silica magnetic NPs.

350 mg of NaCl were added in a solution 1 M of acetic acid (0.915 mL of CH_3COOH 100% in 16 mL of H_2O). In two different flasks of 50 mL, Co@SiO_2 MNPs in ethanol (25 mL, 0.6 mg/L) were dried. In flask A: 100 µL of DY630-TES (0.56 µmol), 0.218 mL acetic acid 1 M, and 25 µL of TEOS (0.112 mmol) were added. In flask B: 400 µL of DY630-TES (2.24 µmol), 0.875 mL of acetic acid 1 M, and 100 µL of TEOS (0.448 mmol) were added. The flasks were sonicated for 30 minutes and then shaken during 2 hours at 40 °C. After this time the Co-FMNPs were washed with water and finally stored in 5 mL of absolute ethanol. The Co-FMNPs were characterized by TEM and UV-VIS.

UV-VIS: λ_{abs}= 636 nm, λ_{em}= 661 nm (EtOH).

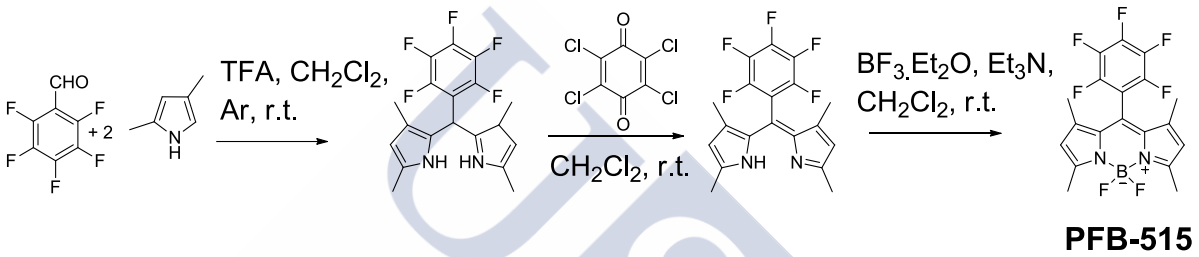
TEM: it was difficult to assess whether an additional SiO_2 layer grew around the MNPs due to the heterogeneous size distribution of the starting Co@SiO_2 NPs (see Figure 175 in the Annex part).

7. Synthesis of fluorescent BODIPY dyes

Boron-dipyrromethene (BODIPY) dye were prepared following synthetic protocols described in the literature for similar compounds.[262,263]. Once prepared, the dyes were stored in dry at 4 °C and protected from light.

7.1. Synthesis of PFB-515

[(4,4-difluoro-1,3,5,7-tetramethyl-8-pentafluorophenyl-4-bora-3a,4a-diaza-s-indacene)]



Scheme 63. Synthesis of PFB-515.

Pentafluorobenzaldehyde (647.2 mg , 3.30 mmol) and 2,4-dimethyl-1H-pyrrole (924.5 mg , 9.71 mmol) were dissolved in CH_2Cl_2 (5 mL) under argon. Then a few drops of trifluoroacetic acid were added. The reaction mixture was kept in the dark and stirred for 4 h at room temperature until the aldehyde was consumed (monitored by TLC). In the next step, oxidation of the intermediate was performed by adding tetrachloro-*p*-benzoquinone (chloranil) (789.4 mg, 3.21 mmol) dissolved in CH_2Cl_2 (30 mL). The reaction mixture was stirred for 1 h. Finally, a solution of boron trifluoride diethyl etherate (6.63 mL, 52.33 mmol) was added together with triethylamine (6.46 mL, 46.35 mmol). The reaction was stirred for 2 additional hours. The crude reaction mixture was washed with H_2O and extracted with CH_2Cl_2, the organic phase was dried with $MgSO_4$ and the solvent was removed under reduced pressure. The crude product was firstly purified with flash column chromatography on silica gel (hexane-ethylacetate with 15:1 to 9:1 *v/v* gradient) and then on neutral aluminium oxide (hexane-ethylacetate with 33:1 to 18:1 *v/v* gradient). PFB-515 was obtained as orange crystals with a green glow (205.0 mg, 15% yield).

^{1}H-NMR (300 MHz, $CDCl_3$, δ): 6.06 (s, 2H, CH), 2.57 (s, 6H, CH_3), 1.62 (s, 6H, CH_3).

[262] G. Vives, G. Giansante, R. Bofinger, G. Raffy, A. del Guerzo, B. Kauffmann, P. Batat, G. Jonusauskas, N.D. McClenaghan, *Chem. Commun*., **2011**, *47*, 10425–10427.

[263] O. Galangau, C. Dumas-Verdes, R. Méallet-Renault, G. Clavier, *Org. Biomol. Chem.,* **2010**, *8*, 4546–4553.

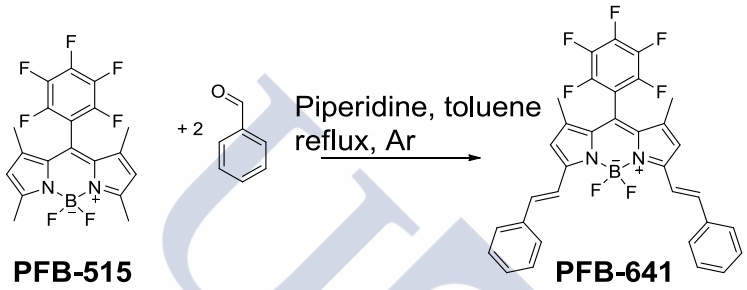
^{19}F NMR (300 MHz, $CDCl_3$, δ from $CFCl_3$): -140.33 (dd, 2F, ^3J = -21.5 Hz; ^4J = 7.1 Hz), -146.84 (q, 2F, $^1J_{F-B}^{(app.)}$ = 32.0 Hz), -151.56 (t, 1F, ^3J = -19.7 Hz), -160.58 (m, 2F).

MS (ESI+): m/z $[M+Na]^+$ calculated for $[C_{19}H_{14}BF_7N_2 + Na]^+$ 437.103, found 437.105.

UV-VIS: λ_{abs} = 515 nm (EtOH).

7.2. Synthesis of PFB-641

[(4,4-difluoro-1,7-dimethyl-3,7-distyril-8-pentafluorophenyl-4-bora-3a,4a-diaza-s-indacene).]



Scheme 64. Synthesis of PFB-641.

PFB-515 (51.81 mg, 0.13 mmol), benzaldehyde (0.040 mL, 0.36 mmol) and piperidine (0.025 mL, 0.26 mmol) were dissolved in anhydrous toluene (2 mL) under argon. The reaction mixture was refluxed for 24 h protected from light. The crude product was cooled to room temperature and the solvent was removed under vacuum. Purification was carried out by silica-gel column chromatography (hexane-dichloromethane with 1:0 to 2:1 *v/v* gradient). PFB-641 was obtained as a dark blue solid (6.81 mg, yield 13%).

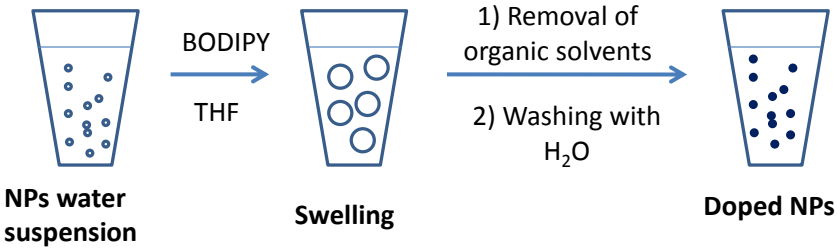
^{1}H-NMR (300 MHz, $CDCl_3$): δ (ppm): 7.63-7.81 (m, 6H, CH_{Ar} and CH=CH), 7.30-7.47 (m, 8H, CH_{Ar} and CH=CH), 6.74 (s, 2H) 1.57 (s, 6H, CH_3).

MS (MALDI-TOF/TOF): m/z [M] calculated for $C_{33}H_{22}BF_7N_2$ 590.18, found 589.99.

UV-VIS: λ_{abs} = 641 nm (EtOH).

8. Fluorescent doping of MNPs-COOH with BODIPY dyes

8.1. General protocol



Scheme 65. Swelling procedure for doping MNPs-COOH with BODIPY dyes.

The commercial aqueous suspension of Estapor® magnetic particles (100 μL, *c* = 100 mg solid/mL) was firstly diluted with water (900 μL) and then THF was added for swelling of the polystyrene NPs. Immediately after, a volume of the corresponding PFB dye solution in THF was incorporated. For the PFB-641 dye, 39, 78, 156, 195 or 234 μL of a 3.84×10^{-4} M stock solution (samples *a* to *e*), and 200 or 250 μL of a 6.00×10^{-4} M stock solution (samples *f* and *g*) were used (Table 23, left); in the case of the FMNP-515 *a* and *b* samples, 67 or 125 μL of a stock solution of PFB-515 in THF ($c_{Stock} = 3.85 \times 10^{-4}$ M) were added, respectively (Table 23, right). The corresponding mixture was stirred in a vortex for 1 h at 600 rpm, and finally, the particles were washed three times with H_2O with the aid of a neodymium magnet, and re-suspended in 1.7 mL of the same solvent. No fluorescence in the supernatant was detected after the third washing indicating the absence of dye leaching. The NP suspension was stored at 4 °C in the dark.

Table 23. Volumes of PFB stock solutions and of THF added for the preparation of FMNPs.

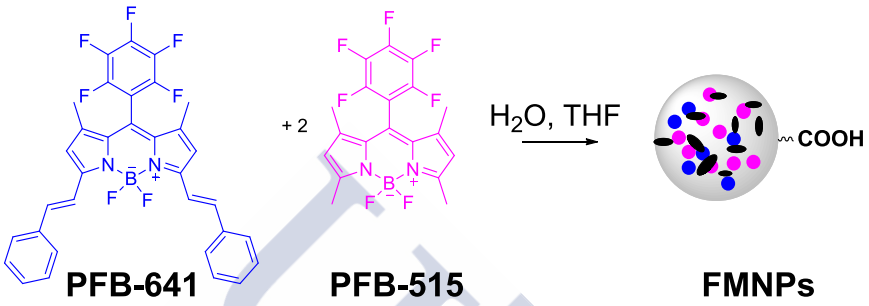
FMNP-641	V_{stock} [μL]	V_{THF} [μL]
a	39[a]	211
b	78[a]	172
c	156[a]	94
d	195[a]	55
e	234[a]	16
f	200[b]	50
g	250[b]	0

FMNP-515	V_{stock} [μL]	V_{THF} [μL]
a	125[c]	125
b	167[c]	83

Stock solution of PFB-641 dye in THF [a] 3.84×10^{-4} M, [b] 6.00×10^{-4} M; [c] Stock solution of PFB-515 dye in THF 3.85×10^{-4} M.

The amount of PFB dyes was varied in the different batches, but the total amount of THF was always kept at 250 μL mL^{-1} of H_2O in order to ensure a reproducible swelling of the polystyrene MNPs-COOH. The optimal dye concentration was determined for the PFB-641-doped FMNPs: *ca.* 5 nmol dye per mg of NPs provided the maximum fluorescence intensity (see part xcvb).

8.2. Preparation of FRET fluorescent magnetic nanoparticle (FMNPs-ET)



Scheme 66. Preparation of FRET MNPs.

The Estapor® magnetic beads were doped with *both* PFB-515 and PFB-641 dyes in a 1:1 or 2:1 (PFB-515/PFB-641) mole ratio. The optimal dye concentration was determined as described above for the PFB-641-doped FMNPs (*ca.* 5 nmol mg^{-1} of FMNPs provided the maximum emission intensity). Keeping constant the total amount of immobilized dye molecules at 9.6 nmol dye per mg of MNPs, the following protocol for the MNPs doping was employed: 1) 100 μL of the commercial MNP suspension (c_0 = 100 mg mL^{-1}) were diluted to 1 mL with water; 2) after adding THF, the suspension was vigorously shaken for a couple of seconds; 3) the corresponding volume of a stock solution containing already a mixture of the PFB dyes in THF was added (for the "FMNP-ETa" NPs, a 1:1 mixture containing 125 μL of PFB-515 dye + 125 μL of PFB-641 was added; for the "FMNP-ETb" NPs, a 2:1 mixture containing 167 μL of PFB-515 + 83 μL PFB-641 was used; in all cases, the c^{PFB}_{stock} was 3.85 x 10^{-4} M); the total volume of THF was always kept at 250 μL mL^{-1} H_2O; 4) the mixture was shaken in a vortex for 3 h at 800 rpm; 5) the FMNP-ET were whashed 3 x 1 mL water with the ai of a neodymium magnet and 6)the FMNPs-ET suspensions were stored at 4 °C in the dark.

9. Foster resonance energy transfer (FRET) assay

9.1. Coupling of the fluoromagnetic nanoparticles to capture antibodies

The selected magnetic FRET nanoparticles (FMNP-ETb those doped with a 2:1 PFB-515/PFB-641 mole ratio) were coupled to the different capture antibodies as follows: 50 μL of fluorescent nanoparticles suspension (containing approximately 0.2 mg of dry

nanoparticles) was washed three times with 500 µL portions of MES buffer (0.1 M MES, 0.15 M NaCl, 0.01% SDS, pH 5.7). The nanoparticles were then activated in 1 mL of MES buffer containing 102 mM EDC and 112 mM sulfo-NHS for 2 h at room temperature (r.t.) in the dark. After activation, the microspheres were washed three times with 500 µL portions of PBSSDS buffer. Then they were incubated in 300 µL of PBSSDS buffer containing 60 µg of capture antibody (either anti-mouse IgM or anti-mouse IgG as positive control) for 4 h at room temperature in the dark. After incubation, the microspheres were washed three times with 500 µL portions of TBSS buffer, and blocked in 1 mL of TBSS buffer for 1 h at room temperature in the dark. After washing three times with 500 µL portions of TBSS buffer, the microspheres were stored in 100 µL of TBSS buffer at 4 °C, protected from light. Additionally, another batch of magnetic nanoparticles were functionalized with neutravidin to be used as positive or negative control in the forthcoming experiments.

9.2. Functionalization of the microwell plates bottom with tacrolimus

The 96-well glass-bottom plates were previously cleaned with Alconox® (Sigma-Aldrich), thoroughly washed with Milli-Q water and rinsed with 96% ethanol. Then, 500 µL of a solution containing 2% APTES in ethanol-water (95:5, *v/v*) was added to each well and incubated for 1 h. The aminated slides were rinsed three times with clear ethanol and stored at 4 °C in the same solvent until use. In the case of poly-L-lysine coating, 500 µL of a solution containing poly-L-lysine 0.01% (w/v) in water was added to each well of the cleaned plates and incubated for 5 min. The coated slides were drained and dried at 60 °C overnight and stored at room temperature. FK506-COOH was immobilized onto the aminated surfaces by adding 200 µL of a 100 µg mL^{-1} FK506-COOH solution containing 100 mM EDC and 50 mM NHS in MES buffer (0.05 M, pH 6.0) into each well. After at least 4 h of incubation, the wells were dumped and washed (3 × 0.5 mL) with MES buffer. As a positive control, 60 µg mL^{-1} D-biotin was used instead of FK506-COOH; the same protocol but in the absence of FK506-CO_2H was employed as negative control. In all cases, the functionalized wells were blocked with PBSS buffer for 1 h, rinsed with deionized water, dried under argon, and either used immediately or stored at 4 °C.

9.3. Immunoassay protocol

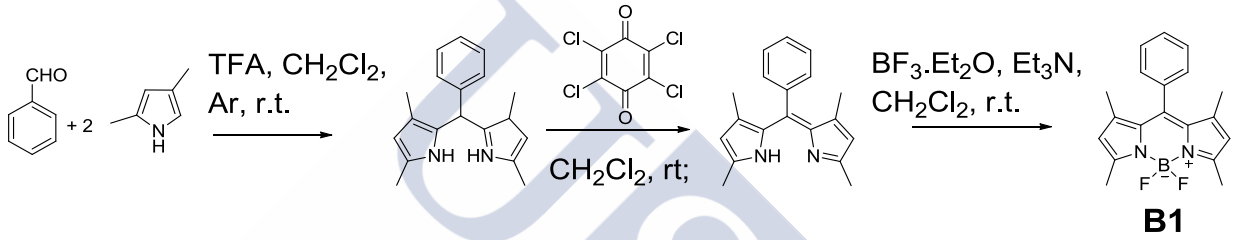
150 µL of FK506 standard solution (in PBS) was mixed with 50 µL of antibody solution (anti-FK506 or anti-biotin antibody, 10 µg mL^{-1} in PBS); then, the mixture was incubated in the FK506-coated well plates for 4 h. The wells were rinsed 3 times with 0.4 mL portions of PBSTM buffer, and 200 µL of a PBS solution containing 3 µg mL^{-1} of fluoromagnetic nanoparticles functionalized with the detection antibody (see below) was added to each well and incubated for 3 h to reveal the surface-bound antibodies. A neodymium magnet used during the incubation step drive them to the bottom of the

well, accelerating their binding to the IgM anti-tacrolimus antibodies attached therein during the assay. The unbound nanoparticles were removed by rinsing with PBSTM (3 × 0.4 mL) before the plate analysis.

10. Synthesis of BODIPY photosensitizing dyes for production of $^1O_2$

BODIPYs photosensitizers were prepared following synthetic protocols described in the literature.[258, 264, 265]

10.1. Synthesis of 5,5-difluoro-1,3,7,9-tetramethyl-10-phenyl-5H-dipyrrolo[1,2-c:2',1'-f][1,3,2]diazaborinin-4-ium-5-uide (B1)



Scheme 67. Synthesis of B1.

B1 was prepared in a three steps, one-pot classical approach. Its synthesis starts with the reaction between 2,4-dimethylpyrrole (1.082 mL, 9.42 mmol) and benzaldehyde (0.383 mL, 3.77 mmol) in CH_2Cl_2 (25 mL). A catalytic amount (*ca.* 0.1 mL) of trifluoroacetic acid was added dropwise to accelerate the reaction. The mixture was stirred overnight. The reaction progress was monitored by TLC until the complete consumption of the benzaldehyde. Then chloranil was added dropwise as oxidation agent and the mixture was stirred for 1 h. Finally boron trifluoride diethyletherate (6.025 mL, 60.3 mmol) and dry triethylamine (7.360 mL, 52.8 mmol) were added. The crude product was washed with saturated NaCl(aq). The organic extracts were dried over $MgSO_4$, filtered and evaporated under reduced pressure. The crude product was purified by silica gel column chromatography (hexane:ethyl acetate 10:2 *v/v*) to afford 1,3,5,7-tetramethyl-8-phenyl-4,4-difluoroboradiazaindacene as a red solid in 29% yield. The chemical structure of B1 was confirmed by mass spectrometry and ^{1}H-NMR.

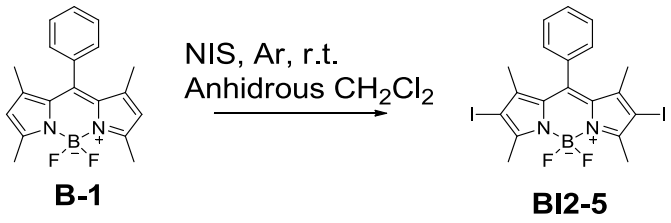
^{1}H-NMR (300 MHz, **$CDCl_3$, δ):** 7.41 (m, 3H, Ar). 7.21 (m, 2H, Ar), 5.91 (s, 2H, Ar), 2.49 (s, 6H, CH_3), 1.30 (s, 6H, CH_3).

MS (ESI+): m/z $[M]^+$ calculated for $C_{19}H_{20}BF_2N_2$: 325.2, found 325.1 and calculated for $[M + Na]^+$ $[C_{19}H_{19}BF_2N_2Na]^+$ 347.15, found 347.1.

[264] Y. Gabe, Y. Urano, K. Kikuchi, H. Kojima, T. Nagano, *J. Am. Chem. Soc.*, **2004**, *126*, 3357–3367.

[265] T. Yogo, Y. Urano, Y. Ishitsuka, F. Maniwa, T. Nagano, *J. Am. Chem. Soc.* **2005**, *127*, 12162–12163.

10.2. Synthesis of 5,5-difluoro-2,8-diiodo-1,3,7,9-tetramethyl-10-phenyl-5H-dipyrrolo[1,2-c:2',1'-f][1,3,2]diazaborinin-4-ium-5-uide (BI2-5)



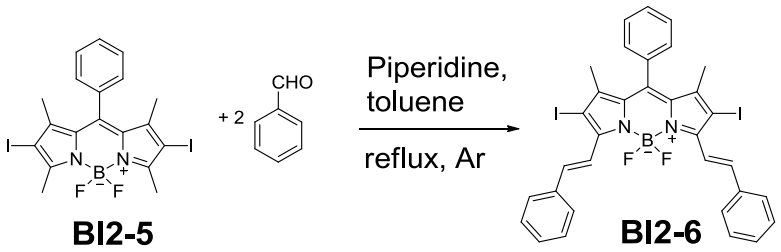
Scheme 68. Synthesis of BI2-5.

BI2-5 was synthesized from B1 (120 mg, 0.37 mmol) by electrophilic iodination with *N*-iodosuccinimide (NIS) (333 mg, 1.48 mmol) in anhydrous CH_2Cl_2 (10 mL) for 1 h. The reaction was protected from light and monitored by TLC while stirred at room temperature until complete consumption of the starting materials. The crude product was purified by silica gel chromatography (hexane–ethyl acetate 10:2 *v/v*). The pure product was obtained as a red solid in 78% yield. The chemical structure was confirmed by mass spectrometry and ^{1}H-NMR.

^{1}H-NMR (300 MHz, $CDCl_3$, δ): 7.44 (m, 3H, Ar), 7.17 (m, 2H, Ar), 2.57 (s, 6H, CH_3), 1.30 (s, 6H CH_3).

MS (ESI-): m/z $[M]^-$ calculated for $C_{19}H_{16}BF_2I_2N_2$ 574.9, found: 574.8.

10.3. Synthesis of 5,5-difluoro-2,8-diiodo-1,9-dimethyl-10-phenyl-3,7-di((E)-styryl)-5H-dipyrrolo[1,2-c:2',1'-f][1,3,2]diazaborinin-4-ium-5-uide (BI2-6)



Scheme 69. Synthesis of BI2-6.

BI2-6 was synthesized by a Knoevenagel condensation between BI2-5 (102.5 mg, 0.178 mmol) and benzaldehyde (0.054 mL, 0.534 mmol). The reaction was performed under

reflux in anhydrous toluene (15 mL). The reaction mixture was monitored by TLC and stirred until complete consumption of the starting materials. The crude product was purified by column chromatography (hexane-ethyl acetate 10:2 *v/v* gradient) to give a deep-purple solid in 20% yield. It was characterized by 1H-NMR and mass spectrometry.

^{1}H-NMR (300 MHz, $CDCl_3$) δ: 8.16 (d, 2H, Ar), 7.74 (s, 1H, Ar), 7.67 (m, 5H, Ar), 7.54 (m, 3H, Ar), 7.41 (m, 6H, Ar), 7.30 (m, 2H, Ar), 1.46 (s, 6H, CH_3).

MS (ESI-): m/z $[M-H]^-$ calculated for $C_{33}H_{24}BF_2I_2N_2$ 751.2, found 752.0.

11.Doping of NPs with the BODIPY photosensitizing dyes

BI2-6 (0.60 mg) was dissolved in 5 mL of THF to prepare a stock solution 0.159 mM. In a 5 mL eppendorf 1800 μL of H_2O, 200 μL of PSt-COOH NPs (Bangs®) or of MNPs-COOH (Estapor®) and 500 μL of BI2-6 stock solution were added and vigorously shaken in a vortex for a few seconds and then at 800 rpm during 3 h. Finally, the NPs were washed by centrifugation three times with water and finally suspended in 3 mL of H_2O. Two duplicates were prepared at the same time using an eppendorf adapter as vortex accessory: **92A** and **92B** with PSt-COOH NPs of 390 nm diameter and M**92C** and **M92D** with MNP-COOH of 300 nm diameter.

The final concentration of BI2-6 in the sample was calculated as follows: 0.0795 μmol (0.159 mM x 0.5 mL) are the moles of BI2-6 added to 2 mg NPs (200 μL NPs c = 10 mg/L) therefore the BI2-6 concentration in NPs is 40 nmol/mg NPs.

12.Doping of polystyrene NPs with ruthenium photosensitizing dyes

To dope Bangs® polystyrene NPs with ruthenium complexit was necessary to optimize the solvents mixture needed for NPs swelling and loading of the RD3 dye. For optimizing doping conditions 390 nm PSt-COOH NPs were used.

12.1. Nanoparticles swelling with different solvent (390 nm PSt-COOH NPs)

Different solvents were tested: acetonitrile (ACN), 1,4-dioxane, tetrahydrofuran (THF) MeOH mixture, N,N-dimethylformamide, dimethyl sulfoxide (DMSO). A stock solution 1.86 x 10^{-4} M of RD3 in each of these solvents was prepared. The swelling process was performed for each solvent as follows: 1) in a 2 mL eppendorf with 900 μL of H_2O, 100 μL of the PSt-COOH NPs and 500 μL of the RD3 stock solution were added. The mixture was kept in a vortex at 800 rpm during 3 h; 2) the PSt-COOH NPs of 390 nm were washed 3 x 1 mL H_2O by centrifugation, suspended in 1 mL of H_2O and stored at 4°C in the dark.

12.2. Swelling with different MeOH-THF proportion (390 nm PSt-COOH NPs)

The composition of the solvent mixture for swelling the PSt-COOH NPs was optimized varying percentages of THF, MeOH and H_2O, but keeping the RD3 moles constant. Stock solutions in methanol at different concentrations were prepared as describe in the **Table 24**.

Table 24. Different stock solutions of the photosensitizer RD3 in methanol used for doping the PSt-COOH NPs.

RD3	[mg]	[nmol]	[mL]	[mM]
SS1	1.61	1.38	3	0.46
SS2	0.8	0.68	3	0.23
SS3	0.52	0.45	3	0.15
SS4	3.14	2.69	3	0.90
SS5	0.54	0.46	0.5	0.92
SS6	0.46	0.39	0.5	0.79
SS7	1.05	0.90	0.5	1.80

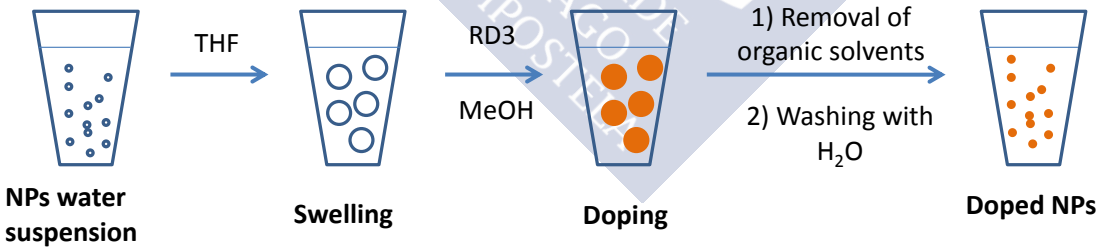
The PSt-COOH NPs were doped as follow: 1) 1 h before starting the doping procedure, 5 mL eppendorf tubes were blocked with casein buffer in order to avoid sticking of the NPs onto the wall tube; 2) after washing the 5 mL eppendorf tubes, 1900 μL of H_2O and 100 μL PSt-COOH NPs were included and shaken in a vortex for few seconds; 3) the corresponding amount of THF (Table 25) was added and the PSt-COOH NPs were kept shaken during 30 minutes; 4) RD3 stock solution in methanol was mixed in the suspension in the proportions that are described in Table 25, the samples were shaken vigorously for few seconds and then at 800 rpm during 3 h; 5) the PSt-COOH NPs were washed by centrifugation with 3 x 1 mL H_2O and finaly suspended in 2 mL of H_2O; 6) the PSt-COOH NPs were stored at 4°C and protected from light.

Table 25. Mol of RD3 and volumes of MeOH and THF used to prepare the PSt-COOH NPs the swelling optimization.

PSt-COOH NPs Batch	*RD3 SS in MeOH* [mM]	*MeOH* [μL]	*RD3* [nmol]	*THF* [μL]	*Mixture (by volume) H_2O/THF/MeOH*
3-1	0.90	50	44.76	200	1/0.1/0.025
3-2	0.46	100	45.90	150	1/0.075/0.05
3-3	0.23	200	45.62	50	1/0.025/0.1
3-4	0.15	300	44.48	100	1/0.05/0.15
4-1	0.46	100	45.90	400	1/0.2/0.05
4-2	**0.23**	**200**	**45.62**	**300**	**1/0.15/0.1**
4-3	0.15	300	44.48	200	1/0.1/0.15
4-4	0.90	50	44.76	450	1/0.225/0.025

The highest degree of doping was achieved using the proportion of THF 150 μL mL^{-1} of H_2O and MeOH 100 μL mL^{-1} of H_2O (sample 4.2 of Table 25).

12.3. Study of RD3 dye loading (390 nm PSt-COOH NPs)



Scheme 70. Procedure for doping the PSt-COOH NPs with RD3.

Once the volume of methanol and THF employed for the swelling has been optimized (the optimum MeOH/THF/H_2O mixture chosen was that providing the most strongly luminescent RD3 doped NPs, sample 4.2 of Table 25), the loading of the RD3 mol was also tune up (

Table 26). Each batch of PSt-COOH NPs prepared here, has an increased amount of moles of ruthenium complex compared to the previous batch. The stokes solutions of RD3 in methanol used were those of Table 24.

The PSt-COOH NPs were doped as follow: 1) 5 mL eppendorf tubes were blocked with casein buffer in order to avoid the staking of the NPs onto the tube wall, one hour before starting the doping procedure; 2) after washing with water the 5 mL eppendorf tubes, 3800 μL of H_2O, 200 μL PSt-COOH NPs and 600 μL of THF were added and the samples kept shakenin a vortex at 800 rpm for 30 minutes; 3) 400 μL of the corresponding RD3 stock solution in methanol was added into the suspension, the eppendorf tubes were shaken vigorously for a few seconds and finally at 800 rpm during 2 hours and 30 minutes in a vortex; 4) the doped PSt-COOH NPs were washed by centrifugation with 3 x 1 mL of water, re-suspended in 5 mL of water, stored at 4°C protected from light.

Table 26 illustrated the concentration of each sample prepared.

Table 26. Concentration of the RD3 stock solution in MeOH and moles of RD3 used for preparing 2 mg of PSt-COOH NPs of 390 nm with photosensitizer loading optimization.

PSt-COOH NPs Batch	*SS* [mM]	*RD3* [nmol][a]
17a	0.23	4.6
17b	0.46	9.2
17c	0.90	17.9
21a	1.0	20.8
21b	1.30	26.0
21c	1.80	35.9

[a] Mol of dye per mg of PSt-COOH NPs (dry weight).

12.4. Preparation of PSt-COOH NPs of 200 nm

Two batches of PSt-COOH NPs of 200 nm each one with different photosensitizer concentrations were prepared. 200 μL of PSt-COOH NPs (c = 10 mg/mL see part 0) of 200 nm and 600 μL of THF were added in 5 mL eppendorf containing 3800 μL of H_2O. The tube was vigorously shaken for a couple of seconds and then for 15 minutes in the vortex at 800 rpm. After this 400 μL of the corresponding stock solution in methanol was added and kept in the vortex for additionally 2 hours and 45 minutes. Then the doped PSt-COOH NPs of 200 nm were washed by centrifugation (3 x 1 mL H_2O) for 20 minutes at 1200 rpm. Finally the samples were suspended in 5 mL of H_2O and stored at 4 °C.

Table 27. Concentration of the RD3 stock solution in MeOH and moles of RD3 used for preparing PSt-COOH NPs of 200 nm with photosensitizer loading optimization.

PSt-COOH NPs Batch	*SS in MeOH* [mM]	*RD3* [nmol][a]
146A	1.26	50.4
146B	0.90	35.8

[a] Moles of dye per mg of PSt-COOH NPs (dry weight).

12.5. Preparation of PSt-COOH NPs of 26 nm

Each sample prepared was doped in a dialysis membrane of ca. 8 cm of length with the following characteristics: Spectra/Por® 7 dialysis membrane, pretreated-rc tubing; MWCO: 15 Kd; Normal flat width: 32 mm; diameter 20.4 mm; Vol length 3.3 mL; total length 5m. Inside the membrane, previously closed in one site with fishing line, the following additions were made: 3800 μL of H_2O, 200 μL of PSt-COOH NPs of 26 nm (c = 9.97 mg/mL see part 0) NPs (suspended in water), 600 μL of THF, 400 μL of RD3 stock solution in methanol, see Table 28 for the concentration of stock solutions.

Table 28. Concentration of the RD3 stock solutions in MeOH and moles of RD3 used for preparing 2 mg of PSt-COOH NPs of 26 nm.

PSt-COOH NPs Batch	*SS in MeOH* [mM]	*RD3* [nmol][a]
14-1	0.22	4.48
14-2	0.44	8.94
14.3	0.67	13.42
14.4	0.90	17.9
14-5	1.11	22.38

[a] Mol of dye per mg of PSt-COOH NPs (dry weight).

Each dialysis membrane containing the PSt-COOH NPs of 26 nm suspension was immersed in a 250 mL beaker full of water. The water was changed four times: after 2, 18, 21 and 25 h. Finally, the PSt-COOH NPs of 26 nm suspension was transferred to a glass vial and the final volume extracted was measured.

12.6. Magnetic nanoparticles doped with RD3

A 0.94 mM stock solution in MeOH of RD3 was prepared dissolving 1.65 mg in 1.5 mL of MeOH. Then 200 μL of MNPs-COOH (Estapor®), 550 μL of THF were added in a 5 mL eppendorf containing 3800 μL of H_2O. The sample was vigorously shaken a few seconds and then at 800 rpm during 20 min in a vortex. After this time 450 μL of the RD3 stock solution in MeOH were added. The MNPs-COOH were shaken in a vortex for additionally 2 h and 45 minutes. Finally the NPs were washed three times with water(3 x 1 mL) with the aid of a neodymium magnet.

13.Determination of the final concentration of PSt-COOH NPs aq. suspensions

To measure the exact concentration of NPs suspension in mg/mL calibration curves were determined for 390 nm and 200 nm PSt-COOH NPs. Three different suspensions of 1 mg/mL of NPs were prepared by diluting 100 μL of commercial NPs in 900 μL of H_2O. The absorption at 600 nm for each of the three NPs suspension 1 mg/mL was measured in triplicate for at least 6 different dilutions (Table 29, Table 30, Table 31). A plastic (PMMA) cuvette of 10 mm x 10 mm with H_2O was used.

Table 29. Concentration in mg/mL in the cuvette and volumes of NPs of 390 nm (1 mg/mL) added in 3 mL of H_2O.

Total volume of 1 mg/mL added [μL]	*Cuvette concentration* [mg/mL]
15	0.0050
30	0.0099
120	0.0385
240	0.0741
480	0.1379
960	0.2424

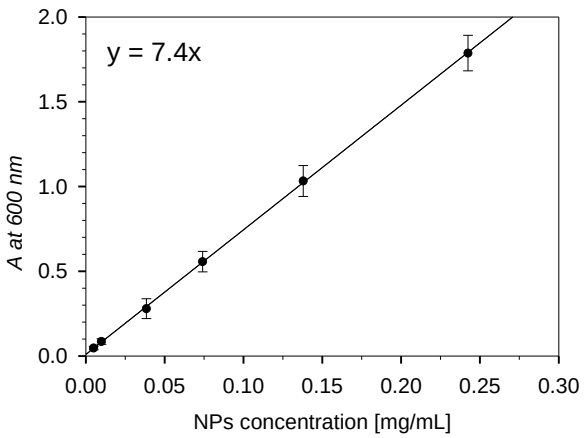


Figure 110. Calibration curve of 390 nm polystyrene NPs (Bangs Laboratories®).

Table 30. Concentration in mg/mL in the cuvette and the volumes of NPs of 200 nm (1 mg/mL) added in 2.5 mL of H_2O.

Total volume of 1 mg/mL added [μL]	*Cuvette concentration* [mg/mL]
10	0.0040
20	0.0080
30	0.0120
40	0.0160
50	0.0200
60	0.0240
70	0.0280
80	0.0320

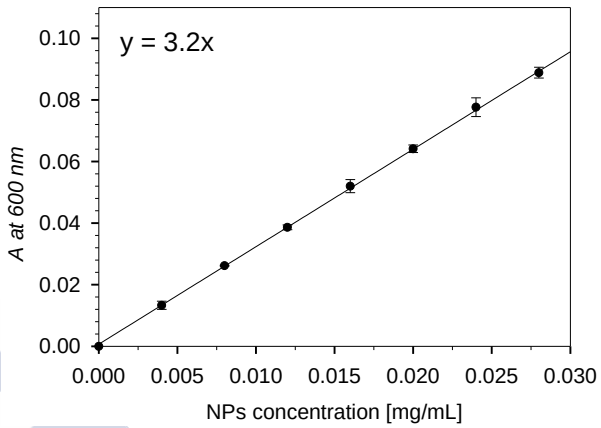


Figure 111. Calibration curve of 200 nm polystyrene NPs (Bangs Laboratories®).

Table 31. Concentration mg/mL in the cuvette and the volumes of MNPs of nm (1 mg/mL) added in 3 mL H_2O.

Total volume of 1 mg/mL added [μL]	*Cuvette concentration* [mg/mL]
10	0.0033
20	0.0067
30	0.0100
40	0.0133
50	0.0167
60	0.0200
70	0.0233

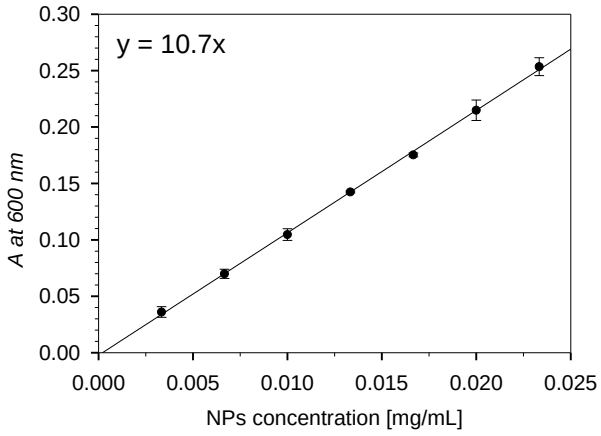


Figure 112. Calibration curve of Estapor® magnetic nanoparticle of 300 nm.

14.Singlet oxygen production quantum yield

For the time-resolved detection at 1270 nm of the $^1O_2$ luminescence the decays were measured with a single photon counting (SPC) laser kinetic spectrometer system from Edinburgh Instruments (UK) LP-900 equipped with a Hamamatsu H10330-45 NIR PMT detector, upon excitation at 532 nm with a Nd:YAG laser head (Minilite II, Continuum, CA).

Each decay was collected with a different energy of the laser pulse, which is measured with a specific energy detector directly plugged into a PC. It can be controlled easily with the integrated software. The decay traces obtained were deconvoluted for the instrumental response and fitted to a double exponential function using the nonlinear Marquardt algorithm included in the Edinburgh Analytical Instruments original software package. It is possible to extract many information from the fitting as (i) the emission lifetimes of the ^{3}MLCT Ru complex τ_{Ru}, (ii) the emission lifetime of $^1O_2$ (τ_Δ), (iii) their contribution in the total lifetime (B in mV). The reduced χ^2 weighed residuals and autocorrelation function were employed to estimate the quality of the fits.

The quantum yield was measured in deuterated water. For this reason the RD3 doped NPs of 20 nm (14-3) hold to be previously dialyzed with D_2O. The membrane used is the same employed in section 12.5 of this chapter. A suspension of 26 nm PSt-COOH NPs (batch 14-3) in 1 mL of H_2O was dialyzed versus 100 mL of D_2O. 3 additional changes of 50 mL of D_2O after 2, 18 and 21 h were made. Then at 25 h from the beginning, the dialysis was finished. 800 μL of NPs suspension in D_2O were obtained after the dialysis.

200 μL of PSt-COOH NPs of 26 nm in D_2O were directly added in a quartz cuvette. The cuvette employed has the chamber wide of 10 mm and it is equipped with a septum needed for the oxygen purge. The large path is used for the excitation of the laser and the short path for the emission of the singlet oxygen phosphorescence. The sample of the cuvette, was purged with oxygen during 30 minutes. The standard used for the measurement of singlet oxygen production quantum yield is the $[Ru(dpds)_3]^{4-}$ dye, it was dissolved in of D_2O, then the solution was passed to a cuvette and purged with oxygen for 30 minutes. Absorption of the sample and of the standard was measured before and after the measurements of singlet oxygen decays. It was necessary to add 100 μL of H_2O in the pure D_2O standard for matching of the singlet oxygen lifetime of 42.03 μs, as observed for the PSt-COOH NPs of 26 nm sample.

The standard and the sample have to be measured in exactly in the same conditions, which are: atmospheric pressure 944 mmHg, temperature inside the holder of the cuvette/laser 27 °C, PMT 10 kΩ, band pass filter of 610 nm and notch filter at 532 nm, slits 2.81 and 2.69 mm corresponding to 1.92 nm and 2.00 nm.

It was observed that the trend in the intensity of the decay changes proportionally with the laser energy. After all this precaution it was possible to proceed to the

measurements for the calculation of singlet oxygen quantum yield. A quintuplet of singlet oxygen measurement for the sample and a triplicate for the reference were done.

Conclusions

Conclusions

The main innovative aspect of this Thesis work has been providing tools for developing novel fluorescence based immunoassays (FIAs) for the detection of three different types of immunossuppresant drugs: tacrolimus (FK506) cyclosporine A (CyA) and mycophenolic acid (MPA): these novel, improved FIAs should facilitate the therapeutic drug monitoring (TDM) of the drugs in transplanted patients. The main contributions of the work have been:

1) ***Chemical derivatization of the immunosuppressants FK506 and CyA with –COOH groups*** for enabling their covalent attachment to surfaces, proteins or fluorophores (derivatization of MPA was not necessary due to the presence of a –COOH group in the original molecule). The most challenging part was the chemical modification of these two molecules due to several reasons: their large molecular size complicates the analytical characterization of the synthetized derivatives; the chemical modification should preserve the binding domains to be recognized by the corresponding antibody in the FIA; the literature describing synthetic protocols for FK506 or CyA derivatization was scarce. Despite all these difficulties three new and stable carboxy-derivatives of CyA were successfully synthesized following straightforward protocols with high reaction yields. The pure –COOH products could be isolated by liquid-liquid extraction without need of further chromatographic purification. A carboxy derivative of tacrolimus was also synthesized with good yield by following a previously described protocol.[266] The fact of having a platform with the carboxylic acid derivatives of the three ISs (FK506-COOH, CyA-COOH and MPA) allows the use of the same chemistry for subsequent chemical transformations and their applicability in multianalyte immunoassays. Additionally, and as far as we know, this work has described for the first time the ***fluorescent labelling of MPA, CyA and FK506*** with a very photostable, strongly emissive NIR probe (λ_{em} > 650 nm), an analogue of the Nile Blue fluorophore, named here ANB.

The usefulness and applicability of these derivatives in different FIA formats for ISs detection, has been demonstrated in the context of the FP7 European Project NANODEM (*NANOphotonic DEvice for Multiple therapeutic drug monitoring*).[267] Additionally: i) as a part of a work of another Doctoral Thesis of the research group, a FPIA assay has been successfully developed for the determination of MPA in the plasma of transplanted patients using the synthetised MPA-ANB probe.[268] This FIA reached a LOD of 0.8 ng mL^{-1} and a dynamic range of 1.7–39 ng mL^{-1} in phosphate buffer; and, ii) it has been

[266] O. Cañadas, Al. Sáenz, G. Orellana, C. Casals, *Anal. Biochem*., **2005**, *340*, 57–65.

[267] EU-FP7 Project NANOphotonic DEvice for Multiple therapeutic drug monitoring (NANODEM), http://nanodem.ifac.cnr.it/

[268] B. Glahn-Martínez, E. Benito-Peña, F. Salis, A B. Descalzo, G. Orellana, María C. Moreno-Bondi, *Anal. Chem.*, **2018**, *90*, 5459–5465.

demonstrated that the ISs labeled with the ANB fluorophore can be used to estimate the free fraction (not linked to plasma proteins) of the three ISs.

2) ***Doping of carboxylated nanoparticles of different chemical composition*** (neat polystyrene, polystyrene with ferrite, or a magnetic cobalt nucleous with a graphene and a silica layer) ***with fluorophores or with photosensitizers*** for singlet oxygen production, depending on the final application. It is expected that the encapsulation of many fluorophores or photosensitizers in a single bead will enhance the signal output (fluorescence or chemiluminescence, depending on the assay format), and therefore, the sensitivity of the bioassays.

1. Derivatization of immunosuppressive drugs for fluorescent labeling and covalent immobilization onto surfaces.

Three different carboxy-CyA derivatives were synthesized with new optimized methods. One of the routes implies the direct modification of the secondary hydroxy group of CyA by a nucleophilic addition to a carbonyl of a diglycolic anhydride. To the best of our knowledge this is the first time that a carboxy-CyA derivative –named CyA-O-COOH– was synthetized in one step and with a very good yield (>80%). The use of a microwaves reactor was critical to the achievement of the sought compound. The formed ester is stable and its hydrolysis was not observed when a fluorescent derivative of CyA-O-COOH, was purified by extraction in slightly acidic conditions. The other two CyA derivatives were synthesized through four steps. The protection (acylation) of the CyA hydroxyl group was necessary to avoid the formation of a deleterious intramolecular cyclic sub-product in both cases. In one of these synthetic routes, a reactive halogen intermediate of CyA was reacted with methyl 3-mercaptopropanoate to yield the named CyA-S-COOH. In the second case, an epoxide of CyA was opened by an ω-aminoester obtaining the called CyA-N-COOH. Both, CyA-S-COOH and CyA-N-COOH, were obtained with high reaction yields.

The corresponding carboxy derivative of tacrolimus FK506-COOH, was obtained with high yield by using carboxymethoxylamine.[1] In Chapter 1, it is shown how FK506-COOH could be successfully immobilized onto an aminated surface.

The obtained carboxylic derivatives of tacrolimus and cyclosporine A are stable and it was demonstrated that such chemical modifications do not interfere in the chemical activity of the drugs, since the immunosuppressive derivatives could be recognized by the corresponding antibodies for their use in immunoassays.

CyA-S-COOH, CyA-O-COOH, FK506-COOH and MPA have been successfully labelled with near infrared fluorescent tags. One of the labels employed was the commercially available Dy636-NH_2 from Dyomics, functionalized with –NH_2 groups and compatibile with the well-established red laser excitation (λ_{abs} = 636 nm and λ_{em} = 667 nm for Dy636-NH_2 in phosphate buffer, pH 7.4). This label was however discarded due to its

very high price, and mainly, because it showed a poor fluorescence in aqueous media. Instead, an analogue of the popular Nile Blue fluorophore was selected. The amino derivative of this dye, ANB, was synthetized in the laboratory. ANB showed similar spectral band position to Dy636-NH_2 (λ_{abs} / λ_{em}= 624 / 677 nm in phosphate buffer, pH 7.4).[269] but it displays almost a five fold more intense fluorescence than Dy636-NH_2 in PBS at pH 7.4 (physiological pH). Moreover ANB is photostable and it is cheaper than Dy636-NH_2 since it can be synthesized in considerably large amounts following a straightforward procedure. The last, allowed adding the dye in a molar excess when reacting with the IS-COOH derivatives for improving reaction yields, something unaffordable with the costly Dy636-NH_2 dye (>80% reaction yield for obtaining FK506-ANB and MPA-ANB and >55% for CyA-ANB).

Fluorescent immunoassays performed by several partners of the EU Project NANODEM put forward the suitability of the IS-COOH derivatives for their use in FIAs. Table 1 shows the LODs achieved for the different ISs within the NANODEM framework, by performing FIAs in different formats. The very demanding limits of detection (LODs) for ISs monitoring in plasma could be achieved for cyclosporine A and mycophenolic acid. In the case of FK506, also the achieved LOD was very close to that required for clinical analysis (targeted LOD = 0.038 ng/mL *vs.* achieved LOD: 0.05 ng/mL).

Table 32. Comparison between the targeted limits of detection (LODs) for levels of ISs in blood patients, with the LODs achieved using the carboxylated or fluorescently doped ISs described in this Thesis work.

Immunosuppressive drug	*Targeted limits of detection (LODs)*	*Achieved LODs in the NANODEM project*
Cyclosporine A[a]	0.250 ng/mL	0.22 ng/mL
Tacrolimus[b]	0.038 ng/mL	0.05 ng/mL
Mycophenolic Acid[c]	5.000 ng/mL	0.19 ng/mL

The IS-COOH derivatives were immobilized over an aminated surface. [a]CyA-N-COOH was incubated with anti-CyA antibody (mouse monoclonal IgG) and labeled (Alexa fluor 647) anti-mouse IgG. [b]FK506-COOH was incubated with FRET NPs functionalized with anti-FK506 IgM antibody. [c]MPA was incubated with FRET NPs functionalized with anti-MPA IgG antibody.

Alternatively, it has been shown that the labeled IS-ANBs can be employed in fluorescence polarization immunoassays. A FPIA was performed with the MPA-ANB

[269] V. H. J. Frade, M. Sameiro T. Gonçalves, J.C.V.P. Moura. *Tetrahedron Lett.*, **2006**, *47*, 8567–8570.

conjugate obtaining excellent results.[268] IS-ANBs were also tested in fluorescent polarization binding assays for the determination of the free IS fraction in the presence of the human serum albumin macromolecule. It was found that for (labeled) cyclosporine A, mycophenolic acid and tacrolimus the free (non-protein bound) fraction (α) are respectively 6%, 3% and 34%. Consequently if properly validated, fluorescence polarization binding assay might be a fast, simple and reproducible method to determine the drug free fraction, a relevant parameter of interest in therapeutic drug monitoring.

2. Fluorescent nanoparticles as markers for sensitive immunoassays

Carboxylated polystyrene nanoparticles decorated with magnetic ferrite nanograins were successfully doped with strongly fluorescent BODIPY dyes using a straightforward protocol by swelling the NPs in a THF:H_2O 0.25/1 *v/v* mixture.[270] The particles were produced with a single BODIPY dye, PFB-515 (λ_{abs}= 515 nm, λ_{em} = 525 nm in EtOH) suitable for excitation with a 532 nm green laser diode, or a new BODIPY dye, PFB-641 (λ_{abs} = 641 nm, λ_{em} = 657 nm in EtOH) suitable for excitation in the red, with emission at λ > 650 nm.[271] The loading of dye in the nanoparticles was optimized to *ca.* 5 nmol per mg of NPs which is the amount providing the maximum emission intensity. It was demonstrated by steady-state (red shift of the emission maximum) and time-resolved measurements (decrease of the fluorescence lifetime) that if the dye loading was higher, inner filter and excited state self-quenching processes can occur. The resulting doped fluoromagnetic nanoparticles are stable in water and dye does not leak from the polystyrene matrix in aqueous buffered solution. The doped magnetic NPs have a relative monodisperse spherical shape (ca. 300 nm diameter), and are quite brilliant, a remarkable feature taking into account the brown colored ferrite layer that covers the polystyrene core. Moreover it was demonstrated that their magnetic properties do not change after the doping procedure. The presence of the –COOH groups on the surface is important for further (bio)conjugation.

The carboxylated polystyrene nanoparticles could also be doped with a combination of both BODIPYs for obtaining an intra-particle FRET system, with a *virtual* Stokes shift of > 150 nm. These FRET NPs have been successfully conjugated to IgG anti-IgM antibodies and are useful as detection probes for immunoassay development. The assay performance improves when exciting the FRET NPs at the FRET donor maximum absorption, at 500 nm and detecting the fluorescence at the acceptor emission at 680 nm (LOD: 1.8 ng/mL), compared to the same nanoparticle-based immunoassay run by directly exciting the PFB-641 FRET acceptor dye at 638 nm (LOD: 2.3 ng/mL). Additionally, the fluorescent FRET nanobeads should also be suitable for detecting

[270] A. B. Descalzo, H.-J. Xu, Z.-L Xue, K. Hoffmann, Z. Shen, M.G. Weller, X.-Z. You, K. Rurack, *Org. Lett.* **2008**, *10*, 1581–1584.

[271] F. Salis, A. B. Descalzo, E. Benito-Peña, M. C. Moreno-Bondi, G. Orellana, *Small,* **2018***, 14,* 1703810.

simultaneously two different immunossuppressants (multianalyte immunoassay) using one single excitation wavelength (excitation of the FRET donor dye and observation either at the donor emission at ca. 550 nm or at the FRET acceptor emission at 650-700 nm).

3. Photosensitizing nanoparticles for singlet oxygen production

A method to successfully dope carboxy-polystyrene beads of 390 nm with a Ru complex (RD3) by swelling in an organic solvent was optimized. The highest degree of doping was achieved using a mixture of H_2O/THF/MeOH 1/0.15/0.1 *v/v/v* as solvent. The optimum loading of the RD3 photosensitizer (that yielding the most emissive particles) was 20.8 nmol per mg of NPs. The characteristic emission of the ^{3}MLCT excited state of the RD3 complex at ca. 640 nm was observed for aqueous suspensions of the doped NPs. The lifetimes of NPs doped with RD3 were measured at three different concentrations of oxygen (0%, 21% and 100%). No significant difference in the lifetime values was observed at 21% and 100% oxygen concentration showing that the polystyrene matrix prevents quenching of the ruthenium ^{3}MLCT excited state by oxygen. In addition, the observed bi-exponential emission decay varies as the loading of the photosensitizer increases, giving information about the NPs site in which the singlet oxygen is produced. The samples that display the shortest lifetime have the RD3 dye located closer to the water, interacting probably by coulombic attraction with the surface carboxylic groups of the nanoparticles. If the concentration of RD3 is increased, the emission lifetime rises again probably because the photosensitizer is now forced to go deeper into the NPs. Unfortunately it was not possible to measure the singlet oxygen production quantum yield for these NPs due to a strong scattering of the light caused by the NPs. In order to minimize scattering, NPs of 26 nm were used instead for quantifying the singlet oxygen production. The optimum loading of RD3 (highest emission intensity per mg of NPs) in this case was 13.4 nmol. The results demonstrated that polystyrene NPs doped with RD3 are suitable to be used as efficient photosensitizers: a larger amount of singlet oxygen is produced when the RD3 dye is encapsulated in NPs than when it is free in solution (Φ_{NPs} (0.50) > Φ_{RD3} (0.42)[272]).

Photosensitizers based on iodinated BODIPY structures (BI2-5, with λ_{abs} / λ_{em} = 532 / 548 nm and BI2-6, with λ_{abs} / λ_{em} = 634 / 650 nm in EtOH) were also prepared as alternative to Ru(II) photosensitizers absorbing at longer wavelengths. The BODIPY dyes avoid the unwanted emission at 1270 nm observed in the case of Ru ^{3}MLCT complexes, which interferes with the $^1O_2$ emission. The NIR emitting BI2-6 dye was used for doping of polystyrene NPs.

The comprehensive study with the polystyrene NPs doped with RD3 paves the way for the development and optimization of a new kind of *donor beads*, alternative to those

[272] G. Orellana, A.M. Braun, *Helv. Chim. Acta* **1996**, 79, 1222–1238.

marketed by PerkinElmer for the *AlphaScreen™ proximity immunoassay*: an assay based on the emission of chemiluminescence that is activated in a set of *acceptor beads* after binding nanoparticles doped with photosensitizers able of photogenerating singlet oxygen (*donor beads*).

USC UNIVERSIDADE DE SANTIAGO DE COMPOSTELA

Annex

Annex

1. NMR and mass spectra of the synthetized compounds

1.1. Cyclosporine A acetate (CyA-Ac)

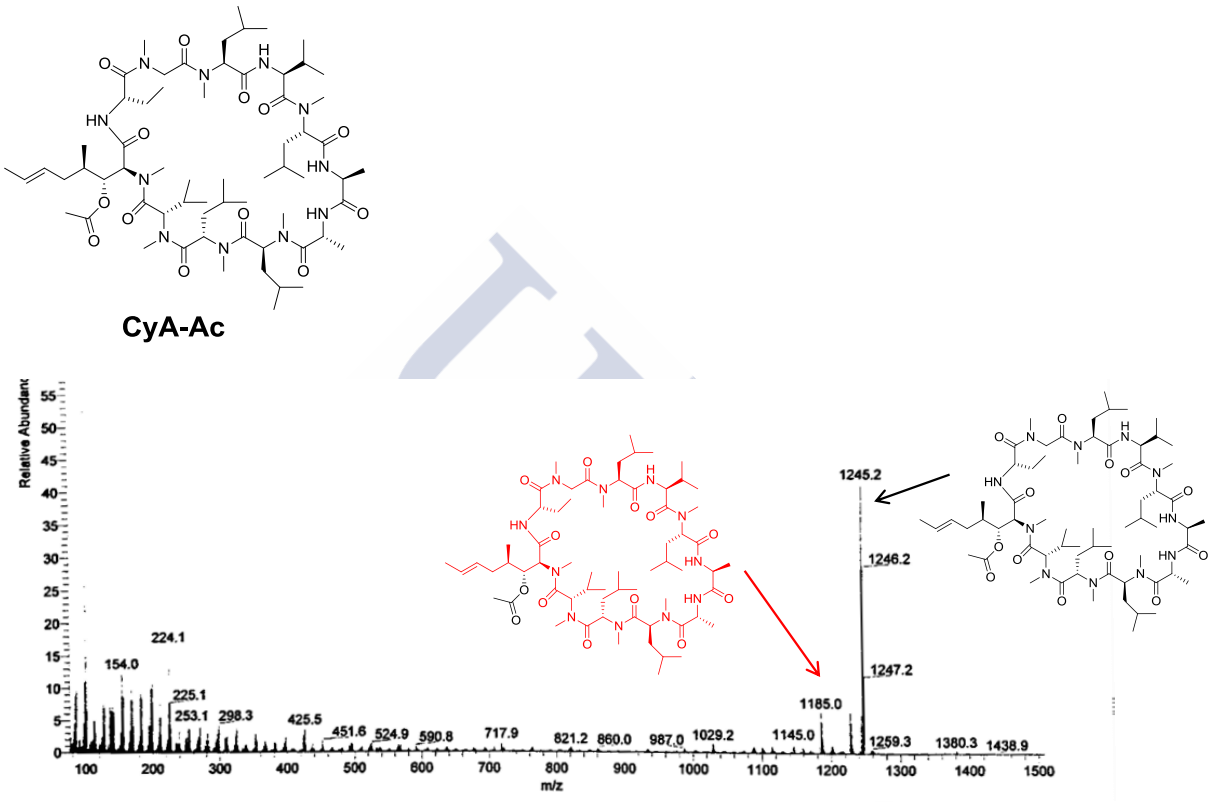


Figure 113. Mass spectrum of CyA-Ac recorded by fast atom bombardment in positive detection mode; m/z $[M+H]^+$ calculated for $C_{64}H_{114}N_{11}O_{13}^+$ 1244.8; found 1245.2.

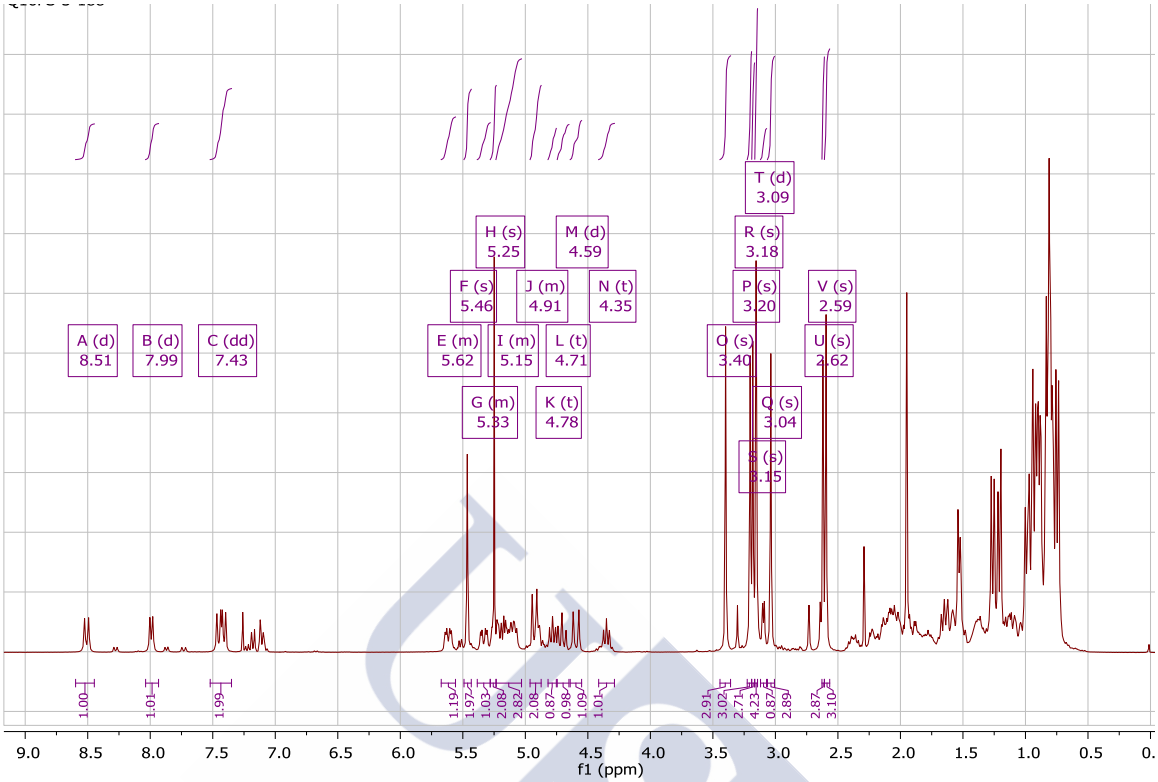


Figure 114. ^{1}H-NMR (300 MHz,$CDCl_3$) of Cyclosporine A acetate (CyA-Ac). Preparation procedure described in the Experimental Part, section 2.1 pag 171.

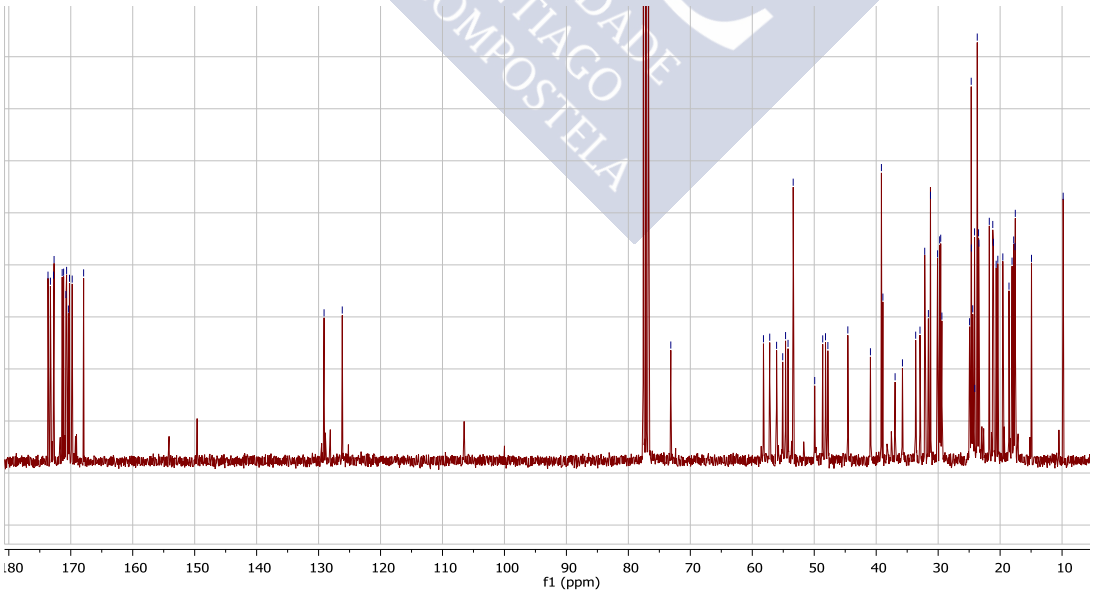
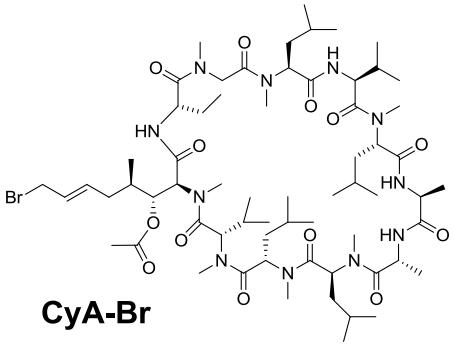


Figure 115. ^{13}C-NMR (75 MHz, $CDCl_3$) of Cyclosporine A acetate (CyA-Ac). Preparation procedure described Experimental Part, section2.1.

1.2. CyA-Br



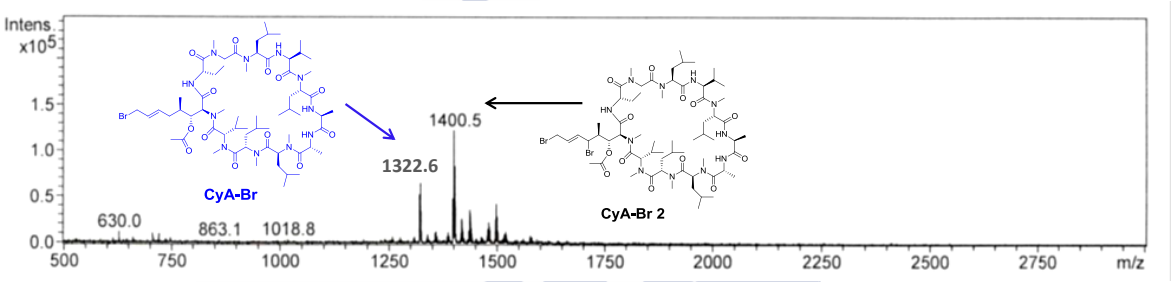


Figure 116. Mass spectrum of CyA-Br by electrospray ionization in negative detection mode **:** m/z $[M–H]^-$ calculated for $C_{64}H_{111}BrN_{11}O_{13}^-$ 1322.8 found 1322.6, (the di-bromine compound was also found at 1400.5 m/z).

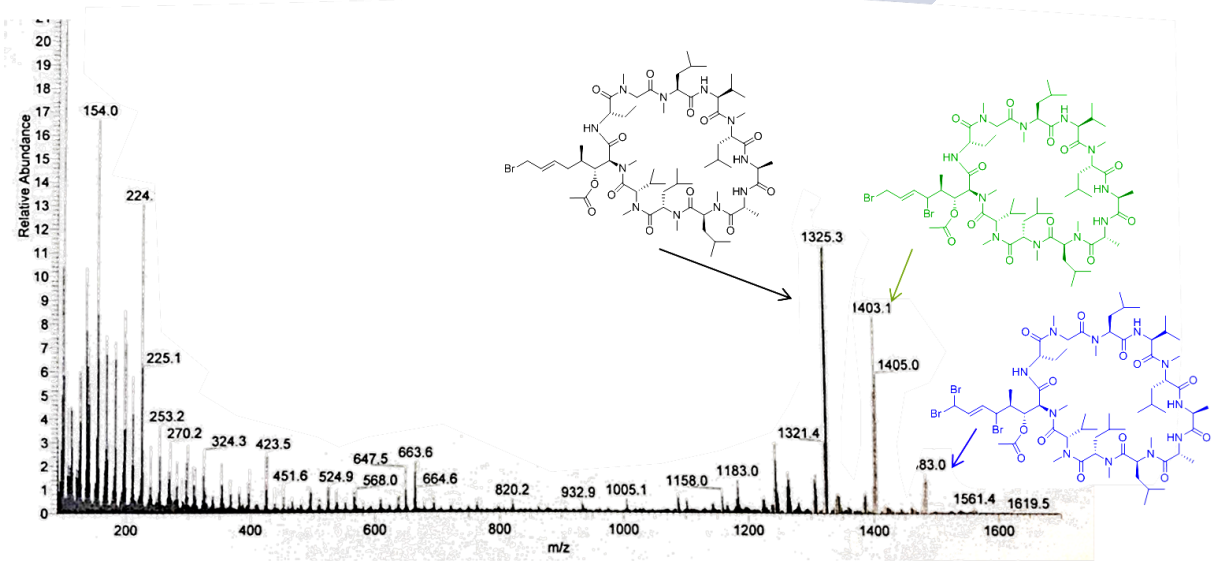


Figure 117. Mass spectrum of CyA-Br recorded by fast atom bombardment in positive detection mode; m/z $[M+H]^+$ calculated for $C_{64}H_{113}BrN_{11}O_{13}^+$ 1324.8 found 1325.3, (the di- and tri- bromine compound were also found at 1403.1 m/z for $C_{64}H_{113}Br_2N_{11}O_{13}^+$, 1483.0 for $C_{64}H_{113}Br_3N_{11}O_{13}^+$m/z).

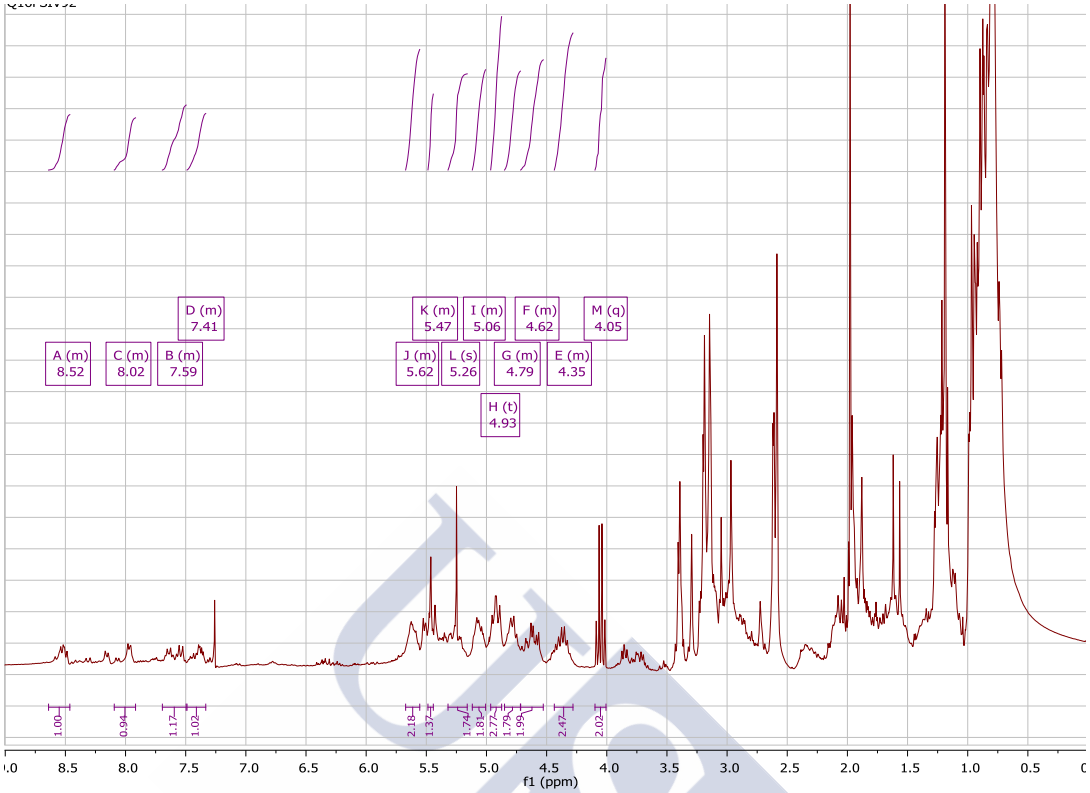


Figure 118. ^{1}H-NMR (300 MHz, $CDCl_3$) of CyA-Br. Preparation procedure described Experimental Part, section2.2.1.

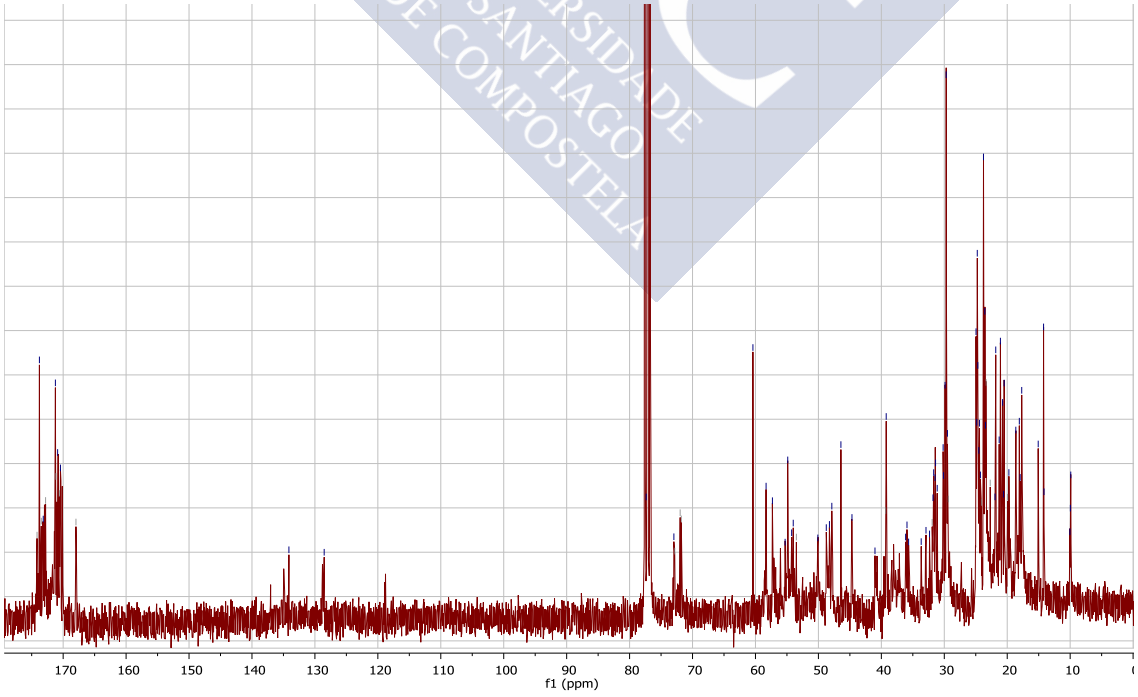
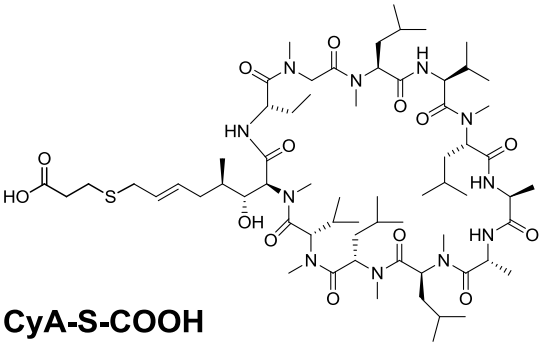


Figure 119. ^{13}C-NMR (75 MHz, $CDCl_3$) of CyA-Br. Preparation procedure described Experimental Part, section 2.2.1.

1.3. CyA-S-COOH



CyA-S-COOH

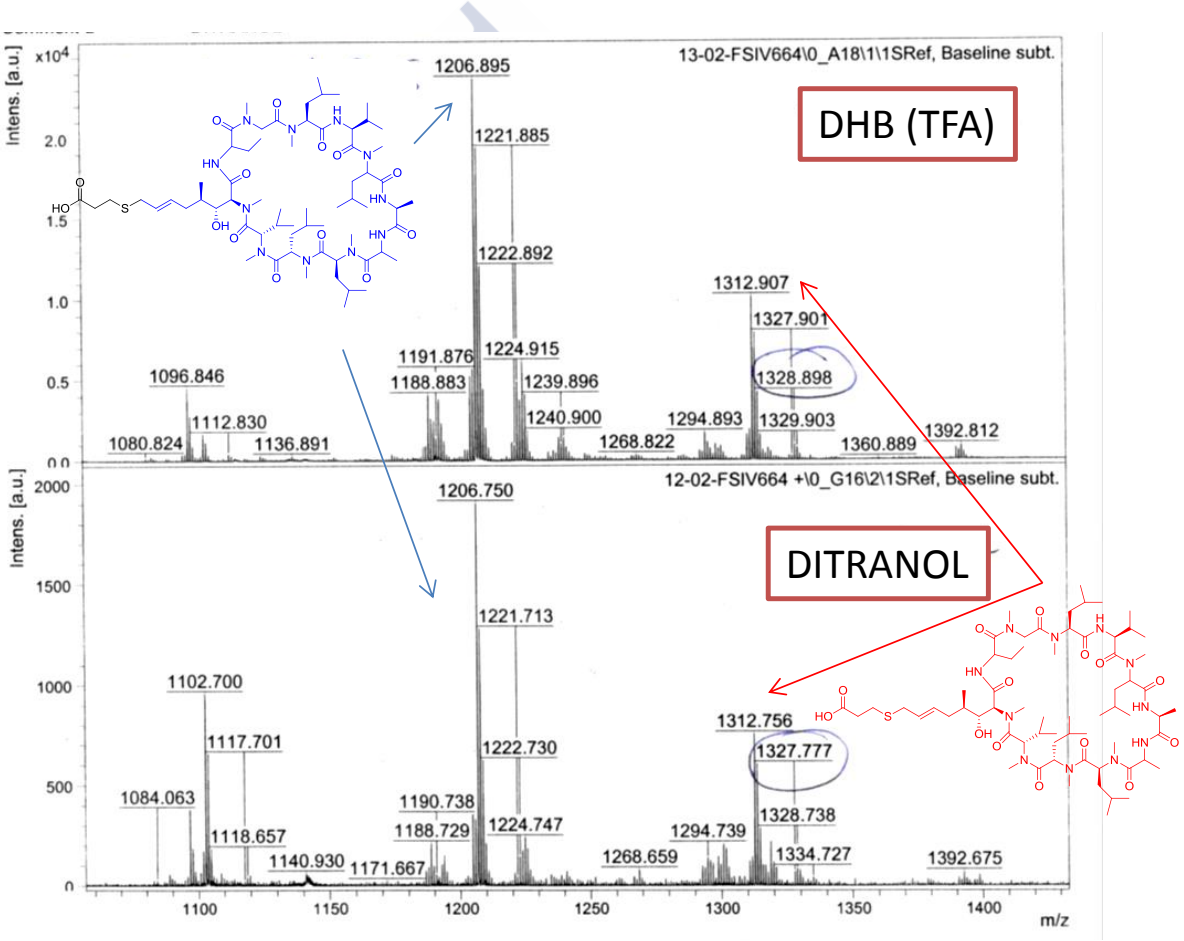


Figure 1. Mass spectra of CyA-S-COOH recorded with two different matrix (DBH 2,5-dihydroxy benzoic acid with TFA up and ditranol down) in MeOH by MALDI TOF/TOF; m/z $[M+Li]^+$ calculated for $[C_{65}H_{115}LiN_{11}O_{14}S]^+$ 1312.9, found 1312.9 and m/z $[M+Na]^+$ calculated for $[C_{65}H_{115}N_{11}NaO_{14}S]^+$ 1328.8, found 1328.9.

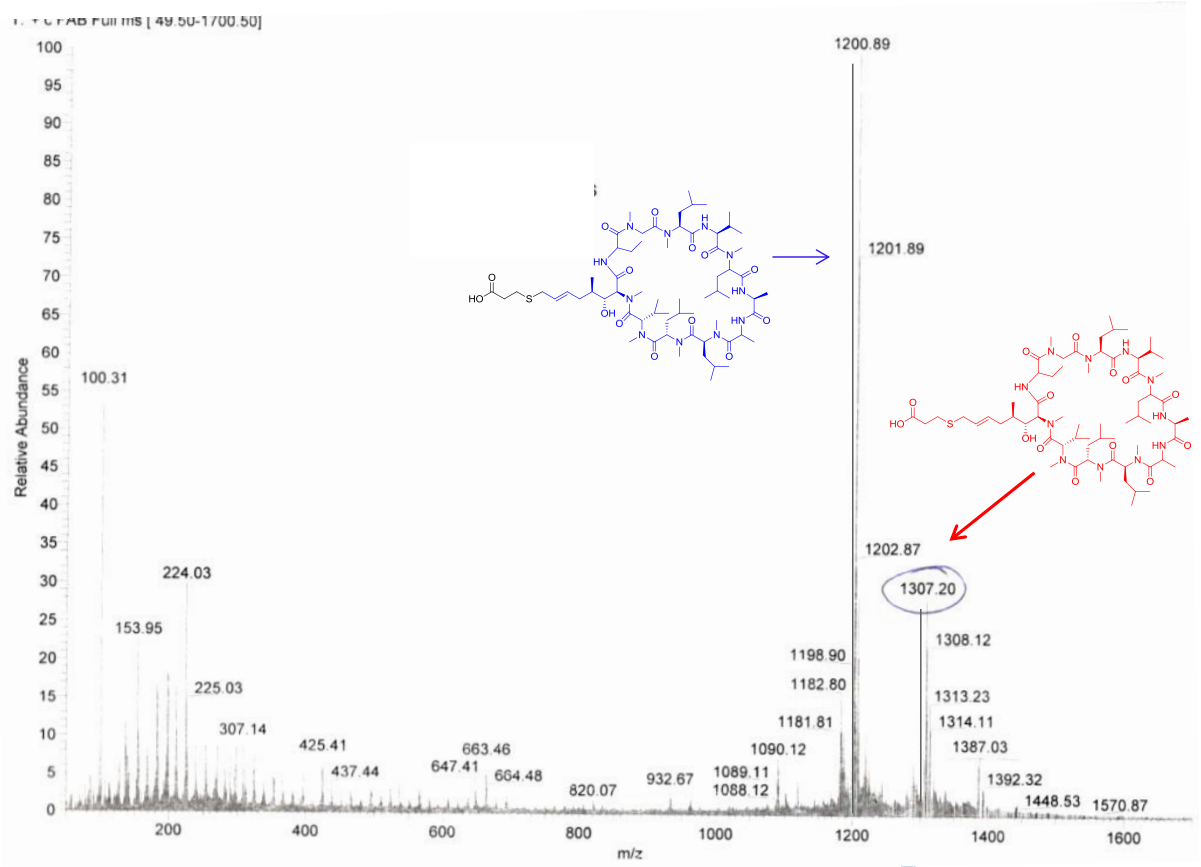


Figure 120. Mass spectrum of CyA-S-COOH recorded by fast atom bombardment in positive detection mode. m/z $[M+H]^+$ calculated for $[C_{65}H_{116}N_{11}O_{14}S]^+$ 1306.8, found 1307.2.

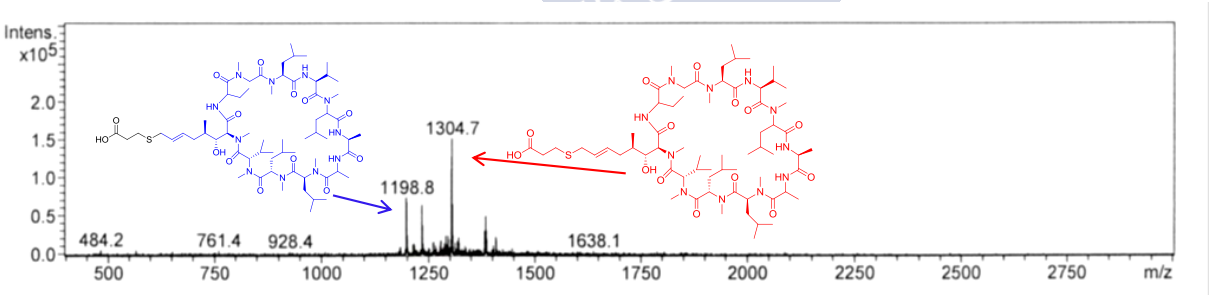


Figure 121. Mass spectrum of CyA-S-COOH by electrospray ionization in negative detection mode : m/z $[M–H]^-$ calculated for $C_{65}H_{114}N_{11}O_{14}S^-$1304.8, found 1304.7.

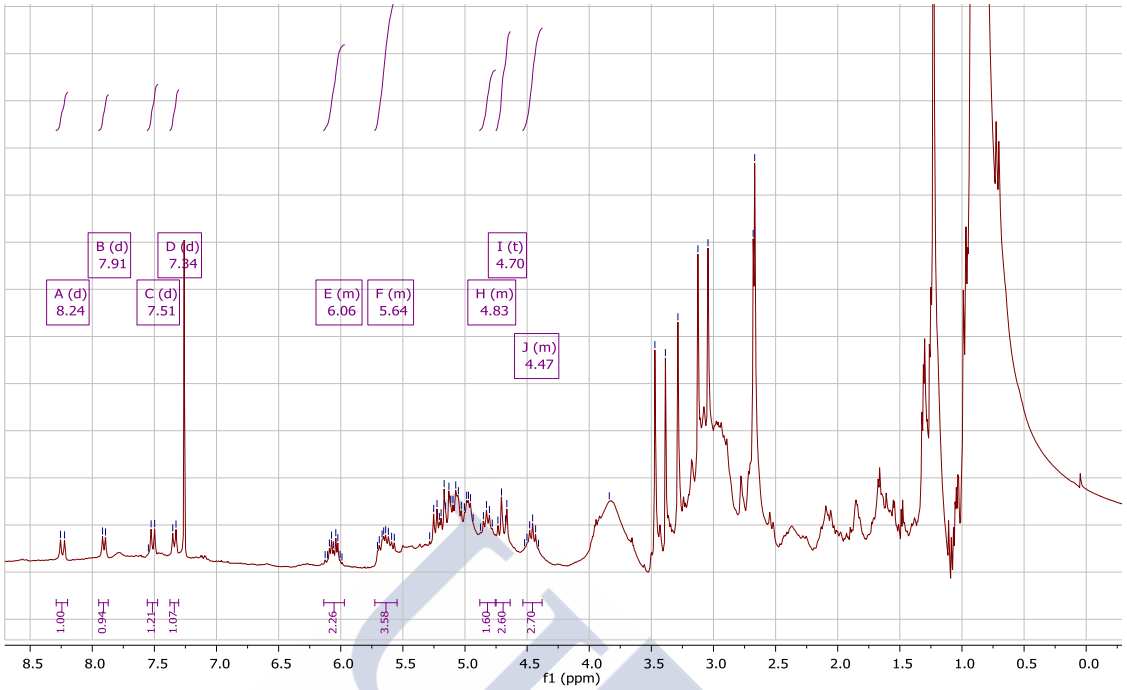


Figure 122. ^{1}H-NMR (300 MHz, $CDCl_3$) of CyA-S-COOH. Preparation procedure described Experimental Part, section 2.2.3.

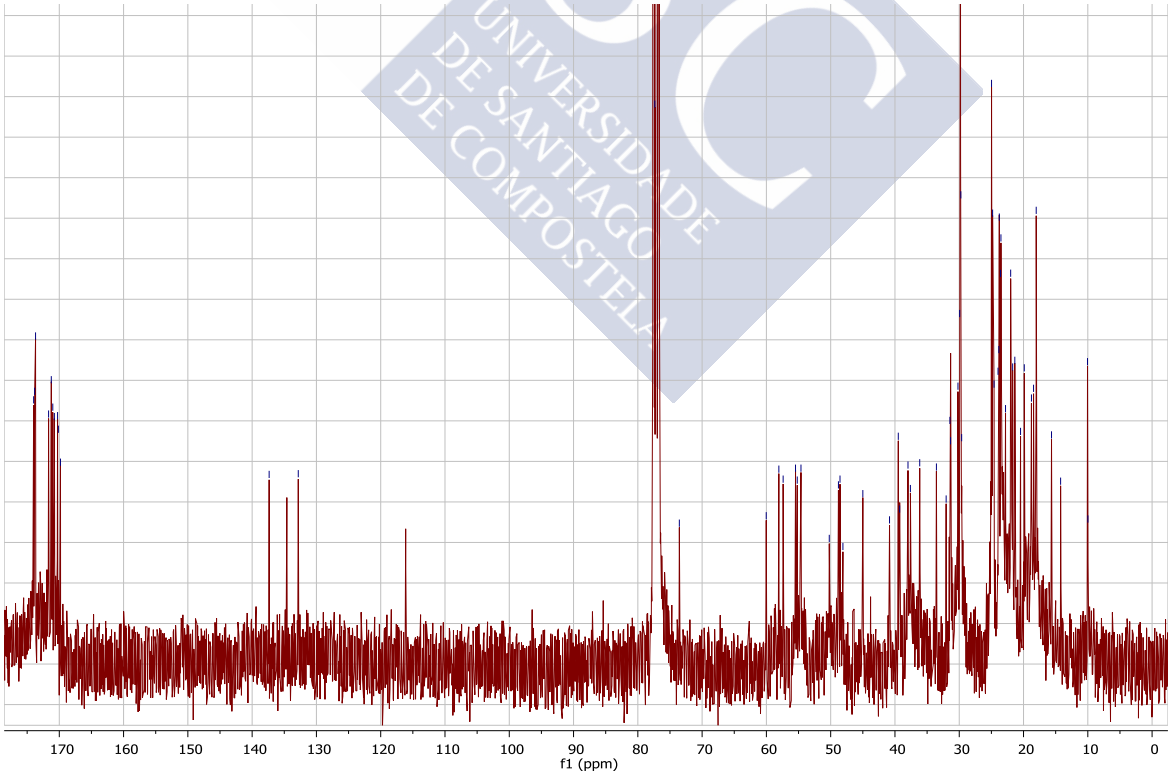
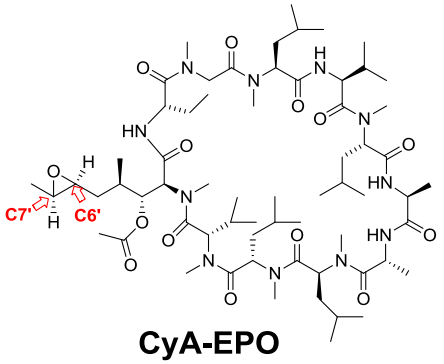


Figure 123. ^{13}C-NMR (75 MHz, $CDCl_3$) of CyA-S-COOH. Preparation procedure described Experimental Part, section 2.2.3.

1.4. CyA-EPO



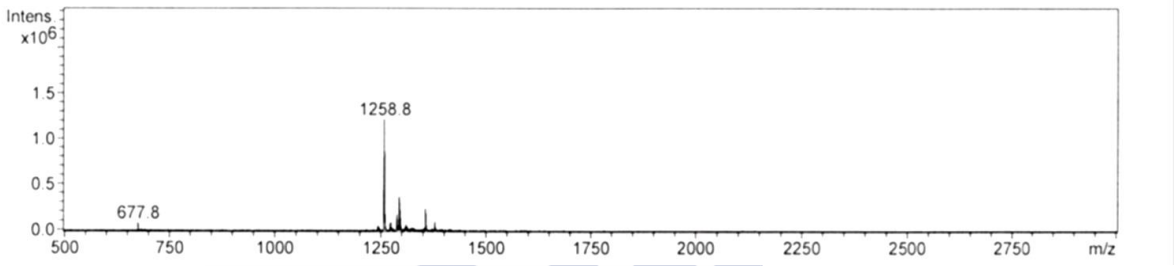


Figure 124. Mass spectrum of CyA-EPO by electrospray ionization in negative detection mode; m/z $[M–H]^-$ calculated for $C_{64}H_{112}N_{11}O_{14}^-$ 1258.9; found 1258.8.



Figure 125. ^{1}H-NMR (300 MHz, $CDCl_3$) of CyA-EPO. Preparation procedure described in Experimental Part, section 2.3.1.

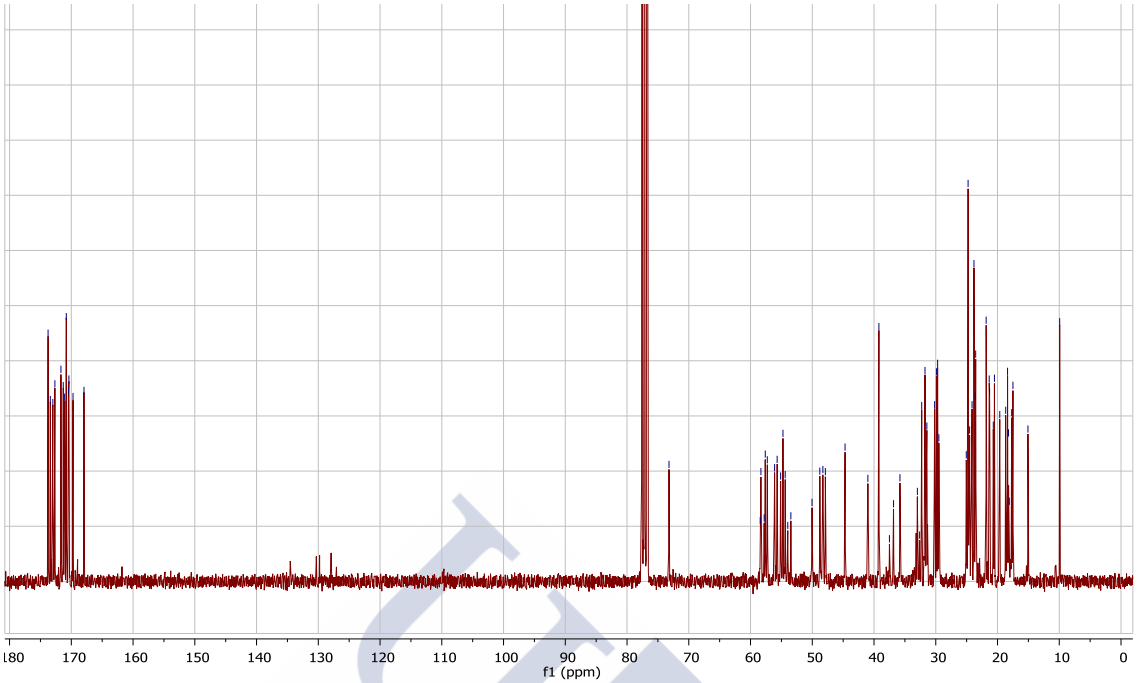


Figure 126. ^{13}C-NMR (75 MHz, $CDCl_3$) of CyA-EPO. Preparation procedure described Experimental Part, section 2.3.1.

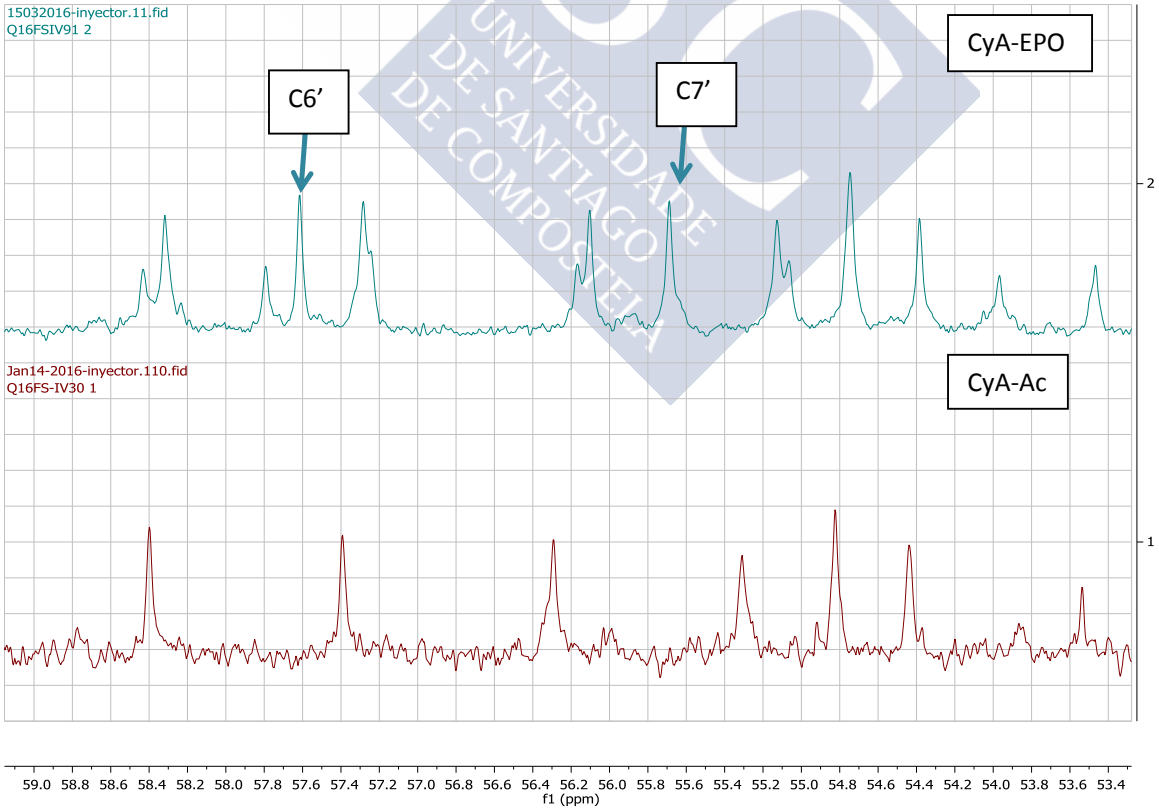
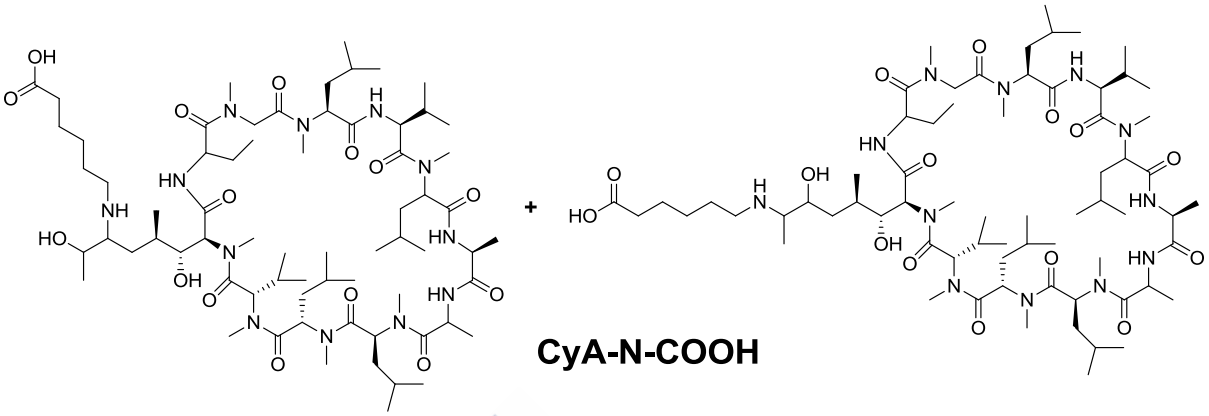


Figure 127. Comparison of the ^{13}C-NMR spectra in $CDCl_3$ of CyA-Ac (brown) and CyA-EPO (green) between 53 and 60 ppm.

1.5. CyA-N-COOH



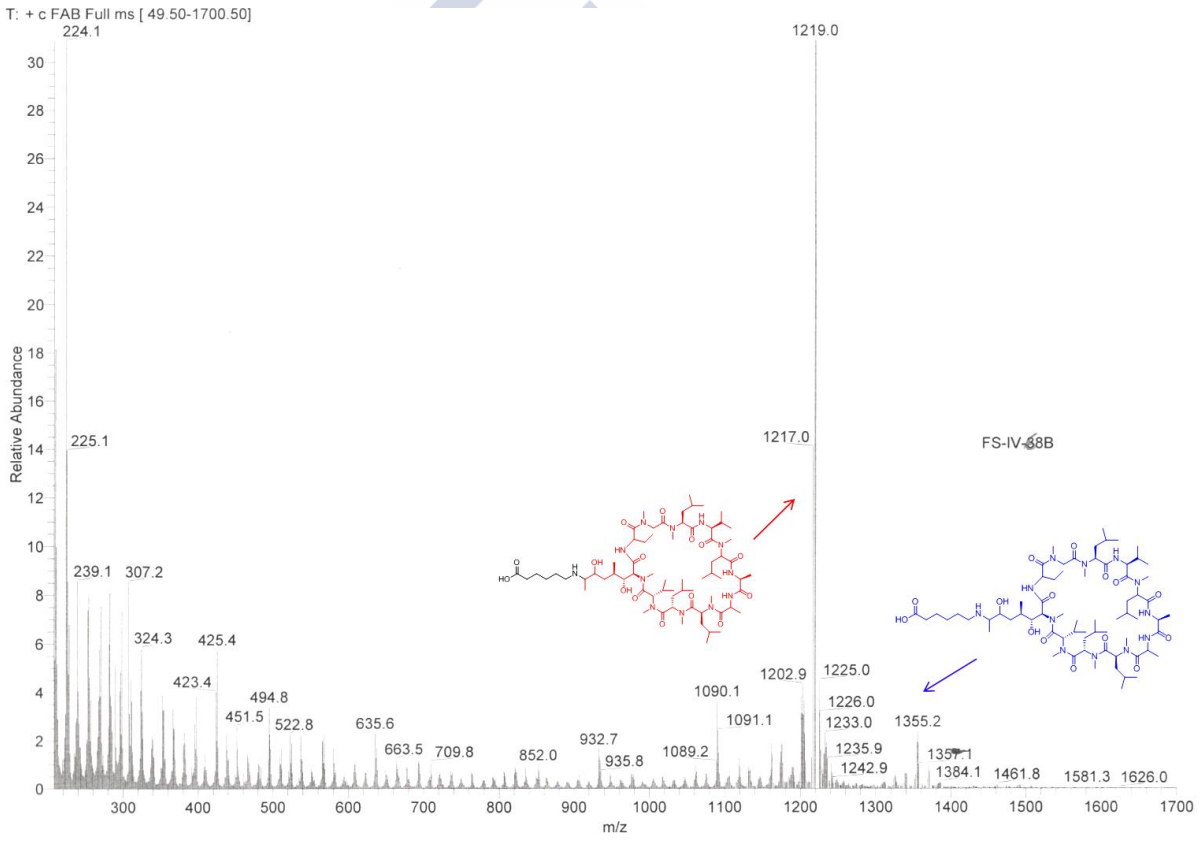


Figure 128. Mass spectrum of CyA-N-COOH recorded by fast atom bombardment in positive detection mode; m/z $[M + Li]^+$ calculated for $[C_{68}H_{124}LiN_{12}O_{15}]^+$ 1355.95; found 1354.43.

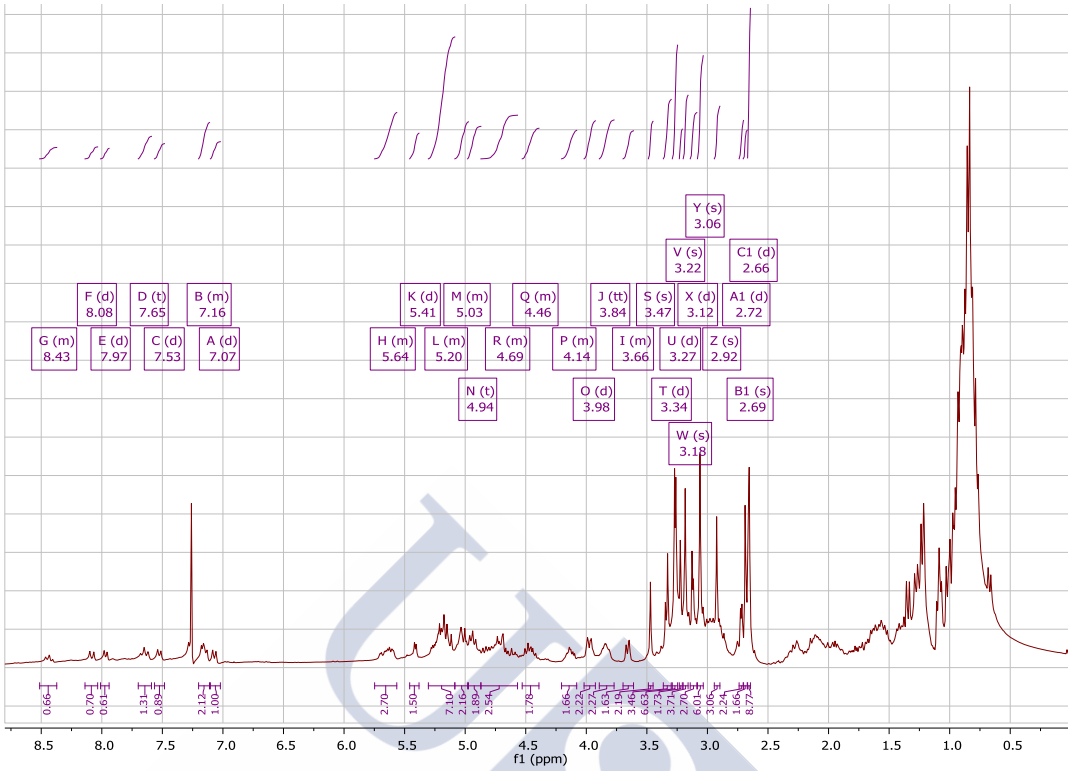


Figure 129. ^{1}H-NMR (300 MHz, $CDCl_3$) of CyA-N-COOH. Preparation procedure described in Experimental Part, section 2.3.2.

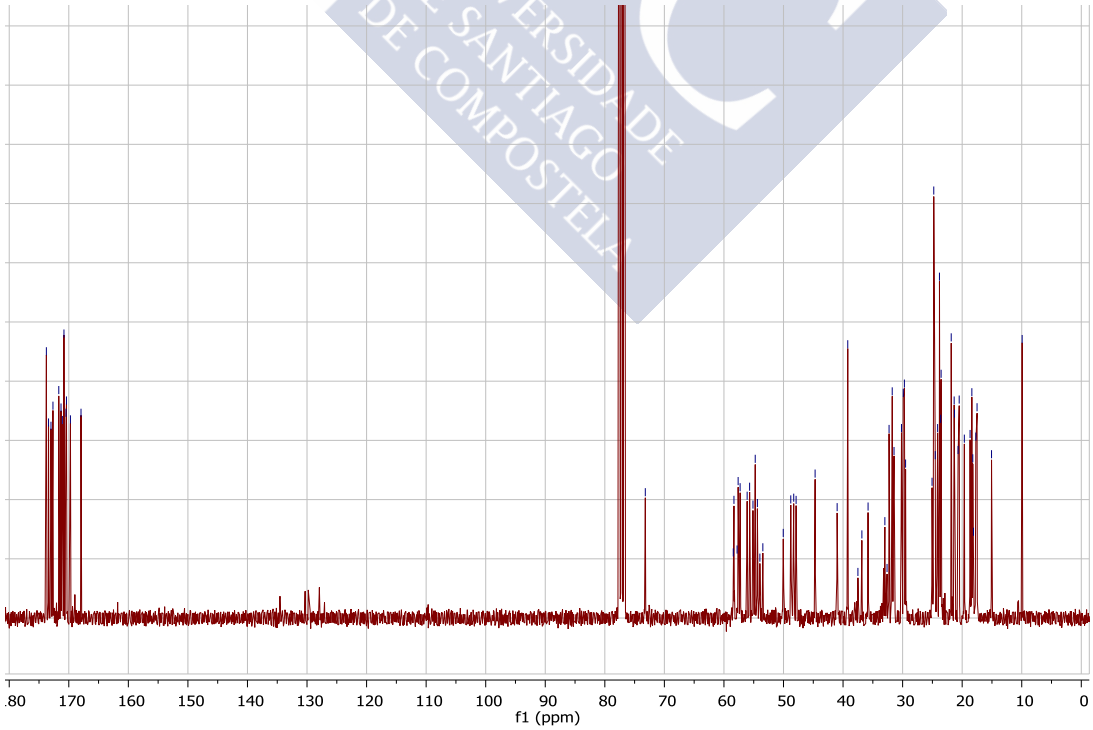
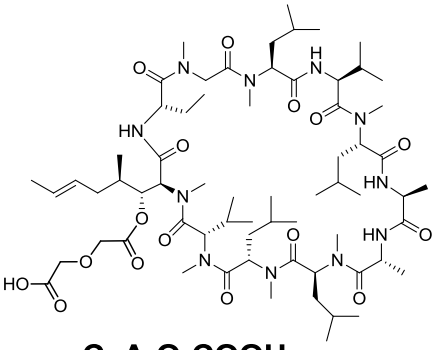


Figure 130. ^{13}C-NMR (75 MHz, $CDCl_3$) of CyA-N-COOH. Preparation procedure described Experimental Part, section 2.3.2.

1.6. CyA-O-COOH



CyA-O-COOH

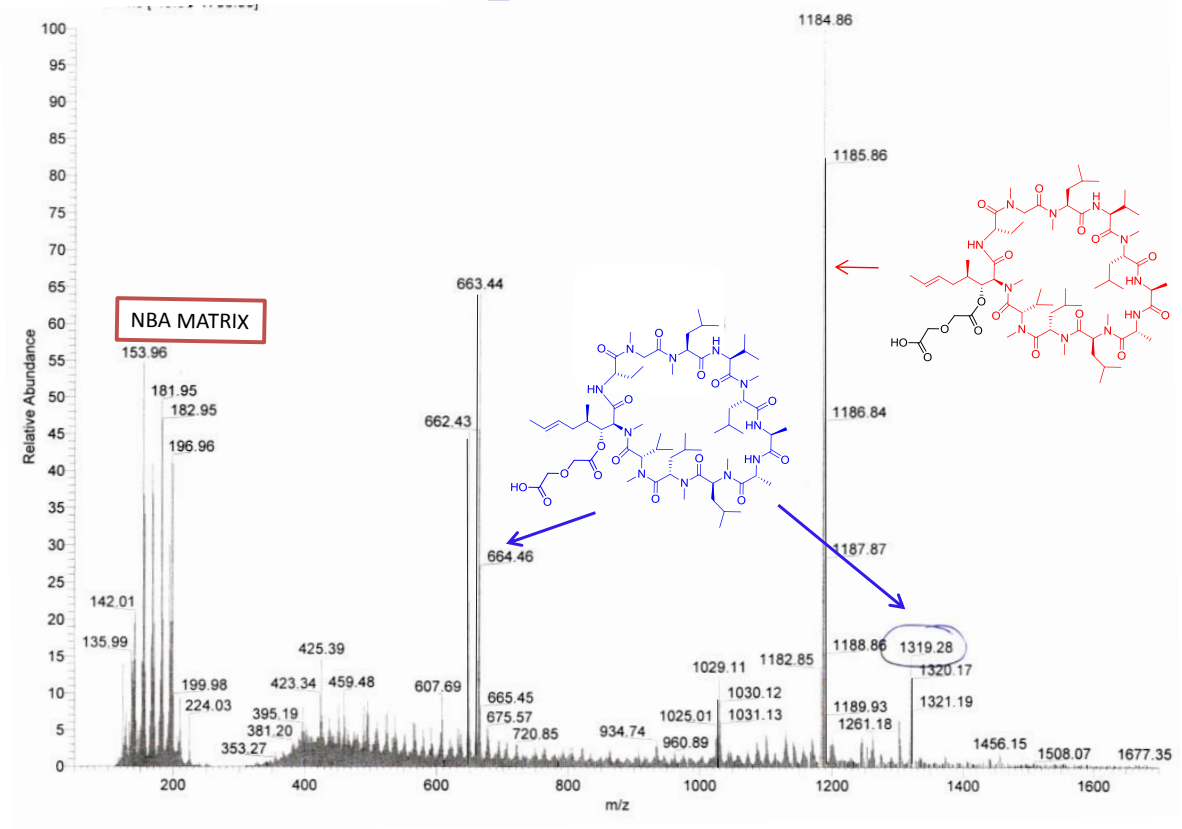


Figure 131. Mass spectrum of CyA-O-COOH recorded by fast atom bombardment in positive detection mode; m/z $[M+H]^+$ calculated for $C_{66}H_{116}N_{11}O_{16}^+$ 1318.85; found 1319.28.

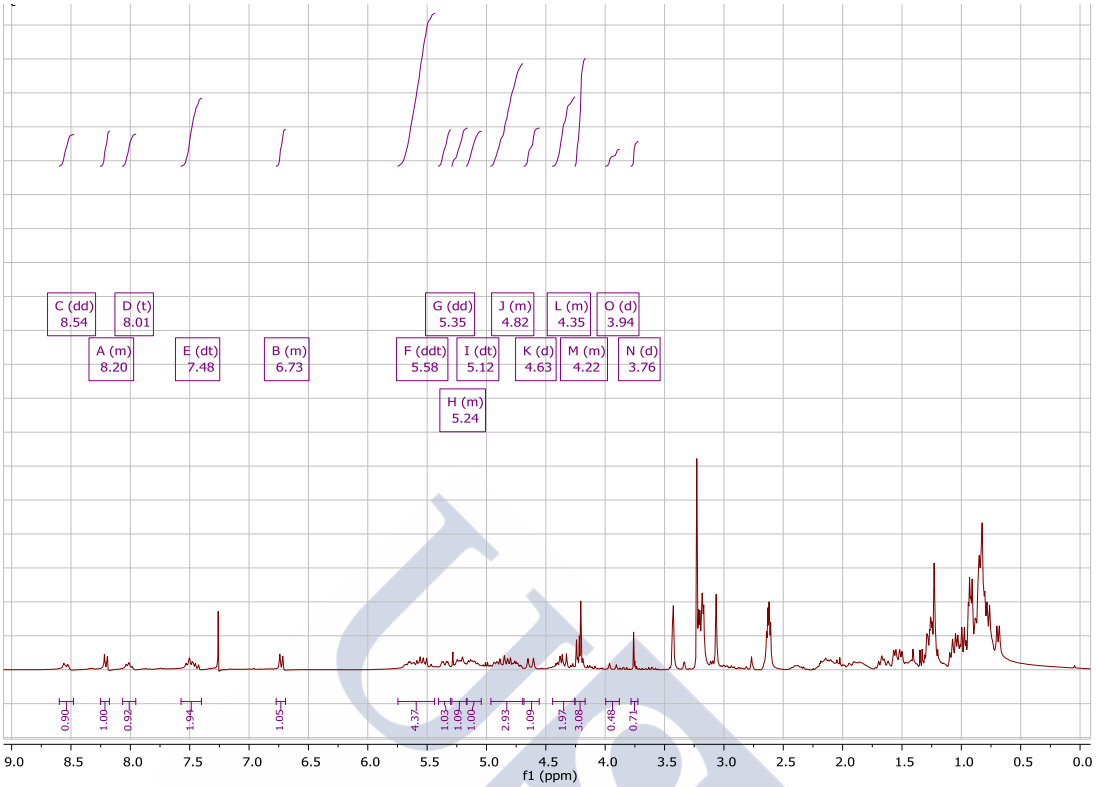


Figure 132. ^{1}H-NMR (300 MHz, $CDCl_3$) of CyA-O-COOH. Preparation procedure described in Experimental Part, section 2.4.

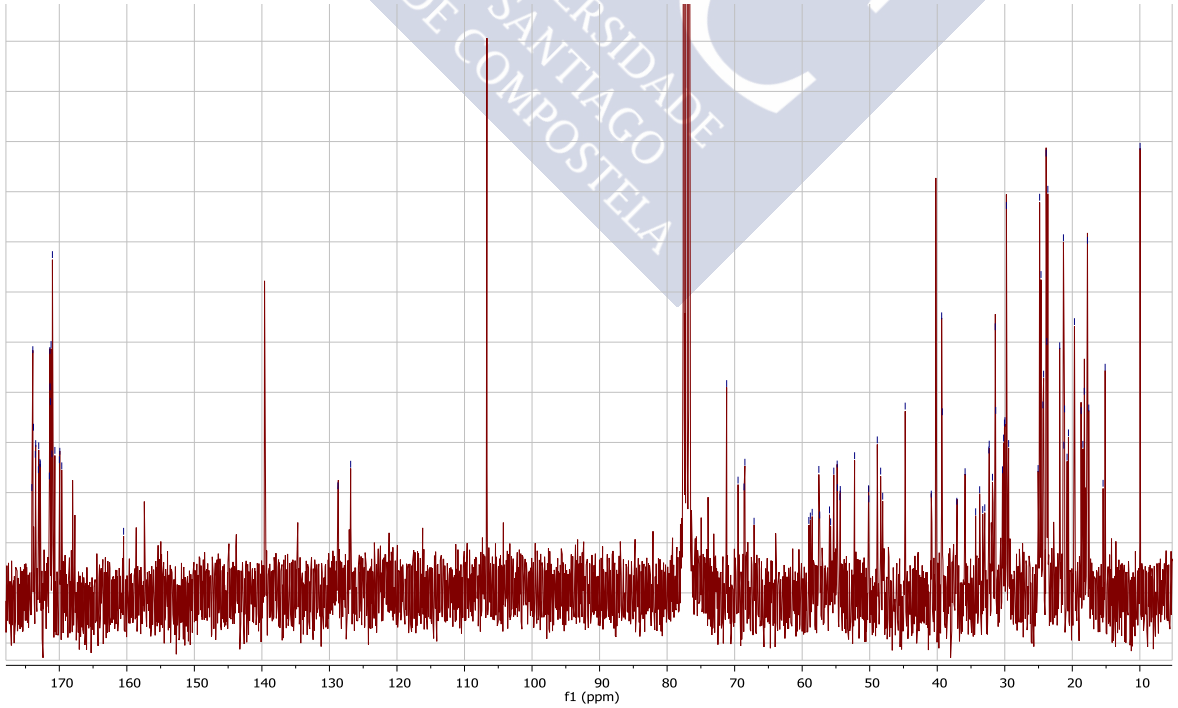
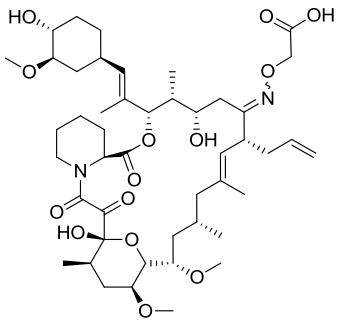


Figure 133. ^{13}C-NMR (75 MHz, $CDCl_3$) of CyA-O-COOH Preparation procedure described in Experimental Part, section 2.4.

1.7. FK506-COOH



FK506-COOH

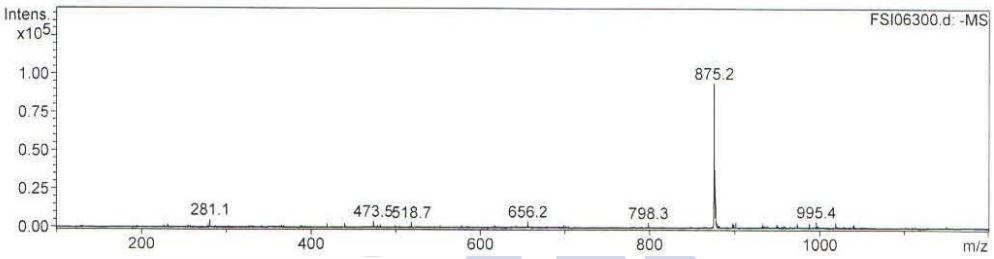


Figure 134. Mass spectrum of FK506-COOH recorded in MeOH by electrospray ionization in negative ion detection mode. m/z: $[M–H]^-$ calcd. for $[C_{46}H_{72}N_2O_{14} – H]^-$, 875.5; found, 875.2.



Figure 135. ^{1}H-NMR (300 MHz, $CDCl_3$) of FK506-COOH. Preparation procedure described in in Experimental Part, section 3.1.

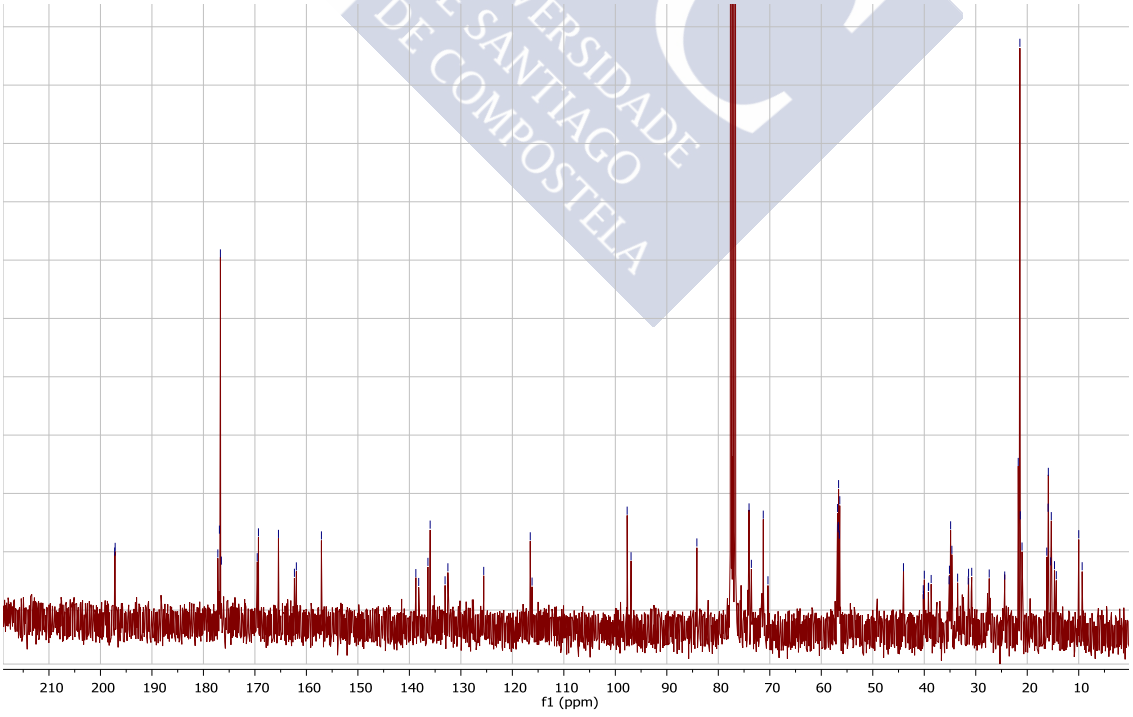


Figure 136. ^{13}C-NMR (75 MHz, $CDCl_3$) of FK506-COOH Preparation procedure described in Experimental Part, section 3.1.

1.8. FK506-DIC

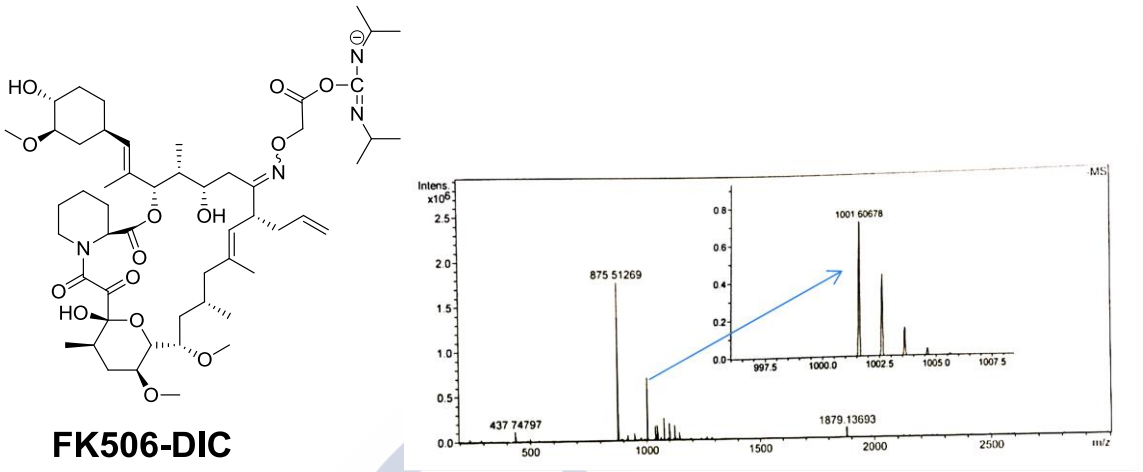
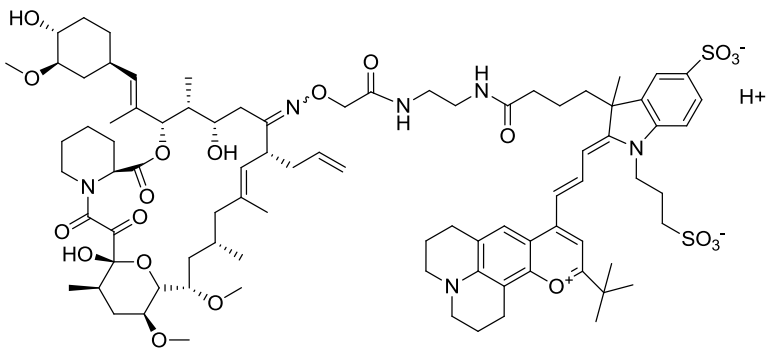


Figure 137. Mass spectrum of FK506-DIC recorded in MeOH by electrospray ionization in negative detection mode; m/z $[M]^-$ calculated for $[C_{53}H_{85}N_4O_{14}]^-$ 1001.61; found 1001.61.

1.9. FK506-DY636



FK506-DY636

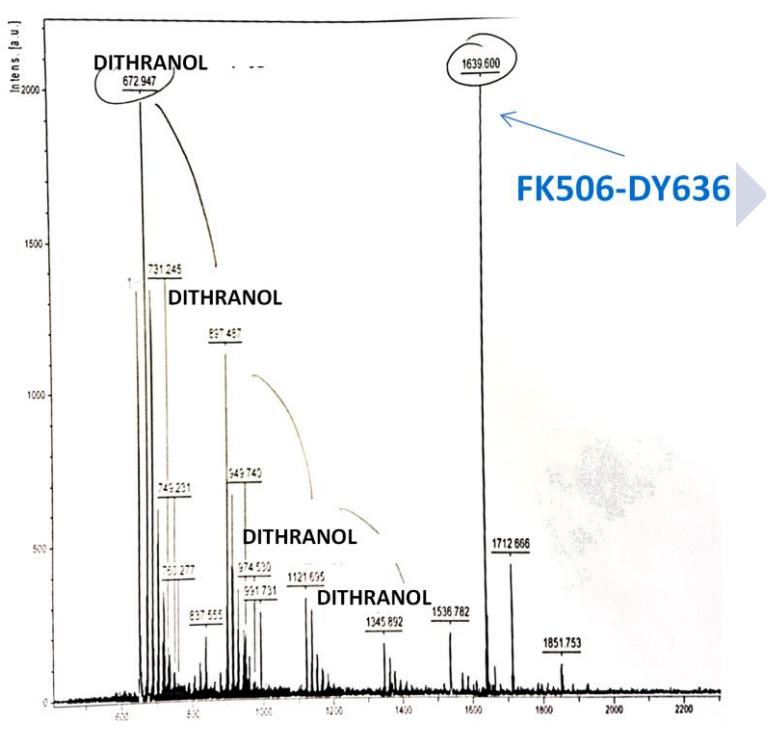
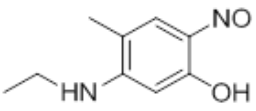


Figure 138. Mass spectra of FK506-DIC recorded by MALDI TOF/TOF; m/z [M] calculated for $C_{86}H_{112}N_6O_{21}S_2$ 1638.81, found 1639.6. Preparation procedure described in Experimental Part, section 3.2.

1.10. 5-ethylamino-4-methyl-2-nitrosophenol



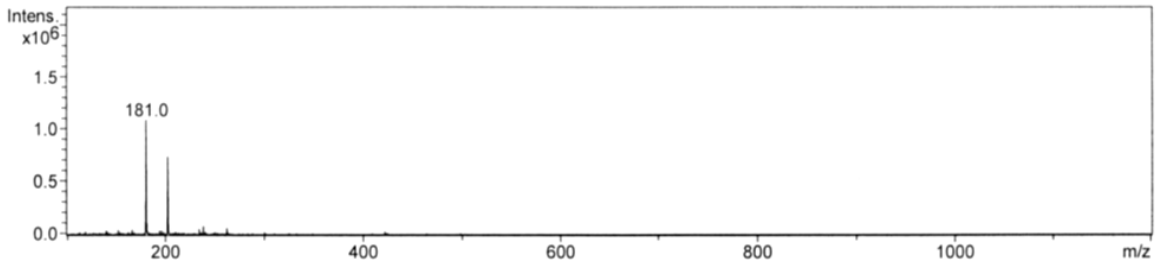


Figure 139. Mass spectrum of 5-ethylamino-4-methyl-2-nitrosophenol recorded by electrospray ionization in positive ion detection mode; m/z [M] calculated for $C_9H_{12}N_2O_2$ 180.09, found 181.0.

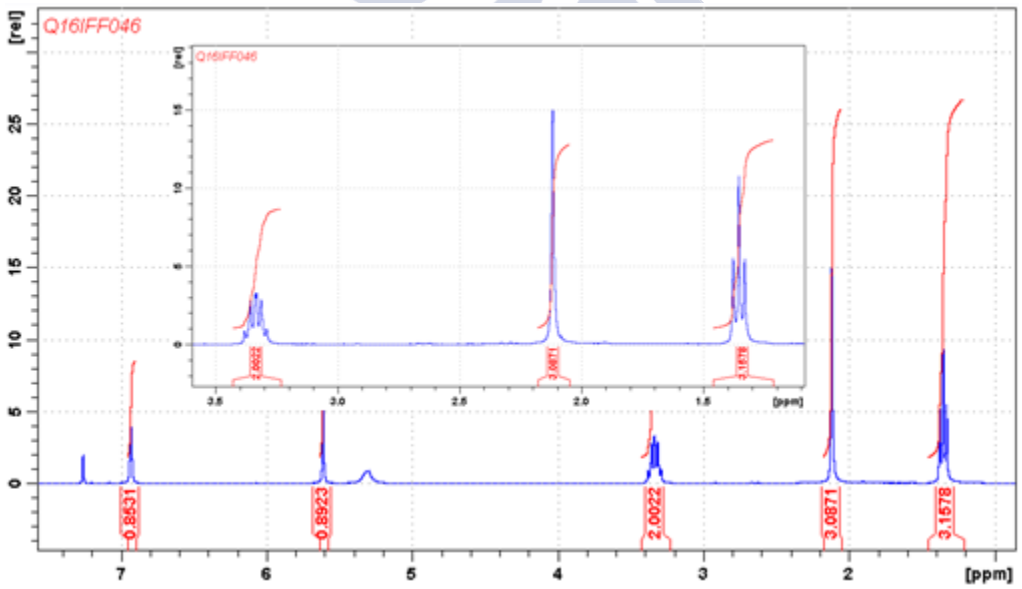


Figure 140. ^{1}H-NMR (300 MHz, $CDCl_3$) of of 5-ethylamino-4-methyl-2-nitrosophenol. Preparation procedure described in Experimental Part, section 4.2.1.

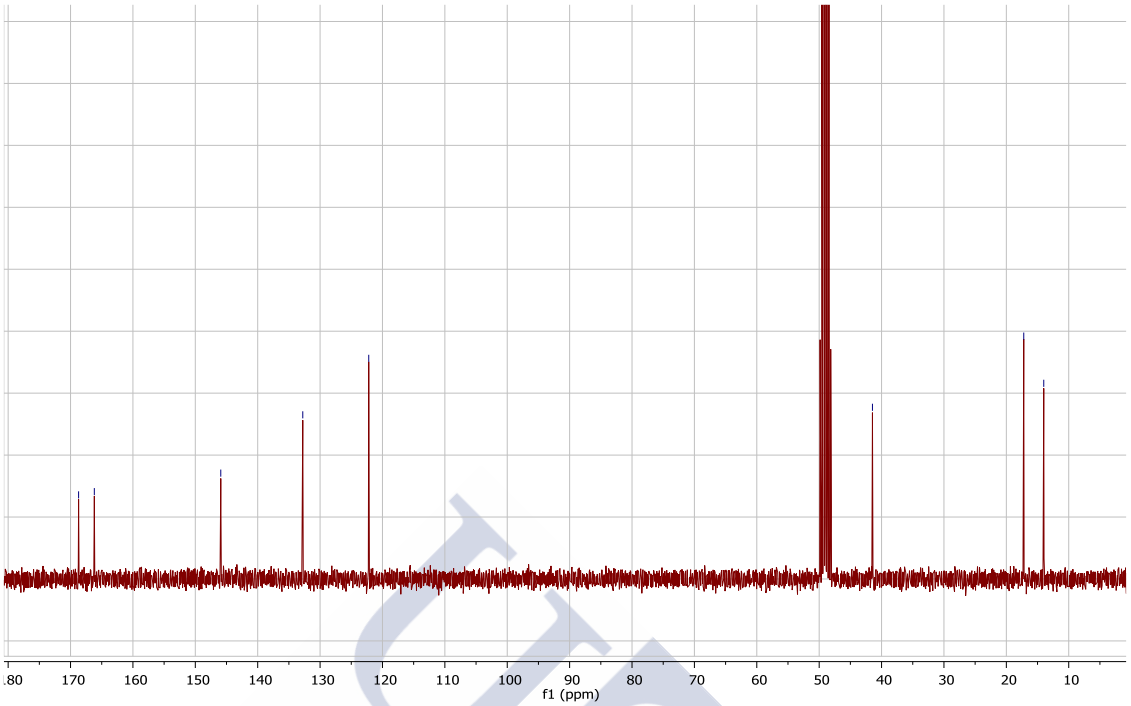
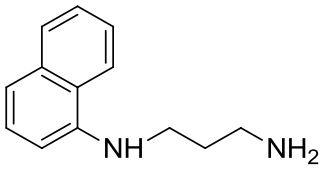


Figure 141. ^{13}C-NMR (75 MHz, CD_3OD) of 5-ethylamino-4-methyl-2-nitrosophenol. Preparation procedure described in Experimental Part, section 4.2.1.

1.11. *N*-(naphtalen-1-yl)propane-1,3-diamine



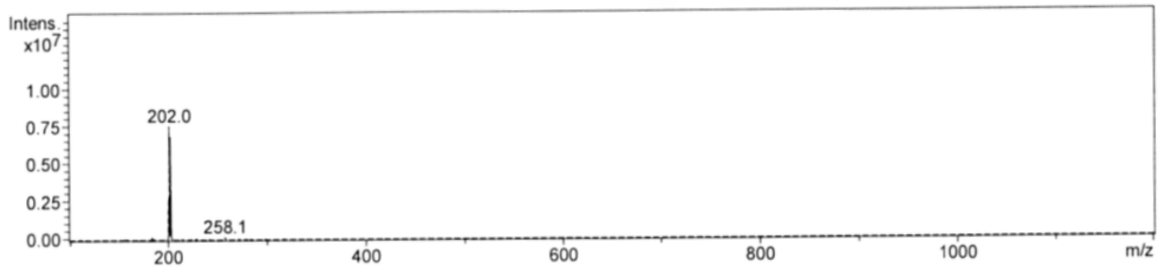


Figure 142. Mass spectrum of *N*-(naphtalen-1-yl)propane-1,3-diamine recorded by electrospray ionization in positive ion detection mode; m/z [M] calculated for $C_{13}H_{16}N_2$ 200.13; found 202.0.

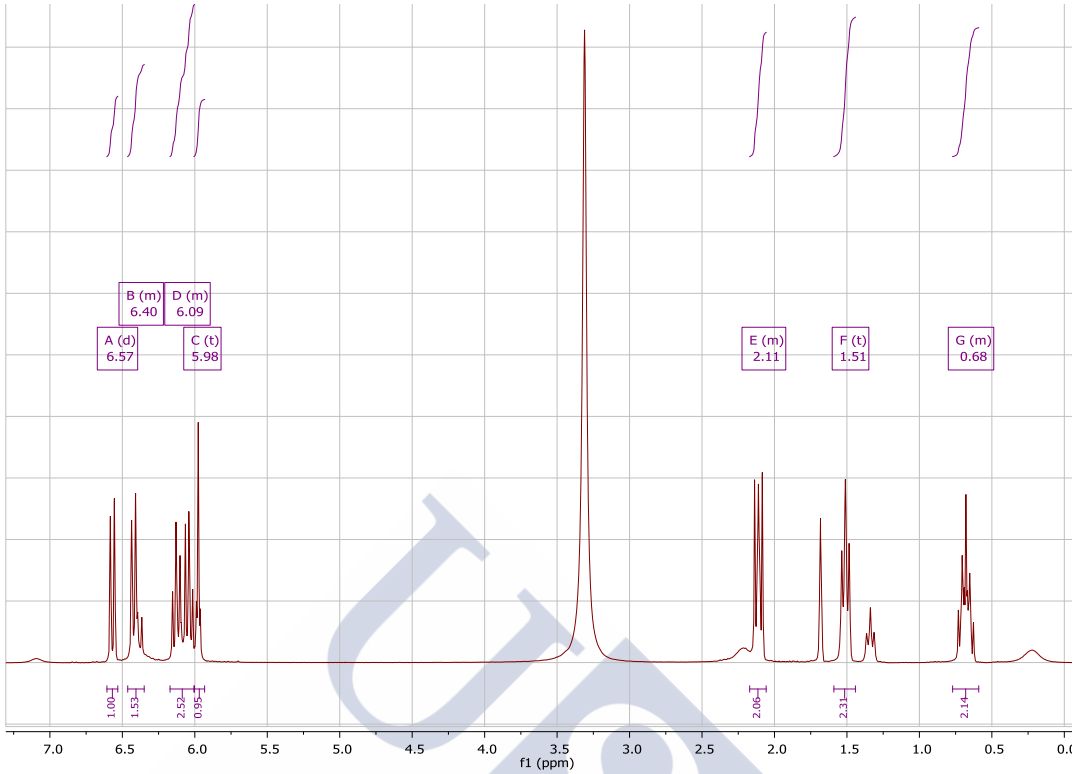


Figure 143. ^{1}H-NMR (300 MHz, CD_3OD) of *N*-(naphtalen-1-yl)propane-1,3-diamine. Preparation procedure described in Experimental Part, section 4.2.2.

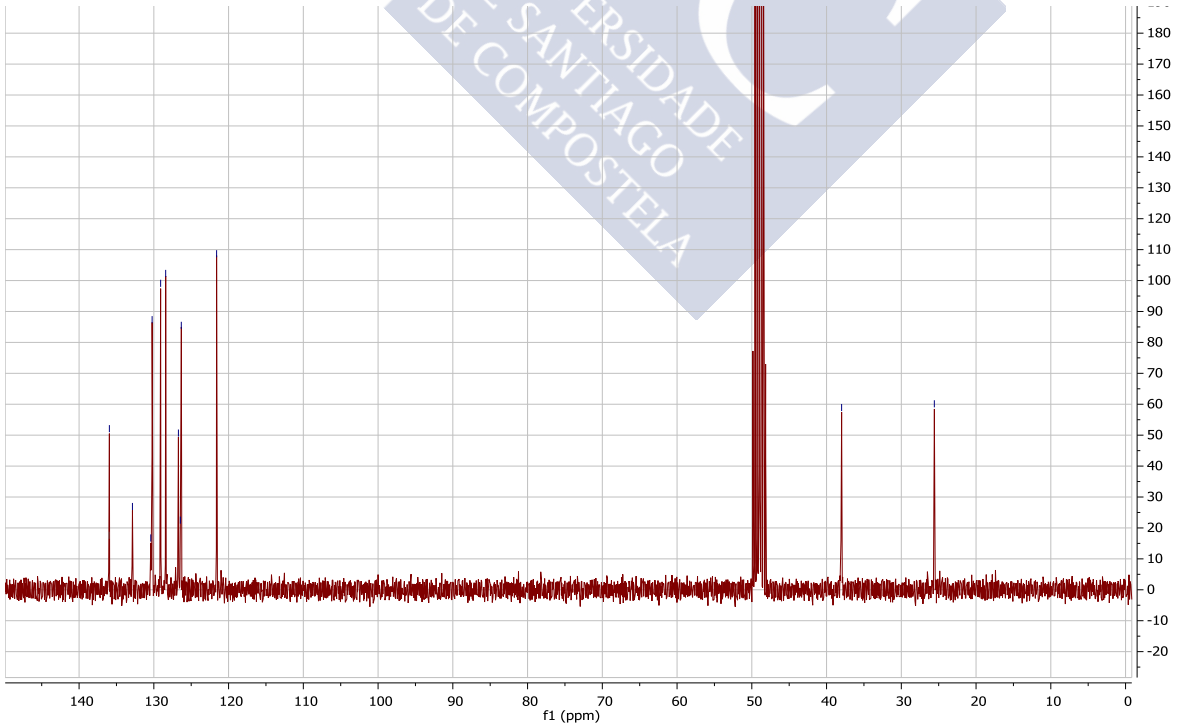
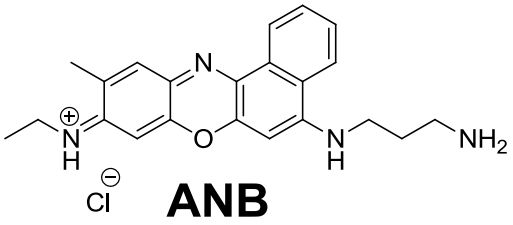


Figure 144. ^{13}C-NMR (75 MHz, CD_3OD) of of *N*-(naphtalen-1-yl)propane-1,3-diamine. Preparation procedure described Experimental Part, section 4.2.2.

1.12. Propylamino Nile Blue (ANB)



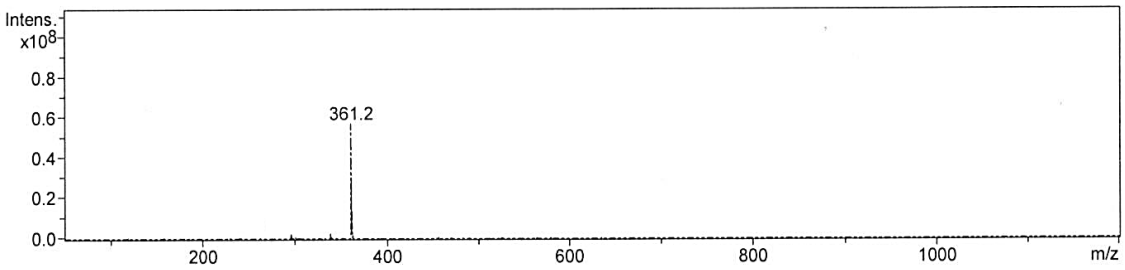


Figure 145. Mass spectrum of ANB recorded by electrospray ionization in positive ion detection mode; m/z $[M]^+$ calculated for $[C_{22}H_{25}N_4O]^+$ 361.20, found 361.2.

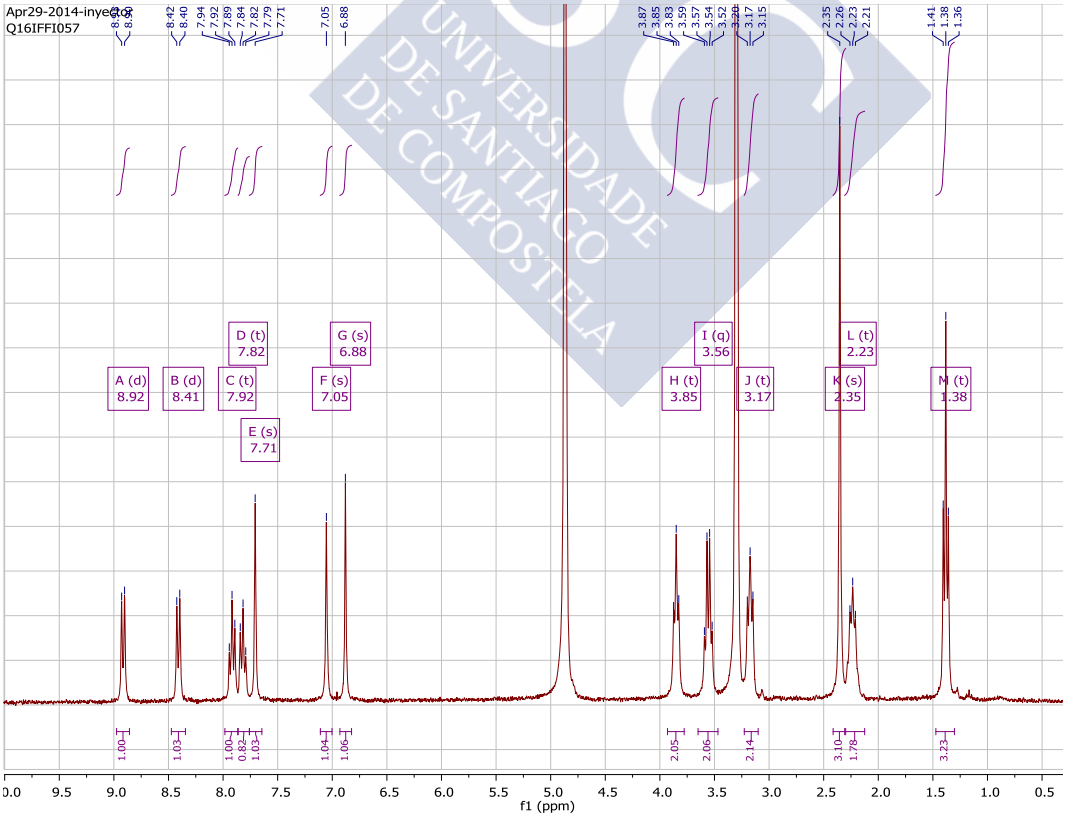


Figure 146. ^{1}H-NMR (300 MHz, CD_3OD) of ANB. Preparation procedure described in Experimental Part, section 4.2.3.

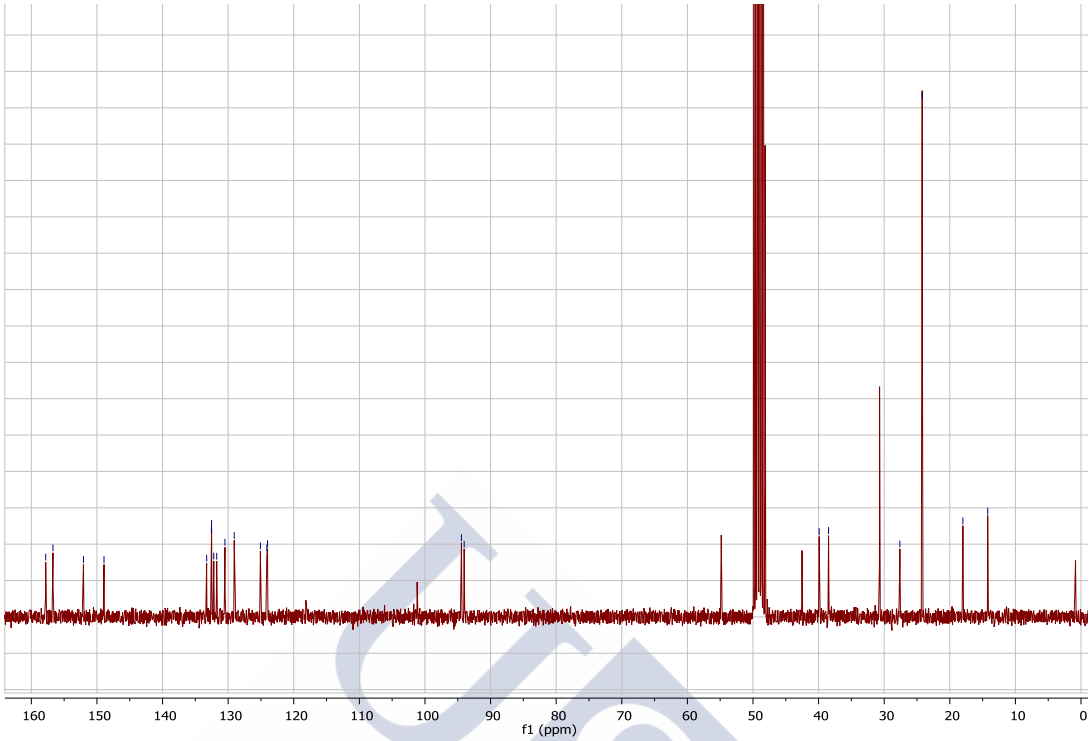


Figure 147. ^{13}C-NMR (75 MHz, CD_3OD) ANB. Preparation procedure described Experimental Part, section 4.2.3.

1.13. CyA-S-ANB

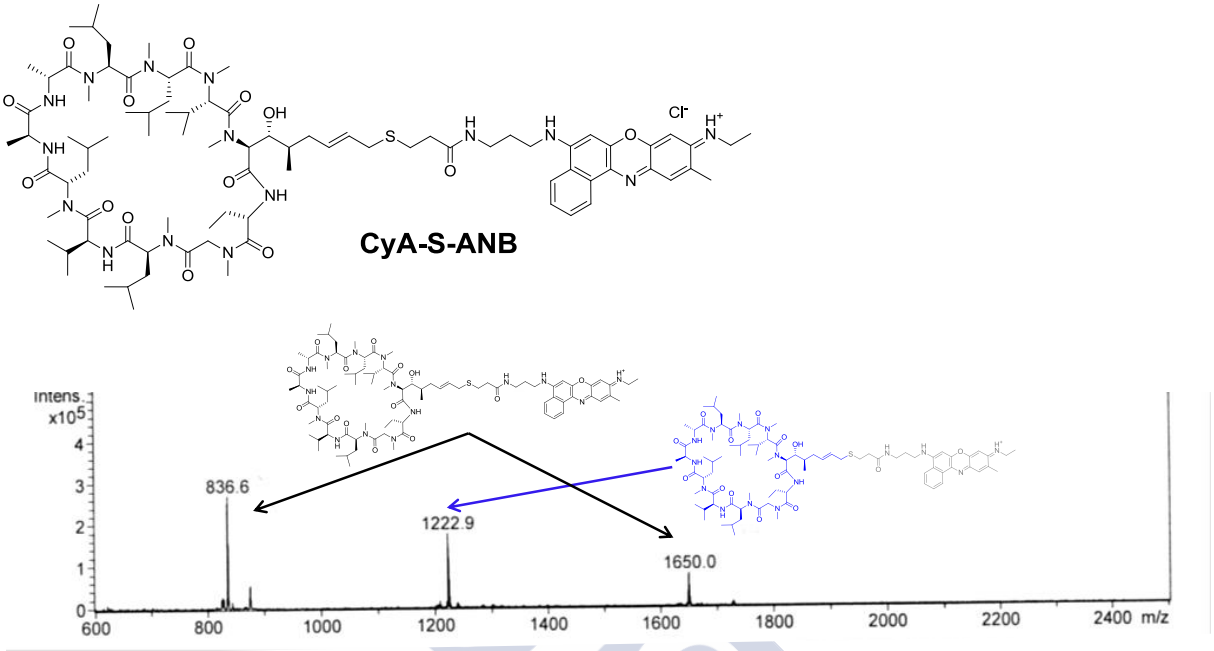


Figure 148. Mass spectrum of CyA-S-ANB recorded by electrospray ionization in positive ion detection mode; m/z $[M]^+$ calculated for $[C_{87}H_{138}N_{15}O_{14}S]^+$ 1649.03 found 1650.0 and also found [M/2 + Na] 836.6.

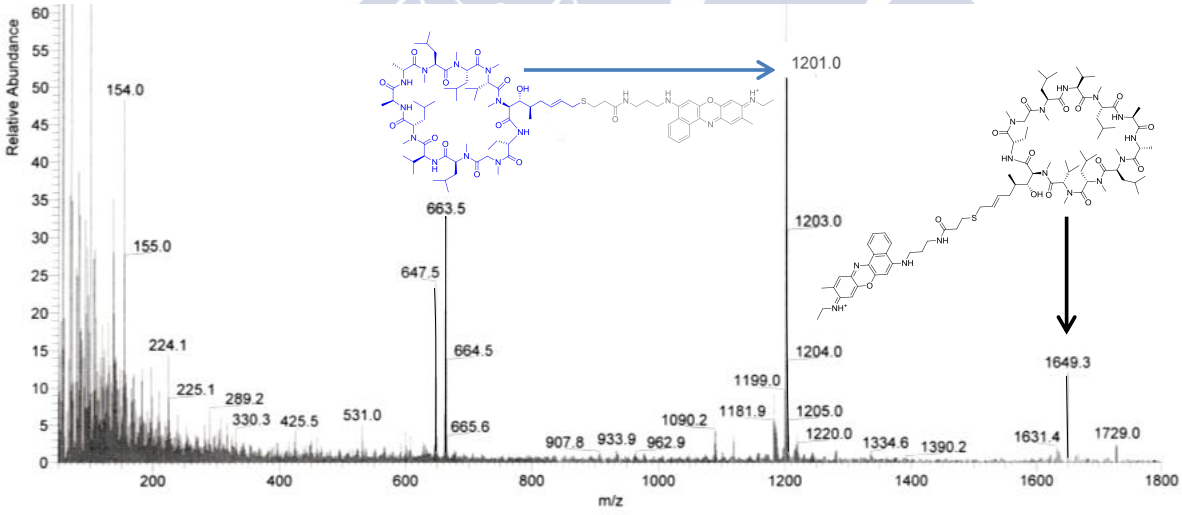


Figure 149. Mass spectrum of CyA-S-ANB recorded by fast atom bombardment in positive ion detection mode; m/z $[M]^+$ calculated for $[C_{87}H_{138}N_{15}O_{14}S]^+$ 1649.03 found 1649.3.

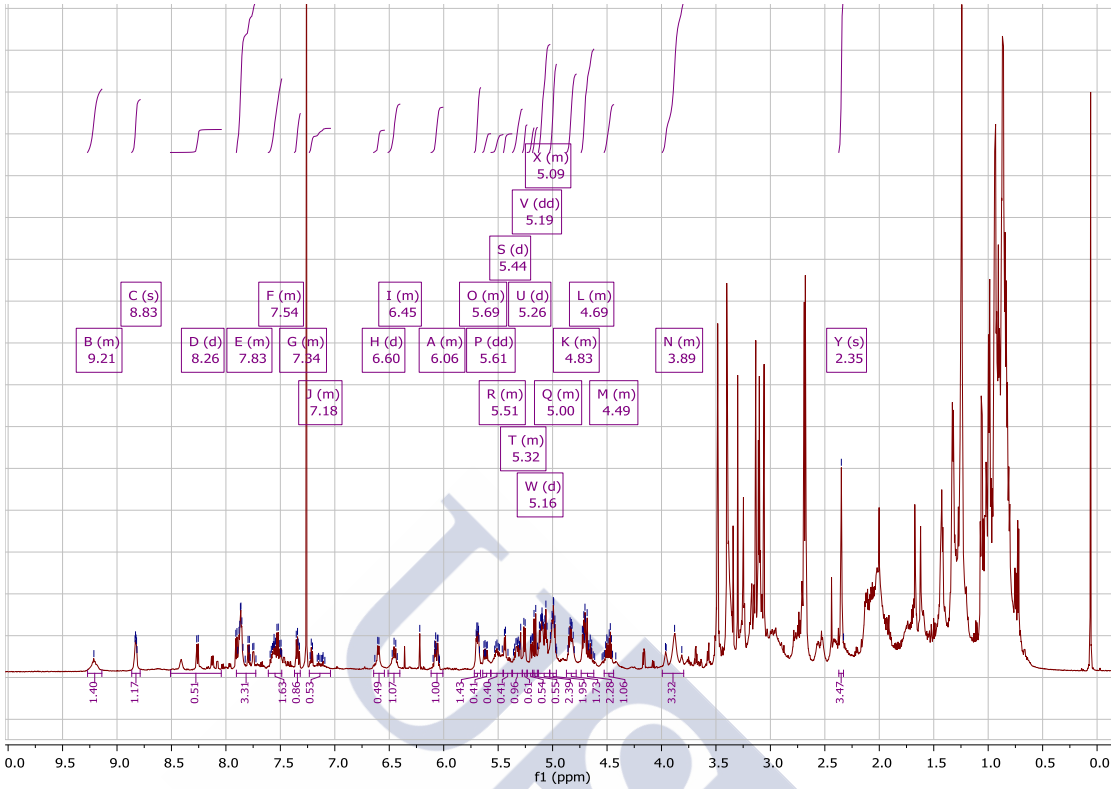


Figure 150. ^{1}H-NMR (700 MHz, $CDCl_3$) of CyA-S-ANB. Preparation procedure described in Experimental Part, section 4.4.

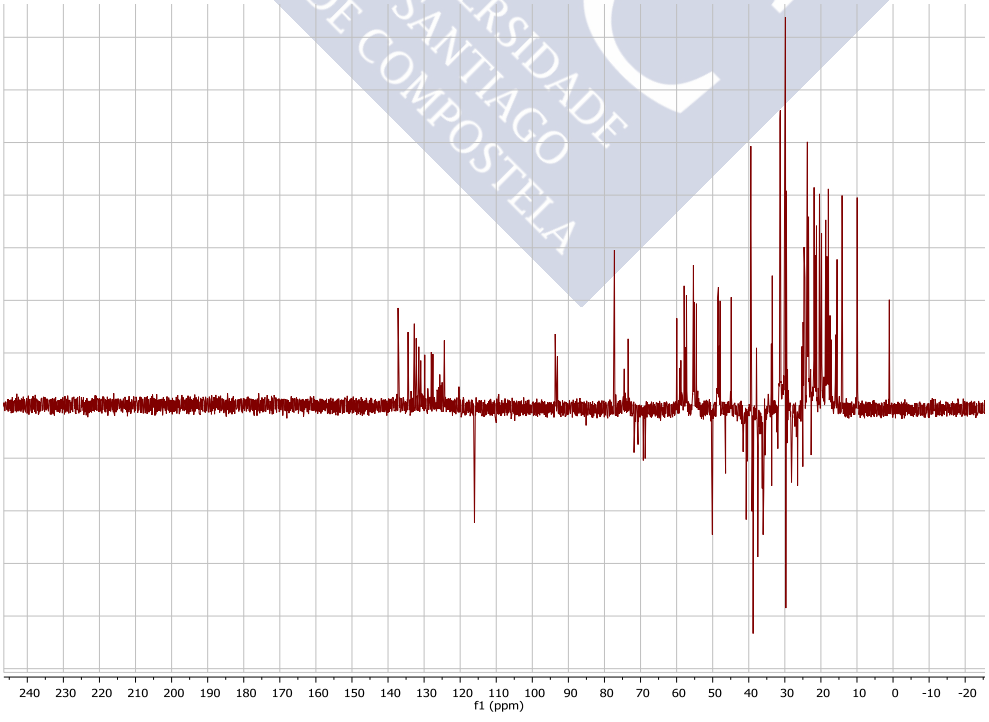
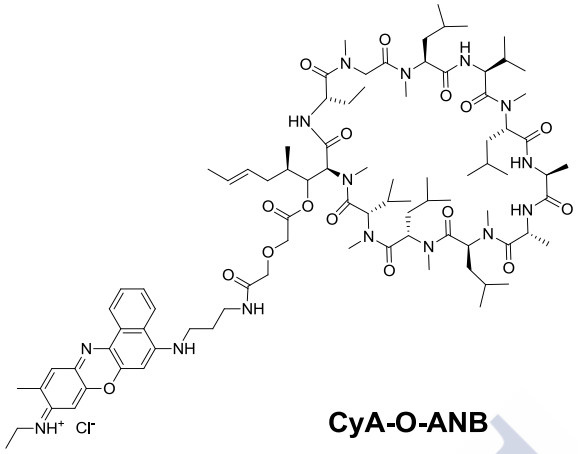


Figure 151. ^{13}C-NMR (176 MHz, $CDCl_3$) CyA-S-ANB in DEPT mode. Preparation procedure described in in Experimental Part, section 4.4.

1.14. CyA-O-ANB



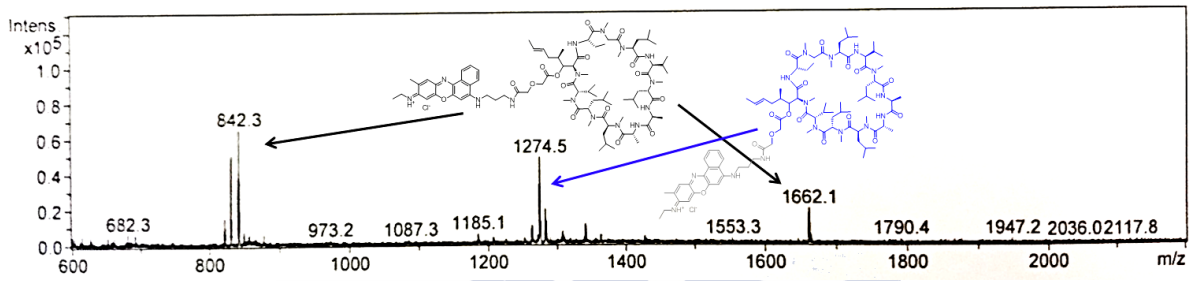


Figure 152. Mass spectrum of CyA-O-ANB recorded by electrospray ionization in positive ion detection mode; m/z $[M]^+$ calculated for $[C_{88}H_{138}N_{15}O_{16}]^+$ 1661.04; found 1662.1, then also found $[M/2 +Na]^+$ 842.3.

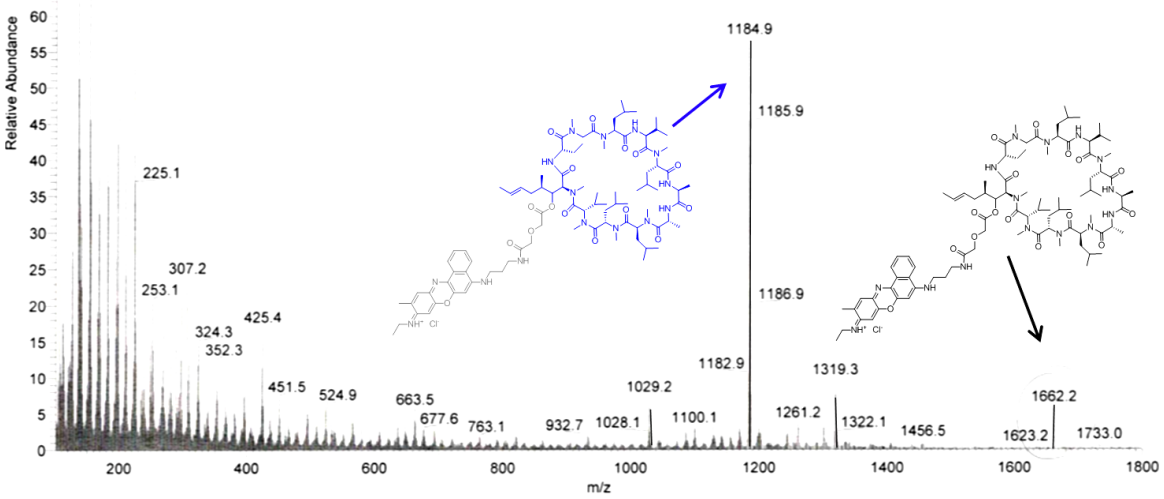


Figure 153. Mass spectrum of CyA-O-ANB recorded by fast atom bombardment in in positive ion detection mode; m/z $[M]^+$ calculated $[C_{88}H_{138}N_{15}O_{16}]^+$ 1661.04; found 1662.2.

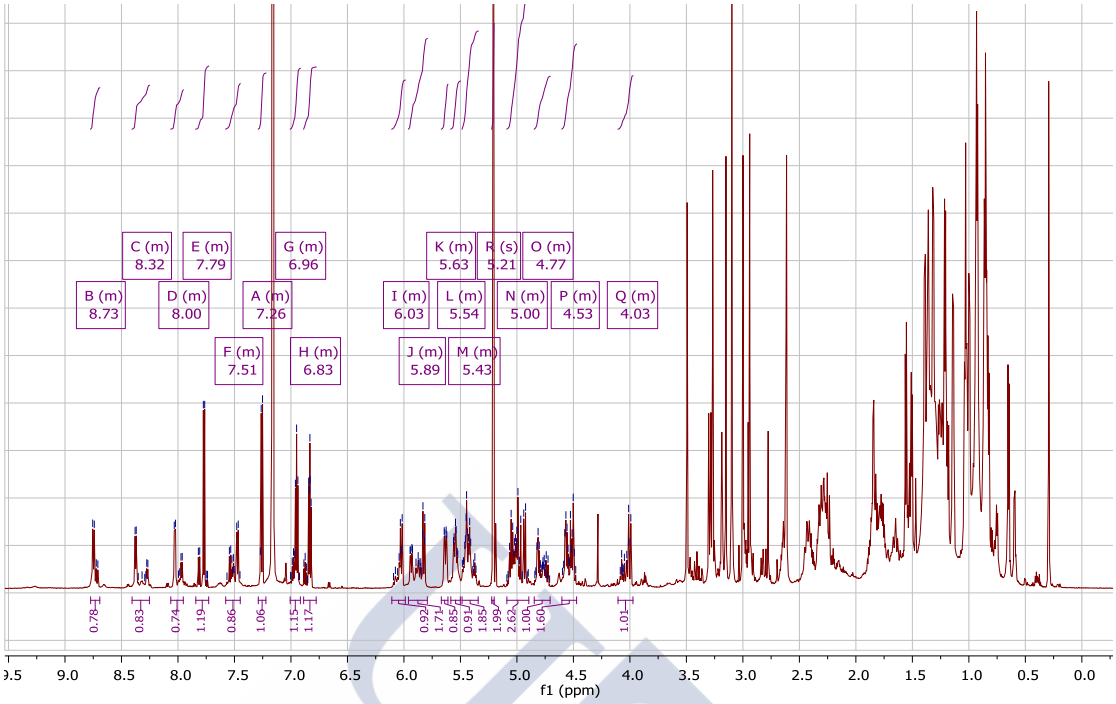


Figure 154. ^{1}H-NMR (700 MHz, $CDCl_3$) of CyA-O-ANB. Preparation procedure described in Experimental Part, section 4.3.

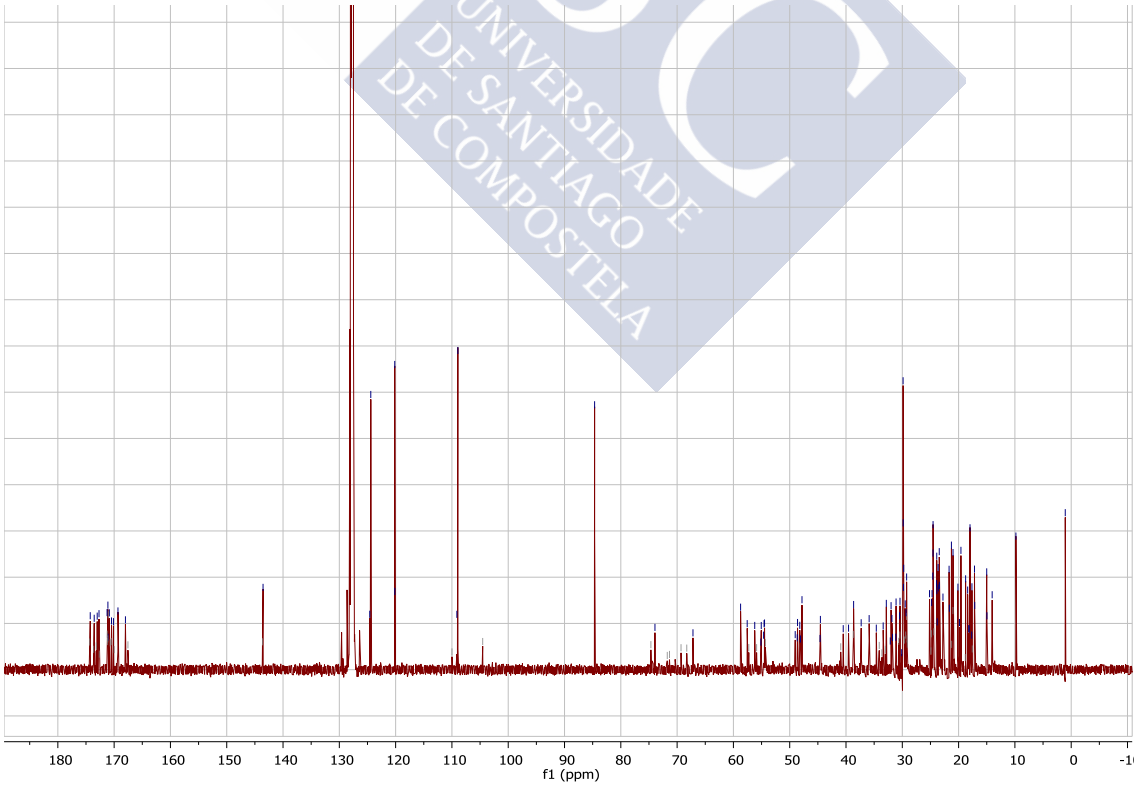
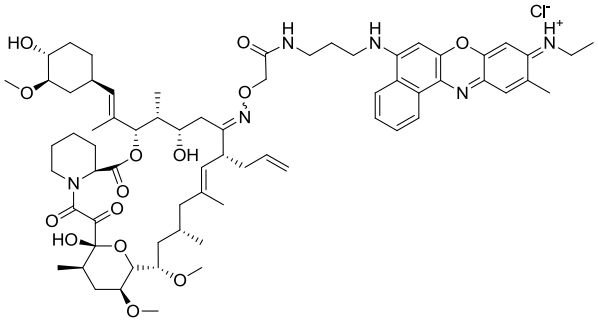


Figure 155. ^{13}C-NMR (176 MHz, C_6D_6) CyA-O-ANB. Preparation procedure described in Experimental Part, section 4.3.

1.15. FK506-ANB



FK506-ANB

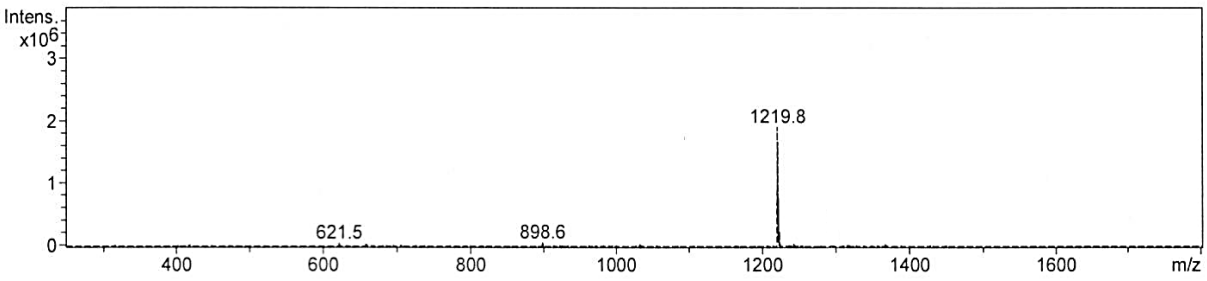


Figure 156. Mass spectrum of FK506-ANB recorded by electrospray ionization in positive ion detection mode. m/z $[M]^+$ calculated for $[C_{68}H_{95}N_6O_{14}]^+$ 1219.69; found 1219.8.

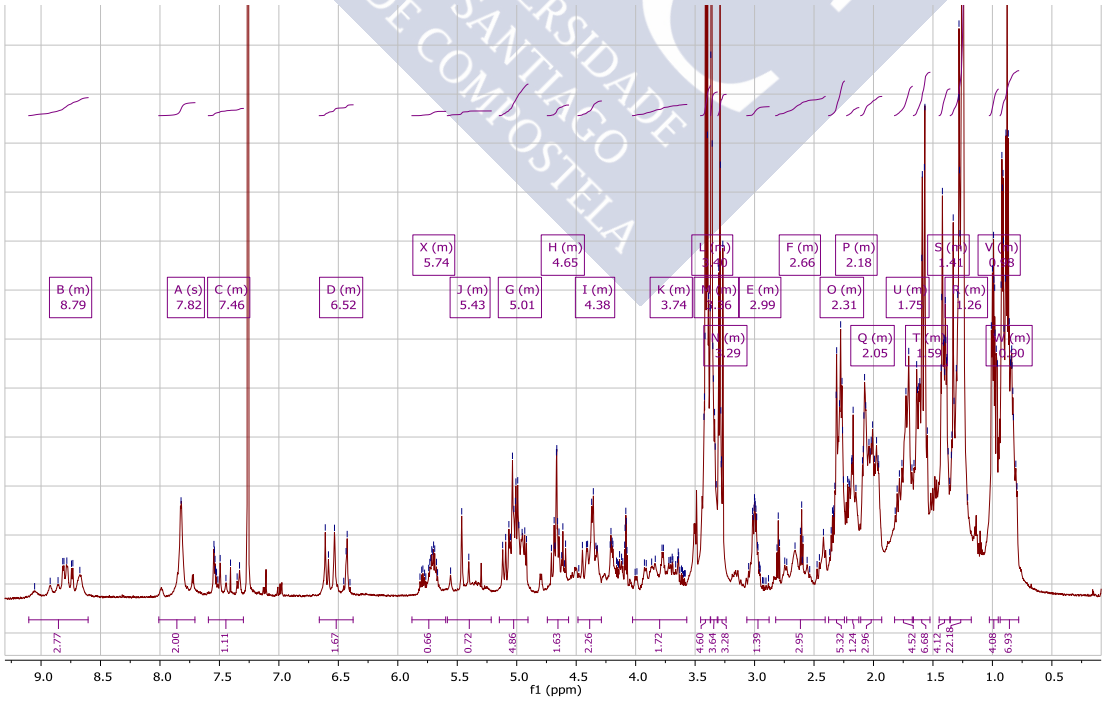


Figure 157. ^{1}H-NMR (700 MHz, $CDCl_3$) of FK506-ANB. Preparation procedure described in Experimental Part, section 4.5.

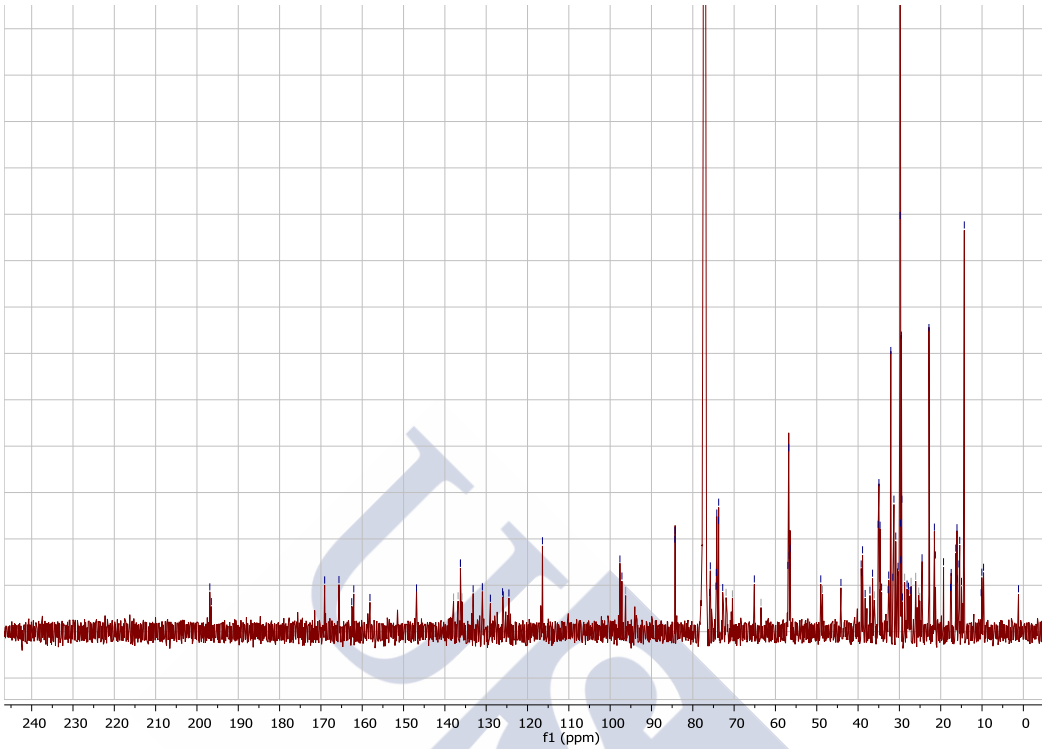
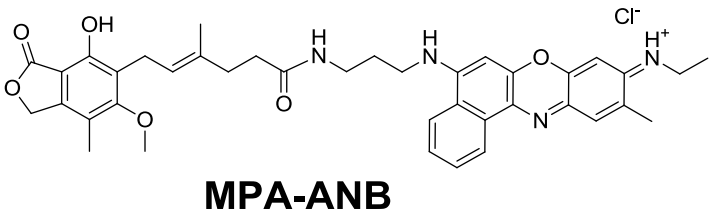


Figure 158. ^{13}C-NMR (176 MHz, $CDCl_3$) FK506-ANB. Preparation procedure described in Experimental Part, section 4.5.

1.16. MPA-ANB



MPA-ANB

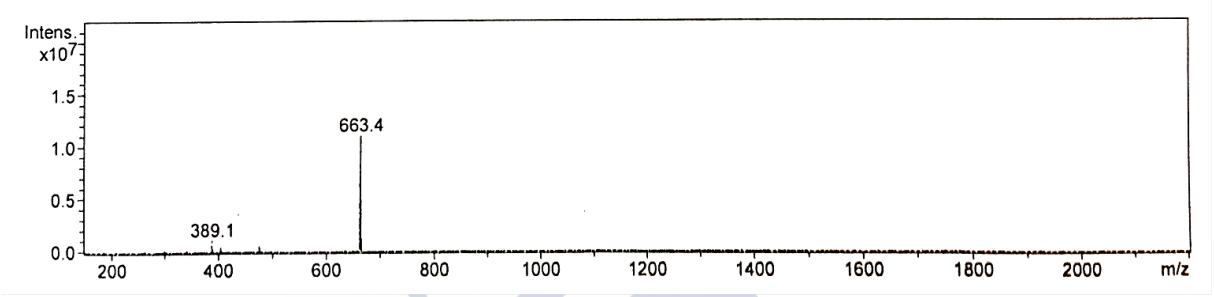


Figure 159. Mass spectrum of MPA-ANB recorded in MeOH by electrospray ionization in positive ion detection mode. m/z $[M]^+$ calculated for calculated for: $[C_{39}H_{43}N_4O_6]^+$ 663.32; found 663.4.

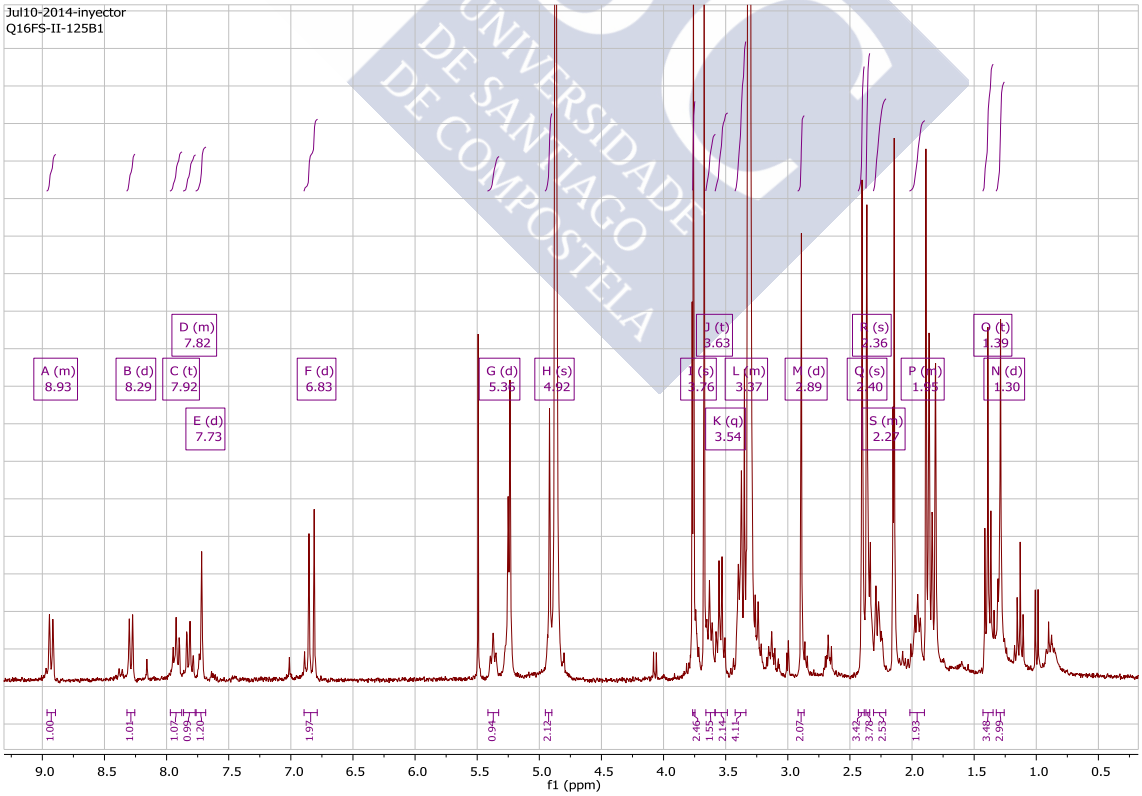
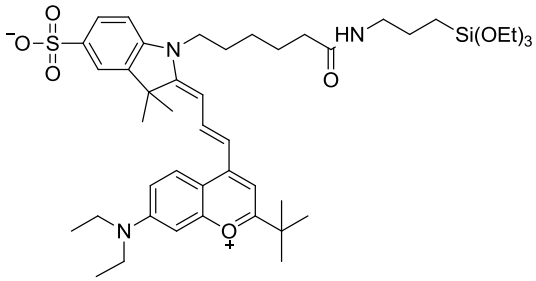


Figure 160. ^{1}H-NMR (300 MHz, $CDCl_3$) of MPA-ANB. Preparation procedure described in Experimental Part, section 4.6.

1.17. Dy630-TES



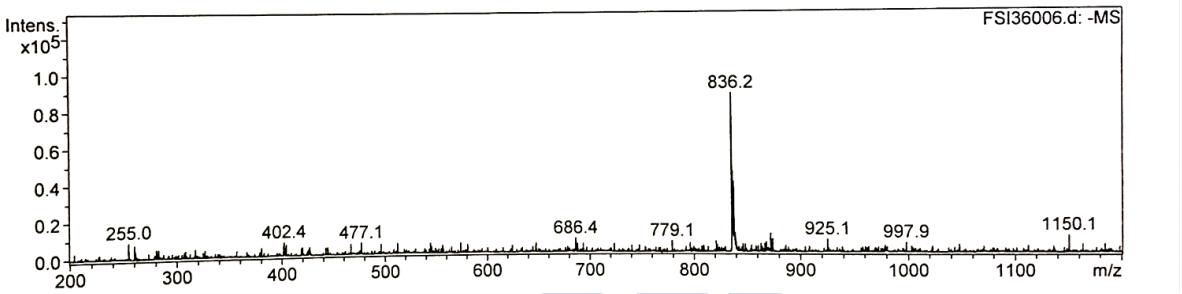
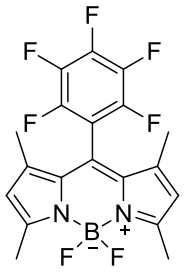


Figure 161. Mass spectrum of Dy630-TES recorded by electrospray ionization in negative detection mode; m/z [M] calculated for $C_{45}H_{67}N_3O_8SSi$, 837.44, found: 836.2.

1.18. PFB-515



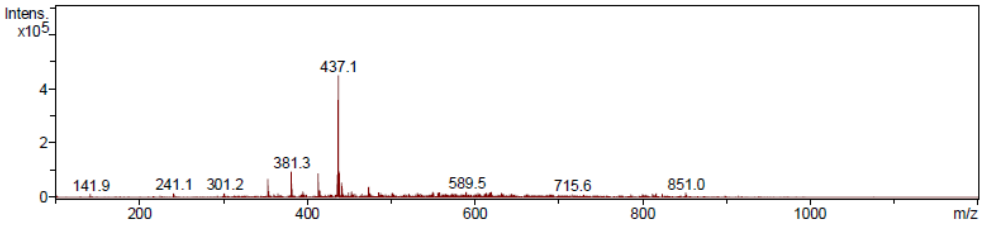


Figure 162. Mass spectrum of PFB-515 recorded by electrospray ionization in positive detection mode; m/z: $[M+Na]^+$ calcd. for $[C_{19}H_{14}BF_7N_2 + Na]^+$, 437.1; found, 437.1.

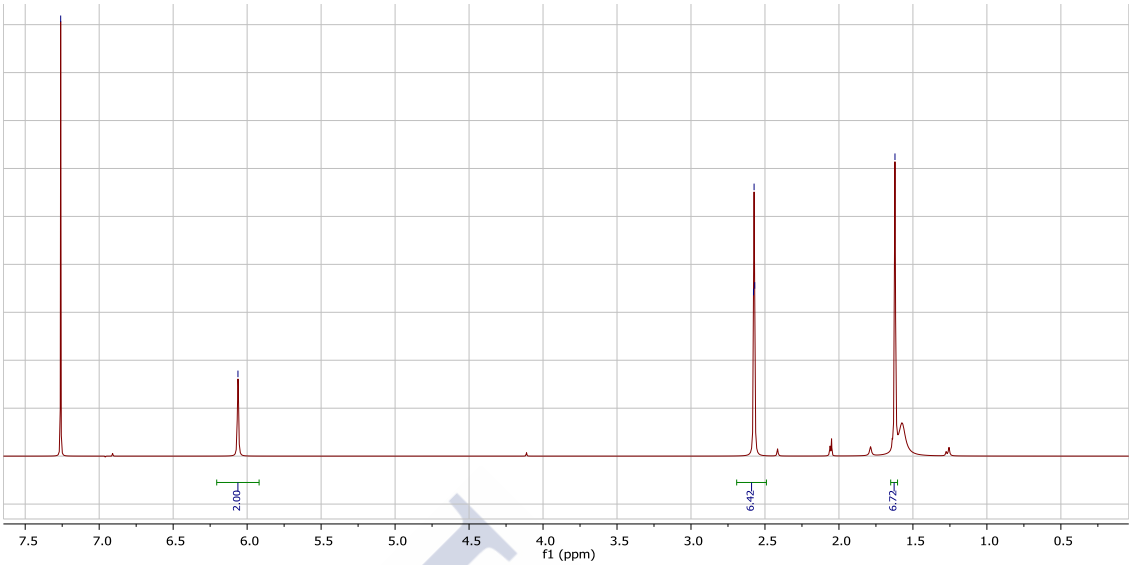


Figure 163. ^{1}H-NMR (300 MHz, $CDCl_3$) of PFB-515. Preparation procedure described in Experimental Part, section 7.1.

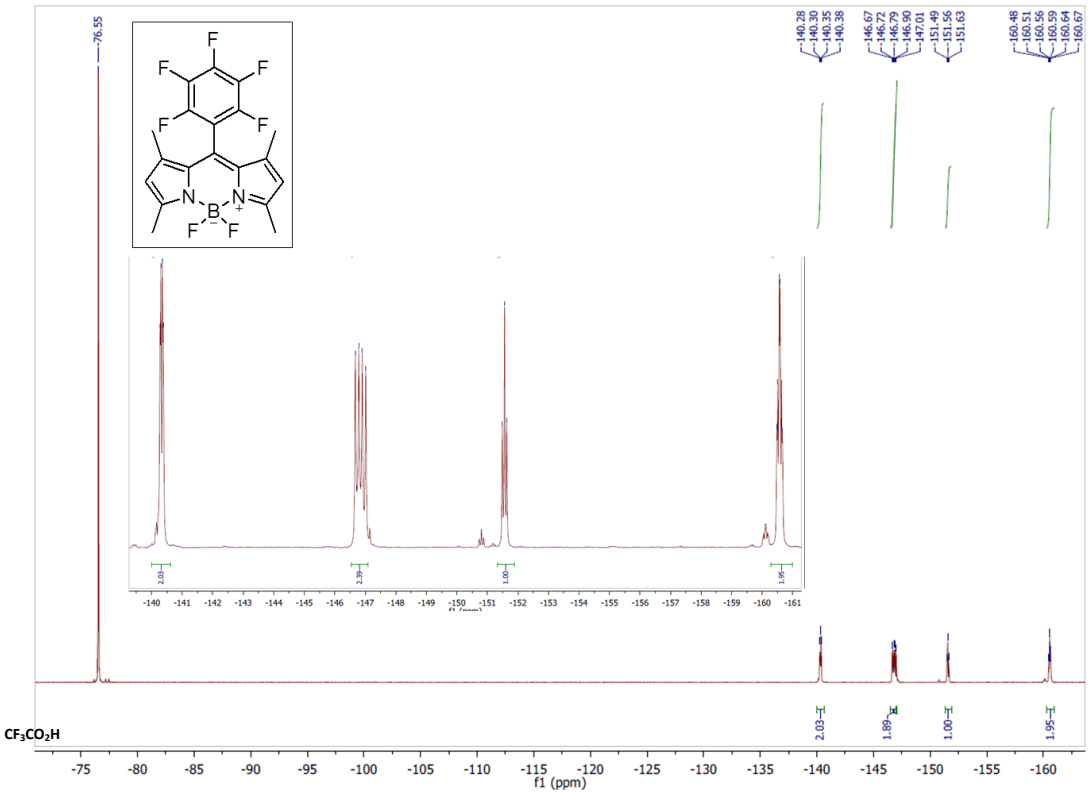


Figure 164. ^{19}F NMR spectrum of PFB-515 (282 MHz, in $CDCl_3$; δ in ppm from $CFCl_3$).

1.19. PFB-641

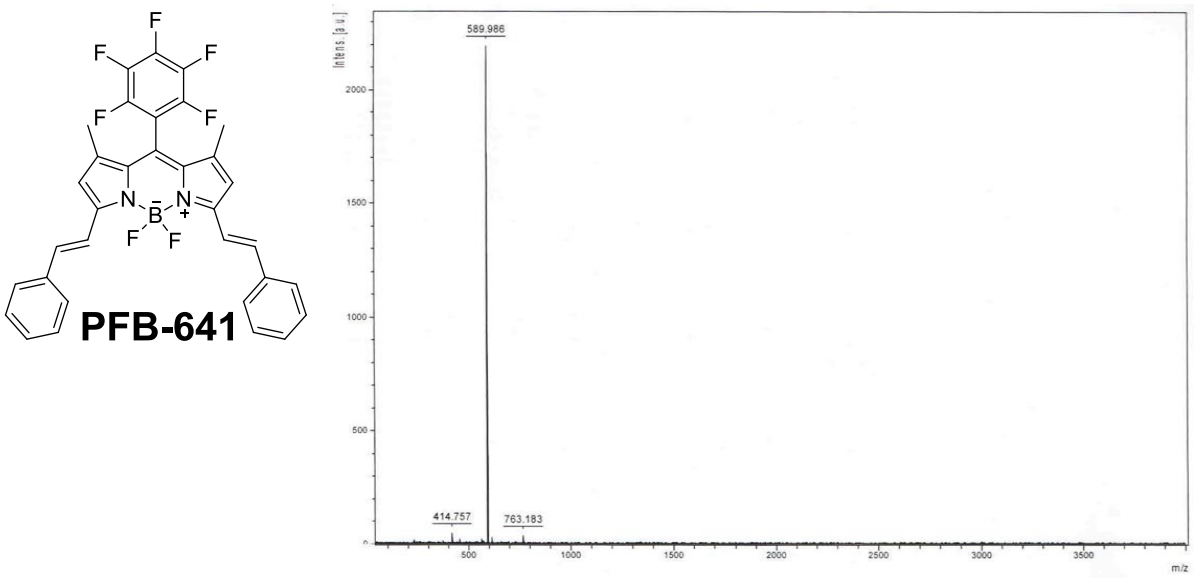


Figure 165. Mass spectrum of PFB-641 recorded by MALDI TOF/TOF; m/z [M]: calcd. for $C_{33}H_{22}BF_7N_2$, 590.18; found, 589.99.

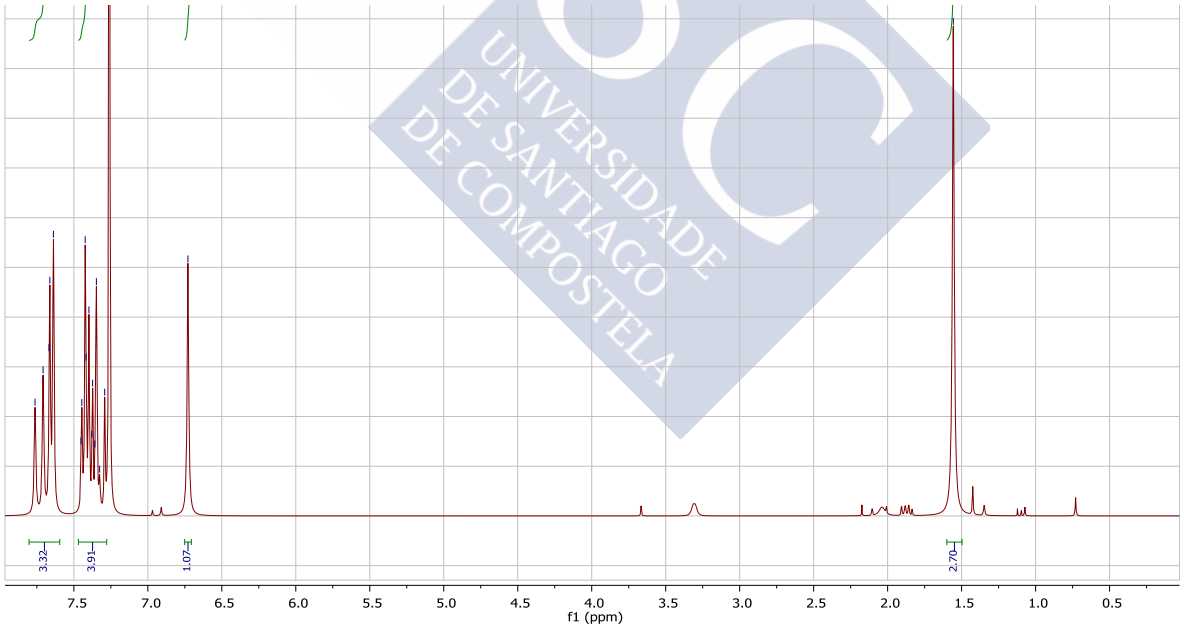


Figure 166. ^{1}H-NMR (300 MHz, $CDCl_3$) of PFB-641. Preparation procedure described in Experimental Part, section 7.2.

1.20. B1

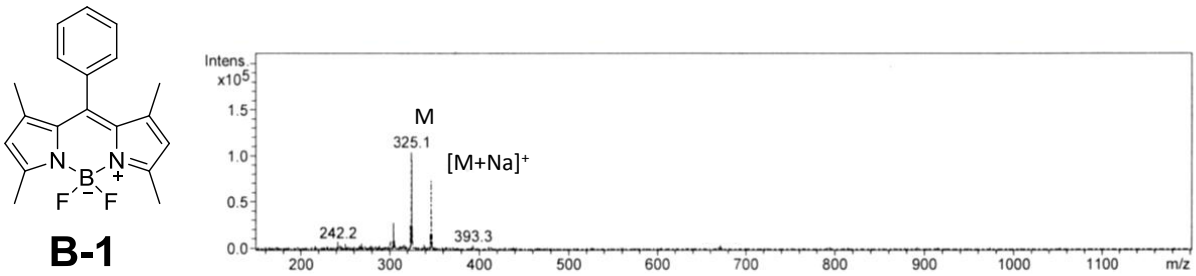


Figure 167. Mass spectrum of B1 recorded by electrospray ionization in positive ion detection mode; m/z [M] calculated for $C_{19}H_{19}BF_2N_2$: 324.16, found 325.1 and calculated for $[M + Na]^+$ $[C_{19}H_{19}BF_2N_2Na]^+$ 347.15; found 347.1.

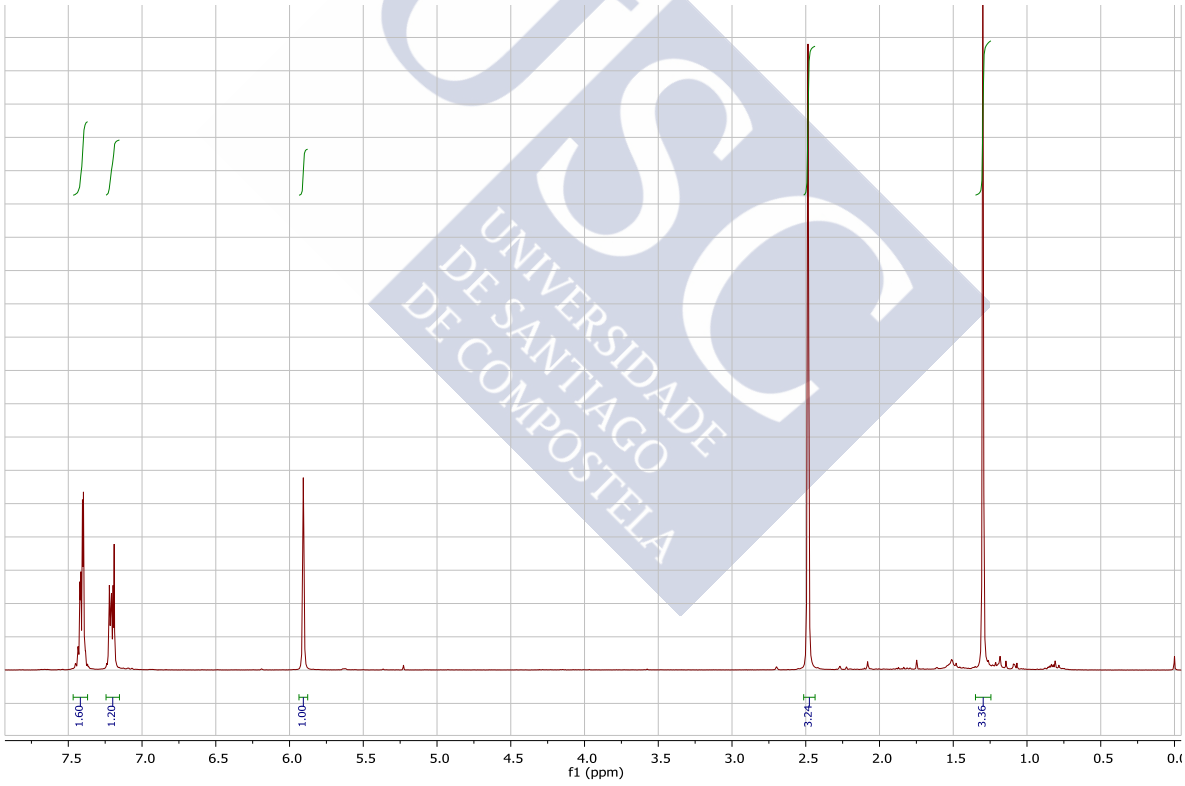
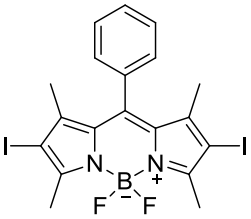


Figure 168. ^{1}H-NMR (300 MHz, $CDCl_3$) of B1. Preparation procedure described in Experimental Part, section, 10.1.

1.21. BI2-5



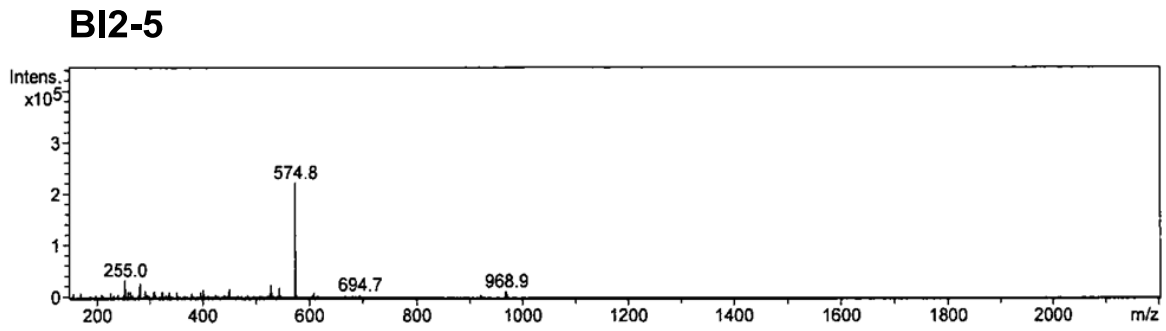


Figure 169. Mass spectrum of BI2-5 recorded by electrospray ionization in negative detection mode; m/z [M] calculated for $C_{19}H_{17}BF_2I_2N_2$ 575.95; found: 574.8.

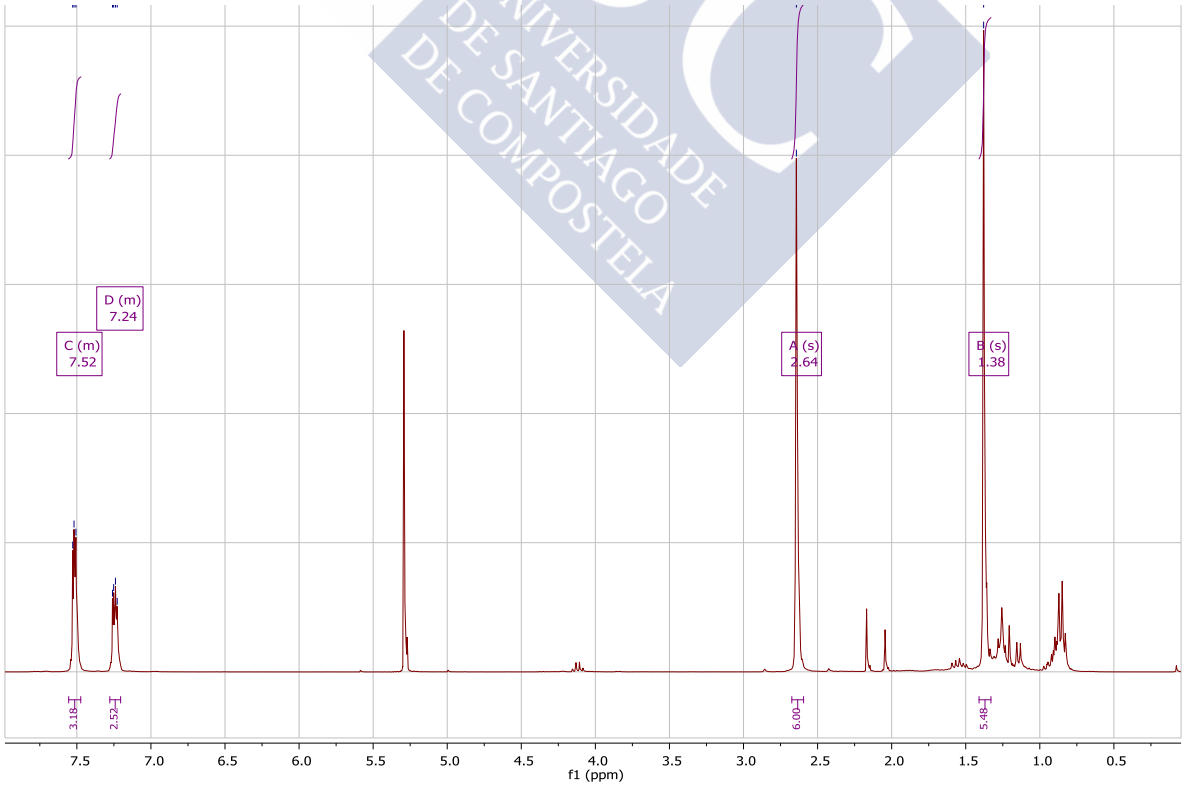
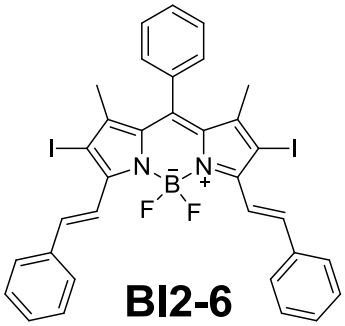


Figure 170. ^{1}H-NMR (300 MHz, $CDCl_3$) of BI2-5. Preparation procedure described in 10.2.

1.22. BI2-6



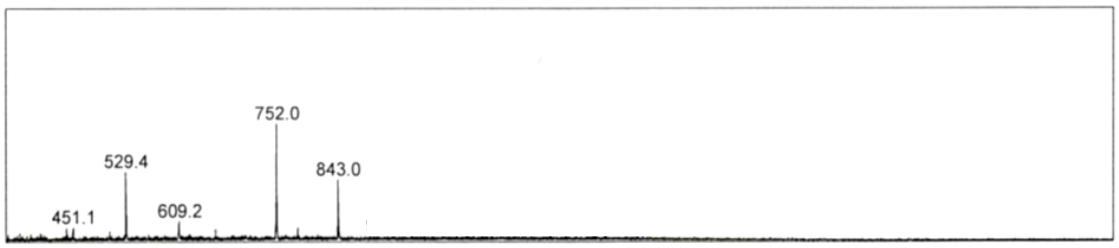


Figure 171. Mass spectrum of BI2-6 recorded by electrospray ionization in negative detection mode; m/z [M] calculated for $C_{33}H_{25}BF_2I_2N_2$ 752.02; found 752.0.

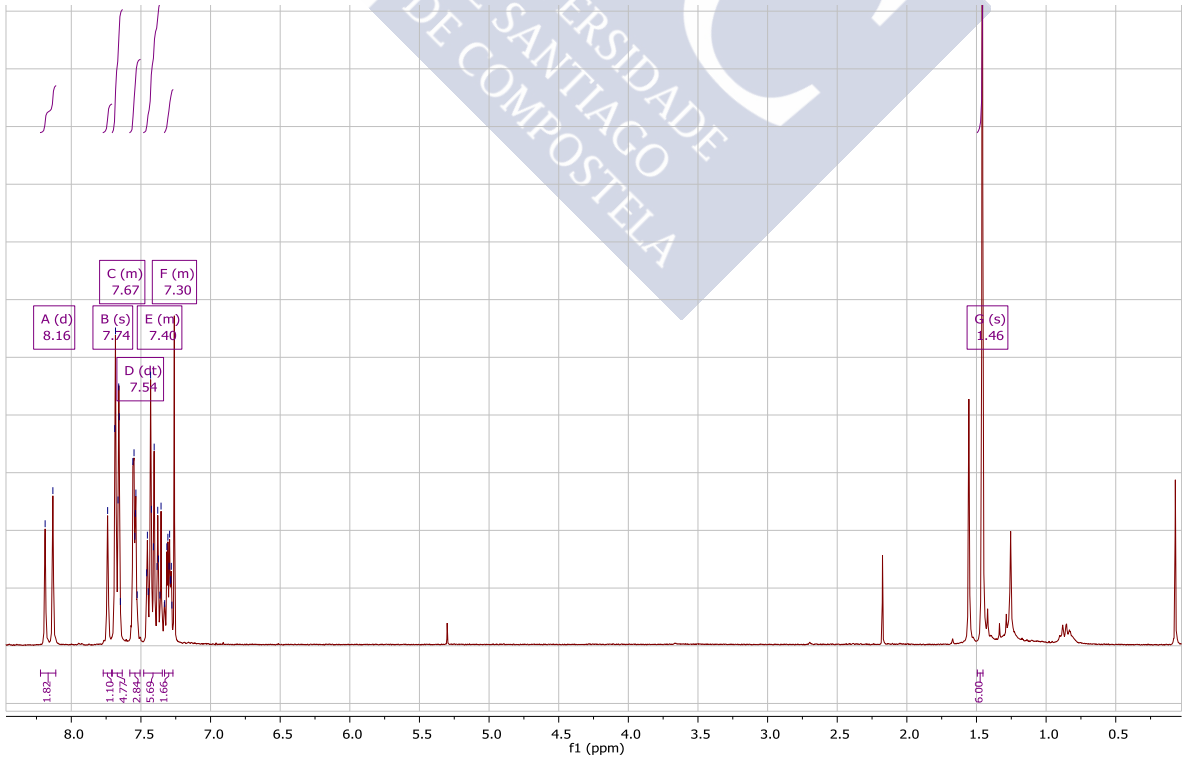


Figure 172. ^{1}H-NMR (300 MHz, $CDCl_3$) of BI2-6. Preparation procedure described in 10.3.

2. FTIR spectra

2.1. Co@SiO_2 NPs

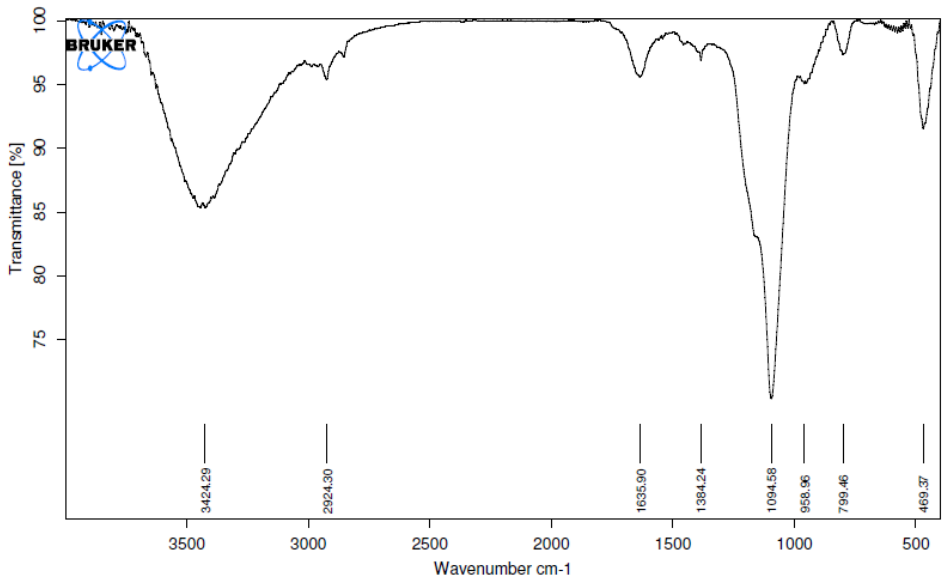


Figure 173. FTIR spectrum of Co@SiO_2 nanoparticles. Preparation procedure described in 6.1.

3. TEM images

3.1. Co-NH_2 magnetic nanoparticles

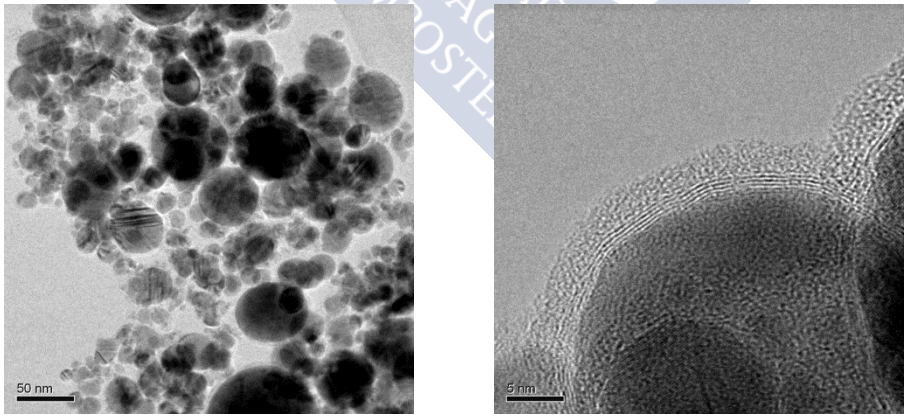


Figure 174. TEM images of commercial Co-NH_2 MNPs described in section 2 of Chapter 2 of Results and discussion Part.

3.2. $Co@SiO_2$ magnetic nanoparticles

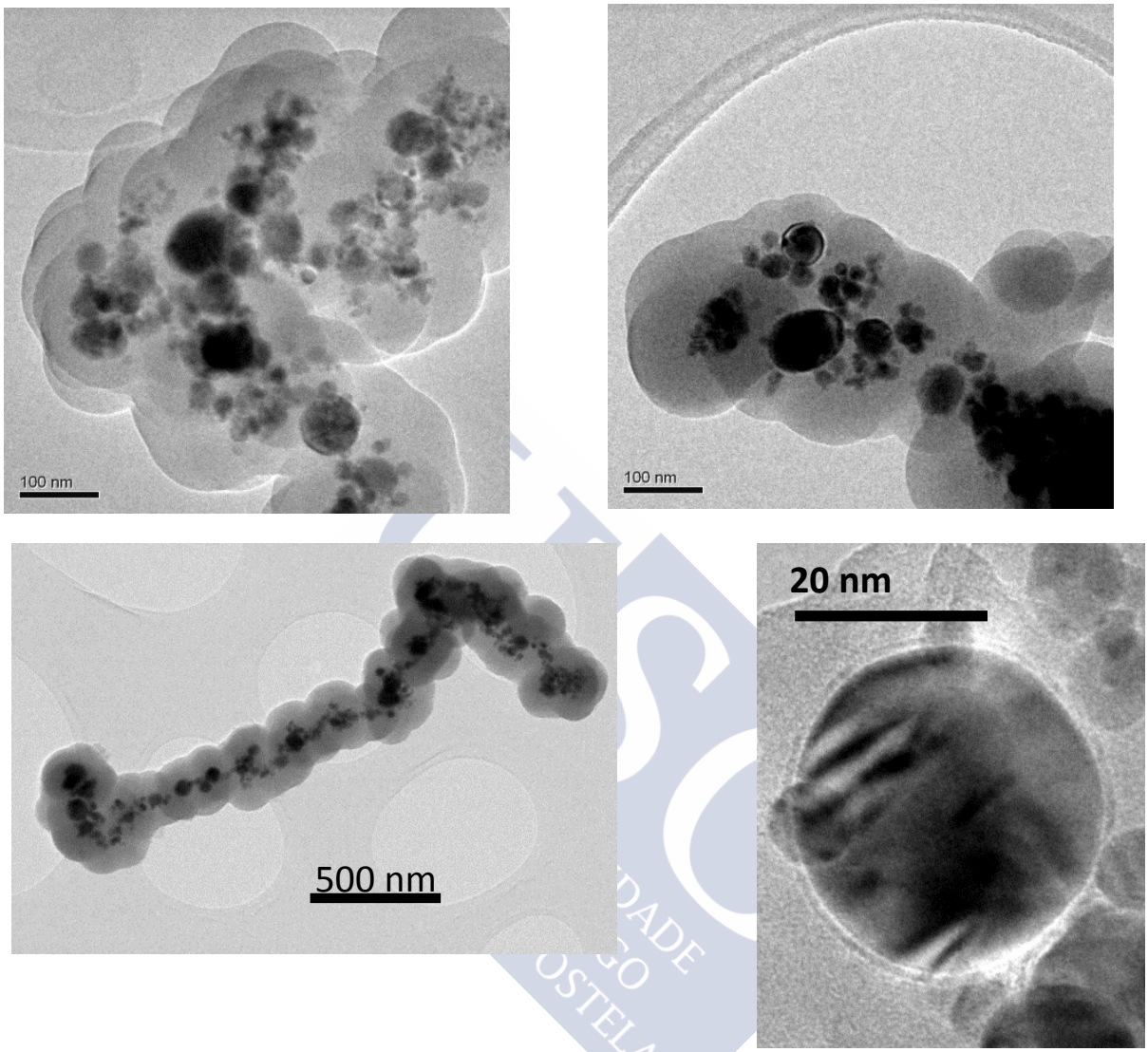
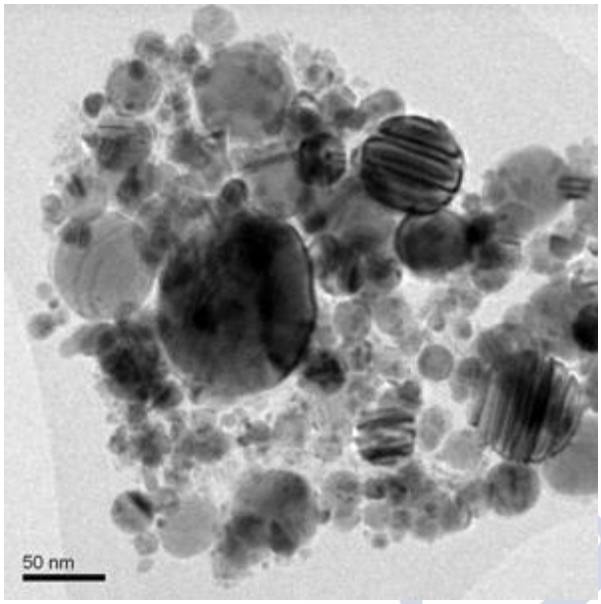


Figure 175. TEM images of $Co@SiO_2$ magnetic nanoparticles. Preparation procedure described in 6.1.

3.3. TurboBeads® with vinyl groups



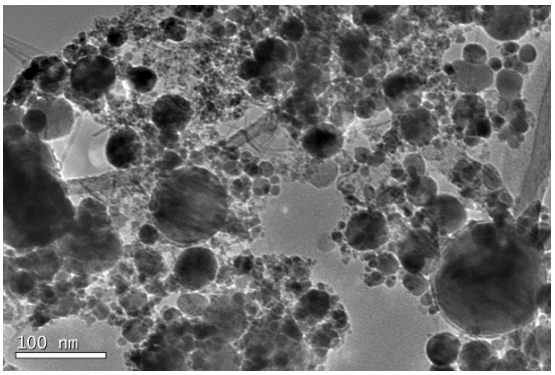


Figure 176. TEM images of commercial Co-St MNPs described in section 2 of Chapter 2 of Results and discussion Part..

3.4. NPs provided by Bangs Laboratories®

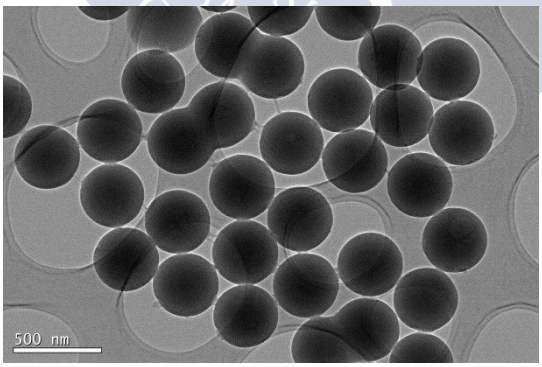


Figure 177. TEM image of commercial carboxylated polystyrene NPs of 390 nm described in section 0 of Chapter 3 of Results and discussion Part.

1.1. Magnetic NPs provided by Estapor®, Merck Millipore

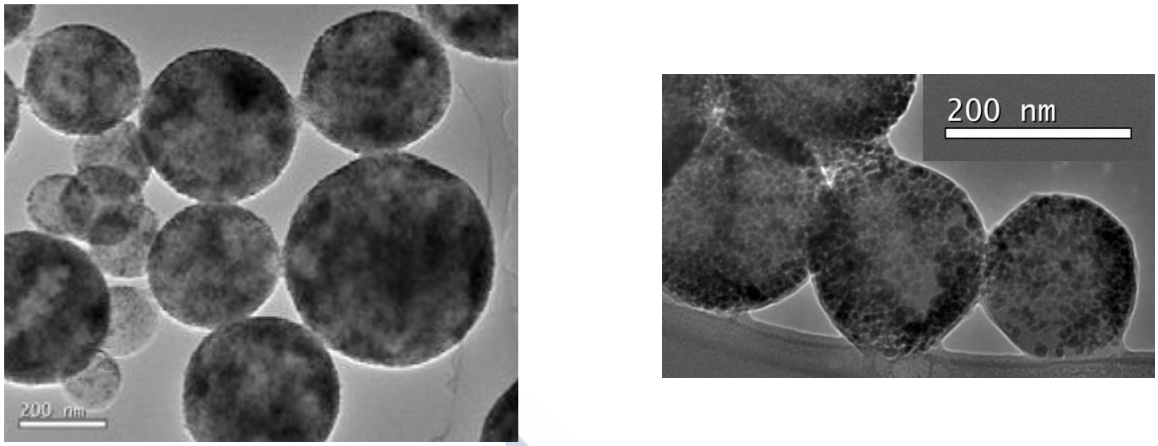


Figure 178. TEM images of commercial carboxylated magnetic NPs made by polystyrene embedded with ferrite nanograins, described in section 3 of Chapter 2 of Results and discussion Part.

Resumen

1. Introducción

El trasplante de células, tejidos, y sobre todo, órganos, es una de las áreas más desafiantes y complejas de la medicina moderna. Algunas de las áreas clave para el tratamiento médico son los problemas del rechazo de trasplantes, durante los cuales el cuerpo tiene una respuesta inmune al órgano trasplantado. Esto posiblemente conlleve un fracaso del trasplante y a la necesidad de eliminar inmediatamente el órgano del receptor. Por estos motivos, los pacientes que han sufrido un trasplante de órgano han de ser tratados con medicamentos inmunosupresores (ISs) que inhiben la respuesta inmune del cuerpo al nuevo órgano trasplantado. De particular interés son los inhibidores de la calcineurina: ciclosporina A (CyA) y tacrolimus (FK506), así como ácido micofenólico (MPA) que inhibe una enzima necesaria para el crecimiento de células T y B.

A pesar del gran éxito del empleo de ISs para realizar transplantes seguros, aún hoy en día la terapia inmunosupresora presenta algunas dificultades como:

1) La estrecha ventana terapéutica que presentan los ISs complica la administración de la dosis correcta del medicamento. Una dosis insuficiente puede conllevar el rechazo del órgano transplantado, y una sobredosis producir efectos secundarios peligrosos.

2) Los ISs presentan una alta variabilidad ínter e intra-paciente en los parámetros farmacocinéticos. Por lo que complica más la administración de la dosis correcta a cada paciente.

3) Estudios clínicos recientes han indicado que la monitorización de la fracción libre de los ISs (aquélla que no va unida a proteínas), es la responsable de la actividad farmacológica, y por tanto, refleja mejor los niveles tóxicos o insuficientes del fármaco. Estudios recientes muestran que se puede esperar un progreso sustancial en los resultados clínicos si se efectúa una monitorización continua de la fracción libre de IS con respecto al control farmacológico convencional. Sin embargo medir la fracción libre de los ISs es difícilmente practicable en la rutina clínica porque el proceso para obtenerla es lento y costoso, ya que representa sólo 1-3% de la dosis administrada.

En la actualidad, la monitorización terapéutica de medicamentos (TDM de su *acrónimo en inglés*) en pacientes post-trasplantados es una práctica habitual. La TDM consiste en la medición de la concentración de un fármaco en la sangre para garantizar que sus niveles permanezcan dentro del rango deseado. Las mediciones se realizan normalmente por métodos de cromatografía líquida acoplados a la detección por espectrometría de masas HPLC o LC-MS, y proporcionan información sobre los niveles de IS totales (libres y unidos a las proteínas).

El desarrollo de métodos analíticos alternativos a los cromatográficos, tales como aquéllos basados en inmunoensayos (IAs), es necesario para optimizar una TDM para inmunosupresores que sea eficaz, permitiendo una monitorización (semi)continua y personalizada. Se espera que en un futuro próximo las técnicas de análisis basadas en IAs reemplazarán progresivamente el análisis por LC-MS / MS en los hospitales como una técnica

rutinaria. Algunas de las ventajas de los IAs son su rapidez, bajo coste instrumental, menor necesidad de personal cualificado por su simplicidad de manejo, y la posibilidad de realizar simultáneamente multitud de análisis.

El objetivo principal de esta Tesis por tanto, es la preparación de reactivos (moléculas y nanomateriales) necesarios para el desarollo de varios tipos diferentes de inmunoensayos fluorescentes (FIAs). Los analitos de interés son tres de los fármacos inmunosupresores más extendidos para su administración en pacientes recién transplantados: tacrolimus, ciclosporina A y ácido micofenólico. Se explorará el uso de distintas técnicas fotoquímicas de amplificación óptica para la mejora de la sensibilidad de los métodos analíticos:

1) *Inmunoensayos de fluorescencia (FIA)*. Los FIA son hoy en día una de las metodologías más aplicadas a los biosensores ópticos en muchos campos de investigación, especialmente en el análisis clínico. La mayoría de los métodos de FIA se basan en el uso de sondas fluorescentes orgánicas o nanopartículas fluorescentes que se emplean para marcaje del analito diana o de un anticuerpo. Una variante interesante de FIAs son los ensayos basados en la medida de *polarización de fluorescencia (FPIAs)*. La ventaja de los FPIAs es que permiten la realización de ensayos en fase homogénea, en lo cuales no se requiere la etapa de lavado para eliminación del exceso de analito marcado con el fluoróforo, ya que únicamente aquél marcador que permanece unido al elemento de reconocimiento (el anticuerpo) posee una emisión con un grado de polarización distinto a la del fluoróforo libre. Para optimizar la sensibilidad de los FIAs se desarrollarán estrategias que permitan aumentar lo máximo posible la relación señal/ruido: i) *empleo de fluoróforos brillantes que operen en la ventana biológica* de 650-900 nm para minimizar problemas de dispersión de luz o de absorción y autofluorescencia de muestras biológicas; ii) *encapsulación de marcadores en NPs* para aumentar la intensidad de la señal; iii) generación de procesos FRET (*Förster resonance energy transfer*) intrapartícula que permitan recoger la fluorescencia con la menor dispersión de luz posible (problema que se agrava cuando se trabaja con NPs) y iv) empleo de *NPs magnéticas* que permiten la preconcentración y localización de la muestra.

2) *Inmunoensayos de quimioluminiscencia de proximidad (CLIA)*. En este ensayo, un tipo de nanopartículas (*NPs dadoras*) están codificadas con un fotosensibilizador que produce grandes cantidades de oxígeno singlete. Estas nanopartículas se funcionalizan con el anticuerpo de reconocimiento requerido. Un segundo conjunto de NPs (*NPs aceptoras*) se derivatizan con el antígeno correspondiente y se dopan con un aceptor de oxígeno singlete que genera un producto de oxidación inestable que emite energía al descomponer. Dicha energía es transferida a un colorante fluorescente que está co-encapsulado en las NPs aceptoras, con lo que se genera una señal de quimioluminiscencia. La emisión de quimioluminiscencia sólo se produce si existe un evento de enlace antígeno-anticuerpo, ya que en ese caso, las NPs dadoras y aceptoras están lo suficientemente próximas para la difusión del $^1O_2$ reactivo.

Por otro lado, una parte fundamental de esta Tesis también ha sido la derivatización química de los ISs con grupos -COOH para permitir su inmovilización covalente en superficies, proteínas o su marcaje fluorescente vía formación de enlaces amida.

2. Derivatización de fármacos inmunosupresores para el etiquetado fluorescente y la inmovilización en superficies.

2.1. Inmunosupresores carboxilados (ISs-COOH).

En esta Tesis, la atención se centra en algunos de los inmunosupresores más relevantes empleados en la actualidad para la terapia inmunosupresora: ácido micofenólico, ciclosporina A y tacrolimus. Respecto la derivatizción de los ISs para permitir su inmobilización en superficies o marcaje fluorescente, en el caso del MPA dicha modificación no es necesaria por poseer ya un grupo -COOH en su estructura. Sin embargo, CyA y FK506 han de ser químicamente modificados para poder introducir una función ácido carboxílico. Estos dos últimos ISs son macromoléculas cíclicas con una estructura bastante compleja, y su derivatización no es una tarea sencilla. Las transformaciones generalmente requieren reacciones de varios pasos y el uso de grupos protectores.

La ciclosporina A es un undecapéptido cíclico, cuyas modificación química se puede realizar a través de la subunidad MeBmt, el único aminoácido de la ciclosporina A que presenta grupos reactivos (un doble enlace y un grupo hidroxilo) en su cadena lateral. Se describe la síntesis de tres tipos de derivados carboxilados de CyA, siguiendo tres rutas sintéticas distintas. En dos de ellas (i) y (ii), fue necesaria la protección previa del grupo hidroxilo presente en CyA:

(i) La primera ruta se lleva a cabo por bromación alílica del carbono terminal C8'de la CyA y subsecuente reacción S_N2 con 3-mercaptopropanoato de metilo para dar el derivado CyA-S-COOH con un 47% de rendimiento tras la hidrólisis alcalina del éster protector.

(ii) La segunda ruta sintética implica una reacción de 4 etapas en la que el punto de partida es la epoxidación del doble enlace C=C, seguido de una reacción S_N2 con un ω-aminoéster. Tras la hidrólisis alcalina del éster protector del grupo -OH, se obtiene CyA-N-COOH como una mezcla de dos regioisómeros (33% de rendimiento). Esto es debido a que el ataque nucleofílico por parte del aminoéster utilizado para abrir el epóxido se produce en ambos C del epóxido.

(iii) La tercera ruta implica la modificación directa del grupo hidroxilo secundario de CyA. Esta novedosa ruta sintética proporciona el carboxi-derivado denominado CyA-O-COOH con un 85% de rendimiento.

Debido a la elevada polaridad de la ciclosporina A, la purificación de sus derivados por cromatografía en columna de gel de sílice no fue posible. Todos los derivados se aislaron mediante extracción líquido-líquido, técnica que afortunadamente fue suficiente para la obtención de los productos carboxilados puros. La estructura de los derivados de la CyA se confirmó por espectrometría de masas (algo complejo en alguno de los casos por la tendencia de algunos derivados de fragmentar, y por la dificultad de encontrar las condiciones adecuadas para la ionización). También se emplearon técnicas de resonancia magnética

nuclear (^{1}H y ^{13}C), con las que, a pesar de la complejidad de las moléculas (todos los derivados de CyA poseen más de 60 átomos de C y más de 100 átomos de H), fue posible asignar algunas de las señales más significativas. En ^{1}H-RMN por ejemplo se observan los enlaces N-H entre 8 y 7 ppm, entre 6 y 4 ppm se aprecian grupos CH unidos a amida, y alrededor de 3 ppm 7 señales intensas de los grupos CH_3 unidos a N peptídicos. En ^{13}C-RMN se aprecian las señales de 12 carbonilos (11 de C=O de amida más 1 C=O del éster protector del grupo -OH) entre 174 y 168 ppm, y a 129 y 126 ppm se observan los dos C vinílicos de la subunidad MeBmt. Señales características resultantes de las reacciones de acilación, epoxidación y apertura del epóxido también se han identificado mediante ^{13}C-RMN.

El tacrolimus o FK506 es una lactona macrólida hidrofóbica de 23 miembros con 14 estereocentros, tres grupos hidroxilo libres, tres dobles enlaces y varios grupos carbonilo. En esta Tesis, la derivatización de FK506 se ha llevado a cabo a través del grupo cetona presente en el C22 mediante una reacción de adición-eleminación con carboximetoxilamina para obtener una oxima mezcla de isómeros Z y E, según el procedimiento descrito por O. Cañadas *et al.* en *Anal. Biochem.* **2005**, *340*, 57 (rendimiento > 80%). Con la derivatización FK506, la señal característica de ^{13}C-RMN a 212 ppm desaparece a la vez que aparece una nueva señal a 156.9 ppm, típica de un enlace C=N de oxima.

2.2. Etiquetado de inmunosupresores con sonda fluorescente NIR.

Para el etiquetado fluorescente de los tres derivados IS-COOH se eligió un colorante de la familia de benzo[a]fenoxazinas, similar al popular fluoróforo *Nile Blue* (NB), que es bastante soluble en agua y tiene un máximo de emisión a 660 nm, en la ventana biológica (Φ_f = 0.01 en H_2O). La síntesis de benzo[a]fenoxazinas implica la condensación de un nitroso derivado aromático y un derivado de naftaleno (5-amino-2-nitrosofenol y 1-aminonaftaleno, respectivamente, para NB) en etanol a reflujo con catálisis ácida. Los análogos del *Nile Blue* con solubilidad en agua mejorada y/o grupos para la bioconjugación se pueden preparar a partir de un naftaleno con los N-sustituyentes apropiados. En esta Tesis, se sintetiza un análogo aminado del *Nile Blue*, denominado ANB, a partir de N^{1}-1-naftalenil-1,3-propanodiamina. ANB con λ_{abs} = 624 nm y λ_{em} = 677 nm en tampón fosfato. ANB ha demostrado ser muy fotoestable y poseer una emisión de fluorescencia prácticamente 20 veces superior a la del NB en medio acuoso (Φ_f = 0.18).

Las tres sondas fluorescentes de los fármacos inmunosupresores se obtienen por formación de enlace amida entre los derivados IS-COOH correspondientes y el ANB, mediante activación previa con EDC/HOBt, (1-etil-3-(3-dimetilaminopropil)carbodiimida y 1-hidroxibenzotriazol, respectivamente) en presencia de trietilamina. Los conjugados de CyA-S-COOH, CyA-O-COOH, FK506-COOH y MPA con ANB se obtuvieron con un rendimiento de > 55%. Los productos fluorescentes se caracterizaron mediante RMN, espectrometría de masas, absorción UV-VIS y espectroscopía de fluorescencia en el estado estacionario y resuelta en el tiempo. La caracterización espectroscópica se llevó a cabo en etanol y en tampón de fosfato a pH 7.4 (medio que simula mejor las condiciones fisiológicas). Los datos fotofísicos confirman la idoneidad de ANB como marcador fluorescente. Se observa además que el marcador

fluorescente no es propenso a la agregación en agua a concentraciones micromolares y que las propiedades espectrocópicas muestran poca variación entre los diferentes conjugados.

Los inmunosupresores marcados con ANB se utilizaron para estudiar la interacción entre los fármacos inmunosupresores y la albúmina de suero humano (HSA) empleando la técnica de polarización de fluorescencia (FP). La albúmina fue seleccionada porque es la proteína más abundante en el plasma sanguíneo. Se demuestra que es posible calcular la fracción libre de los ISs conociendo la constante de disociación K_D. Se obtuvieron curvas de unión total y de unión específica para MPA-ANB, CyA-ANB, FK506-ANB y HSA en las cuales el valor de polarización de fluorescencia se representa frente a la concentración de fármaco en tampón fosfato. Los valores de la constante de asociación especifica entre IS-ANB y HSA en mM^{-1} fueron: 21.3 ± 4.3 para MPA-ANB, 51.3 ± 2.9 para CyA-ANB y 3.1 ± 0.6 para el FK506-ANB. Mientras que la fracción libre que se obtuvo fue 0.069 ± 0.011 para MPA-ANB, 0.030 ± 0.0042 para CyA-ANB, y 0.338 ± 0.014 para FK506-ANB. De acuerdo con estos valores calculados, la ciclosporina A (marcada) muestra la mayor afinidad por HSA mientras que el tacrolimus (marcado) muestra el valor más bajo. Consecuentemente, la fracción libre de FK506-ANB en presencia de HSA es la mayor.

3. Nanopartículas fluorescentes como marcadores para inmunoensayos sensibles.

3.1. Nanopartículas dopadas con sistemas de transferencia de energía resonante Förster (FRET) intraparticula.

En este apartado se describen nanopartículas fluoro-magnéticas (FMNPs) novedosas en las que procesos FRET intrapartícula permiten mejorar los límites de detección en FIAs para detección de inmunosupresores. Las FMNPs se prepararon por dopado con colorantes tipo boro-dipirrometeno (BODIPYs). Estos colorantes fueron seleccionados por presentar un elevado rendimiento cuántico de fluorescencia y una intensa absorción, lo que proporciona una intensa señal analítica. Otra ventaja de los BODIPYs es que poseen una química versátil que permite la introducción de unidades conjugadas adicionales, permitiendo la obtención de cromóforos que absorben en la zona roja-infrarroja del espectro, zona con mínimas interferencias ópticas. Una de las pocas desventajas de este tipo de fluoróforos son los pequeños desplazamientos de Stokes (ca. 10-20 nm) que dificultan una separación adecuada entre la luz de excitación dispersada por las NPs y la detección. En esta Tesis se presenta una estrategia para minimizar este problema mediante la co-encapsulación de dos tipos de BODIPYs en una misma NP, un par dador-aceptor FRET, para obtener sistemas con un desplazameinto virtual de Stokes de > 150 nm con una intensa fluorescencia a > 650 nm.

Para el dopado fluorescente se probaron nanopartículas de distinta composición: sílice, núcleos magnéticos de cobalto recubiertos por una capa de grafeno derivatizable, poliestireno con grupos -COOH superficiales para (bio)conjugación, y poliestireno con grupos -COOH superficiales recubiertas de nanogranos de ferrita magnéticos. La plataforma que fue elegida finalmente fueron las NPs magnéticas carboxiladas de poliestireno, de unos 300 nm de

diámetro, comercializadas por Estapor® (Merck Millipore) con un contenido en nanogranos de ferrita de ca. 55% en peso.

Como fluoróforos, se sintetizaron dos colorantes tipo BODIPY (PFB-515 y PFB-641) con un elevado rendimiento cuántico de fluorescencia. La caracterización espectroscópica de los mismos puso de manifiesto sus idoniedad como marcadores: PFB-515 muestra una λ_{abs} / λ_{em} = 515 / 525 nm en EtOH (Φ_f = 0.87) y PFB-641, con una estructura π-extendida respecto al anterior, muestra un desplazamiento batocrómico con λ_{abs} / λ_{em} = 641 / 657 nm en EtOH (Φ_f = 0.73). Se comprueba que el fluoróforo PFB-641 es fotoestable (únicamente se observa una disminución del 5% de la intensidad de emisión inicial después de 20 horas de irradiación a 635 nm con un láser continuo de 5mW) y una buena superposición espectral entre su banda de absorción y la emisión de PFB-515 (integral de solapamiento espectral J (λ) = 1.35×10^{15} M^{-1} cm^{-1} nm^4, y distancia de Förster R_0 5.2 nm), de modo que se seleccionó el par de BODIPYs como sistema dador (PFB-515) - aceptor (PFB-641) FRET.

El dopado de las NPs magnética de poliestireno se realiza por un método de hinchamiento en mezclas THF:H_2O (0.25/1, *v/v*), realizando un estudio mediante espectroscopía de fluorescencia para ver cómo afecta la carga de BODIPY por mg de NPs a las propiedades fluorescentes. Los resultados revelan un dopado óptimo para valores de *ca.* 5 nmol de BODIPY por mg de NPs. Las MNPs fueron dopados simultáneamente con ambos BODIPY logrando un desplazamiento de Stokes virtual de 150 nm a través de un sistema FRET intraparticula en el que PFB-515 es el dador y PFB-641 el aceptor. Cuando las NPs se dopan con una relación molar 2:1 de PFB-515/PFB-641 se obtiene una fluorescencia más intensa y un tiempo de vida de fluorescencia más largo del aceptor que cuando el dopado es equimolar. Esta observación implica que el proceso FRET mejora debido a la presencia de más "antenas". Cabe resaltar que las FMNPs resultantes son estables en agua y los fluoróforos no lixivian de la matriz de poliestireno en una disolución acuosa tamponada.

3.2. Inmunoensayo competitivo basado en FMNP para tacrolimus.

Las FMNPs FRET han sido empleadas como marcadores en un FIA para la detección de tacrolimus, proporcionando un límite de detección (LOD) de 0.08 ng mL^{-1}, con un rango dinámico (DR) de 0.15–2.0 ng mL^{-1} al realizar el ensayo excitando el dador FRET y observando la fluorescencia sensibilizada del aceptor PFB-641, comparado con un LOD de 2.7 ng mL^{-1} y un DR entre 4.1 y 130 ng mL^{-1} para el inmunoensayo llevado a cabo con excitación directa del aceptor FRET PFB-641 (sin emplear el *modo FRET*). El sistema propuesto sería lo suficientemente sensible para cuantificar el tacrolimus en muestras reales, a que la última recomendación de un panel de expertos europeos en tacrolimus es el desarrollo de métodos analíticos que muestren un límite de cuantificación de hasta 1 ng mL^{-1} para proporcionar concentraciones fiables para la terapia a bajas dosis de tacrolimus.

4. Nanopartículas fotosensibilizadoras para la producción de oxígeno singlete.

El objetivo de esta sección es el dopado de nanopartículas magnéticas de poliestireno con fotosensibilizadores para la producción eficaz de oxígeno singlete. Se espera que la encapsulación en nanopartículas, que permite una mayor concentración de fotosensibilizador, mejore la producción de oxígeno singlete con respecto a los fotosensibilizadores en disolución. Estas NPs podrían usarse en terapia fotodinámica o como NPs productoras de $^1O_2$ en inmunoensayos de proximidad tipo AlphaScreen™ comercializado por PerkinElmer. Este inmunoensayo se basa en la fotogeneración de $^1O_2$ que es capaz de "viajar" desde el NPs dadoras (dopadas con el fotosensibilizador, y funcionalizadas con anticuerpos) a NPs aceptoras (funcionalizadas con el antígeno y dopadas con una molécula que *atrapa* el $^1O_2$ para dar un producto que al descomponer cede energía a un fluoróforo co-encapsulado en las NPs, que entonces emite una señal de quimioluminiscencia). El fenómeno de la quimioluminiscencia sólo se observa cuando las NPs dadora-aceptora están lo suficientemente cerca para la difusión del $^1O_2$, es decir, cuando hay enlace anticuerpo-antígeno. Sólo después que el $^1O_2$ llega a la NP aceptora, la quimioluminiscencia de esta última se activa, lo que conduce a una excelente discriminación del fondo y sensibilidad.

Como fotosensibilizador se ha escogido un complejo de Ru(II): dicloruro de [tris (4,7-difenil-1,10-fenantrolina) rutenio(II)] (RD3). Se optimizó un método para dopar nanopartículas de poliestireno de 390 nm con RD3 por hinchamiento en disolvente orgánicos, estudiando cómo variaba la intensidad de emisión de las NPs según los disolventes utilizados. La mezcla óptima de disolventes resultó ser H_2O:THF:MeOH en proporción 1/0.15/0.1 *v/v/v*. Posteriormente, la carga del fotosensibilizador se optimizó a 20,8 nmol de RD3 por mg de NPs realizando medidas de intensidad de emisión. Además, las mediciones del tiempo de vida de emisión (con un decaimiento de tipo biexponencial, observado también en ausencia de O_2, indicando la existencia de distintos microentornos) proporcionan información sobre la distribución de RD3 en diferentes microambientes de las NPs. Se observa una disminución inicial de el tiempo de vida de *Ru[II], correspondiente a un aumento de la concentración de el RD3, por un proceso de auto-desactivación de luminiscencia. Mientras que si la concentración de RD3 se sigue aumentando, el tiempo de vida vuelve a aumentar probablemente porque el fotosensibilizador ahora se ve obligado a entrar más profundamente en las NPs.

Para la determinación de los valores de rendimiento cuántico de producción de oxígeno singlete Φ_Δ de la NPs de poliestireno dopadas, se emplearon NPs de 26 nm de diámetro en lugar de las de 390 nm, ya que estas últimas daban demasiados problemas de dispersión de luz. Las NPs de 26 nm se doparon con RD3 siguiendo el mismo método optimizado para las NPs de 390 nm. Se perfeccionó un método para determinar el Φ_Δ de una suspensión de NPs en D_2O (en este disolvente la emisión de oxígeno singlete es más intensa que en H_2O) con un sistema de espectrómetro láser cinético. Se monitorizó el decaimiento de el tiempo de vida del $^1O_2$ en su máximo de emisión de fosforescencia a 1270 nm, usando diferentes energías láser (λ_{em} =532 nm). El rendimiento cuántico de producción de $^1O_2$ del fotosensibilizador en las NPs, $\Phi_{\Delta\,NPs}$ puede determinarse mediante calibración frente a un fotosensibilizador de

referencia ($[Ru(dpds)_3]^{4-}$) con un rendimiento cuántico de producción de oxígeno singlete conocido. Se encontró que se produce una mayor cantidad de oxígeno singlete cuando el fotosensibilizador está encapsulado en NPs que cuando está libre en solución ($\Phi_{\Delta\ NPs} = 0.50 > \Phi_{\Delta\ RD3} = 0.42$).

También se sintetizaron dos colorantes tipo BODIPY yodados (BI2-5, λ_{abs} / λ_{em} = 532 / 548 nm, y BI2-6, λ_{abs} / λ_{em} = 634 / 650 nm, en etanol) con alto Φ_Δ como alternativa a los complejos Ru(II) con absorción de luz en el amarillo-rojo. Una de las ventajas de los BODIPYs es que se evita la emisión no deseada a 1270 nm de los complejos ^{3}MLCT de Ru(II), que interfiere con la emisión de $^1O_2$. Otra ventaja es que se encapsulan efectivamente en NPs de poliestireno al ser colorantes más hidrófobos que los complejos de Ru(II). Por ejemplo, BI2-6 se encapsuló exitosamente en NPs de poliestireno por de hinchado de las NPs en mezclas de agua-THF.

5. Conclusiones.

La innovación sustancial de esta Tesis es el desarrollo de nuevas estrategias y herramientas para el desarrollo de IAs para la detección de los inmunosupresores FK506, CyA y MPA.

El desafío más arduo fue la modificación química de los fármacos inmunosupresores necesaria para la introducción de grupos -COOH. Se ha descrito la síntesis de tres nuevos carboxi-derivados de CyA y de un derivado tacrolimus con buenos rendimientos. En consecuencia, se dispone de una plataforma de derivados carboxilados de los tres inmunosupresores examinados, FK506-COOH, CyA-COOH y MPA lo que permite el uso de la misma química para posteriores transformaciones y su aplicabilidad en el inmunoensayos multianalito. Además, la función carboxílica se ha aprovechado para el etiquetado con sondas fluorescentes de infrarrojo cercano. Se ha seleccionado y sintetizado un derivado aminado del *Nile Blue* para etiquetar los fármacos inmunosupresores. Es la primera vez que tales ISs fueron etiquetados con éxito con métodos directos y con altos rendimientos con sondas NIR.

Los derivados IS-COOH e IS-ANB proporcionaron resultados exitosos en inmunoensayos fluorescentes realizados en el marco del Proyecto EU "NANODEM", financiado por el Programa de TIC FP7 *NANOphotonic DEvice for Multiple therapeutic drug monitoring*. Los IS-ANB marcados pueden emplearse por ejemplo en inmunoensayos de polarización de fluorescencia. Por un lado: i) se ha desarrollado con éxito un ensayo FPIA para la determinación de MPA en el plasma de pacientes transplantados empleando la sonda ANB-MPA (parte de un trabajo de otra Tesis Doctoral del grupo de investigación) con un LOD de 0.8 ng mL^{-1} y un DR of 1.7–39 ng mL^{-1} en tampón fosfato; por otro lado ii) se ha demostardo que los IS marcados con ANB se pueden emplear para estimar la fracción libre (no unida a HSA) de IS mediante ensayos FPIA de ciclosporina A, ácido micofenólico y tacrolimus, que fueron respectivamente 6%, 3% y 34%.

Se han preparado con éxito FMNPs empleando NPs de poliestireno carboxilado decoradas con nanogranos de ferrita y fluoróforos BODIPY intensamente fluorescentes usando un protocolo sencillo (hinchamiento de las NPs en mezclas THF:H_2O 0.25/1 *v/v*), encontrando que la cantidad óptima de colorante incorporado era de *ca.* 5 nmol. La combinación de dos tipos de

BODIPY distintos para el dopado ha permitido además obtener FMNPs FRET con un elevado desplazamiento de Stokes virtual de > 150 nm y una intensa emisión a > 650 nm. Las FMNPs resultantes son estables en agua y no se observan pérdidas del BODIPY de la matriz de poliestireno en medio acuoso. La aplicación de las FMNPs FRET en un FIA para la detección de tacrolimus ha demostrado el éxito de la aproximación ya que el ensayo realizado en el *modo FRET* muestra mejor LOD que el mismo ensayo con excitación directa del PFB-641, aceptor FRET. Estas nuevas nanopartículas fluoromagnéticas muestran un rendimiento similar o superior en términos de sensibilidad en comparación con los fluoro-inmunoensayos previamente descritos para tacrolimus.

Y por último, se ha optimizado el dopado de NPs de poliestireno con moléculas fotosensibilizadoras de distinto tipo para la producción eficaz de oxigeno singlete: i) Por un lado, se ha estudiado la preparación de NPs de 390 nm dopadas con un complejo de Ru (RD3). El mayor grado de dopaje se logró utilizando como disolvente la mezcla H_2O/THF/MeOH 1/0.15/0.1 *v/v/v* para el hinchamiento de las NPs. De acuerdo con los resultados obtenidos por espectroscopía de emisión de estado estacionario, la carga óptima del fotosensibilizador RD3 (la que produce las partículas más emisivas) fue de 20,8 nmol por mg de NP. Desafortunadamente, no fue posible medir el rendimiento cuántico de producción de oxígeno singlete para estas NPs por la elevada dispersión de luz. Un problema que se minimizó empleando alternativamente NPs de menor tamaño (26 nm de diámetro). Se desarrolló un método para cuantificar la producción de oxígeno singlete y los resultados demostraron que las NPs de poliestireno dopadas con RD3 producen una cantidad de $^1O_2$ ligeramente superior al propio fotosensibilizador libre en disolución; ii) por otro lado, se prepararon derivados yodados de colorantes BODIPY como fotosensibilizadores alternativos al complejo metálico de Ru(II) para una zona espectral distinta.

Estas nuevas herramientas abren el camino para el desarrollo de nuevos IAs (especialmente para fármacos inmunosupresores) capaces de alcanzar LODs suficientemente bajos. Por lo tanto, si se validan adecuadamente, estos IAs podrían ser sólidas alternativas a las técnicas cromatográficas clásicas (HPLC, LC-MS/MS) para TDM en los laboratorios centrales de los hospitales.